

Last Interglacial (MIS 5e) Palaeoceanography of the Nordic Seas Based on Dinoflagellate Cyst Assemblages

Dissertation

zur Erlangung des Doktorgrades
der Mathematisch-Naturwissenschaftlichen Fakultät
der Christian-Albrechts-Universität
zu Kiel

vorgelegt von

Nicolas Van Nieuwenhove



Kiel, 2008

Referent

Prof. Dr. Wolf-Christian Dullo

Korreferent

Prof. Dr. Priska Schäfer

Tag der Disputation

10. November 2008

Zum Druck genehmigt, Kiel, den

10. November 2008

Der Dekan: Prof. Dr. rer. nat. Lutz Kipp

Summary

Understanding the dynamics of a warm climate is essential in order to assess possible scenarios for future climate evolution. The last interglacial, Marine Isotopic Stage (MIS) 5e, is generally believed to have been warmer than the Holocene, under a comparable orbital configuration, and is thus a good candidate to get more insight in those dynamics. Climate is steered by the rate of overturning of warm surface waters into cool deepwaters. One of these overturning cells is located in the Nordic seas, and the area is thus a key region in terms of climate regulation. Marine sediments from three locations in the Nordic seas have been studied for their dinoflagellate cyst (dinocyst) content in order to reconstruct sea surface conditions (temperature, salinity, sea ice) during MIS 5e. In combination with stable oxygen isotope, ice rafted detritus (IRD) and planktic foraminiferal assemblage data, the variations in the dinocyst assemblage composition reflect a stepwise transition from the final phase of deglaciation (Termination II) into typical interglacial conditions, and the subsequent cooling during glacial inception towards MIS 5d.

The marked presence of the neritic, warm-temperate dinocyst *Lingulodinium machaerophorum* towards the end of Termination II tells us that quite particular water masses entered the southern Nordic seas during the latest deglacial phases of MIS 6. A shift towards the inflow of “more Atlantic” waters and a drastic decrease in both IRD input and stable oxygen isotope values mark the start of MIS 5e. The northward heat flow remained relatively weak during the first ~4-5 kyr of MIS 5e, and at no time an east to west sea surface temperature gradient, as pronounced as at present, appears to have prevailed during that period. Quantitative and qualitative analyses of the dinocyst data from the Vøring Plateau in the eastern Norwegian Sea and comparison with core-top and published data substantiate the existence of distinctly different hydrological surface conditions during MIS 5e with respect to the late Holocene. A higher number of co-dominant, subordinate species in the last interglacial samples suggests that there was a more pronounced seasonality of the surface water at this time. This is supported by the sizeable abundance of *Bitectatodinium tepikiense*, a species virtually absent from the area for most of the Holocene. The seasonality signal is confirmed by transfer function reconstructions, which additionally indicate a stronger stratification of the upper water column during MIS 5e. Low but persistent IRD input during the first ~4.5 kyr of MIS 5e at the Vøring Plateau suggests that prolonged deglacial meltwater input may have caused the stratification and hindered the northward protrusion of Atlantic water masses towards the Arctic.

The abundance maximum of the warm-temperate dinocyst species *S. mirabilis* s.l. between ~117.5 and 116.5 ka reveals that most pronounced, fully marine interglacial conditions prevailed in the (north)eastern Nordic seas only late in the last interglacial. The timing of the optimum is consistent with planktic foraminiferal findings, and contrasts with the early Holocene climatic optimum. Stable oxygen isotope values from planktic foraminifera for the MIS 5e optimum are comparable with average Holocene values, but are generally ca. 0.3‰ higher than those of the earlier part of the last interglacial. These higher $\delta^{18}\text{O}$ values therefore do not reflect optimal interglacial conditions, but corroborate the existence of a differently structured sea surface, as suggested by the dinocyst data.

Whereas the enhanced northward heat flow from the late MIS 5e optimum allowed interglacial conditions to finally develop in the southern Fram Strait, it also appears to have strengthened the southward flow of the East Greenland Current. As a result, cold waters and sea ice were advected towards the eastern Iceland Plateau area, and no late MIS 5e optimum could develop in the uppermost surface waters there.

The work presented here also illustrates that specific ecological constraints can cause different fossil groups to express climate events in a differing way. This clearly stresses the usefulness of combining different proxies for detailed palaeoceanographic reconstructions. Furthermore, the major impact from the enhanced and prolonged influence of Saalian deglacial meltwater on the further development of the last interglacial climate implies that MIS 5e cannot simply be taken as an analogue for the Holocene solely based on insolation forcing.

Zusammenfassung

Für die Vorhersage möglicher zukünftiger Klimaszenarien ist das Verständnis der Mechanismen, die zur Ausbildung eines warmen Klimas führen, von besonders großer Bedeutung. Das letzte Interglazial, das marine Isotopenstadium (MIS) 5e, wird - bei vergleichbaren orbitalen Voraussetzungen - allgemein für wärmer gehalten als das Holozän. Das letzte Interglazial eignet sich daher gut, um die Prozesse, die zu wärmeren Bedingungen führen können, zu untersuchen. Das Klima wird maßgeblich von warmen Wassermassen beeinflusst, die abkühlen, von der Meeresoberfläche in die Tiefe abtauchen, und als kaltes Tiefenwasser in entgegengesetzter Richtung zurückfließen. Eine dieser in die Tiefe abtauchenden Zellen befindet sich im Europäischen Nordmeer. Dieses Gebiet ist somit eine Schlüsselregion für die weltweite Klimasteuerung. Meeressedimente aus drei verschiedenen Gebieten des Europäischen Nordmeeres wurden auf Dinoflagellatenzysten hin untersucht, um die Bedingungen an der Meeresoberfläche (Temperatur, Salzgehalt, Eisbedeckung) während des MIS 5e zu rekonstruieren. Kombiniert mit Ergebnissen der Analyse der stabilen Sauerstoffisotope, des mit dem Eis transportierten Materials (Ice Rafted Debris = IRD) sowie des Gehalts planktischer Foraminiferen spiegelt die Zusammensetzung der Dinoflagellatenzysten eine schrittweise Veränderung von der Endphase der Deglaziation (Termination II) zu typischen interglazialen Verhältnissen und einer nachfolgenden Abkühlung im Zuge des einsetzenden glazialen Stadiums MIS 5d wider.

Die deutlich erkennbare Präsenz von Dinoflagellatenzysten der neritischen, warmgemäßigten Art *Lingulodinium machaerophorum* gegen Ende von Termination II zeigt, dass ganz bestimmte Wassermassen während der letzten Phase des Deglazials MIS 6 in das südliche Nordmeer eindringen. Der verstärkte Einfluss von Atlantischen Wassermassen sowie eine drastische Verringerung des IRD-Materials und der Werte der stabilen Sauerstoffisotope markieren den Beginn von MIS 5e. Der nach Norden gerichtete Wärmestrom blieb während der ersten vier- bis fünftausend Jahre von MIS 5e relativ schwach; ein von Osten nach Westen verlaufender Temperaturgradient an der Meeresoberfläche, wie es ihn heute gibt, existierte nicht. Quantitative und qualitative Untersuchungen der Dinoflagellatenzysten auf dem Vøring-Plateau in der östlichen Norwegischen See sowie der Vergleich mit Sedimentoberflächenproben und mit veröffentlichten Ergebnissen bestätigen die Annahme, dass sich die hydrologischen Verhältnisse an der Meeresoberfläche während des MIS 5e von denen im späten Holozän deutlich unterscheiden. Eine höhere Anzahl von kodominanten untergeordneten Arten in

verschiedenen Proben aus dem letzten Interglazial lässt auf einen verstärkten Einfluss der Jahreszeiten auf das Oberflächenwasser schließen. Dies wird auch von der deutlichen Präsenz von *Bitectatodinium tepikiense* unterstützt, einer Art, die im Holozän auf dem Vøring-Plateau praktisch nicht vorkommt. Der Einfluss der Jahreszeiten wird von Rekonstruktionen mit Hilfe von Transferfunktionen bestätigt. Diese zeigen zusätzlich eine stärkere Schichtung der oberen Wassersäule während MIS 5e an. Geringe, aber stetig vorhandene Mengen an IRD-Material auf dem Vøring-Plateau während der ersten vier- bis fünftausend Jahre im MIS 5e zeigen, dass anhaltende Schmelzwässer für diese Schichtung verantwortlich sein und einen stärkeren Einstrom der Atlantischen Wassermassen nach Norden bis in die Arktis verhindert haben könnten.

Das Maximum warmgemäßiger Dinoflagellatenzysten der Art *S. mirabilis* s.l. zwischen ~117.5 und 116.5 ka verdeutlicht, dass stärker ausgeprägte, vollständig marine interglaziale Bedingungen im nordöstlichen Europäischen Nordmeer nur spät im letzten Interglazial existierten. Der Zeitpunkt des Optimums stimmt mit den Ergebnissen der planktischen Foraminiferenanalyse überein und verdeutlicht den Unterschied zum frühen holozänen Klimaoptimum. Die Werte der stabilen Sauerstoffisotope der planktischen Foraminiferen im MIS 5e-Optimum sind im Durchschnitt mit denen des Holozäns vergleichbar; sie sind allerdings etwa 0.3‰ höher als jene im frühen letzten Interglazial. Diese höheren $d^{18}\text{O}$ -Werte reflektieren daher keine optimalen interglazialen Verhältnisse, bestätigen jedoch die Existenz unterschiedlicher Schichtungen an der Meeresoberfläche, was mit den Ergebnissen der Dinoflagellatenzyste übereinstimmt.

Der stärker nordwärts gerichtete Wärmestrom im späten MIS 5e führte zur Ausbildung interglazialer Bedingungen in der südlichen Framstraße. Gleichzeitig verstärkte sich der nach Süden gerichtete Ostgrönlandstrom. Kaltes Wasser und Meereis wurden in der Folge in das Gebiet des östlichen Island-Plateaus transportiert; hier bildete sich daher in den obersten Wasserschichten kein spätes MIS 5e-Optimum aus.

Die Arbeit veranschaulicht auch, dass Klimaereignisse durch verschiedene fossile Gruppen in speziellen ökologischen Lebensräumen unterschiedlich dargestellt werden können. Dies betont den Vorteil einer detaillierten paläozeanographischen Rekonstruktion mit Hilfe verschiedener, miteinander kombinierter Indikatoren. Weiterhin verdeutlicht der verstärkte und verlängerte Einfluss der Saale-Schmelzwässer auf die weitere Entwicklung des letzten interglazialen Klimas, dass MIS 5e nicht einfach als Analog für das Holozän – allein basierend auf den Einfluss der Sonneneinstrahlung - angesehen werden kann.

Acknowledgements

There are a number of people I would like to thank sincerely for their help in completing this work and their assistance during the past 3 years.

- Prof. Dr. Wolf-Christian Dullo, for the support and encouragements, and the supervision of this work;
- Dr. Henning Bauch, for all the help and support, numerous scientific advice and discussions, all of which helped me to get more insight in the research topic and develop my approach strategy. For his patience when the dinocysts once again didn't feel like cooperating in keeping with the pace of the foraminiferal data production. For his successful assistance in the submission of several proposals. But also for being more than just a supervisor: for instance a reliable team-mate, or challenging opponent during our "Hebbelkicks", the deadly striker he is (or was, at least for one year...). For the enjoyable "Bivalve-parties" and the nice game of snooker (finally!!). For the many interesting history-and-other lessons during coffee- and lunch break – so many, I unfortunately already forgot more than half of them. For giving me the opportunity to join in on a field expedition to northern Russia. And for the many other things impossible to all list here;
- Dr. Jens Matthiessen, for his help in getting me acquainted with the dinocyst taxonomy and providing me with useful literature and his raw data and slides from the Holocene of core M23071, and for his time and help – both via email and in "real-time" – in the determination of "unusual" morphotypes and other strange palynomorphs appearing in my slides;
- Prof. Dr. Jörn Thiede and Dr. Nils Andersen, for supporting the project;
- Prof. Dr. Priska Schäfer, for the help during the final phases of this thesis;
- Dr. Anne de Vernal, Dr. Taoufik Radi, and Maryse Henry, for their hospitality at GEOTOP, Montréal, and their help with the transfer function analysis of my data;
- Dr. Frédérique Eynaud and Dr. Antje Voelker, for providing some of their data;
- Dr. Brian Haley, for improving the English of my manuscripts, and for the occasional times we had a beer (which were way too few – the occasions, I mean);
- Dr. Robert Spielhagen, for the final proofreading and suggestions, and for all useful comments and help during the past years. For giving me the opportunity to join in on a scientific cruise to the Fram Strait. But also for creating the cosy Christmas-atmosphere in the "Gerüchteküche", for all the fun during our "Hebbelkicks", his elaborations on the history of German football, and his expert-view on nearly anything related to football;
- Dr. Heidemarie Kassens, for her help, support and encouragements;

- Dr. Evgenya Kandiano, for all her help, for providing me her foraminiferal data, and for being a fine colleague to work with;
- All the other colleagues from research group FB1, for the nice working environment;
- Angelika Finke, for allowing me to lend some key literature for a really long time;
- Maren Dalock and her colleagues from the administration, for all the help with administrative issues.
- Steffanie Kraft, for her help in the palynological preparation of the samples;
- Irina Polovodova, for her advice during the final stages of this work;
- Asmus Petersen, for an excellent job on making the sieve-tubes;
- Lulzim Haxhijaj, for freeze-drying the samples and isotope analyses, and Dr. Helmut Erlenkeuser and his team from the Leibniz Laboratory for the isotope analyses;
- Dipl. Ing. Torben “wo`s Klagge!?” Klagge, for his technical support, being able to solve really every single computer-related problem and many other dire situations. Without his help, I would have needed another three years to finish;
- Karen Volkmann-Lark, for the secretarial and technical assistance, and useful advice on many other issues;
- Kirstin Werner, for her support during the final phases of this thesis, all her help otherwise, and just because;
- All the colleagues from the “Kaffeerunde” (Robert S., Heidi K., Henning B., Karen V.-L., Dorothea B., Thomas M.-L., Kirstin W., Zhenja K., Nadja K., Matthias G., Ortrud R., Carolyn W., Jens H., Igor D., Torben K., Katharina G.), for the highly pleasant working atmosphere in Gebäude 4;
- Kenneth “Dê’euh” Mertens, Stijn “Postdoctor Love aka Dê’euh-Euh-OokDê’euh” De Schepper, and Dr. Stephen Louwye, for their hospitality in Gent and Bremen, their interesting and useful scientific input, and for the great times we had on conferences and other occasions;
- The “listed sexy palynologists”, vixens Sofia Ribeiro and Anna Pienkowski, for the great fun during dinocyst conferences;
- All my other friends I did not mention yet (Thomas, “Vjeetn”, Jelle, Katrien, Maarten A., Pieter V., Pieter D., “Jo & Bench’n”, Katarina & Alexei, Anke D., Kenny, Broos). The reasons are obvious;
- And finally, but foremost, my family: my dear mother Marijke, my sister Davina, “oma” Georgette, and “Nonkel Wim & Tante Riet & co”, for all their loving support, both moral and logistic, for their patience and understanding, and for providing me from time to time with some delicious Belgian specialties.

Thanks a lot!

This project was made possible thanks to funding from the Deutsche Forschungsgemeinschaft (DFG Project BA1367/6).

Table of contents

Summary/Zusammenfassung	I
Acknowledgements	V
Introduction	1
Chapter I – Preface: Background information on the research area, topic and methods; State of the art	3
1.1 Modern surface circulation in the Nordic seas	3
1.2 The Nordic seas and the last interglacial: state of the art	5
1.2.1 The “Last Interglacial”	5
1.2.2 State of the art	5
1.2.2.1 Intensity and timing of the MIS 5e optimum	6
1.2.2.2 Stability of the MIS 5e climate	6
1.2.2.3 Previous MIS 5e dinocyst studies in the northern North Atlantic	6
1.3 Dinoflagellates and their cysts: ecology, modern distribution, and palaeoceanographic tool	7
1.3.1 Modern dinocyst species distribution	9
1.3.2 Dinocyst assemblages: being aware of the bias	14
1.3.3 Preparation method	15
1.3.4 Quantitative reconstructions: transfer functions	16
Chapter II – Vøring Plateau (Norwegian Sea): Cores M23071 and M23323	17
2.1 Core location and lithology	17
2.2 Core stratigraphy	17
2.3 Age model	20
2.4 Results	20
2.4.1 Proxy-based division of the last interglacial sediment sections	20
2.4.2 Core-top samples	23
2.4.3 Transfer function analysis	26
2.4.4 Planktic foraminifera	27
2.5 Discussion	29
2.5.1 Evolution of the last interglacial climate at the Vøring Plateau	29
2.5.1.1 Latest Termination II (Zone 1)	29
2.5.1.2 Early Last Interglacial (Zone 2)	31
2.5.1.3 Late Last Interglacial (Zone 3)	32
2.5.1.4 Transition towards MIS 5d (Zone 4)	33

2.5.2 Specific palaeoceanographic features of MIS 5e at the Vøring Plateau	35
2.5.2.1 <i>Bitectatodinium tepikiense</i> and the stratification signal	35
2.5.2.2 <i>Spiniferites mirabilis</i> s.l. and the late MIS 5e optimum	36
2.6 Conclusions	40
 Chapter III – Southeastern Fram Strait: Core M23455	 42
3.1 Core location and lithology	42
3.2 Core stratigraphy	42
3.3 Results	43
3.3.1 Qualitative results	43
3.3.2 Transfer function analysis	46
3.4 Discussion	46
3.4.1 The last interglacial optimum in the southeastern Fram Strait	47
3.4.2 Transition to stadial conditions	49
3.5 Conclusions	50
 Chapter IV – Eastern Iceland Plateau (Norwegian Sea): Core MD992277	 52
4.1 Core location and lithology	52
4.2 Core stratigraphy and age model	52
4.3 Results	53
4.3.1 Qualitative results	53
4.3.2 Transfer function analysis	57
4.4 Discussion	58
4.4.1 Latest Termination II (Zone 1)	58
4.4.2 Early last interglacial (Zone 2)	59
4.4.3 Late last interglacial and MIS 5e/5d transition (Zone 3 and 4)	61
4.5 Conclusions	63
 Conclusions	 65
 References	 68
 List of Appendixes	
 Curriculum Vitae	

INTRODUCTION

In the context of present global warming, it is important to understand the dynamics of a warm climate in order to assess possible scenarios for future climate development. The Nordic (Norwegian, Greenland and Iceland) seas is in this respect an essential region to study, since the area and its surface circulation (see **PARAGRAPH 1.1**) plays a key role in climate regulation: as warm surface water moves north via the Gulf Stream/North Atlantic Drift system and flows into the Nordic seas, it cools, becomes denser and sinks to form North Atlantic Deep Water. Continuous formation and outflow of this dense deep water is largely responsible for triggering and sustaining the Meridional Overturning Circulation (MOC), through which the equatorial warmth is distributed polewards. It is believed that disturbances of this system, for instance by a sizeable freshwater input, may cause the climate to shift into different modes (e.g. Rahmstorf, 1995; Marotzke, 2000; Ganopolski & Rahmstorf, 2001; Clark et al., 2002).

The last interglacial, or Marine Isotope Stage (MIS) 5e, is an interesting time interval in the search for analogues for Holocene and future climate development. Both the Holocene and MIS 5e evolved alike in terms of orbital configuration, but it is believed that generally warmer temperatures existed at temperate latitudes during MIS 5e. However, as shown by the state of the art under **PARAGRAPH 1.2**, some controversies exist concerning the climatic development of MIS 5e in the Nordic seas, both with respect to the Holocene, as to MIS 5e itself.

Until now, past sea surface and climate reconstructions at high-northern latitudes have traditionally been done using planktic foraminifera, either directly (assemblage composition changes) or indirectly (isotope analysis). Although planktic foraminifera are undoubtedly a powerful oceanographic tool, they can suffer from low species diversity and carbonate dissolution in the cold (sub-)Arctic waters. Dinoflagellate cysts, the organic remains of specific algae, have the potential to provide a good alternative there. The cysts are highly resistant and therefore mostly preserve well, while assemblages are fairly diverse, even at high latitudes. An overview of the ecology, modern distribution and the use of dinoflagellates and their cysts as palaeoceanographic tool is given under **PARAGRAPH 1.3**. Nonetheless, dinoflagellate cysts have practically never been used for reconstructing last interglacial surface water conditions in the Nordic seas before.

The aim of this study was thus to make sea surface reconstructions with a high temporal resolution for the last interglacial interval in the Nordic seas by using dinoflagellate cyst

assemblages, in order to get more insight into the surface circulation during MIS 5e. More concrete, this involves qualitative and quantitative analysis of the dinoflagellate cyst records and comparison with other data, to trace changes in the intensity and the physical properties (temperature, salinity) of the inflowing water masses, as well as their distribution across the Nordic seas as MIS 5e evolved. One specific aspect was to evaluate how meltwater input from the Saalian deglaciation affected the structure of the upper water column and thus the interglacial surface circulation in the Nordic seas during early MIS 5e, as it is believed that meltwater input might have been more influential due to the larger size of the Saalian ice sheet with respect to the Last Glacial Maximum (Svendsen et al., 2004).

To achieve the goals set for the project, sediment cores were selected from three key locations in the Nordic seas. The first study area is located at the Vøring Plateau in the eastern Norwegian Sea, and is dealt with in **CHAPTER II**. The site directly underlies the present pathway of warm Atlantic water as it moves north and is thus well located to trace changes in the intensity and physical parameters of these water masses as they enter the Nordic seas. The second study area, discussed in **CHAPTER III**, is situated further north along the pathway of the Atlantic water flow, off Svalbard in the southeastern reach of the Fram Strait. Given its location, the site is most prone to be influenced by deglacial processes, and is thus ideally located to evaluate the effects of meltwater input, as well as the northward extent of warm water masses throughout MIS 5e. The final study area is located in the western Norwegian Sea, at the eastern margin of the Iceland Plateau. This site underlies the present position of the Arctic front, where pulses of cold Arctic water masses can mix with warmer waters deriving from the North Atlantic. Sediments at the site are thus likely to register fluctuations in the westward protrusion of Atlantic water masses across the Nordic seas, away from the main flow direction. The results from the study at the eastern Iceland Plateau are presented in **CHAPTER IV**.

Preface

Background information on the research area, topic and methods

State of the art

1.1 Modern surface circulation in the Nordic seas

The modern surface circulation in the Nordic seas is dominated by two main, longitudinally orientated currents, the Norwegian Current in the east, and the East Greenland Current in the west (Fig. 1.1). Due to this configuration of the main current axes, both a distinct S-N and a strong E-W sea surface temperature gradient presently exist in the Nordic seas. An extensive synthesis on the different currents and water masses in the Nordic seas was made by Hopkins (1991). The most relevant surface currents and water masses constituting the general surface circulation pattern in the Nordic seas will be shortly discussed below.

The eastern axis consists of warm and saline water masses originating from the North Atlantic Drift (NAD), the northern continuation of the Gulf Stream system. A minor portion of the NAD branches westward at $\pm 50^{\circ}\text{N}$ towards Iceland and rounds the western part of the island clockwise as the Irminger Current (IC). The main mass of the NAD enters the Nordic seas across the Iceland-Faroe ridge. These water masses continue further north through the Norwegian Sea as the Norwegian Current (NC), eventually entering the Eurasian Basin of the Arctic Ocean through Fram Strait as the West Spitsbergen Current (WSC), and across the Barents Sea as the North Cape Current (NthCC). The NC can be influenced by the fresher waters from the Norwegian Coastal Current (NCC) to the east, a northward flowing marginal current originating from the Baltic Sea. The area influenced by the Atlantic water masses is called the Atlantic Domain (AD).

As the warm Atlantic water masses move north, they cool, become denser and eventually sink to form North Atlantic Deep Water. Continuous formation and outflow of this dense deep water is largely responsible for triggering and sustaining the Meridional Overturning Circulation (MOC), through which the equatorial warmth is distributed polewards. Together with the Labrador Sea, the Norwegian Sea is the main area of deepwater formation in the northern hemisphere, underlining the relevance of the region for palaeoclimate studies.

The inflow of Atlantic water into the Arctic Ocean is counterbalanced by a southward surface outflow of cold and low-salinity water, the East Greenland Current (EGC). The EGC

leaves the Nordic seas through Denmark Strait and delineates the Polar Domain (PD). The EGC is responsible for the cold conditions in the Greenland Sea and along the east coast of Greenland, and drives the deep-water ventilation in the Labrador Sea.

In between the AD and the PD lies the Arctic Domain (ArD), an area made up of mixed water masses bordered by the Arctic front in the east, and by the Polar front in the west. North of Jan Mayen, these water masses basically result from the mixing of branches splitting off westward from the NC with branches deflecting eastward off the EGC. North of Iceland, eastward deflecting waters from the EGC mix with the IC. This new combination of water masses then flows along the northeastern coast of Iceland as the East Iceland Current (EIC), recirculating these mixed waters across the Iceland Plateau in a counter clockwise running gyre system.

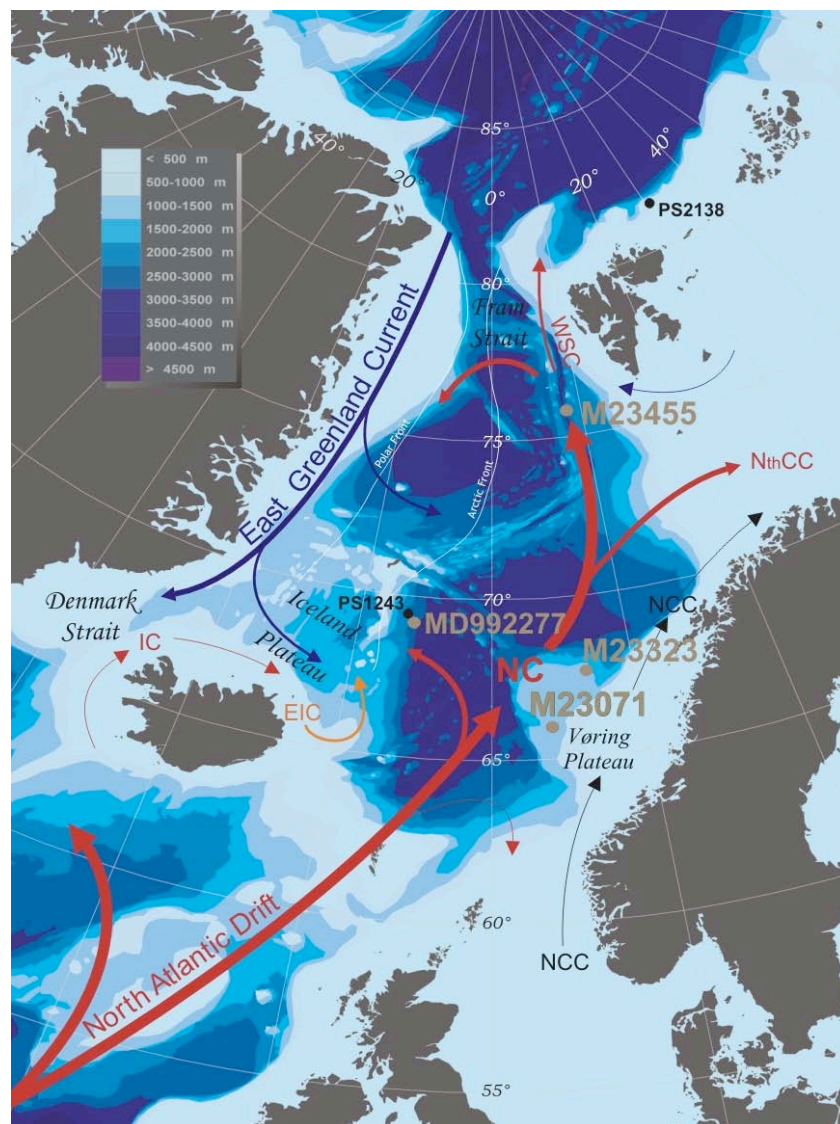


Fig. 1.1: Core locations and modern surface circulation in the Nordic seas. The cores investigated here are shown in grey, black dots show the position of important reference cores for this study. Red arrows represent warm surface currents; blue arrows represent cold surface currents; the orange arrow shows the mixed East Iceland Current (EIC); the black arrow shows the Norwegian Coastal Current (NCC). Other abbreviations: IC, Irminger Current; NC, Norwegian Current; NthCC, North Cape Current; WSC, West Spitsbergen Current.

1.2 The Nordic seas and the last interglacial: state of the art

1.2.1 The “Last Interglacial”

In marine sediment sections, the last interglacial is usually referred to as Marine Isotope (sub-) Stage 5e, or MIS 5e, following the subdivision of Quaternary marine sediments on the basis of stable oxygen isotopes derived from foraminiferal shells (Emiliani, 1955; Shackleton & Opdyke, 1973). Stratigraphical exercises have shown that MIS 5e roughly correlates with the terrestrial Eemian stage (e.g. Shackleton, 1969; Mangerud et al., 1979; Mangerud, 1989). The absolute timing of the onset and the duration of the last interglacial is a topic of debate, due to a scarcity of radiometric datings, difficulties in correlating pollen records across Europe and tying them to the marine isotopic stratigraphy, and uncertainties concerning the synchronicity of interglacial climate development between land and the marine realm (e.g. Sánchez-Goñi et al., 1999; Shackleton et al., 2003). Nonetheless, the onset of the last interglacial is generally believed to be at around 131 to 125 ka for temperate European latitudes (e.g. Shackleton et al., 2003; Beets et al., 2006; Brauer et al., 2007), with interglacial conditions ending at around 116 ka (e.g. Stirling et al., 1998). Determining the timing of the onset is somewhat more complicated for the high latitudes, as it has been shown that a substantial part of high-northern marine sediment sections commonly assigned to MIS 5e on the basis of oxygen isotope chronology belongs stratigraphically to the deglacial phase of the preceding glaciation MIS 6, or the Saalian (Bauch et al., 1996). Highest global sea levels during MIS 5e were on average 4-6 m above the modern sea level 5e (e.g. Chen et al., 1991; McCulloch & Esat, 2000; Thompson & Goldstein, 2005).

1.2.2 State of the art

Many palaeoceanographic studies have focussed on the last interglacial over the past few decades, as MIS 5e is believed to have the potential of providing analogues for Holocene and future climate development. Both the Holocene and MIS 5e evolved alike in terms of orbital configuration (Berger, 1978), and pioneer studies on North Atlantic marine sediments revealed that temperatures during MIS 5e reached similar levels under a comparable ocean circulation regime with respect to the Holocene (e.g. Ruddiman & McIntyre, 1976; Kellogg, 1980; CLIMAP, 1984; Ruddiman et al., 1986). More recent investigations, however, have denoted some considerable differences between both warm periods, revealing two main topics which currently dominate the discussions relating to the last interglacial: the general surface circulation pattern during MIS 5e in the Nordic seas with its feedback on the intensity and timing of the interglacial optimum; and the stability of MIS 5e.

1.2.2.1 Intensity and timing of the MIS 5e optimum

In accordance with the timing of the summer irradiance maxima (Berger, 1978), terrestrial and marine data revealed an early interglacial optimum for both the Holocene (e.g., Koç et al., 1993; Bauch et al., 2001; Calvo et al., 2002; Andersen et al., 2004; Bauch & Erlenkeuser, 2008) and MIS 5e (e.g. Cheddadi et al., 1998; Sánchez-Goñi et al., 1999; Rioual et al., 2001; Rousseau et al., 2006; Bauch & Kandiano, 2007) for Western Europe and the temperate North Atlantic domain, but temperatures were approximately 2°C higher during MIS 5e (e.g. Guiot et al., 1993; Klotz et al., 2003, Kandiano & Bauch, 2003; Kandiano et al., 2004). The general view of a warmer MIS 5e proves to be more complex for the high northern latitudes, as different studies provide apparently contrasting scenarios for the intensity and northward extent of interglacial warmth in the (sub-) Arctic: whereas some suggested a more intense northward heat transport for MIS 5e with respect to the Holocene (e.g. Matthiessen & Knies, 2001; Funder et al., 2002; Grøsfjeld et al., 2006), others have proposed a reduction of the northward heat flow due to a dominantly zonal type of surface circulation during MIS 5e (Bauch et al., 1999; Knudsen et al., 2002). This topic is discussed extensively in CHAPTER II, and addressed in CHAPTER III and IV.

1.2.2.2 Stability of the MIS 5e climate

Another point of discussion is the stability of the last interglacial climate. Arguments have been put forward for one or several cooling events within MIS 5e (Field et al., 1994; Fronval & Jansen, 1996; Maslin et al., 1996; Lehman et al., 2002), possibly accompanied from changes in MOC (Adkins et al., 1997; Oppo et al., 2001). Others have suggested that MIS 5e involves just one, prolonged period of warm conditions (e.g. Kukla et al., 1997, 2002; McManus et al., 2002) with a relatively stable mode of overturning circulation (McManus et al., 1994; Oppo et al., 1997; Chapman & Shackleton, 1999). Unfortunately, the Greenland ice-core records (NGRIP, GRIP, GISP2) cannot clarify this issue, as they either do not cover the full length of the last interglacial (only what seems to be the glacial inception towards 5d) or are disturbed in the last interglacial interval (e.g. Grootes et al., 1993; Fuchs & Leuenberger, 1996; Chappellaz et al., 1997; Landais et al., 2004; NGRIP members, 2004). Although an in depth assessment of MIS 5e climatic variability is not the main goal of the research presented here, the topic is an inherent feature of palaeoclimate proxy records and thus automatically incorporated in the discussions below.

1.2.2.3 Previous MIS 5e dinocyst studies in the northern North Atlantic

So far, reconstructions of past surface water conditions at high-northern latitudes were mainly based on planktic foraminiferal assemblage and stable isotope studies. Although

being a powerful palaeoceanographic tool, foraminifer-based reconstructions in cold regions such as the Nordic seas have their limitations: planktic assemblages usually show a low interglacial species diversity (Bauch, 1997), with one species (*Neogloboquadrina pachyderma* sinistral (s)) sometimes constituting over 90% of the total assemblage in colder regions, while their carbonate composition makes foraminiferal shells susceptible to dissolution. Due to a higher diversity and preservational potential, dinocysts provide a good alternative for palaeoenvironmental studies, and have been used for a number of detailed MIS 5e surface water reconstructions in regions surrounding the Nordic seas: the Baltic/North Sea (Eriksson et al., 1999; Van Leeuwen et al., 2000; Head et al., 2005; Head, 2007); off Western Europe (Sánchez-Goñi et al., 1999, 2000; Eynaud, 1999; Eynaud et al., 2000; Penaud et al., 2008); Norwegian fjords (Dale, 1996); the White Sea region (Grøsfjeld et al., 2006); the Arctic Ocean margin (Matthiesen & Knies, 2001; Matthiessen et al., 2001); and south of Iceland (Eynaud et al., 2004). However, despite the importance of the Nordic seas in terms of climate dynamics, the palaeoceanographical potential of dinocyst assemblages has rarely been applied to last interglacial sections from this region. The work presented here is thus the first to provide detailed MIS 5e dinocyst records from the Nordic seas.

1.3 Dinoflagellates and their cysts: ecology, modern distribution, and palaeoceanographic tool

Dinoflagellates are eukaryotic flagellated algae that formerly belonged to the kingdom Protista (e.g. Fensome et al., 1993) but are now assigned to the kingdom Chromalveolata (Adl et al., 2005). Together with coccolithophorids and diatoms, they constitute a major part of the marine primary productivity, but also occur in fresh water environments (e.g. Pollinger, 1979), and even within sea ice (see review by Matthiessen et al., 2005). Many dinoflagellates are phototrophic and thus obligatorily live within the photic zone, but numerous species have a heterotrophic, mixotrophic, parasitic, or other more complex nutritional and survival strategy (e.g. Gaines & Elbrächter, 1987; Schnepf & Elbrächter, 1992; Smayda & Reynolds, 2003).

The main vegetative stage of dinoflagellates consists of a motile, haploid thecate cell, during which reproduction occurs asexually through binary fission. The vegetative cell is made out of cellulose, a substance that is easily destroyed by bacterial activity and therefore usually is not preserved within the sediments. During the complex life cycle, sexual reproduction can occur, probably triggered by environmental stress. The sexual reproduction process is very diverse among dinoflagellates, but usually involves the fusion of gametes produced by the vegetative cells. In some dinoflagellate species, a non-motile

protective resting cyst or hypnozygote is then formed (Fig. 1.2). This cyst consists of a very resistant, sporopollenine-like organic compound (Fensome et al., 1993; Head, 1996; Versteegh & Blokker, 2004), and it is this resting cyst that is preserved in the sediments. After a variable but obligatory dormancy period, the dinoflagellate leaves the resting cyst or “germinates” through an opening called the archeopyle, and resumes its motile stage as haploid vegetative cell (Evitt, 1985; Pfister & Anderson, 1987; Fensome et al., 1993). Depending on the species, germination usually occurs between late winter and spring, presumably triggered by ameliorating environmental conditions. The formation of a hypnozygote thus appears to be a survival strategy to get through winter, but can also act as a quick response to environmental stress, or as a seed bank for new dinoflagellate populations (Dale, 1983).

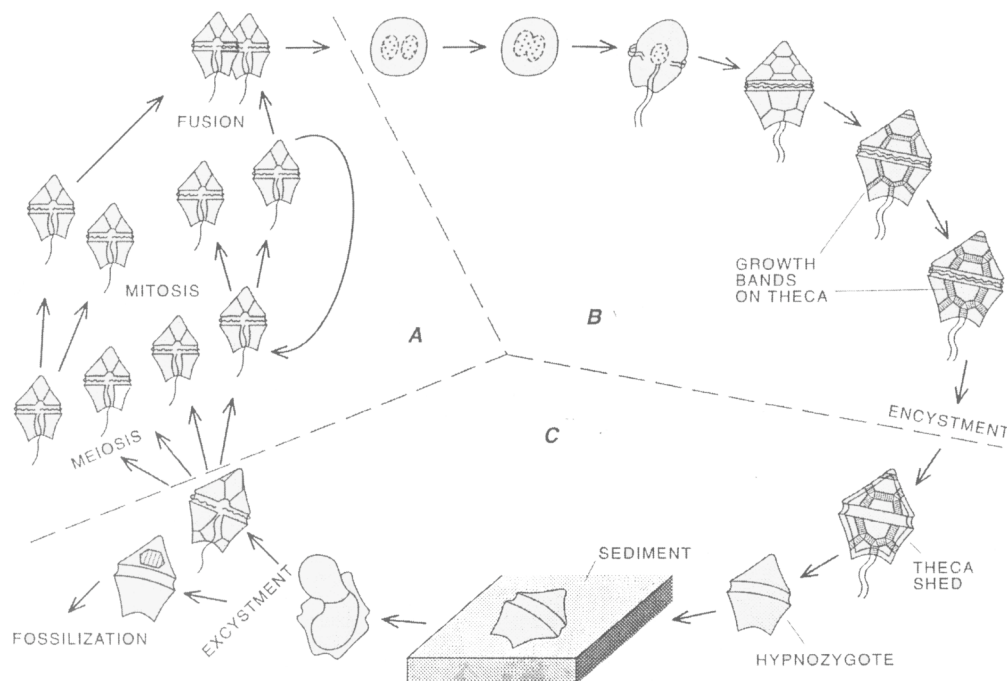


Fig. 1.2: Idealized dinoflagellate life cycle involving sexual reproduction and cyst formation. (A) Cells in this segment are motile and haploid (B) Cells in this segment are motile and diploid (nucleus dotted) (C) Cells in this segment are nonmotile (except for the excysted cell shown in the left) and diploid. Hachured area in the discarded cyst at the bottom left represents the archeopyle (from Fensome et al., 1996).

The hypnozygote, in palaeontological studies normally referred to as “dinoflagellate cyst” or “dinocyst”, is characterised by a tabulation pattern, which may or may not reflect the arrangement of the thecal plates. The presence of a tabulation pattern is the determining feature separating dinocysts from other palynomorphs such as acritarchs, and can be expressed in various ways through different types of ornamentation (ridges along plate boundaries, position of spines or processes, etc) or the shape of the archeopyle (Evitt, 1985).

1.3.1 Modern dinocyst species distribution

A number of extensive surface sediment studies has established the relationship between dinoflagellate cyst assemblage distribution and upper water mass properties in the Nordic seas and adjacent areas (Fig. 1.3) (e.g., Matthiessen, 1995; Rochon et al., 1999; de Vernal et al., 2001, 2005; Marret et al., 2004). Consequently, changes of dinocyst assemblages within and over glacial-interglacial times can be used to evaluate past changes in upper ocean properties; in particular, sea surface temperature (SST) and salinity (SSS), and nutrient availability (Dale, 1996). As reference for a better understanding of the following chapters, an overview of the distribution of the most common cyst species in relation to sea surface conditions is provided alphabetically below. Additional information about the grouping of certain taxa and morphotypes is also given. The taxonomical nomenclature used here conforms to Head (1996), Rochon et al. (1999), Head et al. (2001, 2006) and Fensome & Williams (2004). All dinocyst species recovered are listed author-named in Table 1.1.

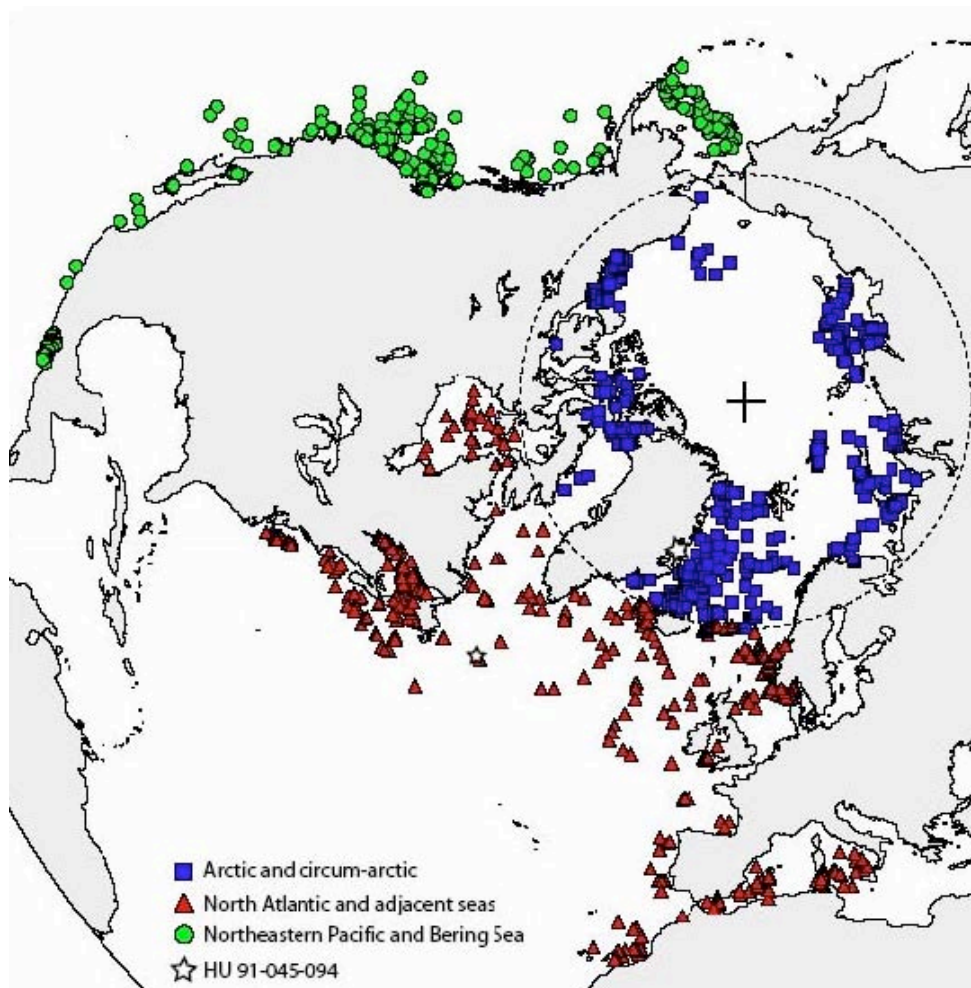


Fig. 1.3: Locations of the core-top samples included in the 'n=1171' reference dinocyst database for which the relation between assemblage composition and sea surface parameters has been established. This 'n=1171' dataset is used in the transfer function reconstructions (from Radi & de Vernal, 2008).

Ataxiodinium choane (Plate 2)

Ataxiodinium choane is a cold to (sub-) tropical, coastal to open oceanic species with tolerance to lower salinities (Brenner, 2005) and a preference for eutrophic conditions. The species usually occurs in core-top samples from the North Atlantic/Nordic Seas in low numbers only (Rochon et al., 1999; Marret and Zonneveld, 2003).

Bitectatodinium tepikiense (Plate 8)

Bitectatodinium tepikiense has a present-day distribution that is closely related to the transitional zone between the subpolar and temperate zones in the Norwegian Sea (Dale, 1996). Higher abundances of *B. tepikiense* can indicate seasonally strong fluctuations, with very cold winters (mean temperature as low as 0°C) and warm summers (15°C and more) (Marret and Zonneveld, 2003). Combined with the fact that it can tolerate salinities down to 30, *B. tepikiense* can be an indicator of seasonally stratified surface water masses, as illustrated by its high present-day occurrence at the mouth of the Gulf of St. Lawrence and other embayments (Rochon et al., 1999).

Brigantedinium spp. (Plate 9)

Brigantedinium spp. comprises *B. simplex*, *B. cariacense*, and spineless round brown cysts that cannot be determined on species level because of bad preservation or unfavourable orientation. As *Brigantedinium* spp. includes several species, the taxon is distributed under a wide range of temperatures, salinities and sea ice conditions (de Vernal et al., 2001). High portions of *B. simplex* are indicative for colder conditions (Matthiessen, 1995). *Brigantedinium* cysts are produced by heterotrophic dinoflagellates and their occurrence is therefore largely dependent on the availability of food, such as diatoms (e.g. Gaines & Elbrächter, 1987). They can effectively cope with prolonged periods of sea ice cover, and are particularly abundant in regions of high productivity, such as upwelling areas (e.g. Wall et al., 1977) or at sea ice margins (Mudie & Short, 1985).

Impagidinium pallidum (Plate 3)

Impagidinium pallidum has its present-day highest occurrence in the Iceland and Greenland Seas (Matthiessen, 1995; Rochon et al., 1999; Marret et al., 2004). It shows a strong relation with sea ice cover (de Vernal et al., 2001). *Impagidinium pallidum* is thus regarded as a polar oceanic species.

Impagidinium spp. (Plate 3)

Impagidinium spp. comprises all *Impagidinium* specimens that cannot be determined to any degree of certainty at the species level – however certainly excluding *I. pallidum*, since this species can easily be recognised by its characteristic pale appearance – and the temperate-subtropical set of *Impagidinium* species (*I. aculeatum*, *I. paradoxum*, *I. patulum*, *I. sphaericum*, *I. striatum*; Matthiessen, 1995). Of all species grouped under *Impagidinium* spp., *I. sphaericum* has at present the northernmost extent, albeit only occurring beyond 65°N in association with the warm water penetration of the NAD (Matthiessen, 1995; Rochon et al., 1999). It is also the only species from the *Impagidinium* group that does not show an oligotrophic behaviour (Devillers & de Vernal, 2000).

Lingulodinium machaerophorum (Plate 4)

Lingulodinium machaerophorum is a neritic, temperate to tropical species that at present has its highest abundances in the eastern North Atlantic in the Strait of Gibraltar and further north along the western Iberian coastline and the Bay of Biscay up to the southwestern Swedish and Norwegian coast (Rochon et al., 1999; Persson et al., 2000; Marret & Zonneveld, 2003). The species is distributed within a very broad salinity range and has been recorded from brackish to fully marine environments, but is most abundant in areas with sea surface salinity above 36. According to Lewis & Hallett (1997), summer temperature is the controlling factor in the occurrence of *L. machaerophorum*, and the species has rarely been recorded from areas with summer SST below 10°C (see refs. in Marret & Zonneveld, 2003). Additionally, blooms of *L. polyedrum*, i.e. the motile stage of *L. machaerophorum*, can occur during periods when a warm, nutrient-rich and well-stratified upper water column with little or no turbulence exists (see refs. in Marret & Zonneveld, 2003). Although turbulence can be a limiting factor for the growth rate of *L. polyedrum* (Blanco, 1995), it does not prevent the species from being present in mixed, turbulent water masses (e.g. Marret & Scourse, 2002).

Nematosphaeropsis labyrinthus (Plate 1)

The present maximum occurrences of the subpolar-temperate species *Nematosphaeropsis labyrinthus* are situated in the ArD and south of Greenland, where cold water from the EGC and Labrador Current, respectively, mix with warm Atlantic water brought in by the IC (Rochon et al., 1999; Marret et al., 2004). Although *N. labyrinthus* (-like) cysts have been found in sediments from brackish environments (Pospelova et al., 2004), the species is considered to represent fully marine conditions. A positive correlation of *N. labyrinthus* with February nutrient content was shown by Devillers & de Vernal (2000).

Operculodinium centrocarpum (Plate 1)

Operculodinium centrocarpum is a cosmopolitan species that tolerates a wide range of temperature and salinity (Dale, 1996; Rochon et al., 1999; de Vernal et al., 2001), opportunistically able to adapt quickly to changing or unstable environments (Dale, 1996). In the northern North Atlantic and Nordic seas, high concentrations of *O. centrocarpum* appear to be associated with the pathway of the warm, saline NAD (e.g. Harland, 1983; Matthiessen, 1995; Rochon et al., 1999). Morphotypes with variations in ornamentation of the cyst wall and the length and shape of the processes seem to characterise cold and/or less saline environments (Dale, 1996; de Vernal et al., 2001).

Cyst of *Pentapharsodinium dalei* (Plate 4)

Cysts of *Pentapharsodinium dalei* occur in a wide range of temperature and salinity conditions, and can tolerate sustained sea ice cover (de Vernal et al., 1998, 2001), but are only present in large numbers where SSTs are at least 4°C (Rochon et al., 1999). Cysts of *P. dalei* were recovered in higher amounts from Norwegian and western Atlantic fjord systems and embayments (e.g. Dale, 1976) and along the northern margin off Iceland (Marret et al., 2004). Stratified conditions with considerable seasonal temperature gradients therefore seem to favour the occurrence of the species.

Spiniferites elongatus s.l. (Plate 6 & 7)

The species and morphotypes included in the *Spiniferites elongatus* s.l. group as used here vary depending on the study area (cf. Rochon et al., 1999). In the data from the Vøring Plateau (cores M23071 and M23323), the group only includes *S. elongatus* s.s. and *S. cf. elongatus* sensu Harland & Sharp 1986. In the other cores, the group comprises *S. elongatus* s.s. and the sporadically occurring species *S. frigidus* and *Rottnestia ampicavata*. The latter two species, which are characterised by a more pronounced antapical flange and sutural membranes compared to *S. elongatus* s.s., are related to cold, Arctic water masses (e.g. Harland et al., 1980; Harland, 1982). At present, *S. elongatus* s.s. is ubiquitous in the northern North Atlantic, occurring under a wide range of temperatures, salinities and up to a few months of sea ice cover (Rochon et al., 1999; de Vernal et al., 2001), but its distribution pattern on the northern Iceland shelf reveals that the *sensu stricto*-morphotype has stronger affinities with the cold-temperate domain (Marret et al., 2004). In contrast, the *S. cf. elongatus* morphotypes, characterised by a strong reduction of the process tips and antapical flange (Plate 6, pict. 7-12; Plate 7, pict. 1-7), were described by Harland & Sharp (1986) from sediments from the Norwegian Sea and, thus, seem to be related to the warm-temperate domain of the Nordic seas.

Spiniferites lazus (Plate 4)

Spiniferites lazus has only been recovered from surface sediments underlying fully marine coastal areas of Western Europe and is thus a typical Atlantic-water species. It requires high salinities (preferably >34) and its occurrence spans a wide interval of (temperate) temperature conditions (Marret & Zonneveld, 2003).

Spiniferites mirabilis s.l. (Plate 5)

Spiniferites mirabilis s.l. includes *S. mirabilis* and *S. hyperacanthus*, since determination on species level can be hampered by unfavourable orientation. Highest present-day occurrences of this warm-temperate, oceanic to neritic taxon in the North Atlantic are registered in the Bay of Biscay and off the Iberian margin, where relative abundances of greater than 40% can be seen (Rochon et al., 1999; de Vernal et al., 2005). *Spiniferites mirabilis* s.l. is generally absent from areas with summer SSTs below 12°C and salinity below 28.5, and thrives optimally when winter SSTs are between 10 and 15°C and summer SSTs are above 15°C (de Vernal et al., 1998). In the North Atlantic, abundances of *S. mirabilis* s.l. correlate negatively with nutrient content (Devillers & de Vernal, 2000), but the global dataset reveals that the species can also be prominently present in eutrophic environments (Marret & Zonneveld, 2003).

Spiniferites ramosus s.l. (Plate 4 & 5)

In addition to typical *Spiniferites ramosus* cysts, the *S. ramosus* s.l. group also includes cysts of *S. bulloides* and *S. ramosus* (-like) cysts whose processes are exclusively gonal but otherwise not typical for the species. These processes usually are wider, and can have more pronounced flanges in between them or even become fused into “geminal processes” (see Plate 5, pict. 1-3).

Although *S. ramosus* s.l. also occurs in the tropics (Marret & Zonneveld, 2003), it is generally considered to be a temperate to cold taxon, which can occur under a wide range of seasonally strongly fluctuating temperature and salinity conditions, able to tolerate seasonal sea ice cover (de Vernal et al., 1998; Rochon et al., 1999). The significant morphological variation within the *S. ramosus* s.l. group is probably a response to specific ecological conditions.

Table 1.1: Dinocyst species, author-named, recovered from the studied core sections.

<i>Achomosphaera</i> sp. Evitt 1963
<i>Ataxiodinium choane</i> Reid 1974
<i>Bitectatodinium tepikiense</i> Wilson 1973
<i>Brigantedinium cariacense</i> (Wall 1967) Lentin & Williams 1993
<i>Brigantedinium simplex</i> Wall 1965 ex Lentin & Williams 1993
<i>Dubridinium</i> sp. Reid 1977
<i>Impagidinium aculeatum</i> (Wall 1967) Lentin & Williams 1981
<i>Impagidinium pallidum</i> Bujak 1984
<i>Impagidinium paradoxum</i> (Wall 1967) Stover & Evitt 1978
<i>Impagidinium patulum</i> (Wall 1967) Stover & Evitt 1978
<i>Impagidinium sphaericum</i> (Wall 1967) Lentin & Williams 1981
<i>Impagidinium strialatum</i> (Wall 1967) Stover & Evitt 1978
<i>Islandinium minutum</i> (Harland & Reid in Harland et al. 1980) Head et al. 2001
<i>Lejeunecysta</i> spp. (Artzner & Dörhöfer 1978) Lentin & Williams 1976
<i>Lingulodinium machaerophorum</i> (Deflandre & Cookson 1955) Wall 1967
<i>Nematosphaeropsis labyrinthus</i> (Ostenfeld 1903) Reid 1974
<i>Operculodinium centrocarpum</i> sensu Wall and Dale 1966
<i>Operculodinium centrocarpum</i> – <i>Arctic morphotype</i> sensu de Vernal et al. 2001
<i>Operculodinium centrocarpum</i> – <i>cezare morphotype</i> Head 2007
Cyst of <i>Pentapharsodinium dalei</i> Indelicato & Loeblich III 1986
Cyst of <i>Polykrikos kofoidii</i> Chatton 1914
Cyst of <i>Polykrikos schwartzii</i> Bütschli 1873
<i>Pyxidinoopsis reticulata</i> (McMinn & Sun 1994) Marret & de Vernal 1997
<i>Quinquecuspis concreta</i> (Reid 1974) Harland 1977
<i>Rottnestia amphicavata</i> Dobell & Norris in Harland et al. 1980
Cyst of <i>Scrippsiella trifida</i> Lewis 1991
<i>Selenopemphix quanta</i> (Bradford 1975) Matsuoka 1985
<i>Spiniferites belerius</i> Reid 1974
<i>Spiniferites bulloides</i> (Deflandre & Cookson 1955) Sarjeant 1970
<i>Spiniferites</i> cf. <i>elongatus</i> sensu Harland and Sharp 1986
<i>Spiniferites elongatus</i> Reid 1974 <i>sensu lato</i>
<i>Spiniferites frigidus</i> Harland & Reid in Harland et al. 1980
<i>Spiniferites hyperacanthus</i> (Deflandre & Cookson 1955) Cookson & Eisenack 1974
<i>Spiniferites lazus</i> Reid 1974
<i>Spiniferites membranaceus</i> (Rossignol 1964) Sarjeant 1970
<i>Spiniferites mirabilis</i> (Rossignol 1964) Sarjeant 1970
<i>Spiniferites pachydermus</i> (Rossignol 1964) Reid 1974
<i>Spiniferites ramosus</i> (Ehrenberg 1938) Mantell 1854 <i>sensu lato</i>
<i>Spiniferites</i> spp. Mantell 1850
<i>Trinovantedinium applanatum</i> (Bradford 1977) Bujak & Davies 1983
<i>Votadinium spinosum</i> Reid 1977

1.3.2 Dinocyst assemblages: being aware of the bias

Several processes can play an important (biasing) role during the transformation of a living dinoflagellate community into the final fossil dinocyst assemblage, and all of these must be considered during palaeoceanographical interpretation of an assemblage composition as it appears under the microscope.

A first bias comes from the fact that only about 10-15% from the known present dinoflagellates produces fossilizable cysts during their life cycle (e.g. Dale, 1976; Head, 1996). Thus, a fossil assemblage can inherently only provide an estimate for the diversity of the living assemblage from which it originated.

Dinocysts have a sedimentary behaviour comparable to fine silt and can therefore be subject to transport as they sink to the seafloor. However, laboratory experiments indicate that cysts sink relatively rapidly in the water column (e.g. Anderson et al., 1985; Zonneveld & Brummer, 2000), and it is generally believed that transport by currents over long distances has only minor influences. Hence, the environmental conditions of the (quasi) overlying surface water are well reflected by the assemblages in the bottom sediments (see discussions in Marret & Zonneveld, 2003, and Matthiessen et al., 2005). If not completely in situ, the dinocysts can at least give insight into the prevailing currents and their physical parameters that might have brought the cysts into the area where they eventually settled.

Palynomorphs, including dinocysts, in general have a high preservational potential. For organic matter, oxygen is generally the most destructive agent, and it has been shown that well-oxygenated bottom sediments can cause species-selective degradation of dinocysts (see review by Zonneveld et al., 2008). Whereas the cysts of phototrophic gonyaulacoids are moderately sensitive to fairly resistant to oxidation, cysts produced by heterotrophic peridinioids species appear to be very sensitive to the presence of oxygen and are likely to be removed rapidly from the assemblages under well-oxygenated conditions (Kodrans-Nsiah et al., 2008).

An additional bias can come from microbial degradation and species-selective grazing by benthic deposit feeders. These processes, however, appear to be of minor importance for the common fossil cysts, as the benthic grazers seem to prefer naked, non-fossilizable and thus easily degradable cysts (Persson & Rosenberg, 2003).

1.3.3 Preparation method

The samples selected for dinoflagellate cyst analysis were all processed using traditional palynological preparation techniques. In a first step, carbonate was removed from the material by adding 50 to 200 ml (depending on the amount of sediment and the carbonate content of the sample) cold 8-10% hydrochloric acid (HCl) to the weighed, freeze-dried material. During this step, a known number of *Lycopodium clavatum* tablets (Batch nr. 483216, X=18 583 for one tablet, s=±1708) was added as a spike in order to calculate absolute concentrations following the method of Stockmarr (1971). After the chemical reaction had finished, the material was neutralised and washed through a 150 µm and 6 µm polymer mesh to remove all Ca²⁺-ions and the coarse and fine fraction, respectively, before any further chemical treatment. In a second step, ±200 ml cold 40% hydrofluoric acid (HF) was added in order to remove siliciclastic components. The material was left to settle for 5 to 7 days, after which it was neutralised and washed through a 6 µm polymer mesh, and centrifuged in order to concentrate the final residue. Occasionally, fluorosilicates had

formed during HF-treatment. In this case, a second HCl-treatment was done in order to dissolve and remove them again. Finally, the residue was mounted on microscopic slides in glycerine jelly using a pipette, and sealed with paraffin wax. No staining, oxidation or sonication was done. Dinocysts were counted using a Zeiss Axiophot light microscope at 200x, 400x and 1000x (oil immersion) magnification. Relative abundances of species are calculated based on the total sum of species excluding reworked cysts and unidentified taxa, whereas the latter are included for calculating absolute cyst concentrations.

1.3.4 Quantitative reconstructions: transfer functions

A number of statistical methods have been developed for quantitatively reconstructing different sea surface parameters (temperature, salinity, sea ice cover) based on fossil assemblages. These methods have used multiple regression calculations (e.g. Imbrie & Kipp, 1971), modern and revised analogue approaches, and neural network techniques (see overview in Guiot & de Vernal, 2007). For dinocyst assemblages, the best-analogue technique is most frequently used, as it provides the best, i.e. most reliable and realistic results (de Vernal et al., 2001; T. Radi, personal communication). The best-analogue technique has originally been developed by Overpeck et al. (1985) and Guiot (1990) for pollen assemblages, and was adapted for dinocyst assemblages by de Vernal et al. (2001, 2005). This technique involves a logarithmic transformation of the relative abundances (in per mille) of all taxa prior to analysis in order to increase the weight of rare species, which presumably have narrower ecological requirements. The 5 closest analogues are then searched for amongst the modern spectra on the basis of even weighting of the taxa through use of the “R” software package (R Development Core Team, 2007). The modern database currently consists of a total of 1171 surface samples from Arctic, North Atlantic and North Pacific basins (Fig. 1.3; Radi & de Vernal, 2008). The most probable estimate for a specific hydrological parameter is calculated as the average of the 5 closest analogues inversely weighted by their respective distance. If the distance between the fossil assemblage and a modern analogue exceeds a threshold value, inherently determined by the technique, the analogue is rejected. A confidence interval is calculated from the variances in the set of analogues around the most probable estimate. The degree of accuracy of the approach can be assessed by comparing measured modern values with the estimated values reconstructed from the core-top sample.

Vøring Plateau (Norwegian Sea)

Cores M23071 and M23323

The results from core M23071 have been published in:

Van Nieuwenhove et al., 2008

Van Nieuwenhove & Bauch, 2008

Cores M23071 and M23323 were both recovered from the Vøring Plateau in the Norwegian Sea, directly underlying the present pathway of the warm NC (Fig. 1.1). In this way, they are ideally located to trace changes in the intensity and the physical parameters of the inflowing warm Atlantic waters, both throughout the last interglacial and with respect to the late Holocene. In addition, the NAD/NC system oceanographically connects the study site to other MIS 5e dinocyst study areas just outside the Nordic seas (Matthiessen & Knies, 2001; Eynaud et al., 2004).

2.1 Core location and lithology

Core M23071 was retrieved from the southwestern Vøring Plateau (67°05.1'N, 2°54.4'E) at a water depth of 1306 m (Gerlach et al., 1986). Surface waters at site M23071 have at present winter and summer temperatures of 6.3 and 10.6°C, and salinities of 35.2 and 35.0, respectively (Boyer et al., 2006). Core site M23323 is located on the northern Vøring Plateau (67°46'N, 5°55'E), at 1286 m water depth (Hirschleber et al., 1988). The site has at present surface waters with winter and summer temperatures of 6.4 and 10.7°C, and salinities of 35.1 and 34.9, respectively (Boyer et al., 2006).

The interglacial intervals of cores M23071 and M23323 consist mainly of brown-grey clays, silts and sands. The sand fraction is largely composed of foraminiferal shells, a typical feature of late Pleistocene interglacial sediments from the area (Gerlach et al., 1986). High contents of ice rafted debris (IRD) characterise the glacial, deglacial and stadial intervals.

2.2 Core stratigraphy

The stratigraphic subdivision of cores M23071 and M23323 (Fig. 2.1) is based on radiocarbon dates, the identification of discrete tephras with known ages for the younger parts of the core, and stable oxygen isotopes derived from the planktic foraminifer *Neogloboquadrina pachyderma* left-coiling (s) (Vogelsang, 1990; Voelker, 1999; Rumohr &

Bauch, unpublished). A low-resolution downcore oxygen isotope stratigraphy back to Termination II was originally established by Vogelsang (1990) for core M23071, and by Rumohr (unpublished) for core M23323. A high-resolution $\delta^{18}\text{O}$ record was created by Voelker (1999) for the Holocene section of core M23071. For the present study, cores M23071 and M23323 were resampled at 1 cm steps from 577 cm and 720.5 cm depth downwards, respectively, in order to establish a high-resolution stable oxygen isotope record spanning MIS 5e and reaching further down across Termination II into stage 6. Oxygen isotope analyses were carried out using 25-30 specimens (200 μm average size) of the polar species *Neogloboquadrina pachyderma* (s). Stable isotope ratios were measured at the Leibniz Laboratory of Kiel University using the fully automated Kiel Carbonate Preparation Device and a Finnigan MAT 251 mass spectrometer system. The analytical accuracy of this system is ± 0.07 ‰ for $\delta^{18}\text{O}$ and all measurements were calibrated on the Pee Dee Belemnite isotope scale (PDB).

The isotope curves are typical for the Nordic seas, showing a stepwise decrease in $\delta^{18}\text{O}$ from MIS 6 into MIS 5e during Termination II (e.g. Fronval & Jansen, 1997; Bauch et al., 2000a), and having the lowest isotope values seen in the Holocene and last interglacial (e.g. Vogelsang, 1990; Bauch et al., 1999) (Fig. 2.1). The *Pullenia bulloides* horizon and more highly resolved oxygen isotope data from this specific interval (Fig. 8 in Haake et al., 1992; Voelker, 1999) clearly identify the stratigraphic position of substage 5a in core M23071. Oxygen isotope values and the amount of IRD (counted in the >150 μm size-fraction and expressed as grains per gram of dried sediment) confirm the position of MIS 5e below.

It has been shown that a substantial portion of Nordic seas sediments commonly assigned to MIS 5e belongs stratigraphically to the deglacial phase of the Saalian (Vogelsang, 1990, Fronval et al., 1995, Bauch et al., 1996). The combination of high sediment input, via iceberg-rafting of terrestrial material from the Scandinavian mainland (e.g., Baumann et al., 1995; Bauch et al., 1999), and at the same time large freshwater fluxes from melting icebergs, results in extended core sections with low $\delta^{18}\text{O}$ values. Hence, the interval from approximately 710 to 656 cm core depth in core M23071, and from 890 to 850 cm core depth in core M23323 represents the latest phase of Termination II, rather than full-interglacial conditions *sensu stricto* (see Bauch et al., 1996). In contrast, the overlying sections with low oxygen isotope values are characterised by more uniform pelagic sedimentation without significant IRD content up to 625 and 755 cm, respectively (Fig. 2.1). These intervals therefore correspond to the “real”, full-interglacial part of cores M23071 and M23323.

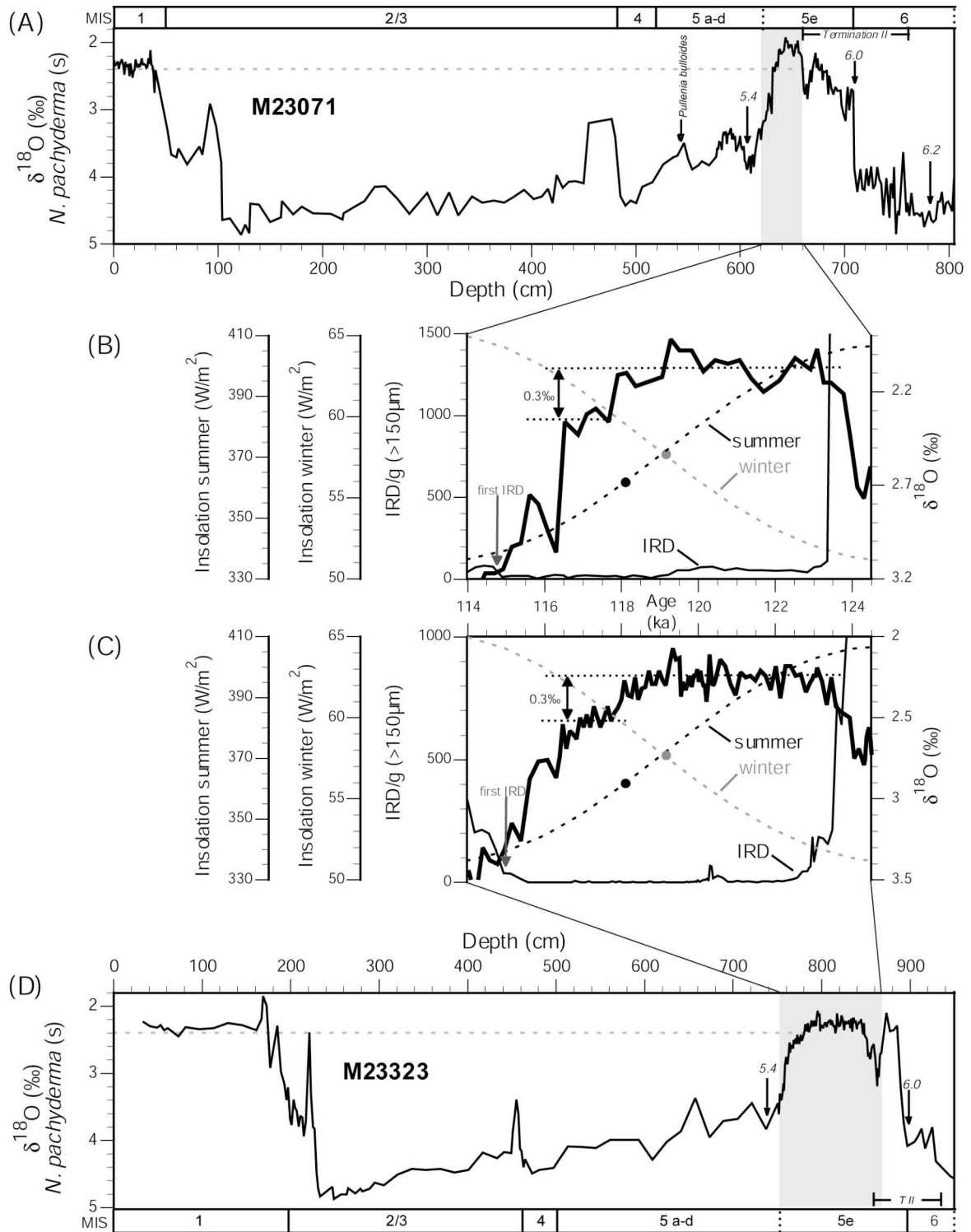


Fig. 2.1: (A) and (D) Planktic foraminifer stable oxygen isotope stratigraphy of core M23071 and M23323, respectively, plotted against depth (data from: Vogelsang, 1990; Voelker, 1999; Rumohr & Bauch, unpublished; LIONS project framework). The dashed grey line indicates the average Holocene $\delta^{18}\text{O}$ value, for comparison with MIS 5e. (B) and (C) Stable oxygen isotopes and ice rafted debris (IRD) content for core M23071 and M23323, respectively, and summer and winter insolation at 65°N [computed with ANALYSERIES 2.0 (Paillard et al., 1996) using the Laskar et al. (2004) data] for the last interglacial interval studied, plotted against age. The dots on the insolation curves represent the present-day values. Note the ca. 0.3 ‰ difference (arrow in between dotted grey lines) between the average value for the largest, first part of MIS 5e and the short plateau from the latest phase, for which fully marine interglacial conditions are interpreted (see main text). The latter value corresponds well with the average Holocene value.

2.3 Age model

The age model for MIS 5e from core M23071 was developed by identifying major SPECMAP events in the $\delta^{18}\text{O}$ record (Martinson et al., 1987) and correlating these marker points to the $\delta^{18}\text{O}$ record of core PS1243 (Fig. 2.2) (Appendix A). The latter core has relatively constant sedimentation rates across MIS 5e and a well-established age model for the last 450 kyr (see Bauch, 1997; Bauch et al., 2000b; Bauch & Erlenkeuser, 2008). The age model of core M23323 (and MD992277; see CHAPTER IV) was then developed by correlating significant features in the $\delta^{18}\text{O}$ record with core M23071 and/or PS1243 (Fig. 2.2) (Appendix A). Our derived age model agrees well with recent findings for the last interglacial sea level maximum (Rohling et al., 2008), i.e. the interval with the lowest oxygen isotope values (Fig. 2.3).

2.4 Results

Due to high cyst abundances in the samples, a statistically significant number of dinocysts could usually be counted at species level. Thus, 500 cysts or more were counted for all samples, except for samples 663 and 650 in core M23071, and samples 852.5 to 868.5 in core M23323. Counting such a high number of cysts per sample assures statistical robustness of the dataset and allows confidently assessing relative abundance changes of low-percentage species. Percentage abundances of each species were calculated based on the total sum of specimens excluding unidentified taxa and reworked specimens (Jurassic To Neogene). The raw palynomorph counts can be found in Appendix B.

Throughout the full-interglacial sections analysed, assemblages are dominated by *O. centrocarpum*, whose cysts usually make up between 50 and 70% of the total number of dinocysts (Fig. 2.4). *Bitectatodinium tepikiense* and *N. labyrinthus* are the subordinate species. *Bitectatodinium tepikiense* has a rather constant relative abundance of $\pm 8\%$ in core M23071, and a more variable and slightly lower relative abundance in core M23323. The species occasionally peaks above 10% in both cores (Fig. 2.4). *Nematosphaeropsis labyrinthus* on average makes up 5% of the assemblages, increasing in relative abundance towards the end of the M23071 interval, but more frequently reaching relative abundances over 10% in core M23323 (Fig. 2.4). *Brigantedinium* spp. also makes up a considerable part of the assemblages in the lower half of both interglacial sections (Fig. 2.4).

2.4.1 Proxy-based division of the last interglacial sediment sections

Considering the overall picture, the assemblage compositions and changes throughout the studied intervals from both cores are fairly similar. This allowed to divide the sections into 4 different zones, based on the combined changes in the dinocyst assemblage

composition and the stable isotope and IRD records (Fig. 2.4). The following paragraphs will give an overview of these changes and the assemblage compositions typifying each zone.

Zone 1

M23071: 663 – 656 cm

M23323: 868.5 – 850.5 cm

Lowermost zone 1 is characterised by high amounts of IRD and heavy $\delta^{18}\text{O}$ values, which both decrease significantly towards the top of the zone, and low absolute abundances of dinocysts per gram dry sediment. Due to the low cyst abundances, less than 100 cysts could be determined to species level in most of the samples from this interval, and (fluctuations in) relative abundance should therefore be interpreted accordingly. The occurrences of *L. machaerophorum*, *S. ramosus* s.l. and *Spiniferites* spp. are nevertheless significant, especially in the lower parts of zone 1 in core M23323, where analysis reached further back into the IRD-rich sediment section. The relative abundance of the above-mentioned species decreases drastically towards the top of zone 1, coincident with a significant increase in the relative abundance *O. centrocarpum*. Also noteworthy is the regular presence of *I. pallidum*, and the occasional occurrences of *S. mirabilis* s.l. and *S. lazus*.

Zone 2

M23071: 655 – 641 cm

M23323: 848.5 – 810.5 cm

IRD persists at low levels in zone 2, with a slight increase towards the top of the zone. The increase is most clearly seen in the northern core M23323, where IRD content is also lower in the preceding interval. After the increase, IRD content drops to near-zero values. The dinocyst assemblages are fairly stable in zone 2, and can be regarded typically interglacial, continuously dominated by *O. centrocarpum*. The latter species shows a significant decrease in the lower part of zone 2 in core M23071, mainly due to an increase of *Brigantedinium* spp. Such increase is less obvious in core M23323. The most significant feature of zone 2 is the abundance maximum of *Impagidinium* spp. extending over the entire interval. The taxon is slightly more abundant in the southern core. Noteworthy is also the peak of *S. mirabilis* s.l. in core M23323 at the top of zone 2, towards the end and directly after the phase of IRD increase. This feature is not seen in core M23071.

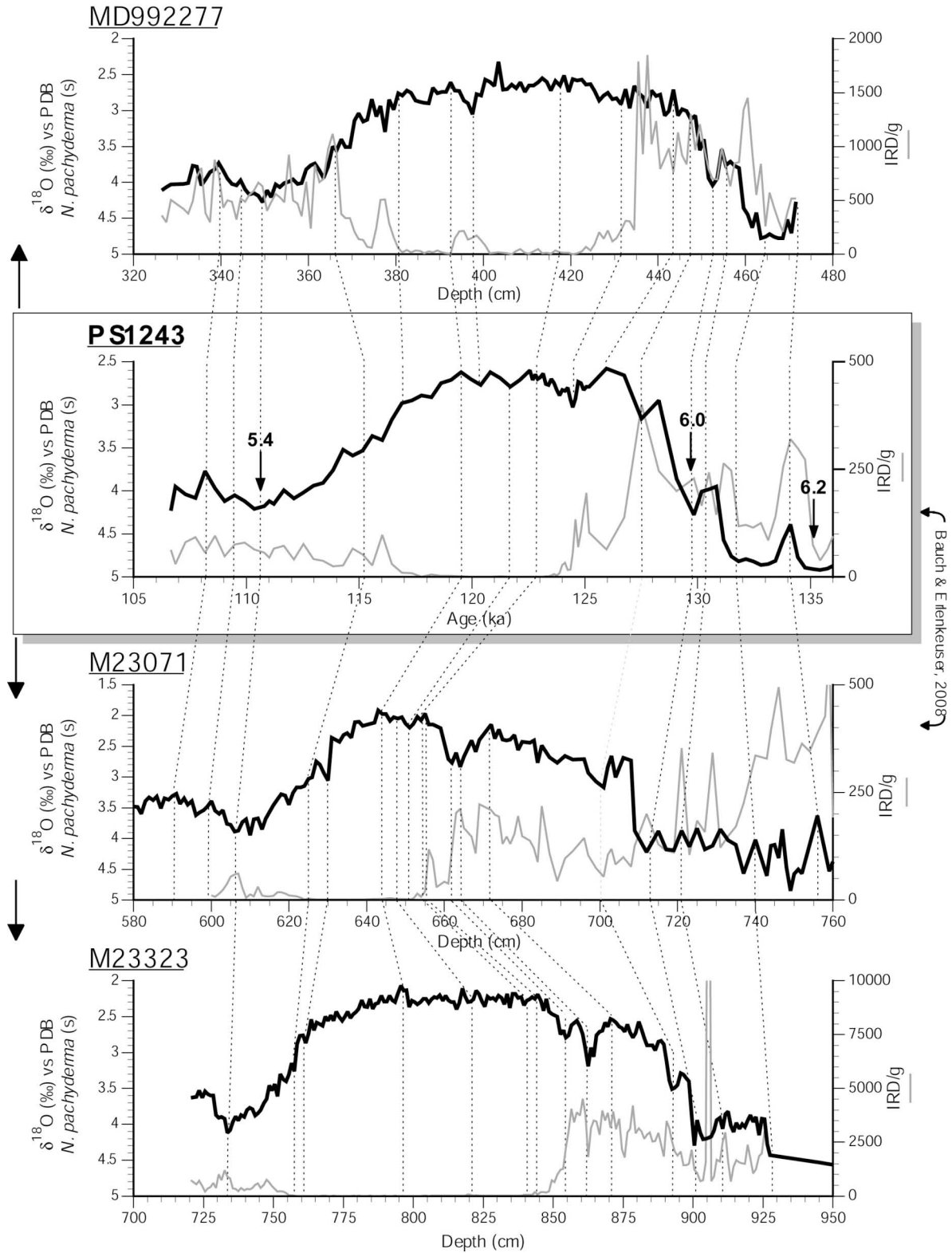


Fig. 2.2: Correlation points in the planktic foraminiferal $\delta^{18}\text{O}$ (and IRD) records used in developing the age models for cores M23071, M23323 and MD992277. The established age model of core PS1243 (Bauch, 1997; Bauch et al., 2000b; Bauch & Erlenkeuser, 2008) was taken as reference for the age model of core M23071 (Bauch & Erlenkeuser, 2008). The age model for cores M23323 and MD992277 was then developed by correlating significant features in the respective $\delta^{18}\text{O}$ record with core M23071 and/or PS1243.

Zone 3

Zone 3 covers the interval with very low IRD content. In the northern core M23323, zone 3 can be divided into zones 3A and 3B. Only zone 3B can be recognised in core M23071.

Zone 3A

M23323: 808.5 – 790.5 cm

Zone 3A is characterised by a significant increase of *S. lazus* and a marked increase of *N. labyrinthus* immediately following the drop in IRD from the top of zone 2. The abundance high of *S. lazus* persists well into zone 3B. *Brigantedinium* spp. peaks intermittently to relative abundance values around 8%.

Zone 3B

M23071: 640 – 629 cm

M23323: 788.5 – 760.5 cm

In both cores, the base of zone 3B is characterised by the virtual disappearance of *Brigantedinium* spp. and a marked increase in the relative abundance of *S. elongatus* s.l. Cysts of *P. dalei* have their highest occurrence in core M23323 within zone 3B, in contrast to core M23071, where the species' abundance is at its lowest values in zone 3B. The relative abundances of *S. ramosus* s.l. start to increase steadily from the base of zone 3B upwards. A conspicuous abundance maximum of *S. mirabilis* s.l. occurs towards the top of the interval.

Zone 4

M23071: 628 – 620 cm

M23323: 758.5 – 750.5 cm

A sudden increase of the $\delta^{18}\text{O}$ values marks the beginning of zone 4, followed by the recurrence of IRD. A considerable number of species become less abundant, to be replaced by *S. ramosus* s.l. and *N. labyrinthus*. Absolute cyst concentrations fall back throughout the zone, towards values comparable to those from zone 1.

2.4.2 Core-top samples

In order to have a modern-day reference to directly compare the last interglacial dinocyst dataset with, the core-top sample of cores M23071 and M23323 has also been analysed. The core-top sample of core M23071 had already been studied by Baumann & Matthiessen (1992), but was recounted to allow optimal comparison, quantitatively and qualitatively, with the samples from MIS 5e.

The high species-diversity of the MIS 5e dinocyst assemblages, where a considerable number of different species generally contribute sizeably to the total assemblage composition, contrasts strongly with the quasi-monospecific assemblages from the core-top samples. *Operculodinium centrocarpum* constitutes $\pm 83\%$ of the core-top assemblages, and only *N. labyrinthus* and cysts of *P. dalei* have relative abundances above 1% (Fig. 2.5). The dinocyst assemblage in the core-top samples can be regarded as representative for the modern and average late Holocene sea surface conditions at the Vøring Plateau, since the assemblage composition remained relatively constant in core M23071 for the last ~7 kyr (Baumann & Matthiessen, 1992).

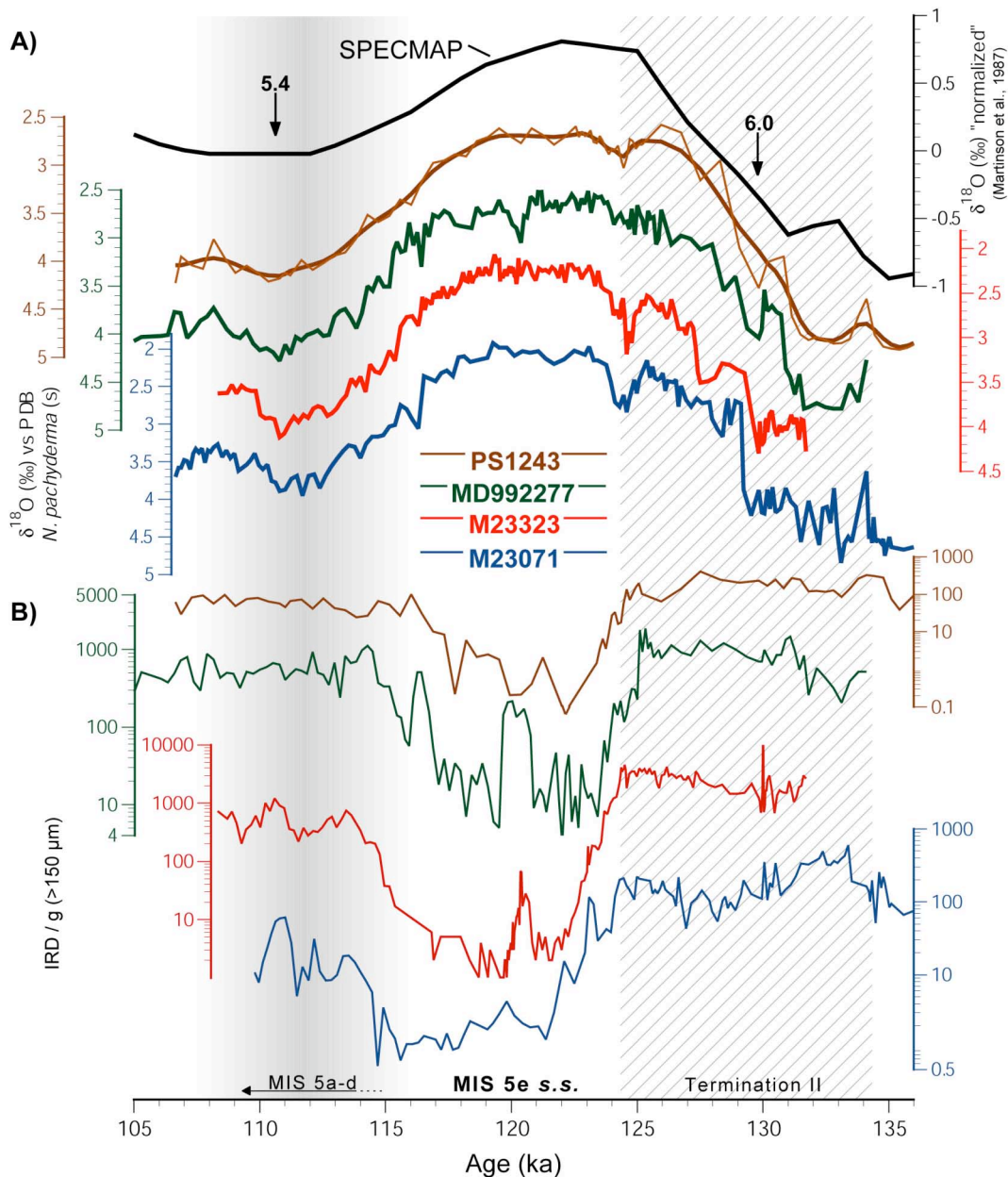


Fig. 2.3: Results from the age model development. Shown are the stable oxygen isotope (A) and IRD (B) records for cores PS1243, M23071, M23323 and MD992277, for the interval from latest Termination II (hatched), over MIS 5e into MIS 5a-d (shaded). The trend of the smoothed $\delta^{18}\text{O}$ curve of PS1243 (thick brown line) agrees well with the stacked SPECMAP isotope curve (Martinson et al., 1987). The “early” light values in the Nordic seas cores with respect to the SPECMAP curve result from meltwater overprint, as can be deduced from the high IRD content for these specific sections. Note the logarithmic scale for the IRD curves.

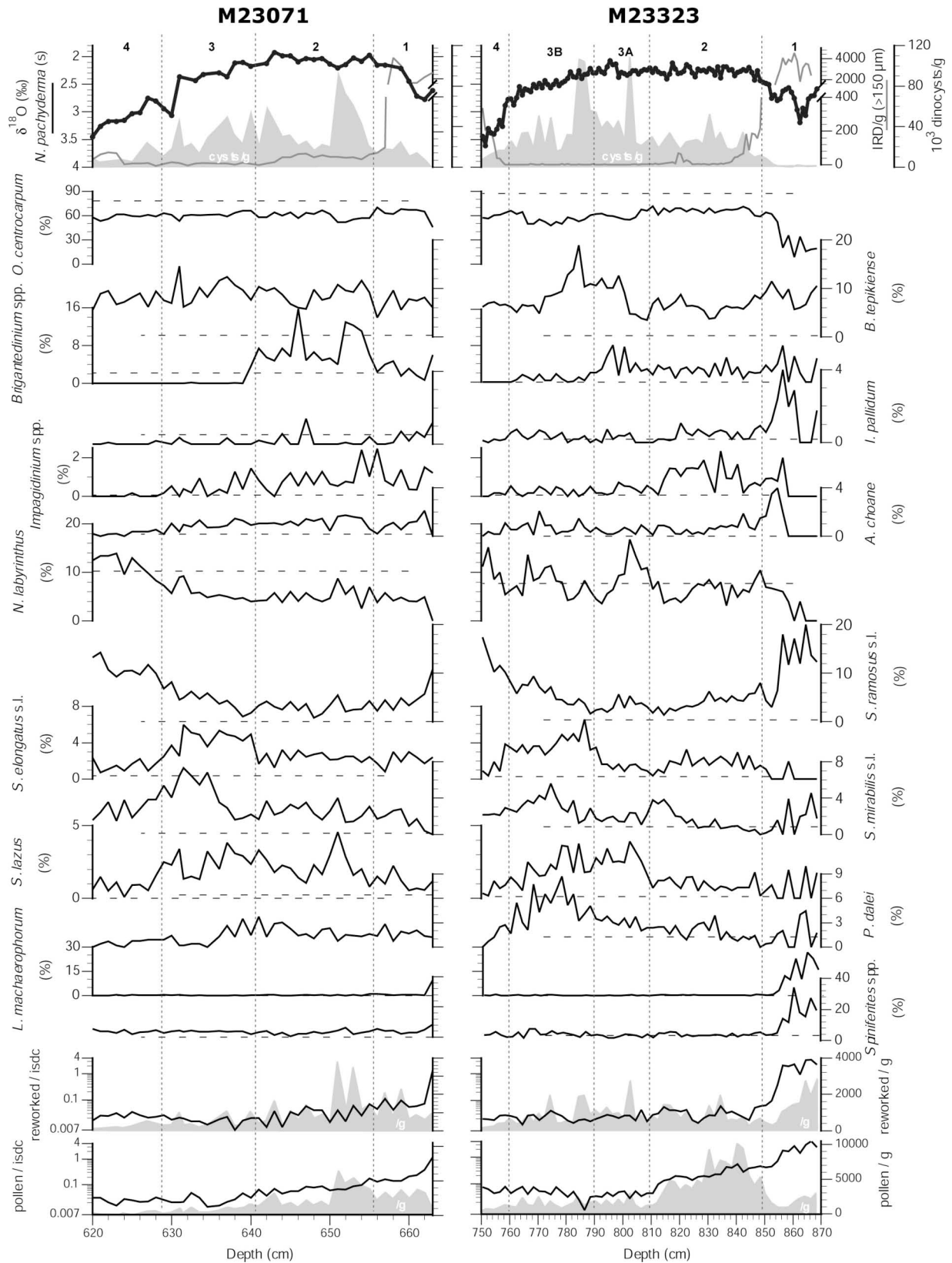


Fig. 2.4: Oxygen isotopes, IRD, and total concentrations and relative abundance fluctuations of the most abundant dinocyst species, reworked dinocysts, and pollen grains throughout the studied interval of core M23071 and M23323, plotted against depth. Also shown is the division of the studied sections into zones, as they are referred to in the text. The dashed horizontal line in each diagram represents the relative abundance of the respective species in the core-top sample from the core. Note that the ratios of reworked dinocysts and pollen grains to in situ dinocysts (isdc) are plotted on a logarithmic scale.

2.4.3 Transfer function analysis

The transfer function exercise was able to find 5 analogues for all samples with the exception of a number of samples from zone 1 in core M23323 (Tables 2.1 & 2.2).

Analogues that could be found for the samples from zone 1 had distances to the fossil assemblages close the threshold value beyond which an analogue is rejected. The reconstructions for zone 1 are therefore not taken into account. The distances between the assemblages from the overlying MIS 5e section and the modern analogues are also rather large, especially compared to the core-top sample, but they still remain well below the threshold value (Tables 2.1 & 2.2).

The results from the transfer function analyses show significant fluctuations occurred during MIS 5e in the reconstructed parameters, and trends are most clearly depicted in core M23071 (Fig. 2.6). Winter and summer SST reconstructions vary from 1.6 to 9.2°C and from 11.2 to 21.4°C, respectively, for core M23071, and from 3.9 to 8.4°C and from 11.1 to 20.1°C, respectively, for core M23323. The summer SSTs of 20°C and more, and the short-term changes of over 5°C during the earliest phase of MIS 5e could be a real signal, but should be regarded cautiously. The distances to their closest analogues are among the highest of all the reconstructions (Tables 2.1 & 2.2), and their analogue sites are situated most distally, in the western North Atlantic off the American and Canadian coast. After 122 ka, a clear increasing trend is discernable in the winter SST in core M23071, reaching temperatures higher than the present-day (reconstructed) value by ~118.5 ka and exceeding the modern estimate between ~117.5 and 116.5 ka (Fig. 2.6). This signal is not as clearly shown by the best analogue curve in core M23323, but is discernable in the range of the closest analogues, bearing in mind the questionable reconstructions for the early MIS 5e. A similar increasing trend is not found in the summer SSTs, which are otherwise consistently higher than the reconstructed present-day value (Fig. 2.6).

Estimated values for SSS range from 32.5 to 35.0 and from 31.6 to 34.7 for winter and summer, respectively, in core M23071, and from 33.2 to 34.9 and from 32.1 to 34.6 for winter and summer, respectively, in core M23323 (Fig. 2.6). Analogous to the winter SST, salinity gradually increases and reaches highest values in core M23071 between ~118 and 116.5 ka immediately after notable shift of ~1. This trend is again best discernable in core M23323 in the range of reconstructed values. Winter SSS are close to the reconstructed present-day value during the late MIS 5e interval, but never exceed the value of the core-top sample reconstruction (Fig. 2.6).

2.4.4 Planktic foraminifera

Extensive and detailed planktic foraminiferal records are available for Termination II/MIS 5 from both core M23071 and M23323, and will be used in the discussion below in support of the dinocyst assemblage data. Analysis of the planktic foraminifera in core M23071 was done by Dr. Henning A. Bauch, and the results were published in Van Nieuwenhove et al. (2008). The unpublished planktic foraminiferal data from core M23323 were produced by Dr. Evgeniya Kandiano.

Table 2.1: Sample depths, correlated interpolated ages, number of analogues found, and minimum (MinDist) and maximum (MaxDist) distances to the analogues, for core **M23071**.

Depth (cm)	Age (ka)	# Analogues	MinDist (threshold 1.26)	MaxDist
core-top sample		5	0.13	0.18
625	115.15	5	0.46	0.62
626	115.38	5	0.44	0.59
627	115.61	5	0.41	0.55
628	115.84	5	0.46	0.59
629	116.07	5	0.59	0.70
630	116.30	5	0.62	0.71
631	116.53	5	0.78	0.82
632	116.64	5	0.67	0.75
633	116.87	5	0.59	0.68
634	117.10	5	0.70	0.76
635	117.33	5	0.69	0.88
636	117.67	5	0.54	0.65
637	117.90	5	0.49	0.61
638	118.13	5	0.68	0.78
639	118.36	5	0.52	0.63
640	118.59	5	0.66	0.74
641	118.82	5	0.57	0.59
642	119.05	5	0.63	0.74
643	119.28	5	0.53	0.62
644	119.51	5	0.57	0.61
645	119.82	5	0.54	0.58
646	120.13	5	0.55	0.61
647	120.44	5	0.64	0.72
648	120.76	5	0.65	0.74
649	121.07	5	0.61	0.68
650	121.38	5	0.52	0.63
651	121.69	5	0.71	0.82
652	122.10	5	0.61	0.70
653	122.51	5	0.61	0.72
654	122.92	5	0.72	0.75
655	123.09	5	0.62	0.73
656	123.26	5	0.65	0.79
657	123.44	5	0.54	0.63
658	123.61	5	0.69	0.75
659	123.78	5	0.60	0.68
660	123.95	5	0.52	0.61
661	124.13	5	0.51	0.62
662	124.3	5	0.69	0.77
663	124.47	5	0.63	1.05

Table 2.2: Sample depths, correlated interpolated ages, number of analogues found, and minimum (MinDist) and maximum (MaxDist) distances to the analogues, for core **M23323**.

Depth (cm)	Age (ka)	# Analogues	MinDist (threshold 1.28)	MaxDist
core-top sample		5	0.16	0.18
750.5	114.01	5	0.59	0.76
752.5	114.39	5	0.38	0.54
754.5	114.77	5	0.49	0.59
756.5	115.15	5	0.40	0.52
758.5	115.61	5	0.32	0.50
760.5	116.07	5	0.40	0.52
762.5	116.39	5	0.38	0.48
764.5	116.56	5	0.29	0.40
766.5	116.74	5	0.50	0.69
768.5	116.92	5	0.38	0.56
770.5	117.10	5	0.51	0.68
772.5	117.28	5	0.47	0.62
774.5	117.46	5	0.44	0.64
776.5	117.63	5	0.44	0.58
778.5	117.81	5	0.47	0.61
780.5	117.99	5	0.47	0.61
782.5	118.17	5	0.36	0.53
784.5	118.35	5	0.46	0.60
786.5	118.53	5	0.43	0.56
788.5	118.71	5	0.43	0.55
790.5	118.88	5	0.47	0.54
792.5	119.06	5	0.44	0.49
794.5	119.24	5	0.44	0.57
796.5	119.42	5	0.35	0.49
798.5	119.55	5	0.44	0.58
800.5	119.63	5	0.51	0.56
802.5	119.70	5	0.50	0.64
804.5	119.78	5	0.39	0.52
806.5	119.86	5	0.42	0.54
808.5	119.94	5	0.35	0.54
810.5	120.01	5	0.24	0.45
812.5	120.09	5	0.43	0.59
814.5	120.17	5	0.53	0.64
816.5	120.25	5	0.61	0.67
818.5	120.33	5	0.45	0.54
820.5	120.40	5	0.52	0.61
822.5	120.57	5	0.69	0.72
824.5	120.83	5	0.44	0.54
826.5	121.09	5	0.42	0.47
828.5	121.35	5	0.58	0.64
830.5	121.62	5	0.38	0.49
832.5	121.88	5	0.38	0.49
834.5	122.14	5	0.58	0.67
836.5	122.40	5	0.51	0.56
838.5	122.66	5	0.47	0.57
840.5	122.92	5	0.62	0.64
842.5	123.00	5	0.42	0.56
844.5	123.09	5	0.53	0.59
846.5	123.33	5	0.66	0.73
848.5	123.57	5	0.88	0.95
850.5	123.82	5	0.73	0.76
852.5	124.06	5	0.86	0.97
854.5	124.30	5	0.95	1.13
856.5	124.37	1	1.24	1.45
858.5	124.44	0	1.38	1.43
860.5	124.51	2	1.18	1.38
862.5	124.58	5	0.70	0.90
864.5	124.78	0	1.37	1.40
866.5	124.99	5	1.02	1.29
868.5	125.20	5	0.91	1.17

2.5 Discussion

2.5.1 Evolution of the last interglacial climate at the Vøring Plateau

The dominance of *O. centrocarpum* and high cyst concentrations in all our last interglacial samples (Fig. 2.4) indicate that the Vøring Plateau stood under permanent influence of inflowing warm Atlantic water throughout the entire MIS 5e. This differs from assemblages from the South Icelandic Basin (Eynaud et al., 2004) and southern Norwegian coastal areas (Dale, 1996), where *O. centrocarpum* only dominates early and late in the last interglacial, respectively. Still, dinocyst assemblages dominated by *O. centrocarpum* are a common feature of both Holocene and last interglacial sediments from areas influenced by inflowing Atlantic water (e.g. Baumann & Matthiessen, 1992; Eynaud et al., 2004), and the species has been used as a Quaternary tracer for NAD waters as they penetrated into high-northern latitudes (Matthiessen & Knies, 2001; Matthiessen et al., 2001; Grøsfjeld et al., 2006). Indeed, species assemblages at the Vøring Plateau and western Norway became dominated by *O. centrocarpum* after ~7 ka, and this has been interpreted as reflecting the onset of the modern mode of surface circulation (Baumann & Matthiessen, 1992; Grøsfjeld et al., 1999). However, the qualitative existence of an “interglacial type” of surface circulation with inflowing Atlantic water at the Vøring Plateau is the only conclusion that can be derived from the dominance of *O. centrocarpum*.

The rather high-frequency relative abundance fluctuations of a large number of species at the Vøring Plateau, against the background of continuous warm water advection, suggest that sea surface conditions in the area underwent subtle changes in the course of the low-IRD period of MIS 5e. The zones defined above (Fig. 2.4) reflect the different phases in the climate development of MIS 5e.

2.5.1.1 Latest Termination II (Zone 1)

The lowermost zone represents a transitional phase from the deglaciation towards interglacial conditions. This is evidenced by the presence of both cold and warm elements: the high relative abundances of *S. ramosus* s.l. and terrestrial input (IRD, pollen and spores, reworked dinocysts), the persistent occurrence of *I. pallidum* and the dominance of *N. pachyderma* (s) in the planktic foraminiferal assemblages are indicative for cold conditions, but the fairly high species-diversity, the considerable occurrence of *O. centrocarpum* and the occasional peaks of *S. lazus*, *S. mirabilis* s.l. and *L. machaerophorum* reveal pulses of warm Atlantic water masses into the area (Figs. 2.4 & 2.7). The high relative abundances of 20% and more of the latter species, which also appears in last interglacial coastal sequences from fjords around Bergen (Norway) (Dale, 1996), are an interesting feature in this context. Considering the restricted, neritic distribution along the

western European coastline of *L. machaerophorum* at present, this signal is suggestive of the origin and specific physical properties of the surface water masses at the Vøring Plateau at that time. It is noteworthy that the relative abundance of *O. centrocarpum* increases dramatically precisely when *L. machaerophorum* quasi disappears from the assemblages (Fig. 2.4). This seems to suggest a shift from the inflow of coastal towards more open marine water masses.

The warming climate towards the end of the first phase caused glaciers to further retreat from the coastline, thereby reducing iceberg release into the open ocean. This environmental change is consistent with steep reduction in IRD content, the overall changes in the dinocyst assemblages, and the steep increase in the relative abundance of the temperate planktic foraminifer *N. pachyderma* (d), and to a lesser degree *Turborotalita quinqueloba* (Fig. 2.7), mainly at the expense of the polar species *N. pachyderma* (s).

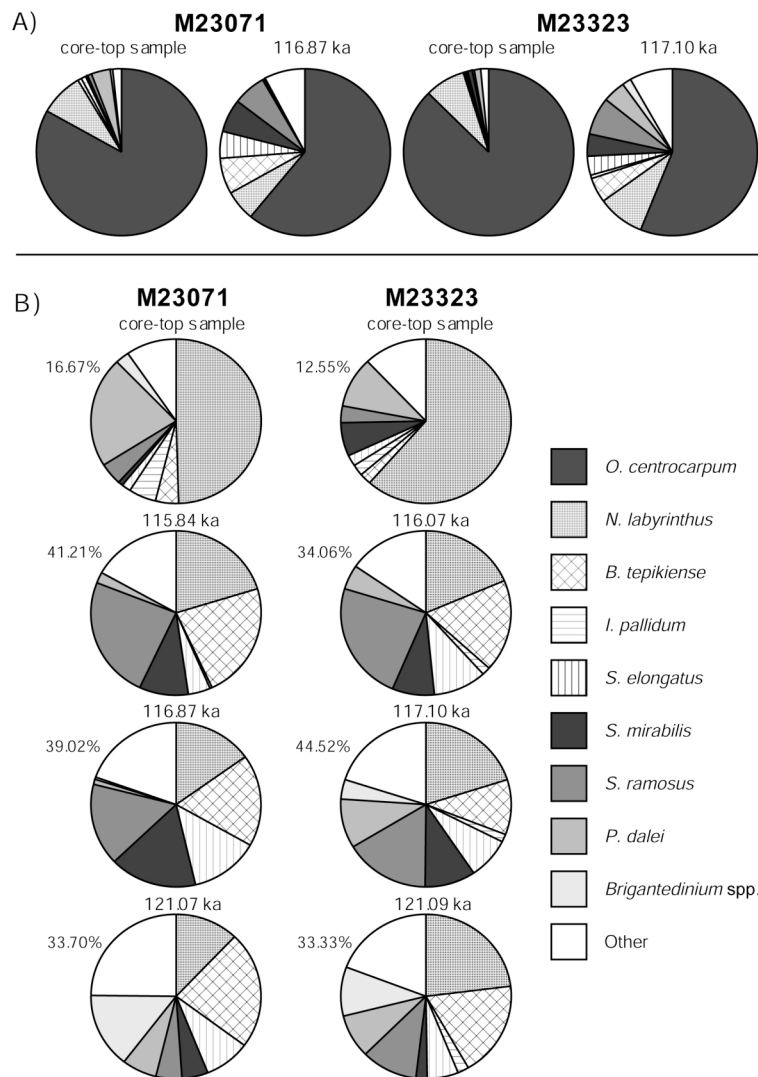


Fig. 2.5: (A) Assemblage composition in the core-top sample and a sample from the last interglacial optimum, for core M23071 and M23323, illustrating the difference in assemblage composition between both phases. (B) Comparison of the composition of the subordinate assemblage (i.e., excluding *Operculodinium centrocarpum*) in the core-top sample with different phases of the last interglacial period, for core M23071 and M23323. The percentage number to the upper left of each diagram gives the percentage of the total assemblage that is represented by the diagram, i.e., 100 minus the relative abundance of *O. centrocarpum* in the respective sample.

2.5.1.2 Early Last Interglacial (Zone 2)

The abrupt decline of IRD at the end of Termination II indicates the end of excess meltwater supply from the retreating Saalian glaciers. Nevertheless, the persistent input of IRD during this phase implies that there were still icebergs reaching the Vøring Plateau after the transitional phase. These also supplied the surface waters with enough nutrients to create favourable growing conditions for the heterotrophic *Brigantedinium* species (see Mudie & Short, 1985; Matthiessen et al., 2005), especially at the southern Vøring Plateau. The terrestrial import shows furthermore from the high concentrations of pollen and spores in the samples (Fig. 2.7).

A continuous inflow of warm-temperate water masses, leading to relatively stable surface conditions for early MIS 5e, might be inferred from the steady assemblage compositions dominated by *O. centrocarpum* with a notable *Impagidinium* spp. occurrence (Fig. 2.4) (Wall et al., 1977; Harland, 1983). The *Impagidinium* group has been related to periods of climatic optima along the Portuguese Margin and the Alboran Sea (Turon & Londeix, 1988; Boessenkool et al., 2001; Turon et al., 2003).

An intriguing feature towards the end of the early last interglacial is the recurrence of larger amounts of IRD, around 120.5 ka (Figs. 2.3 & 2.7). The abundance increase of the polar planktic foraminifer *N. pachyderma* (s) in core M23323 implies a significant cooling at that time, nearly back to glacial conditions (E. Kandiano, unpublished data). Although the IRD increase can also be seen in core M23071, the planktic foraminiferal assemblages in the southern core do not show the cooling event as clearly as in the northern core M23323 (Fig. 2.7). It can be suggested that this might have something to do with differences in the sedimentation regime between the two sites, but this is not a conclusive explanation. Particularly interesting, however, is the fact that the dinocyst assemblages (and, thus, the transfer function reconstructions; Fig. 2.6) do not show any cooling at all. The increase of *S. mirabilis* s.l. would actually rather suggest a considerable warming (Fig. 2.7). An explanation for this apparent contradiction might be in the surface water freshening and a (seasonally) stratified surface water layer caused by the melting of the icebergs. A stratified surface layer could warm easily during summer, thereby creating favourable conditions for *S. mirabilis* s.l. in the very upper water column, and conditions cool enough for the polar foraminifer *N. pachyderma* (s) to persist deeper below. An enhanced meltwater input might also explain why the $\delta^{18}\text{O}$ record does not show the cooling event, either (Fig. 2.7). Concerning the different signal given by the dinocyst and planktic foraminiferal assemblages, it should also be taken into consideration that the enhanced melt-off and the resulting larger input of freshwater presumably not only changed surface ocean salinity and temperature but also nutrients. Since the trophic state of the water masses can be an

important factor controlling dinoflagellate populations (Dale, 1996; Devillers & de Vernal, 2000), this could have influenced both fossil assemblages in quite different, group-dependent ways.

2.5.1.3 Late Last Interglacial (Zone 3)

The virtual disappearance of IRD at the beginning of zone 3 may be considered the actual end of the deglacial phase, and also implies no further meltwater overprint on planktic oxygen isotopes. Zone 3A appears to represent a transitional phase towards full interglacial conditions after the cold event in core M23323. The peak of *N. labyrinthus* would in this respect agree with previous interpretations of an association of this cold indicator species with transitional climatic periods, i.e. glacial-to-interglacial (Baumann & Matthiessen, 1992) as well as interglacial-to-glacial (Eynaud et al., 2004). The increasing abundances of *S. lazus* and subpolar planktic foraminifera clearly point towards ameliorating interglacial conditions from this time on (Figs. 2.4 & 2.7). It is puzzling again that the *S. lazus*-high is only seen in the northern core M23323. Other, more local factors than salinity and temperature probably played a role in causing this signal.

Zone 3B can be recognised in both cores, and represents the final, full interglacial phase of MIS 5e. The relative abundances of the subpolar planktic foraminifera *Globigerina bulloides* and *T. quinqueloba* increase to reach a maximum towards the end of late MIS 5e. Their peak abundances are coeval with the *S. mirabilis* s.l. maximum, between ~117.5 and 116.5 ka (Fig. 2.7). Optimal, most pronounced full-interglacial surface water conditions of the entire MIS 5e are thus interpreted to have existed at the Vøring Plateau during this late phase of the last interglacial. Plotting the relative abundance sum of the warm dincoyst species *Impagidinium* spp., *S. lazus* and *S. mirabilis* s.l. also illustrates the steadily ameliorating interglacial conditions, peaking towards the end of MIS 5e. As can be expected from their respective latitudes, the total sum of warm species is highest in the southern core M23071 (Fig. 2.7).

The high abundances of *S. elongatus* s.l. during the last interglacial optimum might seem contradictory at first sight (Fig. 2.4). However, this phenomenon can be explained when taking into account that the *S. cf. elongatus* morphotype always constitutes an important part of our *S. elongatus* s.l.-group. The persistent and rather high abundance of *N. pachyderma* (s), on the other hand, could be due to the deeper, hence cooler habitat preferred by this polar foraminifer (Bé, 1977). At present, with warm and saline Atlantic water dominating the upper ~700 m of the NC, summer water temperatures at 100 m water depth at the Vøring Plateau are usually below 7°C (Locarnini et al., 2006). Surface samples from the Vøring Plateau area reveal abundances of *N. pachyderma* (s) of 20-30%

(Andersson et al., 2003; see Bauch & Kandiano, 2007), considerably less than what is recorded during MIS 5e. Considering this, it appears as if the upper water structure, i.e. the degree of stratification, is quite different today when compared with the last interglacial.

As observed in the South Icelandic Basin (Eynaud et al., 2004), the high abundances of *S. mirabilis* s.l. do not go in hand with elevated abundances of *Impagidinium* spp. On the contrary, *Impagidinium* spp. percentages decline from the beginning of the late last interglacial onwards, and are negligible in the upper part of the MIS 5e section of both cores (Fig. 2.4). Due to the fact that zone 3B is missing in core M23071, the decline in *Impagidinium* spp. is coeval with the disappearance of *Brigantedinium* spp. and other protoperidinioid cysts in this core. It has been shown that cysts of *Brigantedinium* and *Protoperidinium* species decay more easily under oxygenated conditions (Zonneveld et al., 2008, and references therein). Hence, increased oxygenation of bottom water due to enhanced ventilation might be a possible explanation for the observed decrease in *Brigantedinium* spp. However, the lag between the disappearance of *Brigantedinium* spp. and *Impagidinium* spp. in core M23323, and the fact that Zonneveld et al. (1997, 2001) have shown that *Impagidinium* species are resistant to aerobic decay, implies that the decline of both taxa was not caused by the same event. Thus, as already suggested above, the decline of *Impagidinium* spp. was likely related to a change in the pathway of the inflowing surface water. Such a shift in the position of the NC further east across the Vøring Plateau is conceivable from the stratigraphic position of the highest relative abundances for each of the subpolar foraminifera, especially in core M23071. *Neogloboquadrina pachyderma* (d), which shows its highest modern distribution east and southeast of the Vøring Plateau (see Bauch & Kandiano, 2007), is most abundant during the early last interglacial, synchronous with lowest $\delta^{18}\text{O}$. Decreasing relative abundances of *N. pachyderma* (d) towards the late last interglacial are compensated by the highest abundances of *Globigerinita glutinata*, followed by *G. bulloides* and *T. quinqueloba* (Fig. 2.7). The latter species is considered an Arctic Domain species (Bé & Hutson, 1977). Thus, the actual decline of *N. pachyderma* (d), in parallel with the increase of the other subpolar species, is evidence for an eastward shift in the flow path of the Norwegian Current and an eastward expansion of the cooler ArD during late MIS 5e.

2.5.1.4 Transition towards MIS 5d (Zone 4)

The relative abundance rise of *N. labyrinthus* and *S. ramosus* s.l., already during the latest stages of the thermal optimum, indicates that interglacial surface conditions steadily started to decline towards the 5e/5d transition (Figs. 2.4 & 2.7). This again confirms the association of *N. labyrinthus* with transitional climatic periods (see also above). The end of

full-interglacial conditions is further corroborated here by the coeval increase of oxygen isotope values and polar foraminiferal abundances, and the subsequent recurrence of IRD. The temporal difference between the rise in cold-temperature indicators and renewed IRD input indicates that surface ocean cooling in the Norwegian Sea during the later phase of MIS 5e had a significant environmental impact, eventually leading to a notable regrowth of glacier ice (see Baumann et al., 1995) and/or changes in iceberg drift pattern (Bauch & Kandiano, 2007).

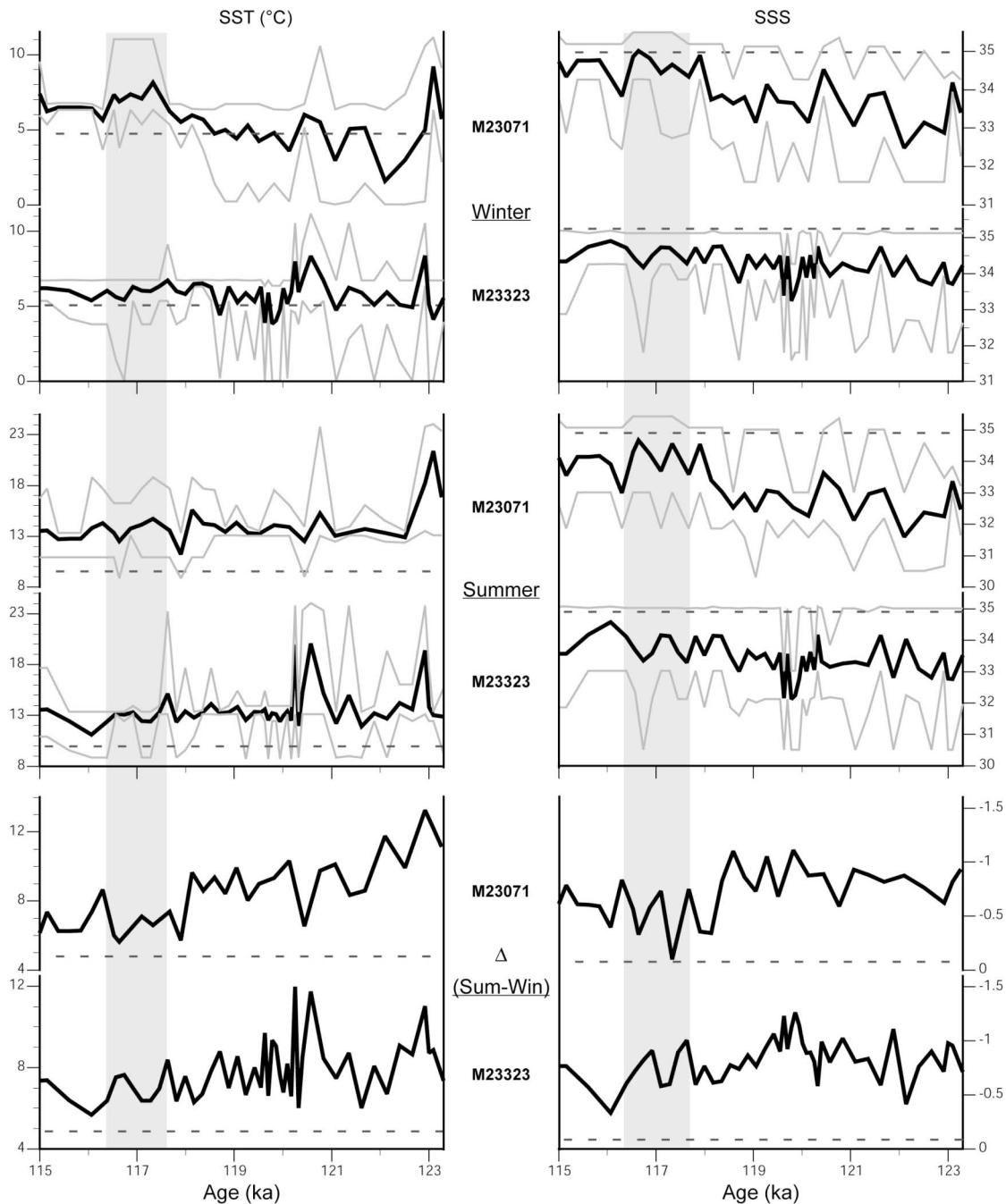


Fig. 2.6: Sea surface temperature (SST) and sea surface salinity (SSS) estimates from the dinoflagellate cyst assemblages for winter and summer, and the difference (Δ) between both, i.e., the seasonal gradient (lower graphs), for core M23071 and M23323. The dashed horizontal lines indicate the values reconstructed from the core-top sample. The relevant trends are best reflected by the reconstructions from core M23071. The grey bar delineates the time interval with optimal, marine interglacial conditions, as suggested by the peak abundance of *Spiniferites mirabilis* s.l. and subpolar foraminifera.

2.5.2 Specific palaeoceanographic features of MIS 5e at the Vøring Plateau

2.5.2.1 *Bitectatodinium tepikiense* and the stratification signal

An interesting feature of MIS 5e is the considerable difference in dinocyst assemblage compositions when compared with the core-top samples (Fig. 2.5). A preservational bias overprinting on the assemblages is unlikely because most of the dominant species are more or less equally resistant to oxidation (Zonneveld et al., 1997, 2001). The difference between the core-top and last interglacial samples becomes obvious when comparing the assemblage composition of the core-top samples with time slices from MIS 5e, taking into account all species other than *O. centrocarpum* (Fig. 2.5). Although most species frequently observed in the MIS 5e section also occur in the core-top samples, the MIS 5e assemblages may be regarded as “more diverse.” This is because greater numbers of co-dominant subordinate species contribute to the total assemblage composition in the MIS 5e samples, and the share made up by rare species is at least twice as high as compared to the core-top samples. For example, half of the core-top subordinate assemblage is comprised of *N. labyrinthus*, yet this species represents only 8% of the total core-top sample assemblage. The fact that *O. centrocarpum* and *N. labyrinthus* constitute ~90% of the assemblage in the core-top samples is entirely consistent with the full marine conditions that prevail in the Norwegian Sea at present.

Identifying what caused the marked differences between the core-top and last interglacial assemblages is somewhat hindered by the fact that only little is known about the ecological preferences, the timing of cyst formation, and the growth conditions of most of the cyst-forming dinoflagellate species (see Matthiessen et al., 2005). A possible explanation for the assemblage differences may lie in the existence of a more pronounced surface water seasonality during MIS 5e, creating thriving conditions for one or several species at differing times of the year. Evidence for stronger seasonality comes from *B. tepikiense*. This species is virtually absent in samples from the last 7 kyr (Baumann & Matthiessen, 1992), but consistently constitutes 5 to 15% of the last interglacial assemblages at the Vøring Plateau (Fig. 2.4). The general differences between the core-top and MIS 5e assemblages, especially clear with the relative abundances of *B. tepikiense*, point towards dissimilar sea surface conditions during MIS 5e at the Vøring Plateau compared to today. Such a finding has already been suggested for the Arctic margin based on similar observations in dinocyst assemblages (Matthiessen & Knies, 2001; Matthiessen et al., 2001), as well as for the North Atlantic using planktic foraminiferal assemblages (Bauch & Kandiano, 2007).

Further support for a pronounced seasonality comes from the results of the transfer functions, with core M23071 showing the different trends most clearly (Fig. 2.6). These results show considerable differences between summer and winter surface water

temperature and salinity, especially during the first ~5 kyr of MIS 5e. Based on the reconstructed lower salinities, a more stratified upper water column is implied to have been present during MIS 5e. A fresher, and hence more stratified surface layer would store heat more easily during summer, giving rise to warmer than present summer SSTs, but could also facilitate the formation of winter sea ice. Although an enhanced NCC could have contributed in generating the lower salinities, meltwater is the most likely freshwater source since the marked salinity increase occurs after the IRD input had dropped to near-zero levels. This scenario of prolonged meltwater influence during MIS 5e is further supported by *B. tepikiense*: high abundances of this species, comparable to the ones from the last interglacial at the Vøring Plateau, were found in Late Allerød sediments from the Norwegian Channel and the west-Norwegian Voldafjorden (Rochon et al., 1998; Grøsfjeld et al., 1999). The latter two studies related these high abundances to strong seasonal variation and stratification due to a substantial freshwater input by deglacial processes. Similarly, relative abundances of *B. tepikiense* reached up to 30% in core M23071 during the last glacial-Holocene transition (Baumann & Matthiessen, 1992). Much higher relative abundances of the species during MIS 5e with respect to the Holocene were also found south of Iceland (Eynaud et al., 2004), an area also prone to be affected by meltwater input during deglaciations. Ice drifting into our study area would also have replenished the surface layer with nutrients after the spring bloom, allowing phytoplanktic communities to bloom again late in the growing season. Indeed, it has been shown that, in addition to temperature and salinity, the trophic state of the water masses can be an important factor controlling dinoflagellate populations (Dale, 1996; Devillers & de Vernal, 2000).

2.5.2.2 *Spiniferites mirabilis* s.l. and the late MIS 5e optimum

As described above, the timing of the MIS 5e optimum, between ~117.5 and 116.5 ka, is inferred from peak abundances of *S. mirabilis* s.l. and subpolar foraminifera (Fig. 2.7). Several studies have revealed strong affinities of *S. mirabilis* s.l. with the last interglacial in the temperate latitudes (Eynaud, 1999; Sánchez-Goñi et al., 1999, 2000; Penaud et al., 2008) as well as further north in the South Iceland Basin (Eynaud et al., 2004). These studies and our data all show the presence of *S. mirabilis* s.l. throughout the entire last interglacial, but with highest relative values during the second half of MIS 5e. This is best seen in samples from south of Iceland, where relative abundances of *S. mirabilis* s.l. reach over 30% during the late last interglacial (Eynaud et al., 2004). Because this site is hydrographically linked to the Vøring Plateau through the flow path of the NAD, it suggests that *S. mirabilis* s.l. might be a useful indicator for enhanced Atlantic water inflow during the time of interglacial optima in the Nordic seas.

The late MIS 5e marine optimum contrasts with the timing of the Holocene climatic optimum, which occurred during the first half of the Holocene more or less synchronously with relatively high northern summer insolation (e.g. Koç et al., 1993; Bauch et al., 2001; Calvo et al., 2002; Andersen et al., 2004; Bauch & Erlenkeuser, 2008). If the last interglacial climate evolution is taken as an analogue for the Holocene, the present orbital configuration would imply that the time of the Holocene climatic optimum has not been reached yet (Fig. 2.1); Kukla & Galvin, 2004). However, when comparing the Holocene with MIS 5e, one should consider that both interglacials began quite differently. Although the main deglacial phase had largely ended by 123.5 ka, it seems as if the continuing input of freshwater, depicted from the presence of IRD, during the following 4.5 kyr had a significant impact on the development of MIS 5e. The differing interglacial climate evolution between MIS 5e and the Holocene is also evident in variations observed in the dinocyst assemblage composition over these periods. In spite of the climate variability that occurred during the last 7 kyr (see review by Mayewski et al., 2004), dinocyst assemblages are virtually invariant for this time interval (Baumann & Matthiessen, 1992). On the other hand, the last interglacial dinocyst assemblages show considerable fluctuations among the subordinate species (Fig. 2.4). Thus, it appears that short-term surface ocean variability during MIS 5e had a greater impact on the phytoplanktonic communities relative to the late Holocene.

It has been suggested, on the basis of a number of marine sediments cores, that ocean heat flux into the Nordic seas had more pronounced meridionality during MIS 5e compared with the Holocene (Bauch et al., 1999; Knudsen et al., 2002). This scenario seems consistent, at least for the early MIS 5e, with evidence for enhanced inflow of more saline and warmer-than-Holocene waters into the North Sea and Baltic Sea regions (Funder et al., 2002; Head et al., 2005). In this last interglacial scenario, inflowing Atlantic water masses could have moved northward as a subsurface flow below the thin fresh surface layer, or closer to the Norwegian coast than in Holocene times (e.g. Kellogg, 1980; Rasmussen et al., 2003), also as a consequence of a weaker NCC due to Baltic Water seepage along the White Sea/Baltic Sea connection. Indeed, the record of relatively high abundances of *N. pachyderma* (d) may provide the evidence for an existence of Atlantic-derived waters bathing the western and southern coastal areas of Norway during early MIS 5e. These warm waters might also explain the finds of specific interglacial dinocysts in coastal areas (Dale, 1996), as well as the other “warm” fossil evidence found along northern Russia (Funder et al., 2002), while the northern Nordic seas and Fram Strait remained relatively cold (Köhler & Spielhagen, 1990; Hebbeln & Wefer, 1997; Bauch et al., 1999). A cold Arctic gateway, however, does not exclude brief spells of enhanced Atlantic water also reaching the northern Nordic seas and the Arctic Ocean (Hald et al., 2001; Matthiessen & Knies, 2001). Furthermore might the lag between a relatively rapid sea level rise, caused by global

deglaciation, and the slower isostatic recovery of the previously icesheet-covered land have eased the protrusion of Atlantic water masses onto the northern Russian shelf, enabling the incursion of “Atlantic” components along northern Russia (Funder et al., 2002; Grøsfjeld et al., 2006)

It is interesting to see that the planktic oxygen isotope values of *N. pachyderma* (s) from the late-MIS 5e optimum are comparable to the average Holocene ones (Fig. 2.1), but that the MIS 5e $\delta^{18}\text{O}$ record does not reflect the late-MIS 5e thermal optimum, as found in the fossil assemblage records. On the contrary, the $\delta^{18}\text{O}$ values from the optimum are on average about 0.3‰ higher than those from the preceding ~5.5 kyr of MIS 5e (Figs. 2.1, 2.4 & 2.7). The estimated 4 to 6 m higher global sea level of MIS 5e (e.g. Chen et al., 1991; McCulloch & Esat, 2000; Thompson & Goldstein, 2005) can only account for a minor part of this isotopic difference between the average Holocene and MIS 5e values. Because of the light values during most of MIS 5e, it is therefore often suggested that the climate of the last interglacial was warmer than the Holocene. For the mid-latitude North Atlantic sector, warmer last interglacial temperatures are confirmed for both the ocean surface and terrestrial realm (e.g. Ruddiman, 1986; Guiot et al., 1993; Kandiano et al., 2004). On the other hand, planktic foraminiferal census data from sites further north, in the eastern Norwegian Sea, indicate notably warmer surface waters prevailed in the Holocene (Risebrobakken et al., 2003) compared to the last interglacial (Rasmussen et al., 2003; Van Nieuwenhove et al., 2008), suggesting a steeper, meridional temperature gradient in the eastern Nordic seas in MIS 5e compared with the Holocene (Bauch et al., 1999; Knudsen et al., 2002). As salinity also influences the oxygen isotope signal derived from planktic foraminifera, it seems likely that the decreasing isotopic trend after the end of Termination II was still biased by light isotope input from meltwater. This freshwater input would amplify the $\delta^{18}\text{O}$ signal of surface warming of the progressing interglacial, at least for a certain time. The results from the transfer function reconstructions appear to confirm the meltwater bias: reconstructed last interglacial SSS values are below the core-top values for most of MIS 5e, but SSS estimates and the seasonal differences in SST and SSS come closest to the reconstructed modern values precisely during the interval of interglacial optimum, between ~117.5 and 116.5 ka (Fig. 2.6). Hence, all the records seem to point toward the development of a surface circulation similar to today, bringing relatively more warm Atlantic water and milder winter conditions in the Norwegian Sea for the time between ~117.5 and 116.5 ka. The data from the dinocyst assemblages thus favour the conclusion that the light oxygen isotopes of the preceding ~5.5 kyr of MIS 5e are the result of a differently structured, presumably more stratified upper water column with considerable freshwater input.

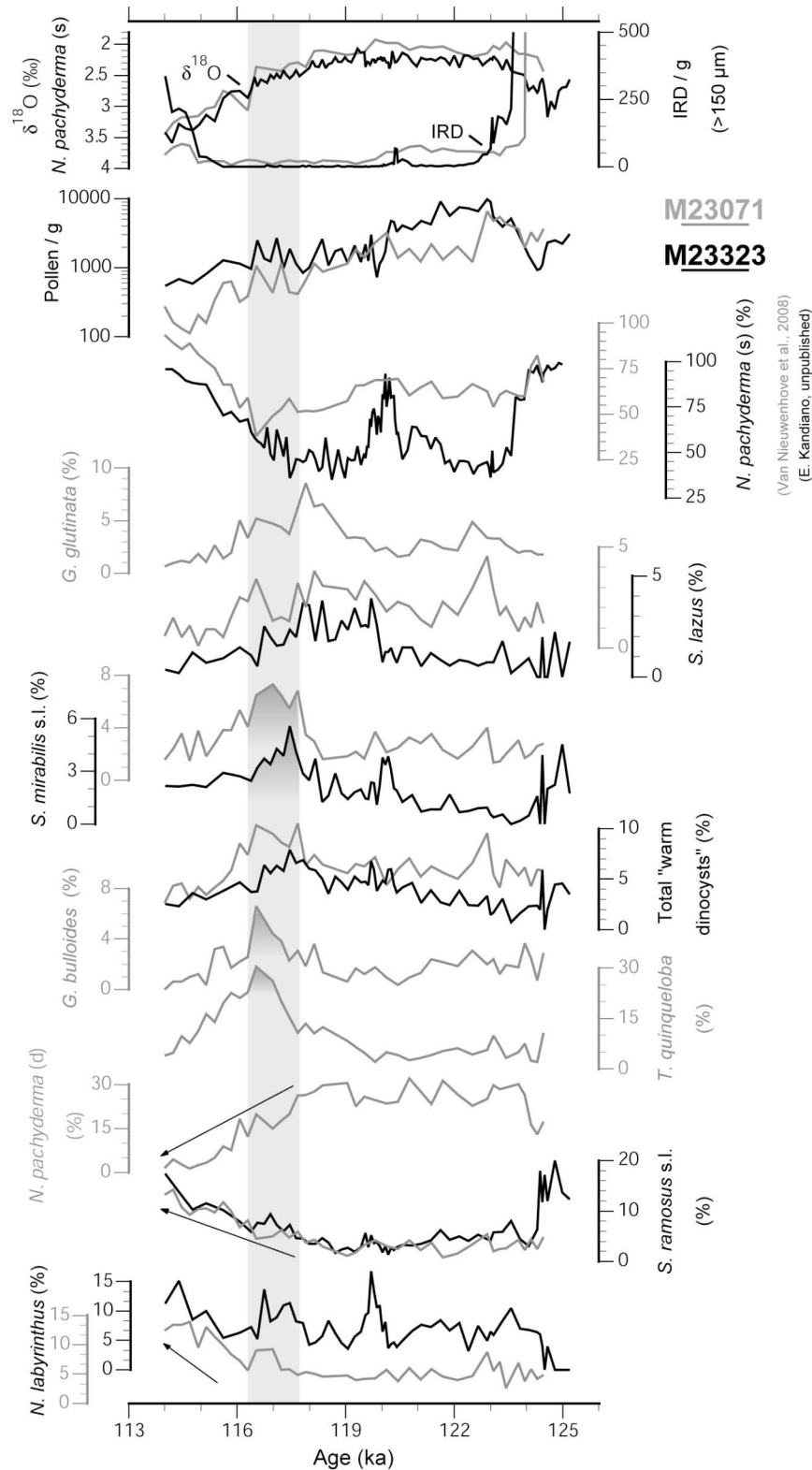


Fig. 2.7: Abundance fluctuations of selected dinocysts and foraminifer species at the Vøring Plateau, with respect to the $\delta^{18}\text{O}$, IRD and pollen records, reflecting the most significant features of MIS 5e plotted against age. Note that the pollen data are plotted on a logarithmic scale. The data from core M23071 are shown in grey, the data from core M23323 in black. A mid-MIS 5e cooling is only clearly registered in core M23323, by a return to nearly glacial abundance values of *Neogloboquadrina pachyderma* (s) (E. Kandiano, unpublished data), and an apparently contradictory peak of *Spiniferites mirabilis* s.l. (see main text for discussion). Favourable marine conditions are recognised late in MIS 5e, as indicated by the co-occurring peaks (shaded) of *S. mirabilis* s.l. and the subpolar foraminifera *Turborotalita quinqueloba* and *Globigerina bulloides*. Also notice the remarkable match of the *S. ramosus* s.l. record in both cores, and also of *Nematosphaeropsis labyrinthus* during the transition towards MIS 5d. Note furthermore the phase relation of *N. labyrinthus* and *N. pachyderma* (s), illustrating the cooling towards MIS 5d, and the antiphase behaviour of *S. ramosus* s.l. and *N. pachyderma* (d).

2.6 Conclusions

Dinocyst assemblages studied in two cores located at the Vøring Plateau in the eastern Norwegian Sea provided good insight in the environmental changes that occurred in the surface waters in the area from latest Termination II across MIS 5e into the transition towards MIS 5d. Occasional appearances of warm-temperate species during Termination II, at times with still considerable IRD input, reveal first pulses of warm water into the area. Especially noteworthy is the significant abundance of the neritic species *L. machaerophorum* during this phase, which would indicate that quite particular water masses flooded the Vøring Plateau at that time. A shift from the inflow of coastal towards more open marine, Atlantic water masses is suggested by the drastic relative abundance increase of *O. centrocarpum* exactly when *L. machaerophorum* practically disappears from the assemblages. At the same time, IRD drops drastically. This indicates the start of the last interglacial *sensu stricto* (i.e. with low or no IRD), at around 123.5 ka, as also suggested by planktic foraminiferal data (data produced by H. Bauch and E. Kandiano). The dominance of *O. centrocarpum* from that time on implies that the eastern Norwegian Sea was continuously influenced by inflowing warm Atlantic water, but short-term fluctuations among the subordinate species reveals that sea surface conditions underwent subtle changes in the course of MIS 5e. The assemblage variability among dinocysts during MIS 5e contrasts sharply with the stable assemblage composition of the last 7 kyr (Baumann & Matthiessen 1992).

A marked reappearance of IRD and drastic decrease of subpolar planktic foraminifera in core M23323 around 120.5 ka would imply a significant cooling at that time (E. Kandiano, unpublished data). However, such a cooling is not seen in the dinocyst assemblages – the slight increase of *S. mirabilis* s.l. would in fact rather suggest a warming. Presumably, the renewed meltwater input and subsequent stratification allowed the surface waters to take up heat more easily, creating favourable conditions for *S. mirabilis* s.l. in late summer, whereas the planktic foraminifera remained relatively unaffected by the seasonal warming in the uppermost ocean. This feature indicates that different fossil groups can express a climatic event in a dissimilar way, as a consequence of ecological constraints that oblige them to inhabit different water masses and/or depths. This phenomenon clearly stresses the usefulness of combining different proxies for detailed palaeoceanographic reconstructions.

A comparison of the samples from the last interglacial *sensu stricto* with core-top samples and published Holocene dinocyst data at the Vøring Plateau revealed the existence of markedly different hydrological conditions in the upper water column of the Norwegian Sea for both interglacial periods. The assemblage compositions, as well as best-analogue

reconstructions based on them, suggest a more pronounced seasonality of the surface water and a more strongly stratified upper water layer existed during MIS 5e, further implying surface circulation was different during this time. The difference is expressed in the dinocyst data in two direct ways: firstly by *B. tepikiense*, an abundant species in seasonally stratified water masses, which is at present nearly absent in the Norwegian Sea, but constitutes a sizeable fraction of the last interglacial assemblages; secondly by a higher diversity in the last interglacial assemblages, opposed to the practically bi-specific assemblages of the last 7 kyr. Additional evidence for different hydrological surface conditions provided by the dinocyst assemblage data comes from the transfer function reconstructions. These reconstructions show reduced salinities and greater seasonal differences in SST and SSS for the first ~5 kyr of MIS 5e (*sensu stricto*) compared to the late Holocene.

It is conceivable that the evolution of the upper water layer during the last interglacial was dissimilar to that of the Holocene, in spite of the oft-cited “analogous boundary conditions.” The prolonged influence of Termination II, delimited by IRD and thus indicating freshwater input continuing to 119 ka, largely prevented the development of an upper water circulation similar to today. The marine optimum was reached only after IRD input had ceased completely; i.e. from ~117.5 to 116.5 ka, as suggested by a marked peak of the warm-temperate dinocyst *S. mirabilis* s.l. coeval with peak abundances of subpolar planktic foraminifera. This late development of the last interglacial optimum is in contrast to the early climatic optimum of the Holocene. The $\delta^{18}\text{O}$ values characterising the MIS 5e climatic optimum are comparable with the average Holocene values, suggesting that the lighter oxygen isotopes typifying the earlier phases of MIS 5e do not reflect optimal interglacial conditions, but rather the existence of a differently structured ocean surface compared to the Holocene.

Southeastern Fram Strait

Core M23455

Core site M23455 is situated in the southeastern Fram Strait, off the southwestern coast of Spitsbergen (Svalbard) (Fig. 1.1). The core underlies the pathway of the WSC, the northern prolongation of the NC as its warm surface waters pass on to Fram Strait and into the Arctic Ocean. The core is thus ideally located to evaluate the northward heat flow towards the Arctic during the last interglacial, and should allow to assess the changes in the WSC as it flows clockwise around Spitsbergen towards the site of a dinocyst study by Matthiessen & Knies (2001) at the northern Barents Sea margin.

3.1 Core location and lithology

Core M23455 was retrieved from 2497 m water depth, at 76°51'N and 8°22'E (Pfannkuche et al., 1993). Surface waters at the site have at present winter and summer temperatures of 1.5 and 5.3°C, and salinities of 34.9 and 34.8, respectively (Boyer et al., 2006). The studied section of core M23455 mainly consists of bioturbated, greyish-brown, foram-dominated fine-sandy silt, with numerous millimetre-sized sediment pellets and dropstones, especially in the upper part.

3.2 Core stratigraphy

The rough stratigraphic subdivision of gravity core M23455-3 is based on planktic oxygen isotope records retrieved from *N. pachyderma* (s) (Kottke, 1998, 1999) aligned to the SPECMAP stratigraphy (Martinson et al., 1987). Lightest values clearly indicate the position of the Holocene and MIS 5e (Fig. 3.1). IRD was counted and the oxygen isotope curve was refined with additional isotope analyses at a 0.5 cm interval for the section from 290.25 to 320.75 cm core depth, which includes the interval from late Termination II to MIS 5d (LIONS project framework). The isotope measurements were carried out at the isotope laboratory at IFM-GEOMAR with a CARBO KIEL automated carbonate preparation device linked to a Finnigan MAT 252 mass spectrometer. The analytical accuracy of this system is ± 0.03 ‰ for $\delta^{18}\text{O}$ and all measurements were calibrated on the Pee Dee Belemnite isotope scale (PDB).

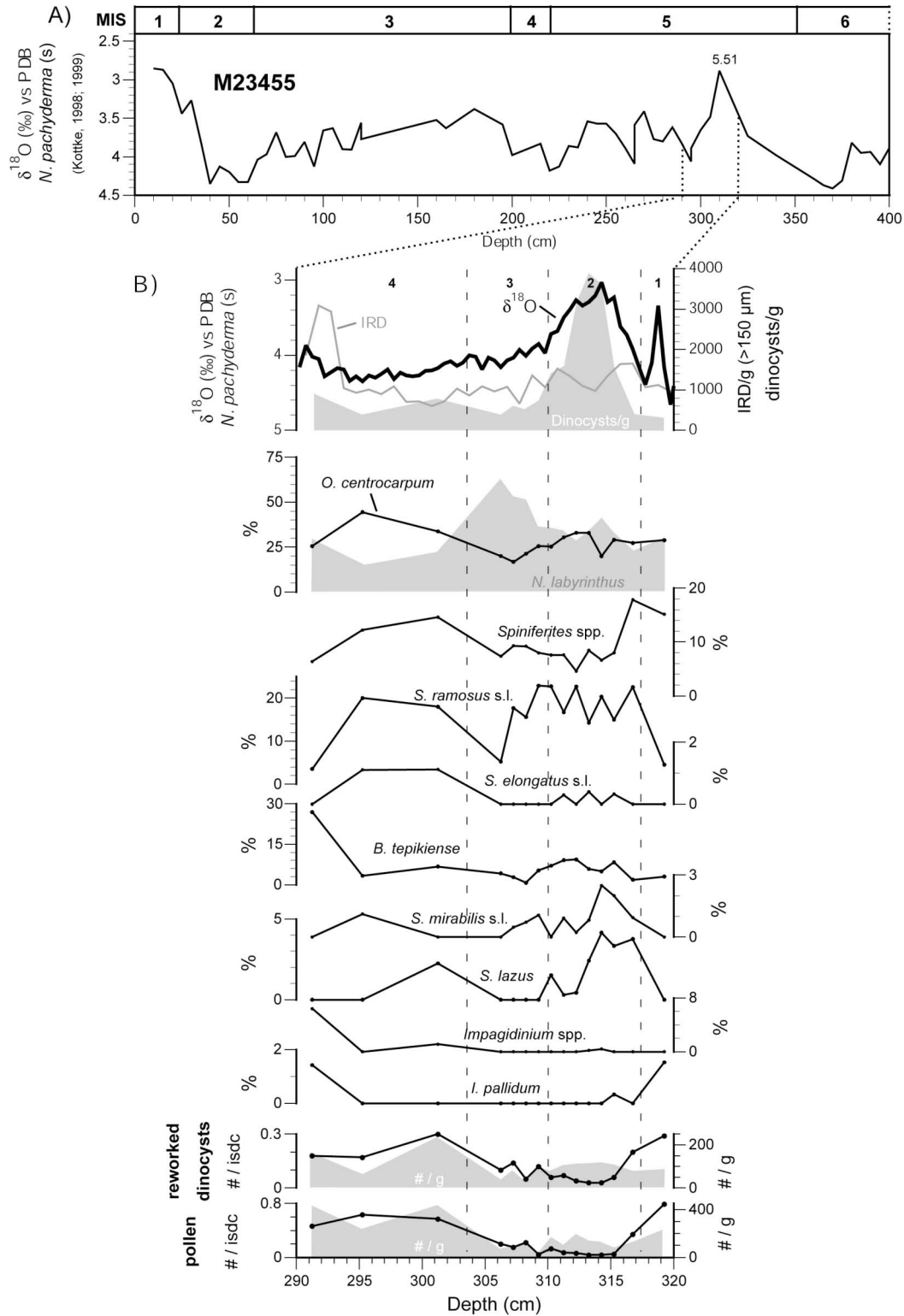


Fig. 3.1: (A) Planktic foraminifer stable oxygen isotope stratigraphy of core M23455, plotted against depth (Kottke, 1998, 1999). Lightest values clearly indicate the position of the Holocene and MIS 5e (B) Oxygen isotopes, ice rafted debris (IRD), and total concentrations and relative abundance fluctuations of the most abundant dinocyst species, reworked dinocysts, and pollen grains throughout the studied interval of core M23455, plotted against depth. Also shown is the division of the studied section into zones, as discussed in the text. "isdc"= in situ dinocysts.

3.3 Results

3.3.1 Qualitative results

Cyst concentrations proved to be low in all samples, varying between 63 and 3869 cysts per dry gram of sediment (<150 µm) (Fig. 3.1). Because of this, and because only a small amount of sediment was available, a statistically significant number of cysts (300 or more; Mertens et al., submitted) could only be counted in samples 311.25 to 313.25 and 315.25. Nevertheless, all samples with a minimum of 100 cysts determined on species level are considered in the discussion. Samples with very low cysts counts (80 and less) were grouped together in some intervals. Values for absolute and relative cyst abundances were then calculated from those grouped samples and considered representative for the assemblage composition in that specific interval. Details can be found in Table 3.1.

Based on the absolute and relative abundance changes of the dinocysts, 4 zones can be distinguished in the studied section (Fig. 3.1). Other, non-dinocyst or -pollen palynomorphs, such as invertebrate eggs and remains of chlorophycean algae (*Botryococcus* spp., *Pediastrum* spp., *Pterospermella* spp.) were present throughout the entire section, albeit without any clear trends in the absolute abundances. The presence of these algal cells, however, indicates that continental freshwater sediment sources continuously affected the area (e.g. Mudie, 1992; Matthiessen et al., 2000) – as also obvious from the presence of IRD across the entire interval. The raw data from the palynomorph analysis can be found in Appendix B4.

Table 3.1: Number of cysts counted in the original samples, and "combined sample" depths for core **M23455**.

sample depth (cm)	cysts counted	"combined sample" depth (cm)
290.25	68	291.25
292.25	78	
294.25	36	295.25
296.25	57	
298.25	24	301.25
300.25	31	
302.25	17	
304.25	21	
306.25	100	306.25
307.25	113	307.25
308.25	149	308.25
309.25	193	309.25
310.25	209	310.25
311.25	344	311.25
312.25	478	312.25
313.25	514	313.25
314.25	246	314.25
315.25	327	315.25
316.25	66	316.75
317.25	45	
318.25	60	319.25
320.25	17	

Zone 1: 320.25 – 317.75 cm core depth

The lowermost zone has low absolute cyst concentrations (< 250 cysts/g) and species diversity. The dinocyst assemblages mainly consist of *O. centrocarpum*, *N. labyrinthus*, *Spiniferites* spp. and cysts of heterotrophic taxa (indeterminable peridinioids, *Lejeunecysta* spp. and *Trinovantedinium applanatum*). Samples from the lowermost interval furthermore contained high amounts of plant pollen and spores and reworked dinocysts (Fig. 3.1).

Zone 2: 317.25 – 310.25 cm core depth

Cyst concentrations increase with an order of magnitude in the second zone, with a maximum of 3869 cysts/g. The interval is characterised by the lightest oxygen isotopes and lowest amounts of pollen/spores and reworked dinocysts. *Operculodinium centrocarpum* and *N. labyrinthus* remain the dominant species, with *S. ramosus* s.l. being the third-most abundant species. *Bitectatodinium tepikiense* constitutes on average $\pm 8\%$ of the assemblages. The warm species *S. mirabilis* s.l. and *S. lazus* have a low-percentage but marked abundance peak in the second interval.

Zone 3: 309.75 – 303.75 cm core depth

The oxygen isotope values in the third zone are substantially higher compared to the previous interval and fluctuate around 4‰. Absolute dinocyst concentrations are again at low values, whereas spores/pollen and reworked cysts become more abundant again. The most distinct feature in the dinocyst assemblages is the dominance of *N. labyrinthus*, which increases mainly at the expense of *S. ramosus* s.l.

Zone 4: 303.25 – 290.25 cm core depth

Many samples from the uppermost interval revealed very low absolute cyst concentrations, which necessitated combined samples in order to attain cyst counts acceptable for statistical interpretation of the data (Table 3.1). Stable oxygen isotope values increase an additional $\sim 0.3\%$, but become lighter again towards the top of the studied interval. This trend towards lower $\delta^{18}\text{O}$ values coincides with an increase of IRD content. The uppermost interval is characterised by high amounts of plant pollen/spores and reworked dinocysts. In the in situ assemblages, *O. centrocarpum* replaces *N. labyrinthus* as the dominant species. *Spiniferites* spp. and *S. ramosus* s.l. are the other most abundant taxa. The uppermost (combined) sample reveals a relative abundance over 25% of *B. tepikiense*, and a $\sim 6\%$ peak occurrence of *Impagidinium* spp.

3.3.2 Transfer function analysis

The modern analogue transfer function technique (de Vernal et al., 2001, 2005) as explained in §1.3.4, was applied on the dinocyst dataset. Although 5 analogues could be found for nearly all (combined) samples, their distances to modern assemblages are usually not far below the threshold value, and the reconstructed temperatures appear unrealistically high (i.e. summer and winter SSTs around 7 and 12°C, respectively, or about 6°C above the modern temperatures at the core site). Core-top assemblages of the high northern latitudes usually contain high amounts of cysts produced by heterotrophic taxa, such as *Brigantedinium* spp. and *Islandinium minutum* s.l. The absence of these cysts from the fossil assemblages, probably due to aerobic decay (Zonneveld et al., 2008), might add to the explanation why consistently higher temperatures are reconstructed. Therefore, a run was done in which cysts from heterotrophic taxa were excluded from the modern and fossil dataset. However, distances again were close to the threshold value, and generally fewer analogues could be found within the modern database. Although winter SSTs were slightly lower compared to the “complete” run, they still remained a questionable 3 to 5.5°C above modern temperatures, whereas summer SSTs did not change at all. More regionally confined runs were done on both the “complete” and the “filtered” datasets for which only modern assemblages north of 65°N were considered, but these, perhaps surprisingly, hardly yielded any analogues. Hence, the results from the transfer function analyses will not be considered in the discussion.

The outcome from this statistical exercise can be found in Appendix C1.

3.4 Discussion

Unfortunately, the low temporal resolution and cyst abundances of the studied section of core M23455 hamper a detailed palaeoceanographic reconstruction for MIS 5e in the southeastern Fram Strait. The low cyst abundances in part reflect the harsh conditions (lower salinities with difficult light regimes due to sea ice cover and high suspension load) in the area during the particular intervals, impeding high primary productivity, but are likely also (partly) due to the low sedimentation rates characterising core M23455. These probably prevented the cysts from becoming buried below the oxygenised upper centimetres of the bottom sediments for a considerable time, leaving them susceptible to aerobic degradation (Zonneveld et al., 2008; see §1.3.2). This might explain why all samples, with exception of the lowermost one, did not yield any cysts from heterotrophic species, despite the fact that these cysts are common in core-top sediments of the area (e.g. Rochon et al., 1999; Marret & Zonneveld, 2003; Baumann, 2007). In fact, high sediment input during the latest deglacial phases might be the reason why some peridinioid

cysts were preserved in the lowermost sample. Interestingly, samples from latest Termination II in a core at the northern Barents Sea margin northeast of Svalbard also yielded high amounts of peridinioid cysts (Matthiessen & Knies, 2001).

3.4.1 The last interglacial optimum in the southeastern Fram Strait

It is apparent from the data that the second interval, from 317.25 to 310.25 cm core depth, covers the sediment section deposited during the “real” interglacial phase with warmest conditions: the maximum of cyst concentrations and noteworthy abundances of a number of temperate species within the plateau of light $\delta^{18}\text{O}$ values represents a clear interglacial signal (Fig. 3.1). As IRD content within the second interval is not significantly different from the under- and overlying core sections, it can be excluded that the light isotopes are solely caused by meltwater overprint on the isotope data.

Last interglacial dinocyst assemblages in core PS2138 at the northern Barents Sea margin (Fig. 1.1; Matthiessen & Knies, 2001; Matthiessen et al., 2001) have a species composition comparable to those from the interglacial optimum in core M23455, albeit that there are some distinct differences in the relative abundances. As in core M23455, the last interglacial section at the Barents Sea margin is characterised by an increase of *S. ramosus* s.l., but the species constitutes only ~5% of the assemblages there, in contrast to the ~20% in core M23455. In general, all subordinate and rare species have lower relative abundances in core PS2138 with respect to M23455. This can be attributed to the fact that *O. centrocarpum* already makes up over 70% of the assemblages in PS2138, whereas the species dominates the assemblages of core M23455 together with *N. labyrinthus* with relative abundances of only ~30%. The relation of *O. centrocarpum* to the advection of warm Atlantic water (e.g. Harland, 1983; Matthiessen, 1995; Rochon et al., 1999), and the lower abundances of the cold taxa *Brigantedinium* spp. and *Impagidinium pallidum* in the MIS 5e section of core PS2138 with respect to surface samples from the continental slope nearby (Mudie, 1992), made Matthiessen & Knies (2001) suggest that SSTs during MIS 5e might have been warmer than today. Three aspects have to be taken into account, though. Firstly, *I. pallidum* is considered a typical open oceanic species (Matthiessen, 1995; Dale, 1996; Rochon et al., 1999), and the lower abundance in the MIS 5e samples could therefore also have resulted from less-oceanic conditions in the area at that time. Secondly, the polar species *Islandinium minutum* s.l. then again is not less abundant in the MIS 5e samples of core PS2138. Most relevant is the fact that high concentrations of *O. centrocarpum* can also result from the opportunistic character of the cyst-producing dinoflagellate, which moreover is known to have a high cyst yield (i.e. the number of cysts produced for a given number of motile cells in the plankton; Dale, 1976). This feature can

allow *O. centrocarpum* to quickly dominate the fossil assemblages, also under adverse conditions.

Clear evidence for warm conditions during MIS 5e is nevertheless presented in core M23455 by the marked abundances of *S. mirabilis* s.l. and *S. lazus* (Fig. 3.1). The relative abundances of both warm species are much higher than for MIS 5e at the Barents Sea margin (Matthiessen & Knies 2001), as well as in core-top sediments from the northern Greenland Sea and Fram Strait area influenced by North Atlantic waters (Rochon et al., 1999; Marret & Zonneveld, 2003; Baumann, 2007). The progressive development of favourable interglacial conditions at core site M23455 appears to be reflected in the arrival of *S. lazus* shortly before *S. mirabilis* s.l. peaks, a feature that is also observed in core M23323 from the Vøring Plateau (Fig. 3.2; see CHAPTER II). Several studies have illustrated how *S. mirabilis* s.l. attained its highest relative abundances during the second half of MIS 5e (Eynaud, 1999; Eynaud et al., 2000, 2004; Sánchez-Goñi et al., 1999, 2000; Penaud et al., 2008; Van Nieuwenhove & Bauch, 2008; Van Nieuwenhove et al., 2008; see CHAPTER II for the latter two studies). Accordingly, the late phase of MIS 5e was interpreted to represent the real, fully marine interglacial optimum in the Nordic seas. Considering the sizeable occurrence of *S. mirabilis* s.l. in the MIS 5e section of core M23455, far north of the species' modern distribution area, and its timing with respect to the *S. lazus* abundance maximum, it can be suggested that only the late, peak interglacial interval is represented in the sediments from site M23455 (Fig. 3.2). This assumption agrees well with planktic foraminiferal findings from core M23455, which show a sole major increase of the warm-water indicative species *T. quinqueloba* within and shortly after the plateau of light oxygen isotopes (E. Kandiano, unpublished data). The coeval peak abundance of *S. mirabilis* s.l. and *T. quinqueloba* is a distinctive feature of the late MIS 5e optimum at the Vøring Plateau (CHAPTER II). In accordance with the data from the Vøring Plateau, it thus seems as if the sizeable deglacial processes during Termination II and early MIS 5e (Spielhagen et al., 2004; Svendsen et al., 2004) only allowed interglacial conditions to develop in the Fram Strait area during the late MIS 5e optimum, when a modern type of surface circulation with enhanced northward heat transport existed in the Nordic seas. The early phase of MIS 5e at the southern Barents Sea margin (i.e. in between the cores from the Vøring Plateau and core M23455) reveals raised abundances of *N. labyrinthus* and *I. pallidum* (Baumann, 2007), supporting the stepwise expansion of interglacial conditions northward along the pathway of the NC as MIS 5e progressed.

It can be argued that the northward heat transport was confined to a small corridor in the eastern Fram Strait (Hebbeln & Wefer, 1997), nevertheless bringing favourable interglacial conditions into the Arctic (Hald et al., 2001; Spielhagen et al., 2004). The higher portion of

warm dinocysts in core M23455 with respect to the northern Barents Sea margin (Matthiessen & Knies, 2001) suggests a considerable surface water temperature gradient along the flow path of the NC/WSC with zonal recirculation of Atlantic surface waters southwest of Svalbard, in compliance with the scenario proposed by Bauch et al. (1999).

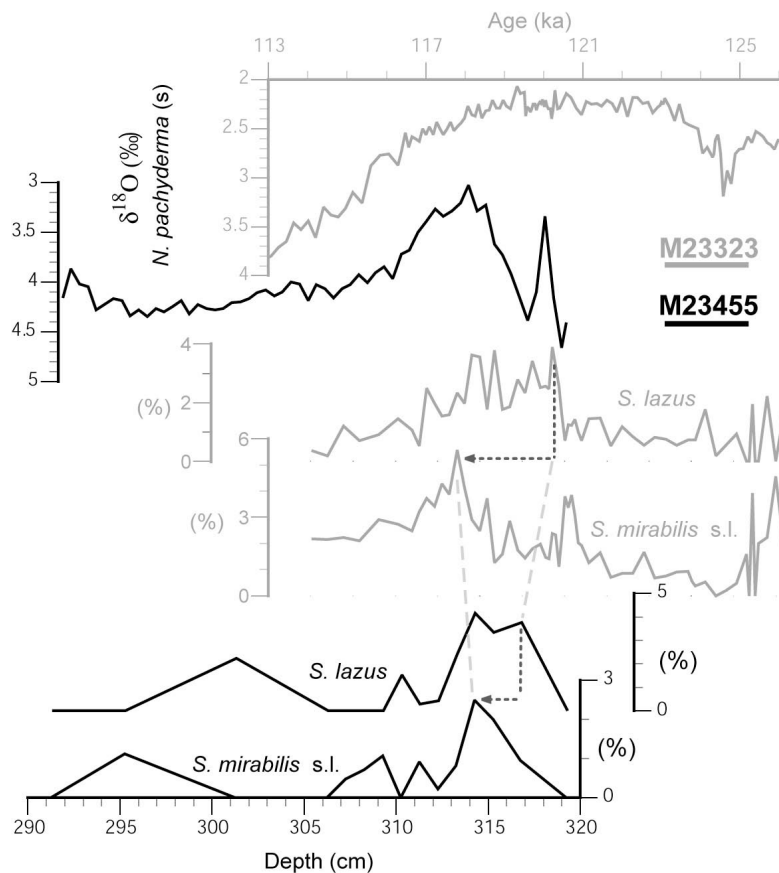


Fig. 3.2: Suggested correlation of the last interglacial section of core M23455 from the southeastern Fram Strait, against depth (black curves), with the records of core M23323 from the Vøring Plateau, against age (grey curves). The stratigraphic position of the *Spiniferites lazus* peak, appearing before the acme of *S. mirabilis* s.l., as well as the quantitative aspects of the peaks in core M23455, compared to core M23323, suggest that only during the late MIS 5e marine optimum, as known from the eastern Norwegian Sea, a typical interglacial environment could develop in the upper ocean of the southeastern Fram Strait.

3.4.2 Transition to stadial conditions

Increasing input of terrestrial plant and reworked material, and dominance of *N. labyrinthus* in the third interval, after the phase of highest productivity, reflect the transition from the interglacial towards the colder stadial MIS 5d (Fig. 3.1). Comparably, a changeover towards assemblages dominated by *N. labyrinthus* in relation to the MIS 5e-5d transition was also observed by Matthiessen & Knies (2001) in core PS2138 from the Barents Sea margin. This once more confirms the association of *N. labyrinthus* with transitional climatic

periods (Baumann & Matthiessen, 1992; Eynaud et al., 2004). The ability of *O. centrocarpum* to quickly exploit favourable seasonal conditions probably explains why the species becomes dominant again afterwards, (presumably) during early MIS 5d. The relative proportions of *O. centrocarpum* and *N. labyrinthus* in this interval of core M23455 compare well with the core-top assemblage of PS1295 (Baumann & Matthiessen, 1992; Matthiessen & Baumann, 1997) situated northwest of core site M23455 in the (colder) Arctic Domain, albeit that there are some marked differences between both cores concerning the subordinate species. The palaeoceanographical significance of the fluctuations among the secondary species within this interval should be questioned in view of the low cyst counts from the respective samples. Still, the increasing IRD content followed by lighter oxygen isotopes points towards enhanced freshwater input, probably causing more pronounced seasonal stratification for this time interval, as suggested by the high relative abundances of *B. tepikiense* in the uppermost samples.

3.5 Conclusions

Low cyst concentrations and species diversity in the samples from the southeastern Fram Strait reveal that relatively harsh conditions prevailed during most of the time covered by the sediment section studied. More favourable, interglacial conditions only existed for a short time. Their arrival shows from the important presence of *S. lazus*, followed by a relative abundance peak of *S. mirabilis* s.l. Taking into account the quantitative and stratigraphic characteristics of the abundance maximum of both species, it seems that only the late, peak interglacial interval as known from the eastern Norwegian Sea is expressed in the sediments from the southeastern Fram Strait. Planktic foraminiferal data from core M23455 appear to confirm this assumption (E. Kandiano, unpublished data). Hence, it seems as if the extensive deglacial processes from late Termination II and early MIS 5e prevented typical interglacial conditions from developing in the southeastern Fram Strait during the first half of MIS 5e. It was only when a modern type of surface circulation with enhanced northward heat transport developed in the Nordic seas, that a typical interglacial environment could build up in the Fram Strait area.

The MIS 5e dinocyst assemblages from core M23455 contain fairly high amounts of warm-indicative species in comparison with both core-top samples from the area and with last interglacial assemblages from further north at the northern Barents Sea margin. This suggests a strong temperature gradient across the Fram Strait along the (modern) pathway of warm Atlantic water masses as they move into the Arctic Ocean. Hence, northward heat transport through the Fram Strait was probably confined to a small corridor in the eastern

Fram Strait, with the main portion of the warm surface water masses recirculating zonally southwest of Svalbard.

After the thermal optimum, surface water conditions rapidly deteriorated towards the cold stadial MIS 5d. As has also been noticed in records from elsewhere (see CHAPTER II), the transition is marked by a steady increase of the relative abundance of *N. labyrinthus*. Freshwater input stratifying the upper ocean probably occasionally created relatively favourable conditions afterwards, allowing “warmer” elements to appear from time to time in the area.

Eastern Iceland Plateau (Norwegian Sea)

Core MD992277

Piston core MD992277 was taken at the eastern slope of the Iceland Plateau, in the western Norwegian Sea (Fig. 1.1). The core site is situated near the present position of the Arctic front, at the outer reaches of cold water masses originating from the EGC. Core MD992277 is thus well suited to trace the western expansion of Atlantic waters within the Nordic seas.

4.1 Core location and lithology

Piston core MD992277 was recovered during the IMAGES V campaign from 2800 m water depth, at 69°15'N and 6°19'W (Labeyrie & Jansen, 2003). Surface waters at the site have at present winter and summer temperatures of 1.8 and 6.7°C, and salinities of 34.9 and 34.7, respectively (Boyer et al., 2006). The interglacial intervals consist of relatively light-coloured greyish-brown clay and sandy mud with high carbonate content, bracketed by sections rich in dropstones.

4.2 Core stratigraphy and age model

No complete oxygen isotope record is available for core MD992277. The stratigraphic framework of the upper 10 meter of the core was therefore established through correlating X-ray fluorescence (XRF) Ca-counts from core MD992277 with carbonate content from the nearby core PS1243, which has an established age model for the last ~450 kyr based on multiple sedimentological records (Fig. 4.1; see Helmke et al., 2005, for more details and references). According to the correlation with core PS1243, MIS 5e is represented in core MD992277 by the interval from around 370 to 430 cm core depth (Fig. 4.1). Oxygen isotope and IRD analyses were conducted in 1 cm steps for the interval from MIS 5d across MIS 5e into Termination II (LIONS project framework). The isotope measurements were carried out at the isotope laboratory at IFM-GEOMAR using a CARBO KIEL automated carbonate preparation device linked to a Finnigan MAT 252 mass spectrometer. The analytical accuracy of this system is ± 0.03 ‰ for $\delta^{18}\text{O}$ and all measurements were calibrated on the Pee Dee Belemnite isotope scale (PDB).

An age model for core MD992277 for the time period from ~105 to 135 ka was developed by correlating marker points in the $\delta^{18}\text{O}$ and IRD record with those records from core PS1243, and linear interpolation between the marker points (Figs. 2.2 & 2.3; Table 4.1) (Appendix A). Major IRD events within the sediment sections of both cores can be assumed to have happened (as good as) synchronously, considering the close vicinity of the core sites.

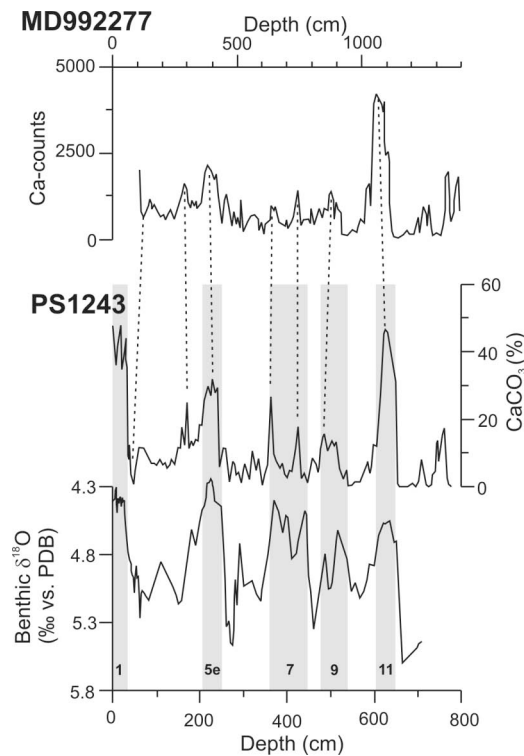


Fig. 4.1: Correlation of MIS 5e in core MD992277 with core PS1243 based on calcium (carbonate) content. MIS 5e is represented in core MD992277 by the interval from around 370 to 430 cm core depth (from Helmke et al., 2005).

4.3 Results

4.3.1 Qualitative results

Absolute cyst concentrations proved to be very low in all the analysed samples, varying between 120 and 1736 cysts per gram dry sediment (<150 μm) (Fig. 4.2). Still, in spite of the large amount of sediment processed (~4-10 g), only a low number of cysts could be counted per sample. It became clear during microscopy work that the major part of the residue left after palynological processing consisted of mineral and amorphous organic material. This material had not been removed during maceration because the use of destructive agents (H_2O_2 , warm HF) was avoided in order not to destroy any palynomorphs. Presumably, the polymer mesh got clogged to a certain extent during sieving, and a considerable amount of palynomorphs remained on the sieve, despite extensive rinsing.

Furthermore, the amorphous organic material often formed a film that was difficult to break down and partly adhered to the sieve tubes. This explains why only a fraction of the added *Lycopodium clavatum* spores was encountered during counting, even though the complete residue had been mounted on slides and studied under the microscope. The loss of material (both *L. clavatum* spores and palynomorphs) is inherent to palynological processing, and the ratio of palynomorph losses with respect to the loss of *L. clavatum* spores depends on the specific techniques applied (Mertens et al., submitted). However, the latter study also proved relative abundances to be reproducible, implying that species are not being lost selectively.

Table 4.1: Number of cysts counted in the original samples, and "combined sample" depths with their respective interpolated ages, for core **MD992277**.

sample depth (cm)	cysts counted	"combined sample" depth (cm)	Age (ka)
361.5	108	361.5	113.41
363.5	90	363.5	113.84
365.5	215	365.5	114.28
367.5	192	367.5	114.71
369.5	160	369.5	115.15
371.5	73		
373.5	129	372.5	115.62
375.5	132	375.5	116.10
377.5	99	377.5	116.42
379.5	95	379.5	116.73
381.5	151	381.5	117.11
383.5	109	383.5	117.55
385.5	182	385.5	117.98
387.5	194	387.5	118.42
391.5	167	391.5	119.29
393.5	357	393.5	119.68
395.5	213	395.5	120.03
397.5	256	397.5	120.38
399.5	247	399.5	120.63
401.5	28		
403.5	111	402.5	121.01
405.5	133	405.5	121.40
407.5	145	407.5	121.65
409.5	66		
411.5	73	410.5	122.03
413.5	83		
415.5	44	414.5	122.54
417.5	58		
419.5	68	418.5	123.05
421.5	87	421.5	123.44
423.5	45		
425.5	49	425.5	123.95
427.5	33		
429.5	107	429.5	124.47
431.5	123	431.5	124.69
433.5	143	433.5	124.90
435.5	57		
437.5	62	437.5	125.33
439.5	30		
441.5	113	441.5	125.75
443.5	77	443.5	125.97

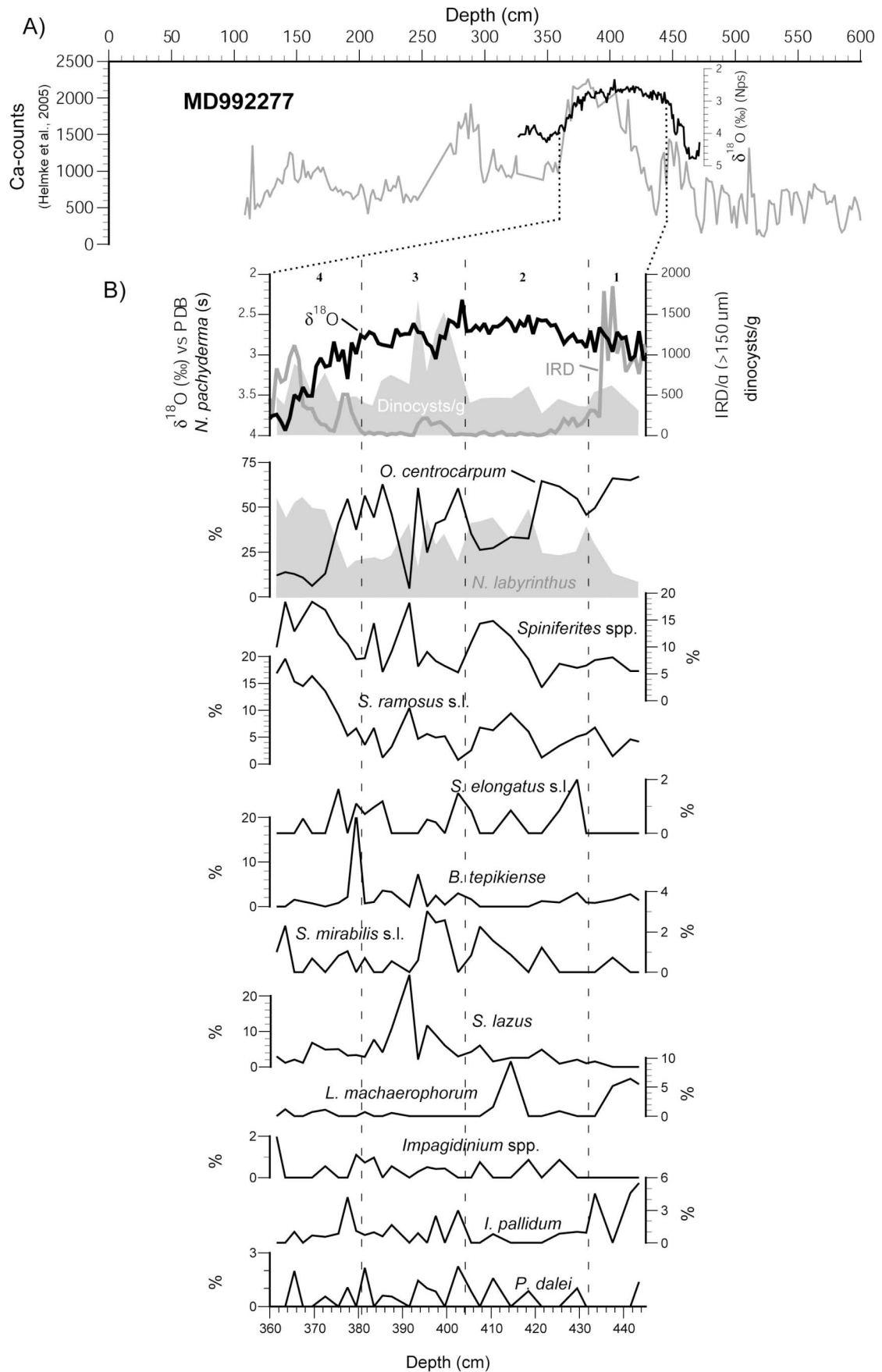


Fig. 4.2: (A) Stratigraphy of the upper 6 m of core MD992277 based on Ca-counts (Helmke et al., 2005), and high-resolution planktic $\delta^{18}\text{O}$ records for the interval from latest Termination II over MIS 5e into the transition towards MIS 5d, plotted against depth. (B) Oxygen isotopes, ice rafted debris (IRD), total cyst concentrations and relative abundance fluctuations of the most abundant dinocyst species in the studied interval of core MD992277, plotted against depth. Also shown is the division of the studied section into zones, as discussed in the text.

All samples where a minimum of ~90 cysts was counted were retained for evaluating assemblage composition changes. Samples had to be combined in some intervals in order to reach a statistically acceptable number of counted cysts. Relative and absolute abundances calculated from these grouped samples were then regarded representative for the specific interval. Details about the grouping can be found in Table 4.1.

Based on changes in assemblage composition, IRD content, and abundances of non-dinocyst palynomorphs, 4 zones could be distinguished within the studied interval (Figs. 4.2 & 4.3).

Zone 1: 443.5 – 433.5 cm core depth

High amounts of IRD, pollen and spores, remains of chlorophycean algae (*Botryococcus* spp., *Pediastrum* spp., *Pterospermella* spp.) and reworked cysts characterise the lowermost interval. *Operculodinium centrocarpum* dominates the dinocyst assemblages, which are completed by considerable abundances of *N. labyrinthus* and *Spiniferites* spp., and to a lesser degree by *L. machaerophorum* and *I. pallidum*.

Zone 2: 431.5 – 405.5 cm core depth

IRD content drops drastically from zone 1 into zone 2, but persists at low levels in the lowermost interval of the second zone. The dominance of *O. centrocarpum* also persists within the latter interval. After that, the relative abundance of the species drops, to be replaced by mainly *N. labyrinthus* and *Spiniferites* spp. Cysts of *P. dalei*, *Impagidinium* spp., *S. elongatus* s.l., *B. tepikiense* and *S. mirabilis* s.l. appear occasionally in zone 2, albeit always in low relative abundances. *Impagidinium pallidum* has its lowest abundances within zone 2, whereas *L. machaerophorum* shows a marked peak of nearly 10% at 414.5 cm core depth.

Zone 3: 402.5 – 381.5 cm core depth

The base of zone 3 shows a recurrence of IRD input, together with a relative abundance high of *S. mirabilis* s.l. and modest peaks of *I. pallidum*. The modest rise of absolute cyst concentrations in this interval should not be overinterpreted in the light of the discussion given under §4.3.1. A marked peak of *S. lazus*, accompanied from higher occurrences of *Spiniferites ramosus* s.l. and *Spiniferites* spp., directly follows the *S. mirabilis* s.l. plateau, and goes at the expense of *O. centrocarpum*, which had become dominant again over *N. labyrinthus*.

Zone 4: 379.5 – 361.5 cm core depth

The uppermost zone features a stepwise reappearance of larger amounts of IRD. A first input phase directly follows a curious acme of *B. tepikiense* and coincides with a subtle peak of *I. pallidum* and higher fluxes of chlorophycean algal cells (*Botryococcus* spp. and *Pediastrum* spp.). Planktic $\delta^{18}\text{O}$ values become higher throughout the uppermost interval. This trend is mirrored in the dinocyst assemblages by increasing relative abundances of *N. labyrinthus*, *S. ramosus* s.l. and *Spiniferites* spp., at the expense of *O. centrocarpum*.

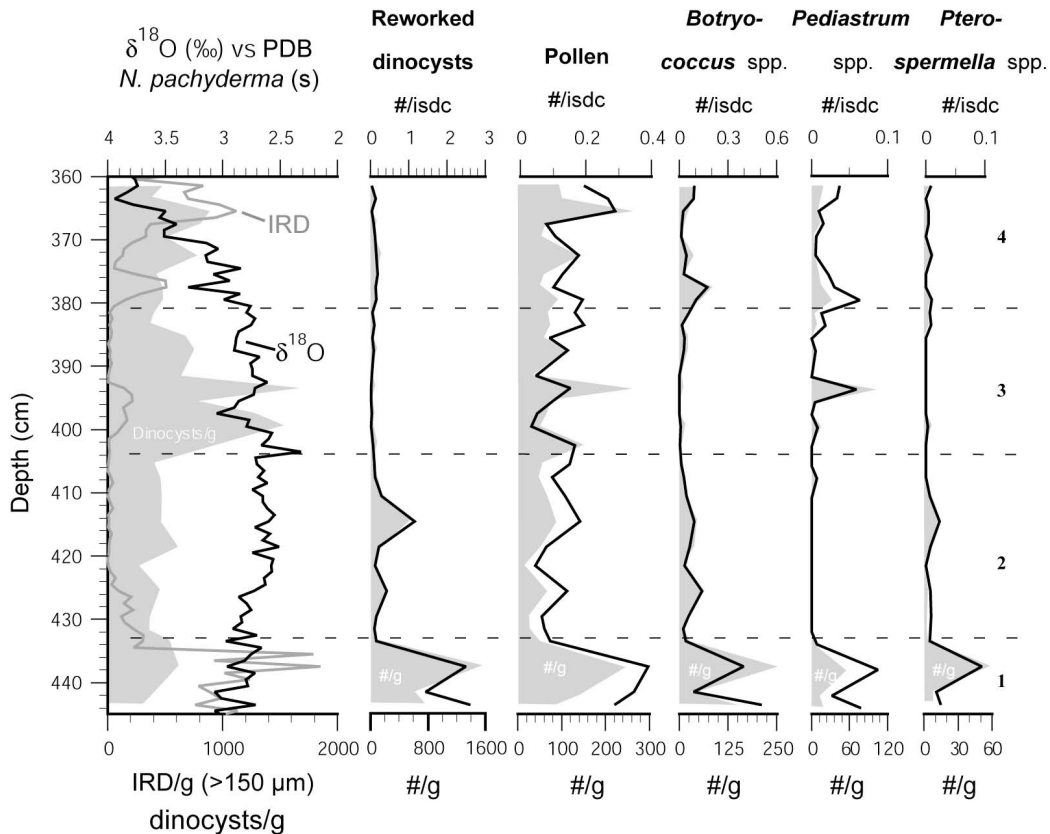


Fig. 4.3: Stable oxygen isotopes, ice rafted debris (IRD), absolute dinocyst concentrations, and abundances of reworked dinocysts, pollen, and chlorophycean algal cells in the studied section of core MD992277, plotted against depth. The shaded area indicates absolute concentrations per gram dry sediment, black lines the ratio of the respective palynomorph (group) to in situ dinocysts (isdc). Also shown is the division of the studied section into zones, as discussed in the text.

4.3.2 Transfer function analysis

Quantitative reconstructions were attempted by applying the modern analogue transfer function technique (de Vernal et al., 2001, 2005; see §1.3.4) on the dinocyst dataset. Five analogues could be found for most of the (combined) samples by the analysis, but the distances between the fossil and modern assemblage often proved to be close to the threshold value beyond which an analogue is rejected. Comparable to core M23455 (CHAPTER III), the reconstructions revealed questionably high SST values (i.e. summer and

winter SSTs around 6 and 10°C, respectively, which is about 4-5°C higher than modern temperatures at the core site and reconstructions for MIS 5e based on planktic foraminiferal assemblages (E. Kandiano, unpublished). This, and the fact that SST/SSS values fluctuate with several degrees/psu between adjacent samples, raises some concern about the reliability of the quantitative reconstructions. Interestingly, modern analogue reconstructions from core-top and latest Holocene dinocyst assemblages from the area (core PS1243) also tend to overestimate SSTs by several degrees (Baumann, 2007).

As for core M23455, a run was done without considering cysts from heterotrophic taxa (see §3.3.2 for rationale), but this did not reveal less questionable results. The outcome of the transfer function exercise will therefore not be included in the discussion, but does, however, point towards surface water conditions during MIS 5e at the eastern Iceland Plateau that have no close analogue in the modern dataset. More details about the quantitative analyses can be found in Appendix C2.

4.4 Discussion

The changes in the proxy records from core MD992277 nicely reflect the evolution of the last interglacial cycle, from latest Termination II over MIS 5e into the transition towards MIS 5d (Figs. 4.2 & 4.3). The data from core MD992277, in this respect, conform well to the records from the Vøring Plateau. A more detailed examination of the data, however, reveals some differences between both areas.

4.4.1 Latest Termination II (Zone 1)

The data from the lowermost zone apparently provide conflicting environmental signals, in containing both cold and warm indicators. This situation is similar to what is observed in the data from the Vøring Plateau for latest Termination II (CHAPTER II), and can be explained more or less in the same way. Occasional pulses of warm water interrupted cold conditions brought about by ice drifting into the area, and created more viable conditions with reduced sea ice cover for temperate dinoflagellate species. As in the eastern Norwegian Sea, the freshwater input from melting icebergs/sea ice is clearly evidenced by considerable quantities of terrestrially-derived material (IRD, reworked cysts, pollen & spores, and freshwater algae) (Fig. 4.3).

The disappearance of *L. machaeorophorum* and subsequent dominance of *O. centrocarpum* during the deglacial/interglacial transition at the Vøring Plateau was interpreted to suggest a shift in the physical properties and/or source area of the water masses reaching the eastern Norwegian Sea (see §2.5.1.1). In contrast, *L. machaeorophorum* persists in core MD992277 at times when *O. centrocarpum* already

dominates the assemblages (Fig. 4.2). The co-occurrence of both species is known from recent sediments (e.g. Persson et al., 2000) and thus not an unusual phenomenon. However, the mere presence of *L. machaerophorum* at site MD992277, and the timing of its appearance, is remarkable, given the neritic, temperate to tropical character of the species. In fact, *L. machaerophorum* has been recorded only once in sediments from open oceanic regions (Marret & Zonneveld, 2003). This provides strong evidence for quite particular warm water masses entering the Nordic seas, which is further supported by an equally enigmatic occurrence of the subtropical-temperate planktic foraminifer *Beella megastoma* during particular intervals of Termination II (Bauch, 1994, 1996; Bauch et al., 2000a; E. Kandiano, unpublished data). The presence of this “Atlantic” water mass indicator was far less pronounced and occurred much later or not at all in the eastern Norwegian Sea than at the Iceland Plateau. Bauch (1996) and Bauch & Erlenkeuser (2008) explained this by a thick freshwater lid from deglacial processes hindering the protrusion of these Atlantic waters into the eastern Norwegian Sea, what seems to agree with the low abundances of the NAD-related dinocyst *O. centrocarpum* during Termination II at the Vøring Plateau (see CHAPTER 2). In this scenario, the high numbers of *L. machaerophorum* for the latter time and area might have been brought in by the NCC, which is presumed to have been more influential at that time (Bauch & Erlenkeuser, 2008). The NCC originates from the Kattegat/North Sea area, where *L. machaerophorum* is abundant at present (e.g. Persson et al., 2000). Differing source areas for the warm water inflow can thus explain why only *L. machaerophorum* is abundant at the Vøring Plateau, whereas both dinocyst species *O. centrocarpum* and *L. machaerophorum* occur together with higher amounts of the planktic foraminifer *B. megastoma* during Termination II at the eastern Iceland Plateau. Further research, however, is needed to find out to what degree the appearance of *L. machaerophorum* is indeed related to the *Beella* events.

4.4.2 Early last interglacial (zone 2)

The onset of “real” interglacial conditions can be interpreted from the drastic drop in IRD at the base of zone 2, at ~124.5 ka (Figs 4.2 & 4.4). However, persisting input of IRD at low yet significant levels, and the rather low species diversity of the dinocyst assemblages reveals that conditions remained relatively harsh during the first phase of MIS 5e in the western Norwegian Sea. The relative abundances of *O. centrocarpum* suggest the presence of Atlantic water masses, but the high cyst yield and opportunistic character of the species (Dale, 1976; 1996) most likely also contributed to its dominance. Other species became more abundant after the virtual cessation of IRD input at ~123.5 ka, but the assemblages still contain rather low numbers of “warm taxa” (*Impagidinium* spp., *S. lazus* and *S. mirabilis* s.l.) when compared with early MIS 5e at the Vøring Plateau. Thus, an

Atlantic inflow into the Norwegian Sea existed during early MIS 5e, but the flux was not sizeable enough to engulf the Nordic seas with warm surface water masses also to the west of the main flow path of the NAD. This seems to contradict the scenario of a less pronounced meridionalism during MIS 5e as proposed by Bauch et al. (1999) and Knudsen et al. (2002). However, core-top assemblages from the central Nordic seas reveal relative abundances around 5% of the polar species *I. pallidum* (Baumann, 2007), which is considerably higher than what is seen in core-top samples from the Vøring Plateau (Baumann & Matthiessen, 1992) and in our MIS 5e material from both the eastern and western Norwegian Sea. Taken at face value, this would confirm a stronger east to west SST gradient during the latest Holocene compared to the last interglacial.

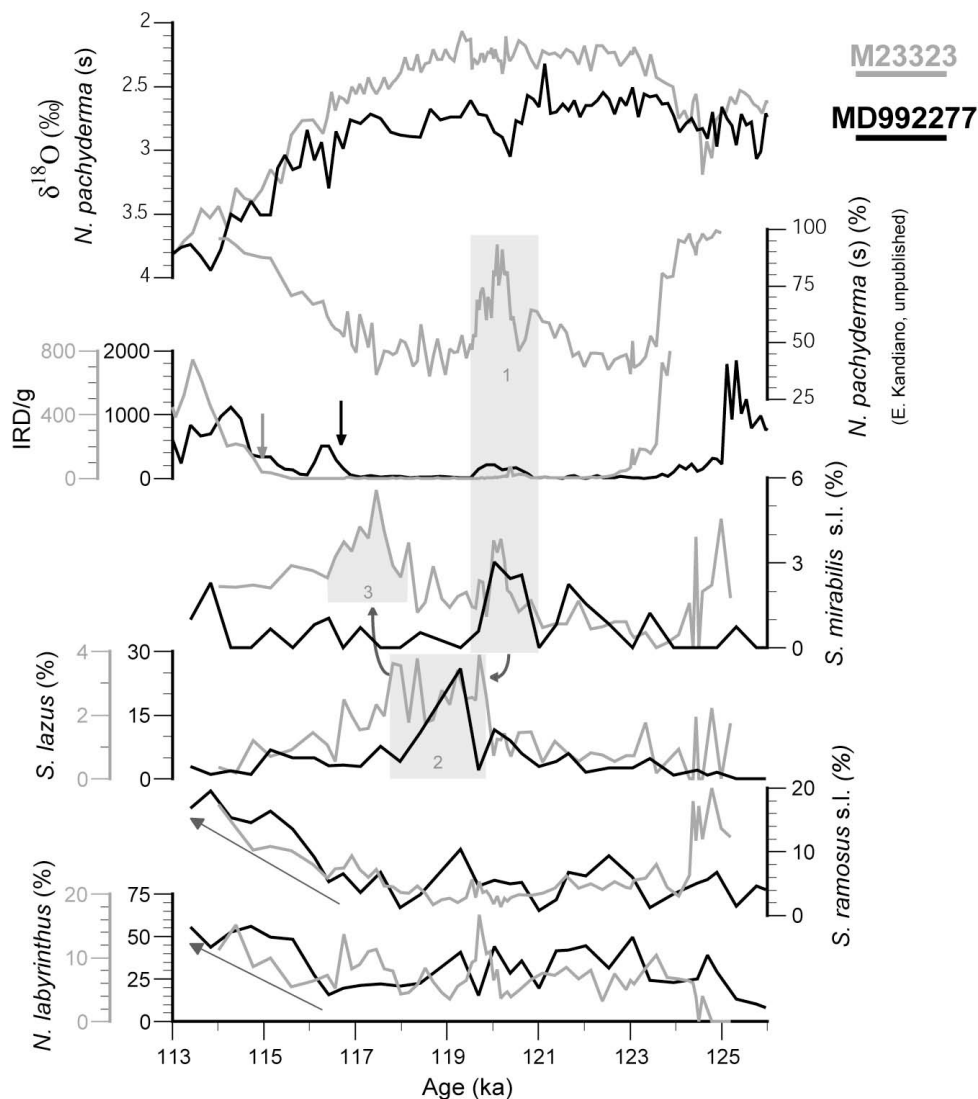


Fig. 4.4: Stable oxygen isotopes, ice rafted debris (IRD), and relative abundances of the polar planktic foraminifer *Neogloboquadrina pachyderma* (s) (E. Kandiano, unpublished data) and selected dinocysts in core M23323 (grey curves) and/or MD992277 (black curves), plotted against age, showing the differences and similarities of the MIS 5e development between the Vøring Plateau and Iceland Plateau. The mid-MIS 5e cooling (grey bar 1) is perceivable in the data from both cores, by a recurrence of IRD and slightly raised abundances of *Spiniferites mirabilis* s.l. This is followed by an abundance maximum of *S. lazus* (grey bar 2), but the late MIS 5e optimum, as suggested by the abundance maximum of *S. mirabilis* s.l., developed only at the Vøring Plateau (grey bar 3). Note furthermore the early return of IRD in core MD992277, and the good fit of the *S. ramosus* s.l. and *Nematosphaeropsis labyrinthus* curves in both cores, and the phased behaviour of both species during the transition towards MS 5d.

The cooler and seasonally less variable oceanic conditions for the first ~3.5 kyr of MIS 5e at site MD992277 with respect to the Vøring Plateau also tell from the higher relative abundances of *N. labyrinthus*, and lower relative abundances of *B. tepikiense* comparable with those in core-top sediments from the area (Baumann, 2007). Of all sites investigated in the study presented here and elsewhere (Matthiessen & Knies, 2001; Eynaud et al., 2004), MD992277 is most distally located from potential iceberg/sea ice sources, and although low amounts of IRD are present throughout the entire MIS 5e interval, a substantial freshwater input to create pronounced seasonality in the surface waters was lacking at the site during early MIS 5e.

4.4.3 Late last interglacial and MIS 5e/5d transition (Zone 3 and 4)

The relatively stable conditions from the early MIS 5e appear to be interrupted around ~120.5 ka, at the base of zone 3. *Impagidinium pallidum* is observed more frequently in this interval (Fig. 4.2), suggesting an increased influence of Arctic surface water masses (cf. Baumann, 2007). IRD and *Pediastrum* cells (Fig. 4.3) indicate that these cold water masses advected ice and thus freshwater towards the core site. The reappearing IRD in core MD992277 is associated with a marked increase of the polar planktic foraminifer *N. pachyderma* (s) (E. Kandiano, unpublished data). This feature is thus very similar to what is seen for mid-MIS 5e in core M23323 at the Vøring Plateau, and suggests a return towards much cooler conditions for that time. However, and again analogous to core M23323, the abundance increase of *S. mirabilis* s.l. within the IRD-enriched interval would suggest warming, rather than cooling (Fig. 4.4). As at the Vøring Plateau, the freshwater input likely created a stratified upper ocean that could take up heat more easily and thereby create favourable conditions for *S. mirabilis* s.l. in late summer, when the species blooms (Reid, 1978). As mentioned above, the stratification at site MD992277 was probably not as pronounced as at the Vøring Plateau, accounting for the low relative abundances of both *B. tepikiense* and *S. mirabilis* s.l.

The raised abundances of *S. mirabilis* s.l. within the IRD-rich section of core MD992277 followed by an increase of *S. lazus* is, again, a feature that was also observed in core M23323. Thus, the stratigraphic and quantitative aspects of this observation reveal that it represents the same event or time interval in both cores, as also suggested by our age model (Fig. 4.4). The rising occurrences of *S. lazus* were interpreted to indicate the start of the late MIS 5e optimum in the eastern Norwegian Sea, culminating between ~117.5 and 116.5 ka just prior to the MIS 5e/5d transition with a marked abundance maximum of *S. mirabilis* s.l. However, such a late acme of *S. mirabilis* s.l. or any other indication for peak interglacial conditions is not seen in the dinocyst data from core MD992277. On the

contrary, the relative abundance increases of *N. labyrinthus* and *S. ramosus* s.l. in association with renewed IRD input and increasing $\delta^{18}\text{O}$ values shortly after the *S. lazus* high (Fig. 4.2), reveal that the upper ocean was already in a transient state towards the colder stadial MIS 5d. Planktic foraminifera, on the other hand, do provide clear evidence for favourable, warm interglacial conditions for the time between the *S. lazus* high and the transition to MIS 5d (E. Kandiano, unpublished data).

The asymmetric response by the dinocyst assemblages in the eastern and western Norwegian Sea bears resemblance to alkenone-based Holocene findings from the Nordic seas. Alkenones used for SST reconstructions derive from marine algae, and thus in essence provide annually averaged temperatures for the same habitat depth as dinocysts. The Holocene data show that during times of enhanced warmth in the eastern Norwegian Sea (e.g. the mid-Holocene thermal optimum; Calvo et al., 2002), U_{37}^k -SSTs on the northern Iceland shelf decrease (Bendle & Rosell-Melé, 2007). At the same time, an increased IRD input is seen on the East Greenland Shelf (Jennings et al., 2002). Such observations are similar to the average situation during years with a positive mode of the North Atlantic Oscillation (NAO). Those years are characterised by an intensification of northerlies along the Greenland coast, negative SST anomalies in the western, and positive SST anomalies in the (north)eastern Nordic seas (e.g. Flatau et al., 2003). This led Bendle & Rosell-Melé (2007) to hypothesise the asymmetry between the eastern and western Nordic seas during the Holocene thermal optimum to be related to (shifts in) the atmospheric circulation and, thus, the mode of NAO. As pointed out by Bendle & Rosell-Melé (2007), though, it is unclear how and whether a decadal-scale phenomenon could explain millennial-scale climate fluctuations. Regardless, it seems reasonable that a more rigorous NAD/NC with enhanced advection of warm waters towards the Arctic Ocean during late MIS 5e intensified the outflow of cold surface waters from the Arctic. Possibly additionally strengthened by enhanced northerlies (Flatau et al., 2003), the EGC might have reached further south and southeast across the Iceland Plateau, advecting cold surface waters and sea ice/icebergs towards site MD992277. The early reoccurrence of IRD around ~117 ka already (Fig. 4.4), i.e. before the sharp increase of oxygen isotope values and accompanied by an abundance peak of *I. pallidum* (Fig. 4.2), appears to evidence the enhanced influence of the EGC at that time. The cold surface waters would also have extended the seasonal presence of sea ice, directly affecting the phytoplanktic communities living in the uppermost water layer. Such a set-up could thus explain why no late MIS 5e optimum is shown by the dinocyst assemblages in core MD992277, whereas the somewhat deeper living planktic foraminifera at first remained relatively unaffected by the cold

conditions in the uppermost surface waters. However, further high-resolution multi-proxy studies at the Iceland Plateau are needed to more precisely assess this scenario.

4.5 Conclusions

The dinoflagellate cyst assemblages from core MD992277 well reflect the environmental changes at the eastern Iceland Plateau from Termination II across MIS 5e into the transition towards MIS 5d. The evolution of the last interglacial cycle at first sight resembles what was seen in the eastern Norwegian Sea. However, detailed analysis reveals the existence of some significant differences with an asymmetric manifestation of the MIS 5e optimum between both sites.

The latest Termination II at the eastern Iceland Plateau reveals the enigmatic presence of the neritic, warm temperate dinocyst *L. machaerophorum*, a feature that might have its counterpart in planktic foraminiferal assemblage records with the appearance of the subtropical species *B. megastoma* during specific phases of Termination II (data from H. Bauch and E. Kandiano). The presence of *L. machaerophorum* (and *B. megastoma*) indicates the inflow of quite particular, “Atlantic” water masses in the western Norwegian Sea during late Termination II. At site MD992277, *L. machaerophorum* co-occurs with *O. centrocarpum*, in contrast to what is seen at the Vøring Plateau. This might imply a different source region from where the former species was advected for both areas.

The first ~3.5 kyr of the last interglacial at the eastern Iceland Plateau were characterised by somewhat cooler and less stratified conditions compared to the Vøring Plateau, as suggested by the relative abundances of *N. labyrinthus* and *B. tepikiense*. At no point, however, an east to west temperature gradient as pronounced as at present, appears to have existed. The insignificant amounts of IRD and chlorophycean algal cells reveal only a weak influence of the polar EGC, but the lack of significant amounts of warm elements (*Impagidinium* spp., *S. lazus* and *S. mirabilis* s.l.) at the same time indicate that the area neither was flooded by warm Atlantic surface water masses. Hence, a fairly weak meridional overturning circulation probably prevailed during early MIS 5e.

A pronounced mid-MIS 5e cold event, clearly discernable in planktic foraminiferal records (E. Kandiano, unpublished data) and indicated by the reappearance of considerable amounts of IRD centred around 120.5 ka, is only weakly expressed by the dinocyst assemblages. In contrast, raised relative abundances of *S. mirabilis* s.l. would rather suggest warming. This contradictory signal was probably caused by pronounced seasonal warming of the slightly fresher upper water layer, and compares well with what was seen in core M23323 at the Vøring Plateau.

In both the eastern and western Norwegian Sea, the cold event is followed by an increase of *S. lazus*. However, the further development of MIS 5e from there on differs drastically between both areas. Whereas a clear late last interglacial marine optimum could be observed at the Vøring Plateau, there are no indications whatsoever in the dinocyst assemblages for a late climatic optimum at site MD992277. On the contrary, the reappearance of IRD and the changes in the dinocyst assemblages suggest the onset of transitional conditions towards MIS 5d shortly after the *S. lazus* high, at around 117 ka. Hence, it is argued that the enhanced overturning circulation of the late MIS 5e in the eastern Nordic seas in turn strengthened the south(east)ward flow of the EGC. This brought cold surface water conditions towards site MD992277, preventing an interglacial optimum from developing in the uppermost ocean at the eastern Iceland Plateau.

CONCLUSIONS

A high-resolution study of dinoflagellate cyst (dinocyst) assemblages from three key locations in the Nordic seas has allowed to make a profound palaeoenvironmental reconstruction of the sea surface conditions (temperature, salinity, sea ice) during the last interglacial, MIS 5e. The palaeoceanographic potential of dinocyst assemblages was clearly illustrated. In addition, comparison of the dinocyst data with other proxy records (planktic foraminifera, $\delta^{18}\text{O}$ and IRD) showed that specific climatic events can be expressed in a differing way by each respective proxy, primarily due to ecological/habitat differences. Concretely, dinocyst assemblages appear to react to environmental changes in the topmost ocean surface, whereas planktic foraminifera register climatic signals from other, probably slightly deeper water masses. This feature clearly underlines the usefulness, or even the need of combining different proxies for refined palaeoceanographic studies.

As had been shown by other studies before, melting of the vast ice sheet that had built up during the penultimate glaciation (MIS 6) provided sizeable amounts of IRD and thus freshwater to the Nordic seas for an extended period, well into times with high summer insolation and light oxygen isotope values. The latest phases of the deglaciation, or Termination II, reveal the unusual presence of the neritic, temperate to tropical dinocyst species *Lingulodinium machaerophorum* in the Norwegian Sea. This feature might have its counterpart in planktic foraminiferal assemblages with the equally enigmatic occurrence of *Beella megastoma* at specific time intervals during Termination II (data from H. Bauch and E. Kandiano), and appears to indicate that quite particular water masses influenced the area at those times. The source area of these water masses might nevertheless have been different for the eastern and western Norwegian Sea, as the assemblages from the latter area contain a stronger “Atlantic” signature. Thus, a thick freshwater lid in the eastern Norwegian Sea probably prevented an easy protrusion of Atlantic water masses towards the Vøring Plateau during latest Termination II.

A shift from the inflow of coastal towards more open marine Atlantic water masses at the Vøring Plateau indicates the start of MIS 5e *sensu stricto* (i.e. with low or no IRD) at around 123.5 ka. The drastic drop in IRD content means that the main deglacial phase had come to an end. However, persisting low amounts of IRD indicate that freshwater input continued for another 4–5 kyr. This prolonged influence of Termination II had a substantial impact on the development of the last interglacial surface circulation in the Nordic seas. Comparison of the MIS 5e dinocyst assemblages with core-top and published Holocene records from the area reveals that MIS 5e was characterised by much stronger stratification and seasonality

in the surface waters than the past 7 kyr. The existence of stratified surface waters shows from the dinocyst data in two direct ways: through high abundances of *Bitectatodinium tepikiense*, an abundant species in seasonally stratified water masses (but at present virtually absent in the eastern Nordic seas), and through a higher diversity in the MIS 5e assemblages, opposed to the practically bi-specific assemblages of the last 7 kyr at the Vøring Plateau. The pronounced stratification and stronger seasonality of MIS 5e is further corroborated by transfer function analysis.

The high relative abundances of *Operculodinium centrocarpum* in the last interglacial assemblages from the Norwegian Sea imply that the area was continuously influenced by inflowing Atlantic water. Sea surface temperatures at the Iceland Plateau appear to have been lower than at the Vøring Plateau, but at no time an east to west temperature gradient as pronounced as at present developed during the first ~4 kyr of MIS 5e. The low amount of cold and freshwater indicators, as well as insignificant abundances of warm species at the Iceland Plateau, would suggest only minor influences from the polar East Greenland Current or Atlantic water masses, respectively, confirming the view of a generally weak meridional overturning circulation during early MIS 5e.

Foraminiferal assemblage data (E. Kandiano, unpublished) and raised IRD indicate a return to much cooler conditions around 120.5 ka. However, the higher share of the warm-temperate species *Spiniferites mirabilis* s.l. in the dinocyst assemblages would rather point towards a warming at that time. Enhanced stratification and warming of the surface waters presumably created favourable seasonal conditions for the dinoflagellate species, and exemplifies the fact that different fossil groups do not necessarily express climatic events in the same way.

Surface water conditions steadily started to improve after the cessation of IRD input, around 119 ka, as illustrated by higher numbers of *Spiniferites lazus* followed by an acme of *S. mirabilis* s.l. The significant relative abundance peak of *S. mirabilis* s.l. at the Vøring Plateau, coeval with high amounts of subpolar planktic foraminifera (data from H. Bauch and E. Kandiano), indicate that optimal, fully marine interglacial conditions could develop only late in MIS 5e, between ~117.5 and 116.5 ka, after IRD and thus freshwater input had come to an end. The results from the transfer function analysis suggest a reduced seasonality with sea surface salinities comparable to modern values, implying that a modern type of surface circulation prevailed in the Nordic seas during late MIS 5e. The stable oxygen isotope values from the MIS 5e optimum are comparable with the average Holocene values, which means that the light values from the preceding phases of MIS 5e reflect the existence of a differently structured ocean surface, rather than optimal interglacial conditions.

The enhanced overturning circulation of late MIS 5e allowed a typical interglacial environment to finally develop further up north along the modern pathway of the Norwegian Current, in the southern Fram Strait, as well. Presumably, the weaker northward heat flow with a substantial body of fresher surface waters from deglacial processes had hindered the warm water masses from becoming manifest at the ocean surface during the preceding phases of MIS 5e. The qualitative aspects of the interglacial optimum in the Fram Strait would nevertheless suggest a distinct temperature gradient with areas further north in the Arctic Ocean, and a zonal recirculation of warm water masses to the southwest of Svalbard.

In contrast with the sites underlying the pathway of the Norwegian Current, no late MIS 5e optimum is shown by the dinocyst assemblages from the eastern Iceland Plateau; the data would in fact suggest that the glacial inception already occurred around 117 ka. Thus, it can be argued that the enhanced NC in turn strengthened the south(east)ward flow of the East Greenland Current, bringing cold surface waters towards the eastern Iceland Plateau and preventing the late MIS 5e optimum from developing properly in the upper ocean. However, further studies at the Iceland Plateau are needed to evaluate this last interglacial scenario.

The late MIS 5e marine optimum contrasts with the early Holocene climatic optimum, which occurred more or less synchronously with relatively high summer insolation. The different conditions with respect to the Holocene under which MIS 5e started, had a major impact on the further development of the last interglacial climate. Hence, MIS 5e cannot simply be taken as an analogue for the Holocene solely based on insolation forcing, but it does have the potential to provide scenarios for a future climate with enhanced freshwater input into the Arctic.

References

- Adkins, J.F., Boyle, E.A., Keigwin, L., Cortijo, E., 1997. Variability of the North Atlantic thermohaline circulation during the last interglacial period. *Nature* 390, 154-156.
- Adl., S.M., Simpson, A.G.B., Farmer, M.A., Andersen, R.A., Anderson, O.R., Barta, J.R., Bowser, S.S., Burgerolle, G., Fensome, R.A., Fredericq, S., James, T.Y., Karpov, S., Kugrens, P., Krug, J., Lane, C.E., Lewis, L.A., Lodge, J., Lynn, D.H., Mann, D.G., McCourt, R.M., Mendoza, L., Moestrup, Ø., Mozley-Standridge, S.E., Nerad, T.A., Shearer, C.A., Smirnov, A.V., Spiegel, F.W., Taylor, M.J.R., 2005. The new higher level classification of eukaryotes with emphasis on the taxonomy of protist. *Journal of Eukaryotic Microbiology* 52, 399-451.
- Andersen, C., Koç, N., Jennings, A., Andrews, J.T., 2004. Nonuniform response of the major surface currents in the Nordic Seas to insolation forcing: Implications for the Holocene climate variability. *Paleoceanography* 19, doi:10.1029/2002PA000873.
- Anderson, D.M., Lively, J.J., Reardon, E.M., Price, C.A., 1985. Sinking characteristics of dinoflagellate cysts. *Limnology and Oceanography* 30, 1000-1009.
- Andersson, C., Risebrobakken, B., Jansen, E., Dahl, S.O., 2003. Late Holocene surface ocean conditions of the Norwegian Sea (Vøring Plateau). *Paleoceanography* 18, doi:10.1029/2001PA000654.
- Bauch, H.A., 1994. *Beella megastoma* (Earland) in late Pleistocene Norwegian-Greenland Sea sediments: stratigraphy and meltwater implication. *Journal of Foraminiferal Research* 24, 171-177.
- Bauch, H.A., 1996. Monitoring Termination II at high latitude: anomalies in the planktic foraminiferal record. *Marine Geology* 131, 89-102.
- Bauch, H.A., 1997. Paleoceanography of the North Atlantic Ocean (68°-76°N) during the past 450 ky deduced from planktic foraminiferal assemblages and stable isotopes. In: Hass, H.C., Kaminski, M.A. (Eds.), *Contributions to the Micropaleontology and Paleoceanography of the Northern North Atlantic*. Grzybowski Foundation Special Publication 5, pp. 83-100.
- Bauch, H.A., Kandiano, E., 2007. Evidence for early warming and cooling in North Atlantic surface waters during the last interglacial. *Paleoceanography* 22, PA1201, doi: 10.1029/2005PA001252.
- Bauch, H.A., Erlenkeuser, H., 2008. A "critical" climatic evaluation of last interglacial (MIS 5e) records from the Norwegian Sea. *Polar Research* 27, 135-151.
- Bauch, H.A., Erlenkeuser, H., Grootes, P.M., Jouzel, J., 1996. Implications of stratigraphic and paleoclimatic records of the last interglaciation from the Nordic Seas. *Quaternary Research* 46, 260-269.
- Bauch, H.A., Erlenkeuser, H., Fahl, K., Spielhagen, R.F., Weinelt, M.S., Andruleit, H., Henrich, R., 1999. Evidence for a steeper Eemian than Holocene sea surface temperature gradient between Arctic and sub-Arctic regions. *Palaeogeography, Palaeoclimatology, Palaeoecology* 145, 95-117.
- Bauch, H.A., Erlenkauser, H., Jung, S.J.A., Thiede, J., 2000a. Surface and deep water changes in the subpolar North Atlantic during Termination II and the last interglaciation. *Paleoceanography* 15, 76-84.
- Bauch, H.A., Erlenkeuser, H., Helmke, J.P., Struck, U., 2000b. A paleoclimatic evaluation of marine oxygen isotope stage 11 in the high Northern Atlantic (Nordic seas). *Global and Planetary Change* 24, 27-39.

- Bauch, H.A., Erlenkeuser, H., Spielhagen, R.F., Struck, U., Matthiessen, J., Thiede, J., Heinemeier, J., 2001. A multiproxy reconstruction of the evolution of deep and surface waters in the subarctic Nordic Seas over the last 30,000 yr. *Quaternary Science Reviews* 20, 659-678.
- Baumann, A., 2007. *Dinoflagellaten-Zysten als Paläoumweltindikatoren im Spätquartär des Europäischen Nordmeeres*. PhD thesis, Universität Bremen.
- Baumann, K.-H., Matthiessen, J., 1992. Variations in surface water mass conditions in the Norwegian Sea: Evidence from Holocene coccolith and dinoflagellate cyst assemblages. *Marine Micropaleontology* 20, 129-146.
- Baumann, K.H., Lackschewitz, K.S., Mangerud, J., Spielhagen, R.F., Wolf-Welling, T.C.W., Henrich, R., Kassens, H., 1995. Reflections of Scandinavian ice sheet fluctuations in Norwegian sea sediments during the past 150,000 years. *Quaternary Research* 43, 185-197.
- Bé, A.W.H., 1977. An ecological, zoogeographic and taxonomic review of recent planktonic foraminifera. In: Ramsay, A.T.S. (Ed.), *Oceanic Micropaleontology*. Academic Press, New York, pp. 1-100.
- Bé, A.W.H., Hutson, W.H., 1977. Ecology of planktonic foraminifera and biogeographic patterns of life and fossil assemblages in the Indian Ocean. *Micropaleontology* 23, 369-414.
- Beets, D.J., Beets, C.J., Cleveringa, P., 2006. Age and climate of the late Saalian and early Eemian type-area, Amsterdam basin, The Netherlands. *Quaternary Science Reviews* 25, 876-885.
- Bendle, J.A.P., Rosell-Melé, A., 2007. High-resolution alkenone sea surface temperature variability on the North Icelandic Shelf: implications for Nordic Seas palaeoclimatic development during the Holocene. *The Holocene* 17, 9-24.
- Berger, A.L. 1978. Long-Term Variations of Daily Insolation and Quaternary Climatic Changes. *Journal of the Atmospheric Sciences* 35, 2362-2367.
- Blanco, J., 1995. Cyst production in four species of neritic dinoflagellates. *Journal of Plankton Research* 17, 165-182.
- Boessenkool, K.P., Brinkuis, H., Schönfeld, J., Targarona, J., 2001. North Atlantic sea-surface temperature changes and the climate of western Iberia during the last deglaciation; a marine palynological approach. *Global and Planetary Change* 30, 33-39.
- Boyer, T.P., Antonov, J.I., Garcia, H.E., Johnson, D.R., Locarnini, R.A., Mishonov, A.V., Pitcher, M.T., Baranova, O.K., Smolyar, I.V., 2006. World Ocean Database 2005. In: Levitus, S. (Ed.), *NOAA Atlas NESDIS 60*. U.S. Government Printing Office, Washington, D.C., pp. 1-190.
- Brauer, A., Allen, J.R.M., Mingram, J., Dulski, P., Wulf, S., Huntley, B., 2007. Evidence for last interglacial chronology and environmental change from Southern Europe. *Proceedings of the National Academy of Sciences of the United States of America* 104, 450-455.
- Brenner, W.W., 2005. Holocene environmental history of the Gotland Basin (Baltic Sea) – a micropalaeontological model. *Palaeogeography, Palaeoclimatology, Palaeoecology* 220, 227-241.
- Calvo, E., Grimalt, J., Jansen, E., 2002. High resolution U^{k}_{37} sea surface temperature reconstruction in the Norwegian Sea during the Holocene. *Quaternary Science Reviews* 21, 1385-1394.
- Chapman, M.R., Shackleton, N.J., 1999. Global ice-volume fluctuations, North Atlantic ice-raffing events, and deep-ocean circulation changes between 130 and 70 ka. *Geology* 27, 795-798.

- Chappellaz, J., Brook, E., Blunier, T., Malaizé, B., 1997. CH₄ and δ¹⁸O of O₂ records from Antarctic and Greenland ice: A clue for stratigraphic disturbance in the bottom part of the Greenland Ice Core Project and the Greenland Ice Sheet Project 2 ice cores. *Journal of Geophysical Research* 102, 26 547-26 557.
- Cheddadi, R., Mamakowa, K., Guiot, J., de Beaulieu, J.-L., Reille, M., Andrieu, V., Granoszewski, W., Peyron, O., 1998. Was the climate of the Eemian stable? A quantitative climate reconstruction from seven European pollen records. *Palaeogeography, Palaeoclimatology, Palaeoecology* 143, 73-85.
- Chen, J.H., Curran, H.A., White B., Wasserburg, G.J., 1991. Precise chronology of the last interglacial period: ²³⁴U-²³⁰Th data from fossil coral reefs in the Bahamas. *Geological Society of America Bulletin* 103, 82-97.
- Clark, P.U., Pisias, N.G., Stocker, T.F., Weaver, A.J., 2002. The role of the thermohaline circulation in abrupt climate change. *Nature* 415, 863-869.
- Dale, B., 1976. Cyst formation, sedimentation, and preservation/factors affecting dinoflagellate assemblages in recent sediments from Trondheimsfjord, Norway. *Review of Palaeobotany and Palynology* 22, 39-60.
- Dale, B., 1996. Dinoflagellate cyst ecology: modeling and geological applications. In: Jansonius, J., McGregor, D.C. (Eds.), *Palynology: Principles and Applications*, vol. 3. American Association of Stratigraphic Palynologists Foundation, Dallas, TX, pp. 1249-1275.
- de Vernal, A., Rochon, A., Turon, J.-L., Matthiessen, J., 1998. Organic-walled dinoflagellate cysts: palynological tracers of sea-surface conditions in middle to high latitude marine environments. *Geobios* 30, 905-920.
- de Vernal, A., Henry, M., Matthiessen, J., Mudie, P.J., Rochon, A., Boessenkool, K.P., Eynaud, F., Grøsfjeld, K., Guiot, J., Hamel, D., Harland, R., Head, M.J., Kunz-Pirring, M., Levac, E., Loucheur, V., Peyron, O., Pospelova, V., Radi, T., Turon, J.-L., Voronina, E., 2001. Dinoflagellate cyst assemblages as tracers of sea-surface conditions in the northern North Atlantic, Arctic and sub-Arctic seas: the new 'n = 677' data base and its application for quantitative palaeoceanographic reconstruction. *Journal of Quaternary Science* 16, 681-698.
- de Vernal, A., Eynaud, F., Henry, M., Hillaire-Marcel, C., Londeix, L., Mangin, S., Matthiessen, J., Marret, F., Radi, T., Rochon, A., Solignac, S., Turon, J.-L., 2005. Reconstruction of sea-surface conditions at middle to high latitudes of the Northern Hemisphere during the Last Glacial Maximum (LGM) based on dinoflagellate cyst assemblages. *Quaternary Science Reviews* 24, 897-924.
- Devillers, R., de Vernal, A., 2000. Distribution of dinoflagellate cysts in surface sediments of the northern North Atlantic in relation to nutrients content and productivity in surface waters. *Marine Geology* 166, 103-124.
- Emiliani, C., 1955. Pleistocene temperatures. *Journal of Geology* 63, 538-578.
- Eriksson, B., Grönlund, T., Uutela, A., 1999. Biostratigraphy of Eemian sediments at Mertunoja, Pohjanmaa (Ostrobothnia), western Finland. *Boreas* 28, 274-291.
- Evitt, W.R., 1985. Sporopollenin dinoflagellate cysts: their morphology and interpretation. *American Association of Stratigraphic Palynologists Foundation*, Dallas, TX, 333 pp.
- Eynaud, F., 1999. *Kystes de Dinoflagellés et Evolution paléoclimatique et paléohydrologique de l'Atlantique Nord au cours du Dernier Cycle Climatique du Quaternaire*. PhD thesis, Université de Bordeaux 1.
- Eynaud, F., Turon, J.-L., Sánchez-Goñi, M.F., Gendreau, S., 2000. Dinoflagellate cyst evidence of 'Heinrich-like events' off Portugal during the Marine Isotopic Stage 5. *Marine Micropaleontology* 40, 9-21.

- Eynaud, F., Turon, J.-L., Duprat, J., 2004. Comparison of the Holocene and Eemian palaeoenvironments in the South Icelandic Basin: dinoflagellate cysts as proxies for the North Atlantic surface circulation. *Review of Palaeobotany and Palynology* 128, 55-79.
- Fensome, R.A., Williams, G.L., 2004. The Lentin and Williams index of fossil dinoflagellates 2004 Edition. *American Association of Stratigraphic Palynologists Contributions Series* 42, 1-909.
- Fensome, R.A., Taylor, F.J.R., Norris, G., Sarjeant, W.A.S., Wharton, D.I., Williams, G.L., 1993. A classification of fossil and living dinoflagellates. *Micropaleontology, Special Paper No. 7*, pp. 1-351.
- Fensome, R.A., Riding, J.B., Taylor, F.J.R., 1996. Dinoflagellates. In: Jansonius, J., McGregor, D.C. (Eds.), *Palynology: Principles and Applications, vol. 1*. American Association of Stratigraphic Palynologists Foundation, Dallas, TX, pp. 107-169.
- Field, M., Huntley, B., Müller, H., 1994. Eemian climate fluctuations observed in a European pollen record. *Nature* 371, 779-783.
- Flatau, M.K., Talley, L., Niiler, P.P., 2003. The North Atlantic Oscillation, surface current velocities, and SST changes in the subpolar North Atlantic. *Journal of Climate* 16, 2355-2369.
- Fronval, T., Jansen, E., 1996. Rapid changes in ocean circulation and heat flux in the Nordic seas during the last interglacial period. *Nature* 383, 806-810.
- Fronval, T., Jansen, E., 1997. Eemian and early Weichselian (140-60 ka) paleoceanography and paleoclimate in the Nordic Seas with comparisons to Holocene conditions. *Paleoceanography* 12, 443-462.
- Fronval, T., Jansen, E., Bloemendal, J., Johnsen, S., 1995. Oceanic evidence for coherent fluctuations in Fennoscandian and Laurentide ice sheets on millenium timescales. *Nature* 374, 443-446.
- Fuchs, A., Leuenberger, M.C., 1996. $\delta^{18}\text{O}$ of atmospheric oxygen measured on the GRIP Ice Core document stratigraphic disturbances in the lowest 10% of the core. *Geophysical Research Letters* 23, 1049-1052.
- Funder, S., Demidov, I., Yelovicheva, Y., 2002. Hydrography and mollusc faunas of the Baltic and the White Sea-North Sea seaway in the Eemian. *Palaeogeography, Palaeoclimatology, Palaeoecology* 184, 275-304.
- Gaines, G., Elbrächter, M., 1987. Chapter 6: Heterotrophic nutrition. In: Taylor, F.J.R. (Ed.), *The biology of dinoflagellates*. Botanical Monographs vol. 21, Blackwell Scientific Publications, Oxford, pp. 224-268.
- Ganopolski, A., Rahmstorf, S., 2001. Rapid changes of glacial climate simulated in a coupled climate model. *Nature* 409, 153-158.
- Gerlach, S.A., Thiede, J., Graf, G., Werner, F., 1986. Forschungsschiff Meteor, Reise 2 vom 19. Juni bis 16. Juli 1986, Forschungsschiff Poseidon, Reise 128 vom 7. Mai bis 8. Juni 1986. *Berichte aus dem Sonderforschungsbereich 313, 4*, Christian-Albrechts Universität, Kiel, pp. 1-140.
- Grootes, P.M., Stuiver, M., White, J.W.C., Johnsen, S., Jouzel, J., 1993. Comparison of oxygen isotope records from the GISP2 and GRIP Greenland ice cores. *Nature* 366, 552-554.
- Grøsfjeld, K., Larsen, E., Sejrup, H.P., de Vernal, A., Flatebø, T., Vestbø, M., Hafliðason, H., Aarseth, I., 1999. Dinoflagellate cysts reflecting surface-water conditions in Voldafjorden, western Norway during the last 11 300 years. *Boreas* 28, 403-415.
- Grøsfjeld, K., Funders, S., Seidenkrantz, M.-S., Glaister, C., 2006. Last Interglacial marine environments in the White Sea region, northwestern Russia. *Boreas* 35, 493-520.

- Guiot, J., 1990. Methodology of the last climatic cycle reconstruction in France from pollen data. *Palaeogeography, Palaeoclimatology, Palaeoecology* 80, 49-69.
- Guiot, J., de Vernal, A., 2007. Transfer functions: methods for quantitative paleoceanography based on microfossils. In: Hillaire-Marcel, C., de Vernal, A. (Eds), *Proxies in Late Cenozoic Paleoceanography*. Elsevier, pp. 523-563.
- Guiot, J., de Beaulieu, J.L., Cheddadi, R., David, F., Poneel, P., Reille M., 1993. The climate in Western Europe during the last Glacial/Interglacial cycle derived from pollen and insect remains. *Palaeogeography, Palaeoclimatology, Palaeoecology* 103, 73-93.
- Haake, F.W., Erlenkeuser, H., Pflaumann, U., 1992. *Pullenia bulloides* (ORBIGNY) in sediments of the Norwegian/Greenland Sea and the Northeastern Atlantic Ocean: Paleo-oceanographic evidence. In: Takayanagi, Y., Saito, T. (Eds.), *Studies in Benthic Foraminifera, Benthos '90*, Tokai University Press, Sendai, Japan, pp. 235-244.
- Hald, M., Dokken, T., Mikalsen, G., 2001. Abrupt climatic change during the last interglacial-glacial cycle in the polar North Atlantic. *Marine Geology* 176, 121-137.
- Harland, R., 1982. Recent dinoflagellate cyst assemblages from the southern Barents Sea. *Palynology* 6, 9-18
- Harland, R., 1983. Distribution maps of Recent dinoflagellate cysts in bottom sediments from the North Atlantic Ocean and adjacent seas. *Palaeontology* 26, 321-387.
- Harland, R., Sharp, J., 1986. Elongate *Spiniferites* cysts from North Atlantic bottom sediments. *Palynology* 10, 25-34.
- Harland, R., Reid, P.C., Dobell, P., Norris, G., 1980. Recent and sub-Recent dinoflagellate cysts from the Beaufort Sea, Canadian Arctic. *Grana* 19, 211-225.
- Head, M.J., 1996. Modern dinoflagellate cysts and their biological affinities. In: Jansonius, J., McGregor, D.C. (Eds.), *Palynology: Principles and Applications*, vol. 3. American Association of Stratigraphic Palynologists Foundation, Dallas, TX, pp. 1197-1248.
- Head, M.J., 2007. Last Interglacial (Eemian) hydrographic conditions in the southwestern Baltic Sea based on dinoflagellate cysts from Ristinge Klint, Denmark. *Geological Magazine* 144, 987-1013.
- Head, M.J., Harland, R., Matthiessen, J., 2001. Cold marine indicators of the late Quaternary: the new dinoflagellate cyst genus *Islandinium* and related morphotypes. *Journal of Quaternary Science* 16, 621-636.
- Head, M.J., Seidenkrantz, M.-S., Janczyk-Kopikowa, Z., Marks, L., Gibbard, P.L., 2005. Last Interglacial (Eemian) hydrographic conditions in the southeastern Baltic Sea, NE Europe, based on dinoflagellate cysts. *Quaternary International* 130, 3-30.
- Head, M.J., Lewis, J., de Vernal, A., 2006. The cyst of the calcareous dinoflagellate *Scrippsiella trifida*: resolving the fossil record of its organic wall with that of *Alexandrium tamarense*. *Journal of Paleontology* 80, 1-18.
- Hebbeln, D., Wefer, G., 1997. Late Quaternary paleoceanography in the Fram Strait. *Paleoceanography* 12, 65-78.
- Helmke, J.P., Bauch, H.A., Röhl, U., Mazaud, A., 2005. Changes in sedimentation patterns of the Nordic seas region across the mid-Pleistocene. *Marine Geology* 215, 107-122.
- Hirschleber, H., Theilen, F., Balzer, W., von Bodungen, B., Thiede, J., 1988. Forschungsschiff Meteor, Reise 7, vom 1. Juni bis 28. September 1988. *Berichte aus dem Sonderforschungsbereich 313, 10*, Christian-Albrechts Universität, Kiel, pp. 1-257.
- Hopkins, T.S., 1991. The GIN Sea – A synthesis of its physical oceanography and literature review 1972-1985. *Earth-Science Reviews* 30, 175-318.
- Imbrie, J., Kipp, N.G., 1971. A new micropaleontological method for quantitative paleoclimatology: application to a late Pleistocene Caribbean core. In: Turekian, K.K.

- (Ed.), *The Late Cenozoic Glacial Ages*. Yale University Press, New Haven, CN, pp. 71-179.
- Jennings, A.E., Knudsen, K.L., Hald, M., Hansen, C.V., Andrews, J., 2002. A mid-Holocene shift in Arctic sea-ice variability on the East Greenland Shelf. *The Holocene* 12, 49-58.
- Kandiano, E.S., Bauch, H.A., 2003. Surface ocean temperatures in the Northeast Atlantic during the last 500,000 years: Evidence from foraminiferal census data and iceberg-rafted debris. *Terra Nova* 15, 265-271.
- Kandiano, E.S., Bauch, H.A., Müller, A., 2004. Sea surface temperature variability in the North Atlantic during the last two glacial-interglacial cycles: comparison of faunal, oxygen isotopic, and Mg/Ca-derived records. *Palaeogeography, Palaeoclimatology, Palaeoecology* 204, 145-164.
- Kellogg, T.B., 1980. Paleoclimatology and paleo-oceanography of the Norwegian and Greenland seas: glacial-interglacial contrasts. *Boreas* 9, 115-137.
- Klotz, S., Guiot, J., Mosbrugger, V., 2003. Continental European Eemian and early Würmian climate evolution: comparing signals using different quantitative reconstruction approaches based on pollen. *Global and Planetary Change* 36, 277-294.
- Knudsen, K.-L., Seidenkrantz, M.-S., Kristensen, P., 2002. Last interglacial and early glacial circulation in the northern North Atlantic Ocean. *Quaternary Research* 58, 22-26.
- Koç, N., Jansen, E., Hafliðason, H., 1993. Paleoceanographic reconstructions of surface ocean conditions in the Greenland, Iceland and Norwegian seas through the last 14 ka based on diatoms. *Quaternary Science Reviews* 12, 115-140.
- Kodrans-Nsiah, M., de Lange, G.J., Zonneveld, K.A.F., 2008. A natural exposure experiment on short-term species-selective aerobic degradation of dinoflagellate cysts. *Review of Palaeobotany and Palynology*, doi:10.1016/j.revpalbo.2008.04.002.
- Köhler, S.E.I., Spielhagen, R.F., 1990. The enigma of oxygen isotope stage 5 in the central Fram Strait. In: Bleil, U., Thiede, J. (Eds.), *Geological History of the Polar Oceans: Arctic versus Antarctic*. NATO ASI Series C: Mathematical and Physical Sciences. Kluwer Academic Publishers, Dordrecht, pp. 489-497.
- Kottke, B., 1998. *Glaziomarine Sedimentation am Knipovitch-Rücken (südliche Framstraße)*. Diploma Thesis, University of Bremen.
- Kottke, B., 1999. Stable isotopes of sediment core GIK23455-3. doi:10.1594/PANGAEA.55465.
- Kukla, G., Galvin, J., 2004. Milankovitch climate reinforcements. *Global and Planetary Change* 40, 27-48.
- Kukla, G., McManus, J.F., Rousseau, D., Chine, I., 1997. How long and how stable was the last interglacial? *Quaternary Science Reviews* 16, 605-612.
- Kukla, G.J., Bender, M. L., de Beaulieu J.-L., Bond, G., Broecker, W. S., Cleveringa, P., Gavin, J. E., Herbert, T., Imbrie, J., Jouzel, J., Keigwin, L. D., Knudsen, K.-L., McManus, J. F., Merkt, J., Muhs, D. R., Müller, H., Poore R. Z., Porter, S. C., Seret, G., Tzedakis, P., Winograd, I. J., 2002. Last interglacial climates. *Quaternary Research* 58, 2-13.
- Labeyrie, L., Jansen, E., 2003. MD114/IMAGES V à bord du Marion Dufresne, Fort de France, 11 juin 1999, Marseille, 20 septembre 1999. *Les rapports de campagnes à la mer, OCE/2003/02*, Institut Polaire Français – Paul-Emile Victor, Brest-Iroise/Plouzané, France.
- Landais, A., Steffensen, J.P., Caillon, N., Jouzel, J., Masson-Delmotte, V., Schwander, J., 2004. Evidence for stratigraphic distortion in the Greenland Ice Core Project (GRIP) ice core during Event 5e1 (120 kyr BP) from gas isotopes. *Journal of Geophysical Research* 109, doi:10.1029/2003JD004193.

- Laskar, J., Robutel, P., Joutel, F., Gastineau, M., Correia, A.C.M., Levrard, B., 2004. A long-term numerical solution for the insolation quantities of the Earth. *Astronomy and Astrophysics* 428, 261-285.
- Lehmann, S.J., Sachs, J.P., Grotwell, A.M., Keigwin, L.D., Boyle, E.A., 2002. Relation of subtropical Atlantic temperature, high-latitude ice rafting, deep water formation, and European climate 130,000-60,000 years ago. *Quaternary Science Reviews* 21, 1917-1924.
- Lewis, J., Hallett, R., 1997. *Lingulodinium polyedrum* (*Gonyaulax polyedra*) a blooming dinoflagellate. *Oceanography and Marine Biology, An Annual Review* 35, 97-161.
- LIONS project – Last Interglacial Ocean of the Nordic Seas. Primary Investigator: Dr. Henning. A. Bauch, in cooperation with Dr. Niels Andersen and Dr. Jörn Thiede; researchers: Dr. Evgeniya Kandiano, Nicolas Van Nieuwenhove.
- Locarnini, R.A.A., Mishonov, A.V., Antonov, J.I., Boyer, T.P., Garcia, H.E., 2006. World Ocean Atlas 2005, Volume 1: Temperature. In: Levitus, S. (Ed.), *NOAA Atlas NESDIS 61*. U.S. Government Printing Office, Washington, D.C., pp. 182.
- Mangerud, J., Sønstegaard, E., Sejrup, H.-P., 1979. Correlation of the Eemian (interglacial) stage and the deep-sea oxygen-isotope stratigraphy. *Nature* 277, 189-192.
- Mangerud J., 1989. Correlation of the Eemian and the Weichselian with deep sea oxygen isotope stratigraphy. *Quaternary International* 3, 1-4.
- Marotzke, J., 2000. Abrupt climate change and thermohaline circulation: Mechanisms and predictability. *Proceedings of the National Academy of Sciences* 97, 1347-1350.
- Marret, F., Scourse, J., 2002. Control of modern dinoflagellate cyst distribution in the Irish and Celtic seas by seasonal stratification dynamics. *Marine Micropaleontology* 47, 101-116.
- Marret, F., Zonneveld, K.A.F., 2003. Atlas of modern organic-walled dinoflagellate cyst distribution. *Review of Palaeobotany and Palynology* 125, 1-200.
- Marret, F., Eiríksson, J., Knudsen, K.L., Turon, J.-L., Scourse, J.D., 2004. Distribution of dinoflagellate cyst assemblages in surface sediments from the northern and western shelf of Iceland. *Review of Palaeobotany and Palynology* 128, 35-53.
- Martinson, D.G., Pisias, N.G., Hays, J.D., Imbrie, J., Moore Jr., T.C., Shackleton, N., 1987. Age Dating and the Orbital Theory of the Ice Ages: Development of a High-Resolution 0 to 300,000-Year Chronostratigraphy. *Quaternary Research* 27, 1-29.
- Maslin, M.A., Sarnthein, M., Knaack, J.-J., 1996. Subtropical eastern Atlantic climate during the Eemian. *Naturwissenschaften* 83, 122-126.
- Matthiessen, J., 1995. Distribution patterns of dinoflagellate cysts and other organic-walled microfossils in recent Norwegian-Greenland Sea sediments. *Marine Micropaleontology* 24, 307-334.
- Matthiessen, J., Baumann, A., 1997. Dinoflagellate cyst records from the East Greenland continental margin during the last 15,000 years: implications for paleoceanographic reconstructions. In: Hass, H.C., Kaminski, M.A. (Eds), *Contributions to the Micropaleontology and Paleoceanography of the Northern North Atlantic*. Grzybowski Foundation Special Publications, vol. 5, pp. 149-165.
- Matthiessen, J., Knies, J., 2001. Dinoflagellate cyst evidence for warm interglacial conditions at the northern Barents Sea margin during marine oxygen isotope stage 5. *Journal of Quaternary Science* 16, 727-737.
- Matthiessen, J., Kunz-Pirrung, M., Mudie, P.J., 2000. Freshwater chlorophycean algae in recent marine sediments of the Beaufort, Laptev and Kara Seas (Arctic Ocean) as indicators of river runoff. *International Journal of Earth Sciences* 89, 470-485.

- Matthiessen, J., Knies, J., Nowaczyk, N.R., Stein, R., 2001. Late Quaternary dinoflagellate cyst stratigraphy at the Eurasian continental margin, Arctic Ocean: indications for Atlantic water inflow in the past 150,000 years. *Global and Planetary Change* 31, 65-86.
- Matthiessen, J., de Vernal, A., Head, M., Okolodkov, Y., Zonneveld, K., Harland, R., 2005. Modern organic-walled dinoflagellate cysts in Arctic marine environments and their (paleo-) environmental significance. *Paläontologische Zeitschrift* 79, 3-51.
- Mayewski, P.A., Rohling, E.E., Stager, J.C., Karlén, W., Maasch, K.A., Meeker, L.D., Meyerson, E.A., Gasse, F., van Kreveld, S., Holmgren, K., Lee-Thorp, J., Rosqvist, G., Rack, F., Staubwasser, M., Schneider, R.R., Steig, E.J., 2004. Holocene climate variability. *Quaternary Research* 62, 243-255.
- McCulloch, M.T., Esat, T., 2000. The coral record of last interglacial sea levels and sea surface temperatures. *Chemical Geology* 169, 107-129.
- McManus, J.F., Bond, G.C., Broecker, W.S., Johnsen, S., Labeyrie, L., Higgins, S., 1994. High-resolution climate records from the North Atlantic during the last interglacial. *Nature* 371, 326-329.
- McManus, J.F., Oppo, D.W., Keigwin, L.D., Cullen, J.L., Bond G.C., 2002. Thermohaline circulation and prolonged interglacial warmth in the North Atlantic. *Quaternary Research* 58, 17-21.
- Mertens, K.N., Verhoeven, K., Verleye, T., Louwye, S., Amorim, A., Ribeiro, S., Deaf, A.S., Harding, I., De Schepper, S., Kodrans-Nsiah, M., de Vernal, A., Henry, M., Taoufik, R., Dybkjær, K., Poulsen, N.E., Feist-Burkhardt, S., Chitolie, J., González Arango, C., Heilmann-Clausen, C., Londeix, L., Turon, J.-L., Marret, F., Matthiessen, J., McCarthy, F., Prasad, V., Pospelova, V., Kyffin Hughes, J.E., Riding, J.B., Rochon, A., Sangiorgi, F., Welters, N., Sinclair, N., Christian, T., Soliman, A., Van Nieuwenhove, N., Vink, A., Young, M. The absolute abundance calibration project: the Lycopodium marker-grain method put to the test. *Submitted to Review of Paleobotany and Palynology*.
- Mudie, P.J., 1992. Circum-Arctic Quaternary and Neogene marine palynofloras: paleoecology and statistical analysis. In: Head, M.J., Wrenn, J.H. (Eds.), *Neogene and Quaternary Dinoflagellate Cysts and Acritarchs*. American Association of Palynologists Foundation, Dallas, TX, pp. 347-390.
- Mudie, P.J., Short, S.K., 1985. Marine palynology of Baffin Bay. In: Andrews, J.T. (Ed.), *Quaternary environments: eastern Canadian Arctic, Baffin Bay and west Greenland*. George Allen & Unwin Ltd., London, pp. 263-308.
- North Greenland Ice Core Project (NGRIP) Members, 2004. High-resolution record of Northern Hemisphere climate extending into the last interglacial period. *Nature* 431, 147-151.
- Oppo, D., Horowitz, M., Lehmann, S.J., 1997. Marine core evidence for reduced deep water production during Termination II followed by a relatively stable substage 5e (Eemian). *Paleoceanography* 12, 51-63.
- Oppo, D.W., Keigwin, L.D., McManus, J.F., 2001. Persistent suborbital climate variability in marine isotope stage 5 and Termination II. *Paleoceanography* 16, 280-292.
- Overpeck, J., Webb, T., Prentice, I.C., 1985. Quantitative interpretation of fossil pollen spectra: dissimilarity coefficients and the method of modern analogs. *Quaternary Research* 23, 87-108.
- Paillard, D., Labeyrie, L., Yiou, P., 1996. Macintosh program performs time-series analysis. *EOS, Transactions of the American Geophysical Union* 77, 379.
- Penaud, A., Eynaud, F., Turon, J.L., Zaragosi, S., Marret, F., Bourillet, J.F., 2008. Interglacial variability (MIS 5 and MIS 7) and dinoflagellate cyst assemblages in the Bay

- of Biscay (North Atlantic). *Marine Micropaleontology*, doi: 10.1016/j.marmicro.2008.01.007.
- Persson, A., Rosenberg, R., 2003. Impact of grazing and bioturbation of marine benthic deposit feeders on dinoflagellate cysts. *Harmful Algae* 2, 43-50.
- Persson, A., Godhe, A., Karlson, B., 2000. Dinoflagellate cysts in recent sediments from the west coast of Sweden. *Botanica Marina* 43, 69-79.
- Pfannkuche, O., Duinker, J.C., Graf, G., Henrich, R., Thiel, H., Zeitzschel, B., 1993. Nordatlantik 92, Reise Nr. 21, 16. März – 31. August. *Meteor Berichte* 93, 4, Universität Hamburg, pp. 1-281.
- Pfiester, L.A., Anderson, D.M., 1987. Dinoflagellate reproduction. In: Taylor, F.J.R. (Ed.), *The Biology of Dinoflagellates*. Botanical monographs vol. 21, Blackwell Scientific Publications, Oxford, pp. 611-648.
- Pollinger, U., 1979. Freshwater ecosystems. In: Taylor, F.J.R. (Ed.), *The Biology of Dinoflagellates*. Botanical monographs vol. 21, Blackwell Scientific Publications, Oxford, pp. 502-529.
- Pospelova, V., Chmura, G.L., Walker, H.A., 2004. Environmental factors influencing the spatial distribution of dinoflagellate cyst assemblages in shallow lagoons of southern New England (USA). *Review of Palaeobotany and Palynology* 128, 7-34.
- R Development Core Team, 2007. R: A language and environment for statistical computing. *R Foundation for Statistical Computing*, Vienna, Austria. ISBN 3-900051-07-0. <http://www.R-project.org>.
- Radi, T., de Vernal, A., 2008. Dinocysts as proxy of primary productivity in mid-high latitudes of the Northern Hemisphere. *Marine Micropaleontology*, doi: 10.1016/j.marmicro.2008.01.012.
- Rahmstorf, S., 1995. Bifurcations of the Atlantic thermohaline circulation in response to changes in the hydrological cycle. *Nature* 378, 145-149.
- Rasmussen, T.L., Thomsen, E., Kuijpers, A., Wastegård, S., 2003. Late warming and early cooling of the sea surface in the Nordic Seas during MIS 5e (Eemian Interglacial). *Quaternary Science Reviews* 22, 809-821.
- Reid, P.C., 1978. Dinoflagellate cysts in the plankton. *New Phytologist* 80, 219-229.
- Rioual, P., Andrieu-Ponel, V., Rietti-Shati, M., Battarbee, R.W., de Beaulieu, J.-L., Cheddadi, R., Maurice, R., Svobodova, H., Shemesh A., 2001. High-resolution record of climate stability in France during the last interglacial period. *Nature* 413, 293-296.
- Risebrokken, B., Jansen, E., Andersson, C., Mjelde, E., Hevrøy, K., 2003. A high-resolution study of Holocene paleoclimatic and paleoceanographic changes in the Nordic Seas. *Paleoceanography* 18, 1017, doi: 10.1029/2002PA000764.
- Rochon, A., de Vernal, A., Sejrup, H.-P., Hafliðason, H., 1998. Palynological evidence of climatic and oceanographic changes in the North Sea during the last Deglaciation. *Quaternary Research* 49, 197-207.
- Rochon, A., de Vernal, A., Turon, J.-L., Matthiessen, J., Head, M.J., 1999. Distribution of recent dinoflagellate cysts in surface sediments from the North Atlantic Ocean and adjacent seas in relation to sea-surface parameters. *American Association of Stratigraphic Palynologists Contributions Series* 35, 1-146.
- Rohling, E.J., Grant, K., Hemleben, C., Siddall, M., Hoogakker, B.A.A., Bolshaw, M., Kucera, M., 2008. High rates of sea-level rise during the last interglacial period. *Nature Geoscience* 1, doi:10.1038/ngeo.2007.28.
- Rousseau, D.D., Hatté, Ch., Guiot, J., Duzer, D., Schevin, P., Kukla G., 2006. Reconstruction of the Grande Pile Eemian using inverse modelling of biomes and $\delta^{13}\text{C}$. *Quaternary Science Reviews* 25, 2806-2819.

- Ruddiman, W.F., Shackleton, N.J., McIntyre, A., 1986. North Atlantic sea-surface temperatures for the last 1.1 million years. In: Summerhayes, C.P., Shackleton, N.J. (Eds.), *North Atlantic Paleoceanography*. Geological Society Special Publications 21, London, pp. 155-173.
- Sánchez-Goñi, M.F., Eynaud, F., Turon, J.-L., Shackleton, N.J., 1999. High resolution palynological record off the Iberian margin: direct land-sea correlation for the Last Interglacial complex. *Earth and Planetary Science Letters* 171, 123-137.
- Sánchez-Goñi, M.F., Turon, J.-L., Eynaud, F., Shackleton, N.J., Cayre, O., 2000. Direct land/sea correlation of the Eemian, and its comparison with the Holocene: a high-resolution palynological record off the Iberian margin. *Geologie en Mijnbouw/Netherlands Journal of Geosciences* 79, 345-354.
- Schnepf, E., Elbrächter, M., 1992. Nutritional strategies in dinoflagellates – a review with emphasis on cell biological aspects. *European Journal of Protistology* 28, 3-24.
- Shackleton, N.J., 1969. The last interglacial in the marine and terrestrial records. *Proceedings of the Royal Society B174*, 135-154.
- Shackleton, N.J., Opdyke, N.D., 1973. Oxygen isotope and palaeomagnetic stratigraphy of equatorial Pacific core V28-238: oxygen isotope temperatures and ice volumes on a 10^5 and 10^6 year scale. *Quaternary Research* 3, 39-55.
- Shackleton, N.J., Sánchez-Goñi, M.F., Pailler, D., Lancelot, Y., 2003. Marine Isotope Substage 5e and the Eemian Interglacial. *Global and Planetary Change* 36, 151-155.
- Smayda, T.J., Reynolds, C.S., 2003. Strategies of marine dinoflagellate survival and some rules of assembly. *Journal of Sea Research* 49, 95-106.
- Spielhagen, R.F., Baumann, K.-H., Erlenkeuser, H., Nowaczyk, R., Nørgaard-Pedersen, N., Vogt, C., Weiel, D., 2004. Arctic Ocean deep-sea record of northern Eurasian ice sheet history. *Quaternary Science Reviews* 23, 1455-1483.
- Stirling, C.H., Esat, T.M., Lambeck, K., McCulloch, M.T., 1998. Timing and duration of the last Interglacial: evidence for a restricted interval of widespread coral reef growth. *Earth and Planetary Science Letters* 160, 745-762.
- Stockmarr, J., 1971. Tablets with spores used in absolute pollen analysis. *Pollen Spores* 13, 616-621.
- Svendsen, J.I., Alexanderson, H., Astakhov, V.I., Demidov, I., Dowdeswell, J.A., Funder, S., Gataullin, V., Henriksen, M., Hjort, C., Houmark-Nielsen, M., Hubberten, H.W., Ingólfsson, Ó., Jakobsson, M., Kjær, K.H., Larsen, E., Kokrantz, H., Pekka Lunkka, J., Lyså, A., Mangerud, J., Matiouchkov, A., Murray, A., Möller, P., Niessen, F., Nikolskaya, O., Polyak, L., Saarnisto, M., Siegert, C., Siegert, M.J., Spielhagen, R.F., Stein R. 2004. Late Quaternary ice sheet history of northern Eurasia. *Quaternary Science Reviews* 23, 1229-1271.
- Thompson, W.G., Goldstein, S.L., 2005. Open-system coral ages reveal persistent suborbital sea-level cycles. *Science* 308, 401-404.
- Turon, J.-L., Londeix, L., 1988. Les assemblages de kystes de dinoflagellés en Méditerranée occidentale (Mer d'Alboran): mise en évidence de l'évolution des paléoenvironnements depuis le dernier maximum glaciaire. *Bulletin des Centres de Recherches Exploration-Production Elf-Aquitaine* 12, 313-344.
- Turon, J.-L., Lézine, A.-M., Denèfle, M., 2003. Land-sea correlations for the last glaciation inferred from a pollen and dinocyst record from the Portuguese margin. *Quaternary Research* 59, 88-98.
- Van Leeuwen, R.J.W., Beets, D.J., Bosch, J.H.A., Burger, A.W., Cleveringa, P., Van Harten, D., Hergreen, G.F.W., Kruk, R.W., Langereis, C.G., Meijer, T., Pouwer, R., de Wolf H., 2000. Stratigraphy and integrated facies analysis of the Saalian and Eemian

- sediments in the Amsterdam-Terminal borehole, the Netherlands. *Geologie en Mijnbouw/Netherlands Journal of Geosciences* 79, 161-196.
- Van Nieuwenhove, N., Bauch, H.A., 2008. Last interglacial (MIS 5e) surface water conditions at the Vøring Plateau (Norwegian Sea), based on dinoflagellate cysts. *Polar Research* 27, 175-186.
- Van Nieuwenhove, N., Bauch, H.A., Matthiessen, J., 2008. Last interglacial surface water conditions in the eastern Nordic Seas inferred from dinocyst and foraminiferal assemblages. *Marine Micropaleontology* 66, 247-263, doi:10.1016/j.marmicro.2007.10.004.
- Versteegh, G.J.M., Blokker, P., 2004. Resistant macromolecules of extant and fossil microalgae. *Phycological Research* 52, 325-339.
- Voelker, A.H.L., 1999. Zur Deutung der Dansgaard-Oeschger Ereignisse in ultra-hochauflösenden Sedimentprofilen aus dem Europäischen Nordmeer. *Report Institut für Geowissenschaften (Kiel University)* 9, pp. 1-278.
- Vogelsang, E., 1990. Paläo-Ozeanographie des Europäischen Nordmeeres anhand stabiler Kohlenstoff- und Sauerstoffisotope. *Berichte aus dem Sonderforschungsbereich 313*, 23, Christian-Albrechts Universität, Kiel, pp. 1-136.
- Wall, D., Dale, B., Lohmann, G.P., Smith, W.K., 1977. The environmental and climatic distribution of dinoflagellate cysts in modern marine sediments from regions in the North and South Atlantic Oceans and adjacent seas. *Marine Micropaleontology* 2, 121-200.
- Zonneveld, K.A.F., Brummer, G.A., 2000. Ecological significance, transport and preservation of organic walled dinoflagellate cysts in the Somali Basin, NW Arabian Sea. *Deep-Sea Research Part II-Topical Studies In Oceanography* 47, 2229-2256.
- Zonneveld, K.A.F., Versteegh, G.J.M., de Lange, G.J., 1997. Preservation of organic-walled dinoflagellate cysts in different oxygen regimes: a 10,000 year natural experiment. *Marine Micropaleontology* 29, 393-405.
- Zonneveld, K.A.F., Versteegh, G.J.M., de Lange, G.J., 2001. Palaeoproductivity and post-depositional aerobic organic matter decay reflected by dinoflagellate cyst assemblages of the Eastern Mediterranean S1 sapropel. *Marine Geology* 172, 181-195.
- Zonneveld, K.A.F., Versteegh, G., Kodrans-Nsiah, M., 2008. Preservation and organic chemistry of Late Cenozoic organic-walled dinoflagellate cysts: A review. *Marine Micropaleontology* 68, 179-197.

List of Appendixes

Appendix A Age-tie points used in developing the age models

Appendix B Raw palynomorph counts data

1. Legend
2. Palynomorph counts from core M23071
 - a. dinoflagellate cysts
 - b. other palynomorphs
3. Palynomorph counts from core M23323
 - a. dinoflagellate cysts
 - b. other palynomorphs
4. Palynomorph counts from core M23455
 - a. dinoflagellate cysts
 - b. other palynomorphs
5. Palynomorph counts from core MD992277
 - a. dinoflagellate cysts
 - b. other palynomorphs

Appendix C Transfer function results

1. Results from the TF analysis of core M23455
2. Results from the TF analysis of core MD992277

Appendix D Plates

Appendix A: Age-tie points used in developing the age models

SPECMAP event	PS1243 depth (cm)	MD992277 depth (cm)	M23071 depth (cm)	M23323 depth (cm)	Age (ka)
5.4	184	339.5	590		108.174
	187	344.5	598		109.482
	190	349.5	606	733.5	110.790
	200	366.5	625	756.5	115.149
			630	761.5	116.296
	204	380.5			116.893
	210	392.5	644	797.5	119.509
	212	397.5			120.380
5.51			647	821.5	120.433
	215		651		121.688
	217				122.560
	220	417.5	654	840.5	122.918
			655	844.5	123.091
			662	854.5	123.400
5.53	233	429.5			124.473
			664	862.5	124.576
	239				125.190
			672	870.5	125.402
6	240	443.5			125.965
	242	447.5		892.5	127.515
	245	452.5	715	900.5	129.840
	246	455.5	721	910.5	130.169
	251	464.5	740	927.5	131.813
	258	471.5	756		134.114
6.2	260		774		134.771
	261		783		135.100

Appendix B1: Palynomorph counts - legend

Acho	Achomosphaera spp.	Spac	Spiniferites pachydermus
Atax	Ataxiodinium choane	Squa	Selenopemphix quanta
Bcar	Brigantedinium cariaeoense	Sram	Spiniferites ramosus (sensu stricto)
Bsim	Brigantedinium simplex	Sramsl	Spiniferites ramosus sensu lato
Bspp	Brigantedinium spp.	Srbc	Spiniferites ramosus/bulloides complex
Btep	Bitectatodinium tepikiense	Sspp	Spiniferites spp.
Dubr	Dubridinium spp.	Stri	Scripsiella trifida, organic remains
Iacu	Impagidinium aculeatum	Tapp	Trinovantedinium applanatum
Imin	Islandinium minutum	Tcfapp	Trinovantedinium? cf. applanatum
lpal	Impagidinium pallidum	Vspi	Votadinium spinosum
lpar	Impagidinium paradoxum	Dindet	Dinoflagellate cyst, indeterminata
lpat	Impagidinium patulum	Drew	Dinoflagellate cyst, reworked
lsph	Impagidinium sphaericum	TOTAL	total in-situ dinocysts counted
lspp	Impagidinium spp.		
Istr	Impagidinium striatum	weight	total weight of freeze-dried sediment processed (in gram)
Lmac	Lingoludinium machaerophorum		
Lspp	Lejeunecysta spp.		
Ncflab	Nematosphaeropsis cf. labyrinthus	*	species present, but not encountered during statistical counting
Nlab	Nematosphaeropsis labyrinthus	?	uncertain determination
Nspp	Nematosphaeropsis spp.	>3	Processes longer than 3µm
OceA	Operculodinium centrocarpum - Arctic morphotype	<3	Processes shorter than 3µm
OceC	Operculodinium centrocarpum - cezare morphotype	Alln	Algal cyst indeterminata
Ocen	Operculodinium centrocarpum	Aspp	Acritarch spp.
OceT	Operculodinium centrocarpum with truncate processes	Botr	Botryococcus spp.
PctA	Protoperidinioid indet. cyst type A	Cycl	Cycliopsella spp.
Pdal	cyst of Pentapharsodinium dalei	Cyma	Cymatiosphaera spp.
Peri	Protoperidinioids indeterminata	Eggln	invertebrate/copepod egg
Pkof	cyst of Polykrikos kofoidii	FoLi	Foraminiferal linings
Pret	Pyxidnopsis reticulata	FuRe	fungal remains
Psch	cyst of Polykrikos schwartzii	Halo	Halodinium spp.
Qcon	Quinquecuspis concreta	LyCo	number of Lycopodium clavatum spores counted
Ramp	Rottnestia amphicavata	LySa	number of Lycopodium clavatum spores added to the sample
Sbel	Spiniferites belerius	Olic	Oligotrichid cyst?
Sbul	Spiniferites bulloides	Pedi	Pediastrum spp.
Scfelo	Spiniferites cf. elongatus sensu Harland & Sharp 1986	PitA	Palynomorph indet. type A
Scfmem	Spiniferites cf. membranaceus	Pter	Pterospermella spp.
Sdel	Spiniferites (cf.) delicatus	Scol	Scolecodont spp.
Selo	Spiniferites elongatus (sensu stricto)	Sigm	Sigmopollis spp.
Selosl	Spiniferites elongatus sensu lato	Tasm	Tasmanites spp.
Sfri	Spiniferites frigidus	TiLo	Tintinid lorica
Shyp	Spiniferites hyperacanthus	TiLo1	Tintinid lorica type 1
Slaz	Spiniferites lazus	TiLo2	Tintinid lorica type 2
Smem	Spiniferites membranaceus	BisPo	Bisaccate pollen
Smir	Spiniferites mirabilis (sensu stricto)	BisPoOth	other Bisaccate pollen
Smirsl	Spiniferites mirabilis sensu lato	Pinus	Pinuspollen
		oP&S	other, non-bisaccate pollen and spores

Appendix B2 a: in-situ dinocyst counts for core M23071

Depth (cm)	Acho	Atax	Btep	Ipal	Ipar	Ipat	Isph	Istr	Ispp	Lmach		Nlab		Nsp	Ocen		OceT	Pret	Selosl		Slaz	Smem		
										<3	>3	Nlab	Ncflab		<3	>3			Selosl	Selo		Scfelo	Smem	Sbel
0.5	0	*	5	6	0	0	*	0	0	0	0	57	0	0	3	565	2	*	0	2	0	1	0	0
620	0	1	28	0	0	0	0	0	0	0	0	63	5	0	2	283	7	0	2	7	3	3	0	0
621	0	0	48	0	0	0	0	0	0	0	0	72	5	0	6	279	3	0	0	4	0	8	0	1
622	0	1	53	*	0	0	0	0	0	0	0	75	5	0	6	303	3	0	4	1	1	3	0	0
623	0	1	36	0	0	0	0	0	0	0	2	75	3	0	3	322	6	1	4	2	2	6	0	0
624	1	0	40	0	0	0	*	0	0	0	0	53	6	0	3	329	8	0	1	1	3	*	0	0
625	0	2	44	0	0	0	0	0	1	0	2	70	4	0	2	315	4	0	5	0	4	5	0	1
626	0	2	48	0	0	0	0	0	0	0	*	61	2	0	5	311	1	0	4	2	6	5	0	0
627	0	2	34	0	0	0	0	0	0	0	*	54	3	0	1	328	4	1	4	0	1	3	0	0
628	0	3	54	1	0	0	0	0	0	0	*	48	2	0	8	321	9	*	5	1	4	9	0	0
629	0	1	42	*	0	0	*	0	1	0	2	41	*	0	2	346	5	2	5	0	9	14	0	0
630	1	6	39	0	0	0	2	0	1	0	1	32	2	0	10	327	8	*	8	8	5	13	0	0
631	0	2	81	2	0	0	0	0	0	0	2	50	1	0	1	291	6	1	7	2	5	19	0	0
632	0	5	32	1	0	0	1	0	1	0	*	48	0	0	12	296	4	0	16	0	15	7	0	0
633	0	4	37	0	0	0	0	0	1	0	0	30	3	1	9	306	7	0	13	6	8	8	1	0
634	0	7	54	0	0	0	2	0	3	0	1	31	2	1	11	300	10	0	12	1	13	7	1	0
635	0	4	46	0	0	0	0	0	0	0	?	27	5	4	10	328	2	0	8	0	12	18	0	0
636	0	4	63	0	0	0	2	0	0	0	0	29	0	0	11	314	9	1	10	1	18	11	0	0
637	0	5	71	2	0	0	1	0	0	0	0	29	3	0	6	321	11	0	11	1	16	22	0	0
638	0	8	59	0	0	0	2	3	2	0	1	25	1	0	16	326	8	1	7	0	19	17	0	0
639	0	7	53	0	0	0	1	0	1	0	0	26	0	0	2	350	10	1	6	3	14	16	0	0
640	0	5	42	0	0	0	3	0	5	0	1	22	1	0	16	338	9	1	6	0	21	13	0	0
641	0	5	50	1	0	0	4	0	0	0	1	20	0	0	4	265	11	0	3	0	5	16	0	0
642	0	6	54	*	0	0	1	0	1	0	2	24	0	0	13	303	13	0	3	0	13	15	0	0
643	0	6	56	0	0	0	*	0	0	0	2	32	1	0	5	338	12	1	2	1	4	10	0	0
644	0	5	46	3	0	0	?	0	4	0	0	20	2	0	11	299	6	0	4	0	13	12	0	0
645	0	7	39	0	0	0	3	0	4	0	0	35	0	0	2	353	15	0	1	0	11	12	0	0
646	0	5	34	0	0	0	1	0	2	0	1	23	4	0	12	300	9	1	5	0	13	8	0	0
647	0	8	33	8	0	0	1	0	6	0	2	33	0	0	3	346	13	0	2	1	11	6	0	0
648	0	6	47	0	0	0	2	???	1	0	1	22	0	0	8	282	8	1	3	0	10	11	0	0
649	0	8	42	0	1	0	1	0	5	0	2	22	0	0	1	345	18	0	3	0	13	9	0	0
650	0	2	38	0	0	0	0	0	3	0	0	22	1	0	10	265	17	?	2	0	8	14	0	1
651	0	9	59	0	0	0	2	0	1	0	2	48	1	0	4	274	7	0	3	0	9	25	0	0
652	0	9	50	*	0	0	2	0	2	0	0	29	*	0	8	255	9	0	4	0	9	15	0	0
653	0	9	52	0	0	0	2	2	0	1	1	40	0	0	4	301	6	?	1	0	13	9	0	0
654	1	8	63	?	?	0	7	0	6	0	0	14	*	0	7	293	8	2	3	0	7	11	0	0
655	0	3	45	2	0	1	4	0	0	0	4	34	1	0	8	263	7	2	3	0	9	4	0	0
656	0	1	21	?	5	0	4	0	4	0	5	20	0	0	10	347	13	2	1	0	8	8	0	0
657	0	4	34	0	0	0	4	0	0	0	3	29	0	0	1	305	8	6	2	0	2	5	0	?
658	0	6	51	*	0	0	2	0	1	0	1	22	*	0	6	322	3	2	1	0	15	12	0	0
659	0	3	32	4	3	1	2	0	2	0	2	28	0	0	4	379	9	1	3	0	8	7	0	0
660	0	6	42	1	0	0	2	0	0	1	1	22	2	0	5	346	11	0	3	0	13	3	0	0
661	0	7	43	4	??	?	2	?	0	0	2	23	0	0	10	371	6	3	4	0	10	4	1	0
662	*	11	43	2	0	0	4	0	4	0	1	26	0	0	5	320	16	2	1	0	8	3	0	0
663	?	0	5	1	0	0	0	0	1	0	8	0	0	0	3	34	1	0	1	0	1	1	0	0

Appendix B2 a: in-situ dinocyst counts for core M23071 (continued)

Depth (cm)	Scfmem	Smirsl			Spac	Sramsl		Sdel	Sspp	Pdal	Stri	lmin	Lspp	PctA	Peri	Qcon	Bspp	Bspp			Squa	Tapp	Tcfapp	Dindet	TOTAL
		Smirsl	Shyp	Sramsl		Srbc	Bcar											Bsim							
0.5	0	1	0	0	0	5	0	0	6	25	1	0	0	0	0	0	3	0	0	2	0	0	4	688	
620	0	6	2	0	0	66	1	0	27	0	0	0	0	0	0	0	0	0	0	0	0	0	7	513	
621	0	7	5	1	0	77	0	0	21	2	0	0	0	0	0	0	0	0	0	0	0	0	17	556	
622	0	11	7	2	0	55	5	0	22	4	0	0	0	0	0	0	0	0	0	0	0	0	16	577	
623	2	4	4	0	0	49	1	0	15	1	0	0	0	0	0	0	0	0	0	0	0	1	9	549	
624	0	13	8	0	?	58	0	0	27	0	0	0	0	0	0	0	0	0	0	0	?	0	10	563	
625	0	6	4	0	0	56	1	0	10	4	0	0	0	0	0	0	0	0	0	0	0	0	16	556	
626	1	7	8	0	0	50	2	0	18	4	0	0	0	0	0	0	0	0	0	0	0	0	11	548	
627	0	14	6	1	1+?	63	1	0	20	5	0	0	0	0	0	0	0	0	0	0	0	0	13	560	
628	0	13	6	3	0	56	1	0	26	5	0	0	0	0	0	0	0	0	0	0	0	0	6	581	
629	1	25	2	3	0	38	0	0	16	5	0	0	0	0	0	0	0	0	0	0	0	0	10	570	
630	4	16	7	0	0	46	0	0	21	8	0	0	0	0	0	0	0	0	0	0	0	0	11	576	
631	0	22	13	1	0	25	0	0	25	1	0	0	0	0	0	0	0	0	0	0	0	0	12	569	
632	0	24	9	5	0	26	*	0	18	1	0	0	0	0	0	0	0	0	0	0	0	0	14	535	
633	0	22	8	4	0	34	0	0	23	2	0	0	0	0	0	0	1	0	0	0	0	0	10	538	
634	0	21	6	2	0	23	2	0	19	2	0	0	0	0	0	0	0	0	0	0	0	0	12	543	
635	0	18	19	1	0	33	0	0	20	?	0	0	0	0	0	0	0	0	0	0	0	1	13	571	
636	0	13	5	1	0	20	0	0	22	7	0	0	0	0	0	0	0	0	0	0	0	1	17	559	
637	0	8	7	2	0	25	0	0	20	15	0	0	0	0	0	0	0	0	0	0	0	0	19	595	
638	2	5	3	1	0	16	0	0	21	7	0	0	0	0	0	0	*	0	0	0	0	0	16	566	
639	1	4	4	2	0	5	1	0	21	19	0	0	0	0	?	0	0	0	0	0	0	*	29	577	
640	0	9	3	0	0	10	0	0	10	8	0	0	0	1	4	0	19	0	1	0	0	0	16	564	
641	1	3	3	2	0	15	1	0	16	18	?	0	0	1	0	?	33	0	3	0	0	1	26	510	
642	1	15	6	0	0	23	1	0	24	7	?	1	0	3	4	1	30	1	0	1	0	0	16	583	
643	2	10	2	0	0	17	0	0	7	16	0	0	0	4	0	2	26	0	1	0	0	0	12	569	
644	0	9	2	2	0	12	1	0	16	16	0	0	1	2	0	0	39	0	0	0	0	0	23	549	
645	0	13	4	2	0	17	6	1	4	13	0	0	0	1	0	0	32	1	0	???	0	0	16	595	
646	0	13	2	1	0	13	0	0	13	8	?	0	1	2	0	1	89	0	*	2	0	2	20	586	
647	0	15	5	0	0	21	0	0	13	9	0	0	0	6	0	0	28	0	0	0	0	0	24	594	
648	2	11	0	0	0	4	0	0	17	5	0	0	0	2	0	1	32	0	0	0	0	0	22	501	
649	2	7	1	1	0	9	0	0	13	12	0	0	0	1	0	2	27	0	0	??	0	1	27	575	
650	1	9	3	0	0	16	0	0	15	11	0	0	0	1	0	1	25	0	0	1	0	1	17	485	
651	0	17	5	0	0	30	0	0	24	4	0	0	0	2	0	?	22	0	0	0	0	0	21	570	
652	0	5	2	0	0	11	0	0	33	8	0	0	0	3	0	??	68	0	0	0	0	0	14	538	
653	0	5	3	0	0	13	0	1	11	8	0	0	0	8	0	?	68	0	0	0	0	1	19	581	
654	1	10	1	0	0	14	0	0	17	7	0	0	0	1	0	0	60	0	0	0	0	0	17	560	
655	0	14	1	0	0	20	1	0	19	8	1	0	0	?	4	2	30	0	0	0	0	0	20	511	
656	0	9	0	0	0	12	0	0	29	7	0	0	0	3	0	1	13	0	0	0	0	1	30	555	
657	0	9	1	0	??	22	0	0	20	14	2	0	0	2	0	0	20	0	0	0	1	0	14	511	
658	2	12	2	0	0	13	0	0	23	4	1	0	0	1	0	2	24	0	1	4	0	0	22	555	
659	0	13	3	0	0	28	0	0	12	11	0	?	0	6	0	1	9	0	0	0	0	1	22	595	
660	0	2	2	1	0	18	0	0	16	9	0	2	0	8	0	2	17	0	0	0	?	1	22	559	
661	1	10	0	0	0	25	1	0	18	12	5	0	2	0	0	1	10	0	0	0	0	0	21	600	
662	3	2	0	0	0	29	1	0	26	7	0	0	0	3	0	*	4	0	0	0	2	2	15	542	
663	0	0	0	0	?	9	0	0	7	1	0	0	0	0	0	0	5	0	0	0	???	0	13	96	

Appendix B2 b: other (palynomorph) counts for core M23071

Depth (cm)	weight	LySa	LyCo	Drew	Aspp	Cyma	EggIn	FoLi	Olic	Pedi	Scol	TiLo	BisPo		oP&S
													Pinus	BisPoOth	
0.5	NN	NN	175	1	2	0	3	16	4	0	1	6	8	8	10
620	1.44	18583	746	8	11	0	0	0	0	0	0	0	1	11	4
621	1.69	18583	1164	14	4	0	1	0	0	0	0	0	1	7	9
622	1.59	18583	1078	14	3	0	1	0	0	0	0	0	0	8	4
623	1.42	18583	1053	17	3	0	2	0	0	0	0	0	1	7	1
624	1.65	18583	864	12	8	0	1	0	0	0	0	0	1	10	5
625	1.41	18583	1167	19	8	0	1	0	0	0	0	0	1	7	6
626	1.43	18583	463	14	4	0	0	0	0	0	0	0	0	6	6
627	1.44	18583	279	12	1	0	1	0	0	0	0	0	2	4	7
628	1.42	18583	394	13	4	0	0	0	0	0	0	0	2	13	4
629	1.58	18583	552	15	3	0	1	0	0	0	0	0	2	9	4
630	1.44	18583	397	10	4	0	0	0	0	0	*	0	1	6	5
631	2.32	18583	91	12	2	0	0	0	0	0	0	0	1	9	2
632	1.52	18583	338	10	9	0	0	1	0	0	0	0	5	7	0
633	1.51	18583	272	8	6	0	0	0	0	0	1	0	17	6	3
634	1.44	18583	499	8	6	0	0	0	0	0	0	0	10	1	6
635	1.33	18583	268	6	5	0	2	0	0	0	0	1	4	2	2
636	1.44	18583	176	10	7	0	4	0	0	0	0	0	6	2	1
637	1.46	18583	146	13	7	0	5	0	0	0	0	0	2	9	2
638	1.43	18583	222	4	11	0	13	0	0	0	0	0	7	6	2
639	1.42	18583	309	9	15	0	8	0	0	1	1	0	3	16	8
640	1.23	18583	149	11	13	0	13	0	0	0	0	5	3	13	2
641	1.33	18583	329	10	20	0	15	0	0	0	1	3	5	11	17
642	1.39	18583	127	5	4	0	14	1	0	0	0	3	3	14	5
643	1.26	18583	184	21	18	0	19	*	0	0	1	3	4	13	23
644	1.41	18583	238	5	16	0	16	1	0	0	1	1	7	7	11
645	1.45	18583	234	21	13	0	19	2	0	0	0	1	8	12	14
646	1.31	18583	381	15	18	0	7	1	0	0	0	1	5	11	17
647	1.36	18583	313	34	17	0	19	0	0	0	1	0	9	26	15
648	1.34	18583	414	20	15	0	11	0	0	0	1	3	12	18	9
649	1.44	18583	319	23	17	0	21	1	0	0	2	1	4	22	24
650	1.46	18583	302	7	10	0	13	0	0	0	1	1	8	13	8
651	1.19	18583	93	23	4	0	13	0	0	0	0	0	5	16	18
652	0.68	18583	201	8	10	0	4	0	0	0	0	1	5	15	15
653	1.17	18583	150	34	15	0	14	0	0	0	1	0	8	29	14
654	1.08	18583	219	14	7	1	5	0	0	0	1	0	17	34	4
655	1.37	18583	329	35	13	0	10	0	0	0	0	2	19	35	35
656	1.53	18583	458	25	13	0	9	0	0	0	0	0	16	36	22
657	1.39	18583	350	56	13	0	5	0	0	3	0	1	9	60	16
658	1.46	18583	409	23	13	0	16	0	0	3	1	1	27	33	17
659	1.44	18583	302	56	5	1	5	0	0	2	3	2	25	44	16
660	1.58	18583	564	30	19	0	4	0	0	1	1	4	47	47	23
661	1.46	18583	508	35	25	0	5	1	0	1	1	1	56	47	40
662	1.63	18583	722	39	19	0	2	0	0	1	0	4	95	81	28
663	1.7	18583	1483	133	15	0	8	1	0	0	3	1	19	65	30

Appendix B3 a: in-situ dinocyst counts for core M23323

Depth (cm)	Acho	Atax	Btep	lacu	lpal	lpar	lpat	lsph	lstr	lspp	Lmach		Nlab	
											<3	>3	Nlab	Ncflab
0.5	0	0	2	0	2	0	0	*	0	0	0	0	56	0
750.5	0	0	34	0	*	0	0	0	0	0	0	1	62	0
752.5	0	2	39	0	0	0	0	0	0	0	0	0	85	0
754.5	0	1	42	0	1	0	0	1	0	0	0	4	50	?
756.5	0	1	37	0	*	0	0	1	0	0	0	0	57	3
758.5	?	6	37	0	1	0	0	*	0	0	0	0	30	0
760.5	0	3	34	0	3	0	0	3	0	0	0	*	35	*
762.5	0	3	29	0	4	0	0	1	0	0	0	2	41	0
764.5	0	5	37	0	2	0	0	0	0	0	0	0	29	0
766.5	0	6	36	0	1	0	0	1	0	0	0	0	77	3
768.5	0	*	36	0	2	0	0	1	0	0	0	2	46	1
770.5	0	13	28	0	4	0	0	1	0	2	0	0	52	*
772.5	0	5	47	0	3	0	0	1	0	1	0	2	62	0
774.5	0	5	47	0	1	0	0	*	0	0	1	1	63	4
776.5	0	1	54	0	2	0	0	3	0	0	0	1	50	2
778.5	0	2	52	0	3	0	0	2	0	0	0	0	44	2
780.5	0	4	72	0	?	0	0	0	0	0	0	0	24	1
782.5	0	3	79	0	1	0	0	1	0	1	0	0	26	1
784.5	0	8	105	0	1	0	0	0	0	0	0	0	32	1
786.5	0	5	58	0	2	0	0	1	0	0	0	*	47	*
788.5	0	4	65	0	0	0	0	2	0	1	0	0	37	3
790.5	0	6	61	0	1	1	0	?	0	0	0	0	26	0
792.5	0	3	67	0	?	?	0	1	0	0	0	0	20	0
794.5	0	3	56	0	4	0	0	*	0	0	0	1	31	0
796.5	0	1	56	0	1	0	0	1	0	0	0	0	36	0
798.5	0	2	69	0	2	0	1	2	0	1	0	0	51	1
800.5	0	4	52	0	2	0	0	3	0	0	0	1	55	1
802.5	0	3	28	0	3	0	0	3	0	0	0	2	99	2
804.5	0	3	26	0	0	0	0	2	0	0	0	0	75	1
806.5	0	6	21	0	0	0	0	1	0	0	0	*	58	0
808.5	0	3	19	0	0	0	0	1	0	2	0	2	60	1
810.5	0	*	38	0	0	0	0	*	0	2	0	1	36	0
812.5	0	6	45	0	1	0	0	*	0	0	0	2	46	0
814.5	0	5	32	0	1	2	0	3	0	0	0	2	21	0
816.5	0	4	35	1	*	1	0	6	0	0	0	1	24	0
818.5	0	4	36	0	1	1	0	6	0	0	0	*	23	0
820.5	0	4	50	0	6	0	0	6	0	0	0	2	22	0
822.5	0	4	35	0	3	1	0	7	0	0	0	1	27	0
824.5	0	2	35	0	2	1	0	7	0	0	0	2	36	0
826.5	0	3	35	0	4	?	0	8	0	0	0	1	43	0
828.5	0	2	32	0	3	3	0	7	0	1	0	1	43	0
830.5	0	4	22	0	2	0	0	6	0	0	0	*	50	0
832.5	0	3	21	0	3	0	0	1	?	0	0	1	36	1
834.5	0	6	34	0	4	0	0	11	0	3	0	*	48	1
836.5	0	5	34	0	3	*	0	3	0	2	0	1	17	0
838.5	0	6	33	0	1	0	0	4	0	1	0	1	41	0
840.5	0	7	33	0	3	0	0	9	0	0	0	1+?	27	0
842.5	0	11	31	0	1	?	0	1	0	0	0	1	35	0
844.5	0	7	37	0	1	0	0	3	0	0	0	0	32	0
846.5	0	10	48	?	4	?	0	4	0	0	0	4	47	1
848.5	0	13	42	0	5	1	0	2	0	0	0	2	56	0
850.5	??	11	51	0	3	1	0	4	0	0	0	1	38	0
852.5	0	19	49	0	5	0	0	4	0	0	0	3	29	0
854.5	0	5	12	0	3	0	0	1	0	0	0	4	8	0
856.5	0	1	4	0	2	0	0	1	0	0	0	6	3	0
858.5	?	0	5	0	1	0	0	0	0	0	0	5	2	0
860.5	0	0	2	0	1	0	0	0	0	0	0	8	0	0
862.5	0	0	3	0	0	0	0	0	0	0	0	5	2	0
864.5	0	0	3	0	0	0	0	0	0	0	0	12	0	0
866.5	0	0	2	0	0	0	0	0	0	0	0	5	0	0
868.5	?	0	6	0	1	0	0	0	0	0	0	9	0	0

Appendix B3 a: in-situ dinocyst counts for core M23323 (continued)

Depth (cm)	<3	>3	Ocen			Pret	Selosl	Selo	Selosl		Sfri	Ramp	Slaz	Smem	Scfmem
			OceT	OceC	OceA				Scfelo	Sfelo					
0.5	4	620	7	1	2	0	0	2	0	0	0	1	0	0	
750.5	2	309	5	?	0	0	5	0	0	0	0	2	0	0	
752.5	2	310	4	?	0	0	0	0	2	0	0	1	0	0	
754.5	2	340	4	0	6	1	1	7	3	0	0	7	0	0	
756.5	3	328	5	0	10	1	1	4	0	0	0	4	0	0	
758.5	3	335	8	0	3	1	0	16	5	0	0	5	0	0	
760.5	5	346	10	0	3	*	0	14	5	0	0	8	0	0	
762.5	6	336	1	0	6	0	0	13	4	0	0	6	0	0	
764.5	3	344	7	2	5	0	0	18	3	0	0	3	0	0	
766.5	0	274	2	0	5	2	0	9	7	0	0	14	0	0	
768.5	4	271	0	0	0	1	0	15	5	0	0	11	0	0	
770.5	2	313	6	3	0	4	1	20	*	0	0	9	0	0	
772.5	1	293	2	1	0	4	0	11	4	0	0	9	0	0	
774.5	3	259	1	0	1	1	1	11	6	0	0	13	0	0	
776.5	1	315	1	0	1	2	1	13	10	0	0	12	0	*	
778.5	2	266	7	0	0	2	2	15	10	0	0	20	0	1	
780.5	1	316	6	3	0	2	1	8	15	0	0	20	0	0	
782.5	3	305	6	0	1	0	1	14	13	0	0	10	0	0	
784.5	1	284	7	0	2	0	0	12	11	0	0	21	0	0	
786.5	2	297	10	0	2	0	2	15	20	0	0	10	0	0	
788.5	1	347	10	0	0	0	0	15	4	0	0	11	0	0	
790.5	6	342	4	0	3	1	0	13	7	0	0	16	0	1	
792.5	9	332	4	0	4	0	0	7	2	0	0	13	0	*?	
794.5	4	318	8	0	4	0	0	7	2	0	0	19	0	0	
796.5	4	316	8	0	2	0	0	5	1	0	0	14	0	0	
798.5	5	306	2	0	1	0	0	5	4	0	0	14	0	0	
800.5	4	299	9	1	2	0	0	4	1	0	0	14	0	0	
802.5	0	316	5	0	1	*	0	2	7	0	0	23	0	0	
804.5	2	314	4	1	1	0	0	4	5	0	0	18	0	0	
806.5	0	366	2	0	0	0	0	5	1	0	0	14	0	1	
808.5	2	352	7	0	0	1	0	4	1	0	0	9	0	1	
810.5	0	388	7	0	2	?	0	1	1	0	0	4	0	0	
812.5	2	338	4	0	0	4	0	4	2	0	0	7	0	0	
814.5	1	384	8	1	1	4	0	2	2	0	0	7	0	0	
816.5	0	352	4	0	1	4	1	5	5	0	0	8	0	0	
818.5	3	329	4	1	3	1	0	4	5	0	0	5	0	0	
820.5	1	386	6	0	1	4	0	7	1	0	1	4	0	0	
822.5	0	355	3	0	0	4	0	13	5	0	0	8	0	2	
824.5	4	362	7	0	1	1	0	5	3	0	0	8	0	*?	
826.5	3	369	4	0	0	1	0	8	3	0	0	3	0	0	
828.5	2	357	9	0	3	1	3	8	3	0	0	7	0	1	
830.5	4	397	5	1	0	2	1	2	6	0	0	5	0	1	
832.5	1	336	3	0	0	2	3	4	4	0	0	3	0	1	
834.5	1	390	6	0	0	*	0	12	3	0	0	5	0	1	
836.5	3	353	3	0	2	2	0	4	7	0	0	4	0	2	
838.5	2	357	5	0	4	2	1	5	2	0	0	3	0	2	
840.5	3	358	5	0	3	4	5	5	6	0	0	4	0	0	
842.5	5	376	4	0	1	3	0	2	4	0	0	4	0	0	
844.5	3	357	5	0	3	4	1	4	9	0	0	4	0	0	
846.5	4	320	9	0	3	2	1	1	4	0	0	10	0	1	
848.5	4	294	10	0	7	3	0	5	3	0	0	1	0	0	
850.5	3	334	9	0	4	3	1	3	2	0	0	3	0	2	
852.5	3	239	17	1	7	4	0	0	0	?	0	4	0	0	
854.5	1	61	2	0	2	1	0	0	0	0	0	0	0	0	
856.5	0	8	1	0	1	0	0	0	0	0	0	0	0	0	
858.5	0	16	2	0	0	0	0	1	0	0	0	1	0	0	
860.5	0	3	0	0	0	0	0	0	0	0	0	0	0	0	
862.5	0	15	2	0	0	0	0	0	0	?	0	0	0	0	
864.5	0	7	0	0	0	0	0	0	0	0	0	1	0	0	
866.5	0	4	0	0	0	0	0	0	0	0	0	0	0	0	
868.5	0	11	0	0	0	0	0	0	0	0	0	1	0	0	

Appendix B3 a: in-situ dinocyst counts for core M23323 (continued)

Depth (cm)	Smirsl			Spach	Sramsl		Sdel	Sspp	Pdal	Stri	Imin	Lspp	PctA	Peri
	Smirsl	Smir	Shyp		Sram	Srbc								
0.5	5	0	1	0	3	0	0	8	9	0	0	0	0	1
750.5	11	1	0	0	96	0	?	19	0	0	0	0	0	1
752.5	10	2	0	0	77	0	0	22	4	0	0	0	0	0
754.5	11	2	0	0	60	0	0	33	7	0	0	0	0	0
756.5	9	1	2	??	62	0	4	20	14	0	0	0	0	0
758.5	15	0	1	0	55	1	0	12	15	0	0	0	0	0
760.5	7	6	2	0	44	0	0	14	9	0	0	0	0	0
762.5	10	4	0	0	33	0	0	31	31	1	0	*	0	1
764.5	12	5	1	0	41	0	2	10	17	1	0	0	?	0
766.5	16	5	0	0	42	0	0	43	12	??	0	0	0	0
768.5	16	3	0	0	51	1	0	41	43	?	0	0	1	0
770.5	12	7	6	0	40	2	0	22	25	*	0	1	0	0
772.5	13	6	3	cf	34	0	0	23	37	0	0	0	0	0
774.5	25	6	0	0	40	0	0	35	30	*	0	0	0	0
776.5	19	4	2	1	28	0	0	27	42	1	0	0	1	1
778.5	13	3	0	0	25	0	0	29	48	0	0	0	0	0
780.5	10	4	0	0	20	0	0	25	29	0	0	0	*	0
782.5	14	6	1	1	20	0	0	20	37	0	0	0	0	0
784.5	5	2	0	0	26	0	0	12	18	0	0	0	3	0
786.5	7	2	0	0	20	0	1	32	23	2	?	0	*	0
788.5	11	3	3	0	10	0	0	19	30	2	0	0	1	0
790.5	6	3	1	0	14	0	0	22	20	2	0	0	5	0
792.5	7	1	0	?	15	0	0	18	18	4	0	0	10	0
794.5	8	2	0	0	11	0	0	9	21	*	0	0	10	1
796.5	7	4	0	0	16	0	0	9	17	1	0	0	12	0
798.5	6	2	0	0	30	1	0	15	15	1	0	0	?	0
800.5	6	2	0	0	16	0	0	23	20	3	0	0	3	0
802.5	10	4	0	0	31	0	0	23	14	1	0	0	1	0
804.5	9	4	0	0	20	0	0	19	21	0	0	0	5	0
806.5	2	3	1	0	21	0	0	11	11	2	0	0	7	0
808.5	10	2	0	0	17	0	0	23	13	*	0	0	4	0
810.5	14	7	0	0	10	0	0	11	13	?	0	0	6	0
812.5	14	2	3	0	17	0	0	27	14	1	0	0	3	0
814.5	16	5	1	0	8	0	0	26	14	1	0	0	5	0
816.5	12	3	2	0	15	0	0	31	9	3	?	0	5	0
818.5	8	2	0	?	11	0	0	26	13	1	0	0	1	0
820.5	10	1	0	0	16	0	0	15	9	2	0	0	2	0
822.5	7	0	0	0	18	0	0	21	5	1	0	0	8	2
824.5	8	1	0	0	17	0	0	15	12	*	0	0	5	0
826.5	2	2	0	0	20	0	0	18	16	0	0	0	2	0
828.5	3	2	0	2	25	0	0	20	18	2	0	0	14	0
830.5	3	2	0	0	37	0	0	19	12	0	0	0	3	0
832.5	7	1	1	0	23	0	0	21	21	2	0	0	14	0
834.5	4	0	0	0	30	0	0	22	5	3	0	0	3	0
836.5	4	0	0	0	22	0	0	14	10	2	0	0	10	0
838.5	4	1	0	0	29	0	0	25	6	1	?	0	2	0
840.5	4	1	0	0	24	0	0	13	4	0	0	0	5	0
842.5	3	0	0	0	23	0	0	21	7	*	0	0	1	0
844.5	2	0	0	0	30	0	1	19	5	0	0	0	0	0
846.5	3	0	0	0	33	0	0	27	8	1	0	0	0	0
848.5	0	0	0	0	43	0	0	30	0	1	0	0	0	0
850.5	1	0	0	?	24	0	0	19	2	0	0	0	1	0
852.5	2	0	0	0	13	0	0	16	2	1	0	0	0	0
854.5	2	0	0	0	8	0	0	6	2	0	0	0	0	0
856.5	0	0	0	0	9	0	0	7	1	0	0	0	0	0
858.5	2	0	0	0	6	0	0	6	0	0	0	0	0	0
860.5	0	0	0	0	6	0	0	12	0	0	0	0	0	0
862.5	1	0	0	?	6	0	0	9	2	0	0	0	0	0
864.5	1	0	0	0	9	0	0	7	2	0	0	0	0	0
866.5	1	0	0	0	3	0	0	7	0	0	0	0	0	0
868.5	1	0	0	0	7	0	0	11	1	0	0	0	3	0

Appendix B3 a: in-situ dinocyst counts for core M23323 (continued)

Depth (cm)	Qcon	Bspp		Pkof	Psch	Squa	Tapp	Tcfapp	Vspi	Dindet	TOTAL
		Bspp	Bcar								
0.5	0	0	0	0	0	0	1	0	0	9	734
750.5	?	0	0	0	0	0	0	0	1	7	559
752.5	0	0	0	0	0	0	0	0	0	11	572
754.5	0	0	0	0	0	0	0	0	0	12	596
756.5	0	0	0	0	0	0	0	?	0	11	581
758.5	0	0	0	0	0	0	0	*	0	11	561
760.5	0	0	0	0	0	0	0	1	0	4	556
762.5	0	3	0	0	0	0	0	1	0	11	578
764.5	0	8	0	1	0	0	0	0	0	10	567
766.5	0	6	0	0	0	0	0	0	0	10	573
768.5	0	2	0	0	0	0	0	0	0	10	564
770.5	0	8	0	2	0	0	0	0	0	11	594
772.5	0	2	0	0	0	0	0	2	0	10	577
774.5	0	2	0	0	0	0	0	0	0	12	568
776.5	0	11	0	0	0	0	0	0	0	9	616
778.5	0	4	0	0	0	0	0	0	0	15	567
780.5	0	0	0	0	0	0	0	0	0	13	575
782.5	0	1	0	0	0	0	0	0	0	13	578
784.5	*	6	0	0	0	3	0	0	0	9	569
786.5	0	2	0	0	0	0	?	0	0	19	581
788.5	?	11	1	0	0	0	0	1	0	15	608
790.5	0	12	0	0	0	1	0	0	0	11	586
792.5	1	15	0	1	0	2	0	0	0	19	575
794.5	4	30	0	2	0	1	0	0	0	12	568
796.5	*	44	0	1	0	1	0	0	0	8	565
798.5	?	7	0	1	0	0	0	0	0	15	562
800.5	0	39	0	5	0	0	0	0	0	15	584
802.5	*	12	0	0	0	0	0	0	0	17	607
804.5	*	20	2	1	0	0	0	?	0	14	572
806.5	0	11	0	2	0	?	0	0	0	9	556
808.5	0	16	0	0	0	0	?	*?	0	13	564
810.5	1	9	0	0	0	0	?	0	0	14	568
812.5	??	18	1	2	0	0	*	0	0	17	582
814.5	1	16	0	0	0	0	1	?	0	11	582
816.5	0	18	0	0	0	0	2	0	0	19	572
818.5	0	4	0	0	0	0	0	0	0	8	501
820.5	0	16	0	0	0	0	0	0	0	16	588
822.5	2	18	0	0	0	0	*	0	0	8	558
824.5	*	9	0	1	0	0	0	0	0	7	551
826.5	*	15	0	3	0	*	0	0	0	7	571
828.5	2	16	0	0	0	0	0	0	0	16	606
830.5	0	6	0	*	0	0	0	0	0	12	603
832.5	1	22	0	0	0	0	1	0	0	10	548
834.5	1	8	0	0	0	0	0	0	0	11	612
836.5	0	27	0	2	0	0	0	0	0	13	549
838.5	0	9	0	0	0	0	0	*	0	9	557
840.5	1	18	0	0	0	0	0	0	0	10	553
842.5	0	4	0	0	0	0	0	1	0	15	555
844.5	1	10	0	2	0	0	0	0	0	10	550
846.5	1	11	0	0	0	0	1	?	0	14	575
848.5	1	11	0	0	0	0	2	0	0	16	552
850.5	1	20	0	0	1	0	2	1	0	16	564
852.5	0	10	0	0	0	0	1	0	0	10	440
854.5	0	5	0	0	0	0	2	1	0	3	129
856.5	0	4	0	0	0	0	1	1	0	3	53
858.5	0	0	0	0	0	0	3	0	0	4	55
860.5	0	2	0	0	0	0	0	1	0	3	38
862.5	0	1	0	0	0	0	2	0	0	1	51
864.5	0	0	0	0	0	0	0	3	0	5	50
866.5	0	0	0	0	0	0	0	0	0	4	26
868.5	0	3	0	0	0	0	2	0	0	4	61

Appendix B3 b: other (palynomorph) counts for core M23323

Depth (cm)	weight	LySa	LyCo	Drew	Aspp	Cyma	Eggin	Foli	Pedi	Scol	TiLo	BisPo		oP&S
												BisPoOth	Pinus	
0.5	1.60	18583	284	0	1	0	1	1	0	0	*	4	12	5
750.5	1.51	18583	936	11	5	0	5	0	0	0	0	8	2	31
752.5	1.84	18583	522	11	7	0	2	0	0	0	2	16	6	13
754.5	1.54	18583	531	11	1	0	5	0	0	0	0	3	6	17
756.5	1.52	18583	427	15	11	0	2	0	0	0	0	10	6	12
758.5	1.60	18583	399	15	3	0	1	0	0	0	1	10	7	27
760.5	1.65	18583	235	14	4	0	*	0	0	*	0	9	7	8
762.5	5.90	55749	333	13	8	0	4	0	*	2	2	2	13	19
764.5	1.60	18583	197	7	2	0	3	1	0	0	0	9	12	22
766.5	6.22	55749	150	15	1	0	2	0	0	0	0	7	13	3
768.5	1.76	18583	362	16	7	0	1	1	0	0	0	10	17	15
770.5	6.17	55749	102	11	4	0	4	0	0	1	0	13	12	6
772.5	1.68	18583	327	15	10	0	3	0	0	*	2	12	7	10
774.5	6.00	55749	107	23	5	0	12	0	0	1	1	6	7	9
776.5	1.78	18583	411	19	9	0	13	1	0	1	3	9	14	22
778.5	1.90	18583	328	14	12	0	22	1	0	1	0	7	7	14
780.5	1.71	18583	195	10	5	0	11	0	0	0	1	8	3	7
782.5	1.71	18583	198	8	4	0	11	0	0	0	1	6	5	18
784.5	1.67	18583	59	9	7	0	18	1	0	0	1	4	3	7
786.5	6.33	55749	49	11	3	0	*	0	0	0	1	3	2	1
788.5	1.42	18583	142	10	4	0	11	0	0	1	3	7	8	4
790.5	1.43	18583	138	12	6	1	10	0	0	0	1	4	9	7
792.5	1.65	18583	173	14	7	0	4	0	0	0	1	7	5	6
794.5	1.59	18583	143	16	5	0	11	1	0	1	2	15	5	6
796.5	1.47	18583	199	14	4	0	8	1	0	1	0	7	6	6
798.5	5.70	55749	118	12	2	0	6	*	0	*	2	6	8	13
800.5	1.44	18583	310	15	3	0	4	5	0	1	2	13	5	12
802.5	6.78	55749	45	16	2	0	*	0	0	0	2	5	5	7
804.5	1.55	18583	287	10	5	0	4	2	0	*	1	11	10	9
806.5	1.43	18583	347	24	3	0	2	1	0	0	0	6	7	6
808.5	1.54	18583	266	7	2	0	0	0	0	0	1	8	10	7
810.5	6.54	55749	160	16	8	0	2	0	0	1	0	8	5	12
812.5	1.40	18583	415	18	1	0	4	3	1	1	2	23	22	10
814.5	1.35	18583	307	32	2	0	7	1	0	1	1	38	29	10
816.5	1.29	18583	245	24	6	0	8	*	0	*	3	35	31	18
818.5	1.38	18583	278	21	3	0	4	0	0	1	1	43	40	14
820.5	1.36	18583	453	22	6	0	4	0	2	0	5	41	57	14
822.5	1.40	18583	302	24	2	0	3	0	4	2	3	39	41	16
824.5	1.36	18583	280	10	1	0	5	0	0	1	3	21	40	14
826.5	1.43	18583	276	8	5	0	1	1	0	0	2	25	60	19
828.5	1.32	18583	377	13	4	0	3	1	0	2	3	36	63	19
830.5	6.40	55749	98	16	5	0	2	0	0	0	1	32	67	9
832.5	1.31	18583	297	14	0	0	1	0	0	0	5	28	83	12
834.5	5.75	55749	168	36	10	0	1	0	0	1	4	24	92	19
836.5	1.37	18583	419	18	6	0	4	1	0	1	2	64	127	43
838.5	1.39	18583	424	21	6	0	1	1	0	3	5	57	136	27
840.5	1.35	18583	401	16	2	0	0	0	1	2	2	83	180	40
842.5	1.31	18583	233	13	3	0	1	0	0	0	5	47	91	16
844.5	1.39	18583	502	10	2	0	1	0	*	*	6	67	117	31
846.5	1.32	18583	782	30	1	0	0	1	0	2	3	66	143	27
848.5	1.33	18583	665	33	3	0	0	0	0	2	2	64	148	46
850.5	1.31	18583	1173	35	2	0	0	1	2	2	10	77	112	44
852.5	1.41	18583	1739	42	2	1	2	2	0	1	4	68	95	36
854.5	1.34	18583	1344	48	2	0	1	0	0	0	5	36	33	23
856.5	1.44	18583	1226	109	2	0	0	0	0	1	2	43	35	18
858.5	1.34	18583	1109	106	2	0	1	1	0	0	1	40	35	18
860.5	1.35	18583	800	88	2	0	1	0	2	0	0	50	43	8
862.5	1.32	18583	426	49	0	0	0	0	0	3	1	28	36	10
864.5	1.29	18583	804	164	2	0	0	0	5	1	0	78	55	18
866.5	1.27	18583	654	89	1	0	0	2	2	3	0	53	37	16
868.5	1.35	18583	653	138	1	0	2	4	1	4	0	79	48	21

Appendix B4 a: in-situ dinocyst counts for core M23455

Depth (cm)	Acho	Atax	Btep	Ipal	Ipar	Ipat	Isph	Lmac	Nlab	Ocen			
										<3	>3	OceA	OceC
290.25	0	0	22	0	0	4	3	0	18	0	10	1	0
292.25	0	0	16	2	0	1	1	0	24	0	24	1	0
294.25	0	0	0	0	0	0	0	0	2	2	15	1	0
296.25	0	0	3	0	0	0	0	0	12	2	19	0	1
298.25	0	0	2	0	0	0	0	0	1	0	9	1	0
300.25	0	0	2	0	0	0	0	0	5	0	8	2	0
302.25	0	0	2	0	0	0	0	0	4	0	7	0	0
304.25	0	0	0	0	0	1	0	0	10	0	3	0	0
306.25	0	0	4	0	0	0	0	0	60	0	17	1	1
307.25	0	0	3	0	0	0	0	0	57	0	17	1	0
308.25	1	0	1	0	0	0	0	0	73	0	23	6	1
309.25	0	0	10	0	0	0	0	0	69	1	40	7	0
310.25	0	0	14	0	0	0	0	0	71	3	41	5	1
311.25	0	0	30	0	0	0	0	1	113	3	90	7	0
312.25	1	0	43	0	0	0	0	0	133	4	132	12	3
313.25	0	1	29	0	1	0	0	0	168	4	152	6	1
314.25	0	0	12	0	0	0	1	0	98	2	43	2	1
315.25	0	0	25	1	0	0	0	0	100	2	83	2	0
316.25	0	0	0	0	0	0	0	*	18	0	11	1	1
317.25	0	0	2	0	0	0	0	1	7	0	16	0	0
318.25	1	0	2	1	0	0	0	0	20	0	12	2	1
320.25	0	0	0	0	0	0	0	0	0	0	4	0	0

Appendix B4 a: in-situ dinocyst counts for core M23455 (continued)

Depth (cm)	Selosl		Sram	Sben	Slaz	Smir	Sspp	Pdall	Dubr	Lspp	Peri	Tapp	Dindet	TOTAL
	Selo	Sfri												
290.25	0	0	3	0	0	0	5	0	0	0	0	0	2	68
292.25	0	0	2	0	0	0	4	0	0	0	0	0	3	78
294.25	1	1	9	0	0	1	4	0	0	0	0	0	0	36
296.25	0	0	9	0	0	0	7	0	0	0	0	?	3	56
298.25	0	0	6	0	0	0	4	0	0	0	0	0	1	24
300.25	1	0	4	0	0	0	7	0	0	0	0	0	2	31
302.25	0	0	3	0	0	0	1	0	0	0	0	0	0	17
304.25	0	0	3	0	2	0	1	0	0	0	0	0	1	21
306.25	0	0	5	0	0	0	7	0	0	0	0	0	5	100
307.25	0	0	19	0	0	*	10	0	0	0	0	0	5	112
308.25	0	0	22	0	0	1	13	0	0	0	0	0	8	149
309.25	0	0	43	0	0	2	15	0	0	0	0	1	5	193
310.25	0	0	45	0	3	0	15	0	0	0	0	0	11	209
311.25	1	0	55	0	1	3	25	0	0	0	0	0	15	344
312.25	0	1	104	0	2	1	21	0	0	1	0	*	19	477
313.25	2	0	71	0	12	4	42	1	1	1	0	0	18	514
314.25	0	0	49	1	10	6	16	0	0	0	0	0	5	246
315.25	1	0	45	0	10	6	24	0	0	0	0	1	27	327
316.25	0	0	20	0	1	0	11	0	0	0	0	0	2	65
317.25	0	0	4	0	3	1	8	0	1	0	0	0	2	45
318.25	0	0	3	0	0	0	7	0	0	1	3	1	6	60
320.25	0	0	0	0	0	0	3	1	0	1	1	2	5	17

Appendix B4 b: other (palynomorph) counts for core M23455

Depth (cm)	weight	LySa	LyCo	Drew	Alln	Aspp	Botr	Cycl	Cyma	Eggl
290.25	1.78	37166	6316	5	0	2	1	0	0	4
292.25	1.74	37166	5496	21	0	0	4	0	0	4
294.25	1.99	37166	8543	8	0	1	3	0	0	1
296.25	1.98	37166	9437	8	0	3	1	0	0	6
298.25	1.99	37166	2583	8	0	0	0	0	0	4
300.25	2.01	18583	3936	6	0	1	0	0	0	2
302.25	2.01	18583	2155	7	0	0	0	0	0	1
304.25	1.99	18583	2371	7	0	1	3	0	0	2
306.25	2.00	18583	4742	10	0	3	0	0	0	5
307.25	1.99	18583	3391	16	0	2	4	0	0	9
308.25	1.96	18583	5236	8	0	3	1	0	0	4
309.25	1.93	18583	4737	24	0	2	6	0	0	10
310.25	1.97	18583	2795	12	0	3	3	0	0	5
311.25	1.95	18583	3947	23	0	0	4	0	0	7
312.25	1.99	18583	2811	17	0	0	3	0	0	9
313.25	1.94	18583	2469	15	0	6	3	0	0	3
314.25	1.95	18583	1271	8	0	1	1	0	0	4
315.25	1.90	18583	3772	21	0	7	2	0	0	7
316.25	1.85	18583	5394	12	0	0	3	0	2	6
317.25	1.93	18583	4861	10	0	4	4	0	0	8
318.25	1.97	18583	4460	10	0	5	5	1	3	8
320.25	1.98	18583	5023	12	7	7	4	0	*	5

Appendix B4 b: other (palynomorph) counts for core M23455 (continued)

Depth (cm)	FoLi	FuRe	Halo	Pedi	Pter	Tasm	TiLo	BisPo		oP&S
								BisPoOth	Pinus	
290.25	0	16	0	0	0	0	0	5	7	24
292.25	1	17	0	0	0	0	0	10	4	18
294.25	0	6	0	0	0	0	1	3	2	17
296.25	0	1	0	0	1	0	0	3	2	32
298.25	0	0	0	0	0	1	0	3		11
300.25	0	3	0	0	0	0	0	2	1	9
302.25	0	3	0	1	0	0	0	3	1	13
304.25	0	4	0	1	0	0	0	3	1	6
306.25	0	6	0	0	0	0	0	3	2	15
307.25	0	7	0	3	1	0	0	6	1	10
308.25	0	3	0	3	0	0	0	4	2	27
309.25	1	6	0	2	0	0	1	3	1	4
310.25	0	3	0	2	0	0	0	8	2	17
311.25	0	4	1	0	1	0	0	5	2	18
312.25	0	5	0	0	0	0	0	3	1	26
313.25	0	2	0	0	0	0	0	4	1	13
314.25	0	2	0	2	0	0	0	1	1	7
315.25	0	6	0	0	0	1	0	1	0	15
316.25	0	13	0	5	1	0	0	2	4	18
317.25	1	8	0	0	2	0	0	1	0	13
318.25	0	1	0	0	0	0	1	4	2	28
320.25	0	10	0	1	3	1	0	4	1	22

Appendix B5 a: in-situ dinocyst counts for core MD992277

Original depth (cm)	Corrected depth (cm)	Acho	Atax	Btep	Iacu	Ipal	Ipar	Ipat	Isph	Ispp	Lmac	Nlab			Ocen			Pret	Scfmem	Sdel	Selo
												Nlab	Ncflab	<3	>3	OceA	OceC				
390.5	361.5	?	0	0	0	0	0	1	0	1	0	56	0	0	12	0	0	0	0	0	0
392.5	363.5	0	0	0	0	0	0	0	0	0	1	37	1	0	12	0	0	0	0	0	0
394.5	365.5	?	0	3	0	2	0	0	0	0	0	104	2	0	25	1	0	0	0	0	0
396.5	367.5	0	1	2	0	0	0	0	0	0	0	104	0	1	19	0	0	0	0	0	1
398.5	369.5	0	0	1	0	1	0	0	0	0	1	73	0	0	9	0	0	0	0	0	0
400.5	371.5	0	0	0	0	0	0	0	0	0	2	37	0	0	4	0	0	0	0	0	0
402.5	373.5	0	0	0	0	1	0	0	1	0	0	52	0	0	19	1	0	0	0	0	0
404.5	375.5	0	0	1	0	1	0	0	0	0	0	33	0	0	48	2	0	0	0	0	2
406.5	377.5	0	0	2	0	4	0	0	0	0	0	15	0	0	51	1	0	0	0	1	0
408.5	379.5	0	0	19	0	1	0	1	0	0	0	18	0	1	32	1	0	0	0	0	1
410.5	381.5	0	0	1	1	1	0	0	0	0	1	30	0	0	78	1	0	0	0	0	1
412.5	383.5	0	0	1	1	1	0	0	0	0	0	23	0	0	46	0	0	0	0	0	1
414.5	385.5	0	0	6	0	1	0	0	0	0	0	35	0	0	105	1	0	0	0	0	2
416.5	387.5	0	0	6	0	3	0	0	1	0	1	42	0	0	83	2	0	0	0	0	0
420.5	391.5	0	0	0	0	0	0	0	0	0	0	63	0	0	7	0	0	0	0	0	0
422.5	393.5	0	0	25	0	3	0	0	0	1	0	53	0	4	204	1	0	0	0	0	0
424.5	395.5	0	0	0	0	0	0	0	1	0	0	87	0	0	46	2	1	0	0	0	1
426.5	397.5	0	0	6	0	6	0	0	1	0	0	69	0	0	100	0	0	0	0	0	1
428.5	399.5	0	0	1	0	?	1	0	0	0	0	83	0	0	99	2	0	0	0	0	0
430.5	401.5	0	0	0	0	1	0	0	0	0	0	11	0	0	11	0	0	0	0	0	0
432.5	403.5	0	0	4	0	3	0	0	0	0	0	15	0	0	70	0	0	0	0	0	2
434.5	405.5	0	0	2	0	0	0	0	0	0	0	50	0	0	41	1	0	0	0	0	1
436.5	407.5	0	1	0	0	0	0	0	1	0	0	56	0	1	34	0	0	0	0	0	0
438.5	409.5	0	0	0	0	1	0	0	0	0	2	21	0	0	24	0	0	0	0	0	0
440.5	411.5	0	0	0	0	0	0	0	0	0	0	36	0	0	11	0	0	0	0	0	0
442.5	413.5	0	0	0	0	0	0	0	0	0	7	21	0	0	26	0	0	0	0	0	1
444.5	415.5	0	0	0	0	0	0	0	0	0	4	16	0	0	13	0	0	0	0	0	0
446.5	417.5	0	0	0	0	0	0	0	1	0	0	28	0	0	15	0	0	0	0	0	0
448.5	419.5	0	0	0	0	0	0	0	0	0	0	30	0	0	23	0	0	0	0	0	0
450.5	421.5	0	0	1	0	0	0	0	0	0	0	20	0	0	52	1	0	0	0	0	0
452.5	423.5	0	0	0	0	0	0	0	0	0	1	5	0	0	35	0	0	0	0	0	0
454.5	425.5	0	0	1	0	1	0	0	0	0	0	13	0	0	22	0	0	0	0	0	1
456.5	427.5	0	0	0	0	0	0	0	0	1	0	9	0	0	15	0	0	0	0	0	0
458.5	429.5	0	0	3	0	1	0	0	0	0	0	25	0	1	53	0	0	0	0	0	2
460.5	431.5	0	0	1	0	1	0	0	0	0	0	42	0	0	49	0	0	0	0	0	0
462.5	433.5	0	0	1	0	6	0	0	0	0	0	39	0	0	66	0	0	0	0	0	0
464.5	435.5	0	0	1	0	0	0	0	0	0	4	7	0	0	39	0	0	0	0	0	0
466.5	437.5	0	0	1	0	0	0	0	0	0	2	8	0	1	36	0	0	0	1	0	0
468.5	439.5	0	0	0	0	0	0	0	0	0	1	3	0	0	13	1	0	0	0	0	0
470.5	441.5	0	0	3	0	5	0	0	0	0	7	11	0	1	68	2	0	1	0	0	0
472.5	443.5	0	0	1	0	4	0	0	0	0	4	6	0	0	47	2	0	0	0	0	0

Appendix B5 a: in-situ dinocyst counts for core MD992277 (continued)

Original depth (cm)	Corrected depth (cm)	Slaz	Smirsl	Spac	Sram	Sspp	Pdal	Bspp	Bspp Bcar	Bsim	Dubr	Peri	Tapp	Tcfapp	Dindet	TOTAL
390.5	361.5	3	1	0	17	10	0	0	0	0	0	0	0	0	7	108
392.5	363.5	1	2	0	17	16	0	0	0	0	0	0	0	0	3	90
394.5	365.5	4	0	0	31	26	4	0	0	0	0	0	?	0	13	215
396.5	367.5	2	0	0	27	29	0	0	0	0	0	0	0	0	6	192
398.5	369.5	10	1	0	24	27	0	0	0	0	0	0	0	0	13	160
400.5	371.5	4	0	0	10	9	1	0	0	0	0	1	0	0	5	73
402.5	373.5	5	0	0	15	22	0	0	0	0	0	0	0	0	13	129
404.5	375.5	6	1	0	11	15	0	0	0	1	0	0	0	0	11	132
406.5	377.5	3	1	0	5	10	1	0	0	0	0	0	1	0	4	99
408.5	379.5	3	0	0	6	7	0	0	0	0	0	0	1	0	4	95
410.5	381.5	4	1	0	5	11	3	0	0	1	1	0	0	0	11	151
412.5	383.5	8	0	0	7	15	0	0	0	0	0	0	0	1	5	109
414.5	385.5	7	0	0	2	9	1	0	0	0	0	0	0	0	13	182
416.5	387.5	20	1	0	6	17	1	1	0	0	0	1	0	0	9	194
420.5	391.5	40	0	0	16	28	0	0	0	0	0	0	0	0	13	167
422.5	393.5	7	2	0	16	22	5	1	0	0	0	0	0	0	13	357
424.5	395.5	23	6	0	11	18	2	0	0	0	0	0	0	0	15	213
426.5	397.5	22	6	0	12	18	2	1	0	0	0	0	0	0	12	256
428.5	399.5	14	6	0	12	15	0	0	0	0	0	0	0	0	14	247
430.5	401.5	2	0	0	0	3	0	0	0	0	0	0	0	0	0	28
432.5	403.5	2	0	0	1	4	3	2	0	0	0	0	0	0	5	111
434.5	405.5	5	1	0	3	13	1	2	0	0	0	0	0	0	13	133
436.5	407.5	8	3	1	9	19	0	0	0	0	0	0	0	0	12	145
438.5	409.5	1	0	0	3	10	0	0	0	0	0	0	0	0	4	66
440.5	411.5	1	2	0	5	9	2	0	0	0	0	0	0	0	7	73
442.5	413.5	3	1	0	8	8	0	0	0	0	0	0	0	0	8	83
444.5	415.5	0	0	0	3	6	0	0	0	0	0	0	0	0	2	44
446.5	417.5	1	0	0	2	6	0	0	0	0	0	0	0	0	5	58
448.5	419.5	2	0	0	5	3	1	0	0	0	0	0	0	0	4	68
450.5	421.5	4	1	0	1	2	0	0	0	0	0	0	0	0	5	87
452.5	423.5	0	0	0	1	2	0	0	0	0	0	0	0	0	1	45
454.5	425.5	1	0	0	2	3	0	0	0	0	0	0	0	0	5	49
456.5	427.5	0	0	0	1	3	0	0	0	0	0	0	0	0	4	33
458.5	429.5	2	0	0	5	6	1	0	0	0	0	0	0	0	8	107
460.5	431.5	1	0	0	6	7	0	0	0	0	0	0	0	0	16	123
462.5	433.5	2	0	0	9	10	0	0	0	0	0	0	0	0	10	143
464.5	435.5	0	0	0	0	1	0	0	0	0	0	0	0	0	5	57
466.5	437.5	0	0	0	1	6	0	0	0	0	0	0	1	1	4	62
468.5	439.5	0	1	0	1	4	0	0	0	0	0	0	2	0	4	30
470.5	441.5	0	0	0	5	6	0	0	0	0	0	0	0	0	4	113
472.5	443.5	0	0	0	3	4	1	0	0	0	0	0	1	0	4	77

Appendix B5 b: other (palynomorph) counts for core MD992277

Original depth (cm)	Corrected depth (cm)	weight	LySa	LyCo	Drew	Aspp	Alln	Botr	Cycl	Cyma	Eggln	FoLi	FuRe	Halo	Olic	Pedi	PitA	Pter	Scol	Sigm	Tasm	TiLo	TiLo1	TiLo2	BisPo			
																									BisPo	Oth	Pinus oP&S	
390.5	361.5	9.37	18583	4237	4	1	0	10	0	0	13	0	6	0	0	4	3	1	0	0	0	0	2	1	5	2	14	
392.5	363.5	9.31	18583	4517	12	1	0	8	0	0	3	0	8	0	0	3	4	0	0	0	0	0	2	1	5	4	15	
394.5	365.5	8.97	55749	13122	6	0	0	5	0	0	7	2	2	0	0	2	0	1	0	1	1	0	1	5	12	10	40	
396.5	367.5	9.67	18583	4607	16	2	2	3	1	0	2	0	3	0	0	3	1	1	0	0	1	0	3	2	1	2	12	
398.5	369.5	7.62	18583	6044	18	3	0	2	0	0	3	0	6	0	0	1	1	0	0	0	0	0	2	4	0	2	15	
400.5	371.5	7.36	18583	4463	11	2	0	6	0	0	2	0	4	0	0	0	2	2	0	0	0	0	1	4	0	1	18	
402.5	373.5	8.12	18583	4912	21	4	5	3	0	0	2	0	3	0	0	1	2	0	0	0	1	0	3	6	2	3	12	
404.5	375.5	8.47	18583	5689	25	6	4	4	0	1	3	0	1	0	1	3	1	0	1	0	2	0	4	7	1	4	12	
406.5	377.5	8.09	18583	3755	14	2	3	17	0	0	3	4	5	0	0	3	6	0	0	0	1	0	6	8	3	1	6	
408.5	379.5	7.95	18583	3667	15	4	2	10	0	0	5	1	5	0	0	6	8	1	0	0	0	0	6	3	4	9	5	
410.5	381.5	7.68	18583	7072	7	10	2	9	0	0	7	1	8	0	0	2	9	1	0	0	1	0	12	13	3	3	19	
412.5	383.5	6.28	18583	5479	11	2	0	2	0	0	3	2	4	0	0	2	17	1	0	0	0	0	9	3	6	4	11	
414.5	385.5	7.19	18583	4993	9	5	0	6	0	0	4	0	4	0	0	0	2	0	0	0	1	0	15	8	3	3	10	
416.5	387.5	7.29	18583	4723	18	4	5	6	0	0	1	7	3	0	0	1	1	0	0	0	0	0	11	14	10	4	14	
420.5	391.5	4.90	18583	4913	6	1	3	0	0	0	3	0	4	0	0	0	1	0	0	0	0	0	0	0	0	2	3	3
422.5	393.5	2.85	37166	7644	8	6	0	1	2	1	12	13	2	2	0	21	0	0	0	0	0	0	25	0	19	18	17	
424.5	395.5	4.20	18583	5349	4	3	2	0	0	0	5	0	1	0	0	1	0	0	0	0	0	1	0	2	2	3	16	
426.5	397.5	3.39	18583	3697	7	6	0	0	0	0	3	1	0	0	0	3	0	0	0	0	1	0	10	8	5	3	5	
428.5	399.5	4.38	18583	2946	3	2	0	2	0	0	3	2	1	0	0	2	0	1	1	0	0	0	0	8	2	3	3	
430.5	401.5	5.38	18583	3405	2	0	0	0	0	0	0	0	1	0	0	0	0	0	0	0	0	0	1	2	3	3	5	
432.5	403.5	5.48	18583	2331	7	5	0	1	0	0	3	2	3	0	2	0	0	0	0	0	0	2	6	6	2	2	8	
434.5	405.5	6.87	18583	6694	13	5	0	2	0	0	4	0	1	0	0	0	0	0	0	0	1	0	4	12	2	1	17	
436.5	407.5	6.88	18583	5863	16	6	7	4	0	0	8	0	5	0	0	1	0	0	1	0	0	0	1	4	1	2	11	
438.5	409.5	7.98	18583	4987	19	8	5	4	0	2	1	0	6	0	0	0	0	0	0	0	1	0	2	0	3	4	5	
440.5	411.5	6.20	18583	5821	22	3	0	2	0	0	0	0	2	0	0	0	0	1	0	0	0	0	2	0	3	3	1	
442.5	413.5	9.26	18583	5828	121	11	0	8	0	0	4	2	0	0	0	0	0	3	0	0	0	0	0	3	2	3	5	
444.5	415.5	6.07	18583	4164	26	4	3	4	0	0	2	1	0	0	0	0	0	0	0	0	0	0	1	3	1	3	9	
446.5	417.5	5.00	18583	2761	15	2	0	5	0	0	1	0	3	0	0	0	1	0	0	0	0	0	2	1	0	4	2	
448.5	419.5	6.06	18583	4902	12	0	0	3	0	0	2	3	1	0	0	0	0	1	0	0	0	0	2	2	1	1	2	
450.5	421.5	6.37	18583	6234	10	1	0	3	0	0	3	2	2	0	0	0	0	0	0	0	0	0	6	8	1	3	0	
452.5	423.5	5.28	18583	3537	14	3	0	6	0	0	1	2	3	0	0	0	0	0	0	0	0	0	2	4	2	2	2	
454.5	425.5	5.04	18583	7475	28	0	1	9	0	0	3	1	0	0	0	0	0	1	0	0	0	0	1	4	2	2	4	
456.5	427.5	4.54	18583	4619	11	0	0	3	0	0	2	0	0	0	0	0	0	0	0	0	0	0	0	1	0	1	3	
458.5	429.5	5.24	18583	5467	17	8	0	6	0	0	2	1	1	0	0	0	0	1	0	0	1	0	4	11	2	1	4	
460.5	431.5	4.66	18583	6350	13	7	0	3	0	0	4	6	3	0	0	0	0	1	0	0	0	0	8	8	3	3	3	
462.5	433.5	4.98	18583	4976	22	7	0	6	0	0	2	7	0	0	2	1	0	1	0	0	0	0	9	10	2	2	9	
464.5	435.5	8.02	18583	4705	67	8	6	11	0	2	21	1	5	0	0	0	0	2	0	0	0	0	2	4	4	3	9	
466.5	437.5	9.29	18583	4594	146	12	0	28	0	2	22	2	1	0	0	7	0	4	0	0	0	0	0	2	14	3	15	
468.5	439.5	9.37	18583	3983	159	8	0	20	0	2	17	1	2	0	0	6	2	8	0	0	2	1	2	0	5	2	3	
470.5	441.5	9.91	55749	15352	162	3	7	10	0	3	9	2	3	0	0	3	3	2	0	0	2	1	14	15	6	7	26	
472.5	443.5	9.37	18583	4987	201	1	4	39	0	2	9	2	4	0	0	5	0	2	0	0	0	1	5	3	9	4	9	

Appendix C1: results from the transfer function analysis of core M23455

Exercise 1: complete dataset (threshold: 1.243)

Depth (cm)	Summer SST (°C)			Summer SSS			Winter SST (°C)			Winter SSS			# ana-logues	Distance	
	min	BEST	max	min	BEST	max	min	BEST	max	min	BEST	max		Min	Max
291.25	7.98	9.48	10.91	34.70	34.94	35.08	2.45	4.66	6.53	34.83	35.04	35.19	5	1.088	1.219
295.25	10.91	13.77	16.24	31.95	34.17	35.44	6.31	8.36	11.02	32.29	34.54	35.49	5	0.693	0.775
301.25	8.74	13.68	17.68	31.86	33.80	35.44	4.12	7.13	11.02	32.29	34.12	35.49	5	1.000	1.092
306.25	3.23	8.33	10.91	31.88	34.30	35.08	-1.24	4.26	6.31	33.88	34.81	35.19	5	0.693	0.826
307.25	8.16	10.23	13.11	33.02	34.49	35.08	4.12	5.70	6.33	34.26	34.87	35.19	5	0.774	0.926
308.25	8.74	11.43	14.76	31.95	34.02	35.08	4.12	6.24	8.65	32.29	34.39	35.19	5	0.817	0.967
309.25	8.74	12.54	16.24	33.02	34.70	35.44	4.12	7.44	11.02	34.26	35.02	35.49	5	0.841	0.946
310.25	8.16	10.74	16.24	34.58	34.96	35.44	4.12	6.55	11.02	34.83	35.11	35.49	5	0.856	1.040
311.25	8.74	12.41	16.24	33.02	34.26	35.44	4.12	6.83	11.02	34.26	34.81	35.49	5	0.766	0.874
312.25	8.16	10.82	16.24	34.58	34.97	35.44	4.12	6.60	11.02	34.83	35.11	35.49	5	0.796	0.957
313.25	8.74	12.38	16.24	33.02	34.22	35.44	4.12	6.76	11.02	34.26	34.79	35.49	5	0.783	0.922
314.25	8.74	12.35	16.24	33.02	34.29	35.44	4.12	6.80	11.02	34.26	34.82	35.49	5	0.988	1.210
315.25	10.91	13.52	16.24	33.02	34.40	35.44	6.31	8.01	11.02	34.26	34.93	35.49	5	0.935	1.037
316.75	10.91	12.03	13.11	33.02	34.03	35.08	6.31	6.32	6.33	34.26	34.71	35.19	2	1.165	1.372
319.25	3.23	3.23	3.23	31.88	31.88	31.88	-1.24	-1.24	-1.24	33.88	33.88	33.88	1	1.163	1.395

Exercise 2: all modern sites considered, Protoperidinioid species not included (threshold: 1.449)

Depth (cm)	Summer SST (°C)			Summer SSS			Winter SST (°C)			Winter SSS			# ana-logues	Distance	
	min	BEST	max	min	BEST	max	min	BEST	max	min	BEST	max		Min	Max
291.25	NA	NA	NA	NA	NA	NA	NA	NA	NA	NA	NA	NA	0	1.584	1.935
295.25	12.36	14.97	16.34	29.86	32.82	35.23	0.29	5.11	9.95	31.15	33.25	35.42	5	0.958	1.070
301.25	12.36	12.36	12.36	34.60	34.60	34.60	7.37	7.37	7.37	35.01	35.01	35.01	1	1.407	1.605
306.25	8.16	10.27	12.36	34.58	34.76	35.06	5.56	6.27	7.37	34.94	35.02	35.10	5	0.951	1.062
307.25	10.43	12.87	15.68	29.86	32.81	34.82	0.29	3.96	7.37	31.15	33.51	35.06	5	1.151	1.216
308.25	9.80	11.35	15.68	29.86	33.87	35.06	0.29	4.89	6.42	31.15	34.27	35.10	5	1.239	1.315
309.25	10.43	12.94	15.68	29.86	32.74	34.82	0.29	3.88	7.37	31.15	33.45	35.06	5	1.209	1.242
310.25	8.16	11.50	15.55	29.94	33.65	34.82	0.39	4.94	7.37	31.19	34.20	35.06	5	1.266	1.442
311.25	10.58	13.41	15.68	29.86	32.50	34.60	0.29	4.14	7.37	31.15	33.38	35.01	5	1.004	1.263
312.25	8.16	11.50	15.55	29.94	33.65	34.82	0.39	4.93	7.37	31.19	34.19	35.06	5	1.102	1.235
313.25	12.36	13.51	15.55	29.94	33.51	35.02	0.39	5.51	7.37	31.19	34.13	35.13	5	1.170	1.301
314.25	NA	NA	NA	NA	NA	NA	NA	NA	NA	NA	NA	NA	0	1.791	1.892
315.25	NA	NA	NA	NA	NA	NA	NA	NA	NA	NA	NA	NA	0	1.590	1.672
316.75	NA	NA	NA	NA	NA	NA	NA	NA	NA	NA	NA	NA	0	1.692	1.963
319.25	3.23	11.31	15.60	28.70	31.11	34.60	-1.24	1.08	7.37	31.03	32.61	35.01	5	0.928	1.131

Exercise 3: only modern sites north of 65°N considered, all species included (threshold: 0.813)

Depth (cm)	Summer SST (°C)			Summer SSS			Winter SST (°C)			Winter SSS			# ana-logues	Distance	
	min	BEST	max	min	BEST	max	min	BEST	max	min	BEST	max		Min	Max
291.25	NA	NA	NA	NA	NA	NA	NA	NA	NA	NA	NA	NA	0	1.088	1.274
295.25	11.47	11.47	11.47	35.03	35.03	35.03	6.31	6.31	6.31	35.19	35.19	35.19	1	0.696	0.994
301.25	NA	NA	NA	NA	NA	NA	NA	NA	NA	NA	NA	NA	0	1.092	1.256
306.25	11.47	11.47	11.47	35.03	35.03	35.03	6.31	6.31	6.31	35.19	35.19	35.19	1	0.756	0.990
307.25	11.47	11.47	11.47	35.03	35.03	35.03	6.31	6.31	6.31	35.19	35.19	35.19	1	0.788	1.118
308.25	NA	NA	NA	NA	NA	NA	NA	NA	NA	NA	NA	NA	0	0.824	1.116
309.25	NA	NA	NA	NA	NA	NA	NA	NA	NA	NA	NA	NA	0	0.841	1.115
310.25	NA	NA	NA	NA	NA	NA	NA	NA	NA	NA	NA	NA	0	1.006	1.269
311.25	11.47	11.47	11.47	35.03	35.03	35.03	6.31	6.31	6.31	35.19	35.19	35.19	1	0.771	1.108
312.25	NA	NA	NA	NA	NA	NA	NA	NA	NA	NA	NA	NA	0	0.897	1.149
313.25	11.47	11.47	11.47	35.03	35.03	35.03	6.31	6.31	6.31	35.19	35.19	35.19	1	0.783	1.052
314.25	NA	NA	NA	NA	NA	NA	NA	NA	NA	NA	NA	NA	0	0.988	1.384
315.25	NA	NA	NA	NA	NA	NA	NA	NA	NA	NA	NA	NA	0	0.963	1.218
316.75	NA	NA	NA	NA	NA	NA	NA	NA	NA	NA	NA	NA	0	1.220	1.558
319.25	NA	NA	NA	NA	NA	NA	NA	NA	NA	NA	NA	NA	0	1.163	1.439

Exercise 4: only modern sites north of 65°N considered, Protoperidinioid species not included: no analogues found

Appendix C2: results from the transfer function analysis of core MD992277

Exercise 1: complete dataset (threshold: 1.226)

Depth (cm)	Summer SST (°C)			Summer SSS			Winter SST (°C)			Winter SSS			# ana-logues	Distance	
	min	BEST	max	min	BEST	max	min	BEST	max	min	BEST	max		Min	Max
361.5	NA	NA	NA	NA	NA	NA	NA	NA	NA	NA	NA	NA	0	1.240	1.368
363.5	10.91	12.02	13.11	33.02	34.04	35.08	6.31	6.32	6.33	34.26	34.72	35.19	2	1.145	1.284
365.5	3.23	9.084	13.47	30.51	32.92	35.08	-1.24	2.606	6.36	31.74	33.98	35.19	5	0.514	0.871
367.5	8.74	12.13	16.24	31.95	34.39	35.44	4.12	7.207	11.02	32.29	34.53	35.49	5	0.879	1.014
369.5	NA	NA	NA	NA	NA	NA	NA	NA	NA	NA	NA	NA	0	1.266	1.405
372.5	3.23	9.126	14.94	30.38	32.98	35.08	-1.24	2.159	6.31	31.76	33.93	35.19	4	0.998	1.259
375.5	6.83	10.71	16.24	33.02	34.52	35.44	3.54	5.994	11.02	34.26	34.88	35.49	5	0.881	0.981
377.5	3.23	8.887	13.35	31.88	34.34	35.08	-1.24	3.959	6.72	33.88	34.85	35.19	5	0.870	0.964
379.5	14.13	15.96	17.68	31.86	34.3	35.44	5.36	8.896	11.02	32.87	34.65	35.49	3	1.025	1.238
381.5	6.83	10.27	13.94	32.13	33.86	34.99	3.54	4.904	6.33	33.83	34.56	35.12	5	0.559	0.713
383.5	3.23	10.03	16.24	31.88	33.67	35.44	-1.24	5.362	11.02	32.29	34.2	35.49	5	0.977	1.130
385.5	3.23	7.447	10.91	31.88	34.36	35.08	-1.24	3.549	6.31	33.88	34.86	35.19	5	0.566	0.699
387.5	7.98	10.91	13.94	32.13	34.04	35.08	2.45	5.041	6.33	33.83	34.68	35.19	5	0.922	0.979
391.5	NA	NA	NA	NA	NA	NA	NA	NA	NA	NA	NA	NA	0	1.413	1.537
393.5	3.23	10.84	13.35	31.88	33.6	35.08	-1.24	4.96	6.72	33.88	34.54	35.19	5	0.571	0.631
395.5	3.23	10.28	14.94	30.38	33.14	35.08	-1.24	3.378	6.33	31.76	34.07	35.19	5	0.770	1.041
397.5	8.7	10.86	13.11	33.02	34.24	35.08	3.8	5.455	6.36	34.26	34.78	35.19	5	0.702	0.847
399.5	8.74	12.59	16.24	33.02	34.72	35.44	4.12	7.492	11.02	34.26	35.03	35.49	5	0.920	1.105
402.5	6.43	7.752	9	34.91	34.97	35.02	3.53	4.309	5.16	35.07	35.09	35.12	5	0.377	0.424
405.5	8.7	11.91	13.47	30.51	32.8	35.08	-0.44	3.499	6.33	31.74	33.61	35.19	5	0.477	0.646
407.5	10.91	10.91	10.91	35.08	35.08	35.08	6.31	6.31	6.31	35.19	35.19	35.19	1	1.155	1.407
410.5	3.23	9.897	14.94	30.38	33.05	35.08	-1.24	3.152	6.33	31.76	34.07	35.19	5	0.742	0.973
414.5	13.11	15.92	18.86	33.02	34.5	36.04	6.33	10.7	15.27	34.26	35.12	36.01	2	1.172	1.274
418.5	3.23	9.179	14.94	30.38	33.35	35.08	-1.24	2.656	6.31	31.76	34.12	35.19	5	0.702	0.851
421.5	8.74	12.19	16.24	34.7	35.13	35.44	4.12	7.614	11.02	34.83	35.21	35.49	5	0.689	0.910
425.5	3.23	8.548	16.24	31.88	34.37	35.44	-1.24	4.006	11.02	33.88	34.86	35.49	5	0.850	0.899
429.5	3.23	7.428	10.91	31.88	34.13	35.08	-1.24	3.13	6.31	33.88	34.7	35.19	5	0.515	0.639
431.5	3.23	7.981	10.84	31.88	34.27	35.05	-1.24	3.347	6.53	33.88	34.78	35.16	5	0.762	0.847
433.5	3.23	7.553	10.84	31.88	34.24	35.02	-1.24	2.626	6.53	33.88	34.75	35.16	5	0.860	0.955
437.5	9.49	12.81	16.24	33.02	34.77	35.44	3.99	7.558	11.02	34.26	35.06	35.49	5	0.884	1.011
441.5	3.23	8.795	14.76	31.88	33.74	35.02	-1.24	3.577	8.65	32.29	34.27	35.16	5	1.088	1.156
443.5	3.23	7.84	10.84	31.88	34.25	35.02	-1.24	3.094	6.53	33.88	34.78	35.16	5	0.716	0.887

Exercise 2: all modern sites considered, Protoperidinioid species not included (threshold: 1.385)

Depth (cm)	Summer SST (°C)			Summer SSS			Winter SST (°C)			Winter SSS			# ana-logues	Distance	
	min	BEST	max	min	BEST	max	min	BEST	max	min	BEST	max		Min	Max
361.5	NA	NA	NA	NA	NA	NA	NA	NA	NA	NA	NA	NA	0	1.982	2.071
363.5	NA	NA	NA	NA	NA	NA	NA	NA	NA	NA	NA	NA	0	1.514	1.871
365.5	3.23	10.33	14.53	30.14	32.42	34.8	-1.24	2.26	7.37	31.57	33.47	35.04	5	1.013	1.260
367.5	10.58	13.94	15.55	29.94	31.42	34.58	0.39	1.619	5.56	31.19	32.22	34.94	4	1.236	1.387
369.5	NA	NA	NA	NA	NA	NA	NA	NA	NA	NA	NA	NA	0	2.128	2.264
372.5	NA	NA	NA	NA	NA	NA	NA	NA	NA	NA	NA	NA	0	1.726	1.789
375.5	NA	NA	NA	NA	NA	NA	NA	NA	NA	NA	NA	NA	0	1.562	1.621
377.5	NA	NA	NA	NA	NA	NA	NA	NA	NA	NA	NA	NA	0	1.427	1.527
379.5	NA	NA	NA	NA	NA	NA	NA	NA	NA	NA	NA	NA	0	1.548	1.742
381.5	8.7	13.14	23.24	32.91	34.08	34.99	4.72	6.416	8.8	33.92	34.68	35.12	5	0.923	1.093
383.5	NA	NA	NA	NA	NA	NA	NA	NA	NA	NA	NA	NA	0	1.698	1.783
385.5	5.22	8.526	12.36	34.6	34.84	34.99	1.35	4.063	7.37	34.98	35.04	35.12	5	0.803	0.900
387.5	NA	NA	NA	NA	NA	NA	NA	NA	NA	NA	NA	NA	0	1.443	1.666
391.5	NA	NA	NA	NA	NA	NA	NA	NA	NA	NA	NA	NA	0	2.135	2.327
393.5	8.7	12.26	13.94	32.13	33.95	35.02	4.72	6.088	7.37	33.83	34.67	35.13	5	1.033	1.084
395.5	23.13	23.21	23.28	32.7	33.03	33.71	8.48	8.883	9.37	33.81	33.94	34.11	4	1.134	1.515
397.5	8.7	13.45	23.24	32.91	34.3	34.99	3.8	5.711	8.8	33.92	34.69	35.12	3	1.239	1.459
399.5	NA	NA	NA	NA	NA	NA	NA	NA	NA	NA	NA	NA	0	1.694	1.800
402.5	5.22	7.773	9.69	34.61	34.88	35.02	1.35	4.039	5.51	34.95	35.05	35.12	5	0.555	0.695
405.5	10.91	12.35	13.11	30.58	32.82	35.08	-0.44	4.02	7.37	31.68	33.61	35.19	5	0.908	1.086
407.5	NA	NA	NA	NA	NA	NA	NA	NA	NA	NA	NA	NA	0	2.052	2.179
410.5	13.11	13.11	13.11	33.02	33.02	33.02	6.33	6.33	6.33	34.26	34.26	34.26	1	1.385	1.507
414.5	NA	NA	NA	NA	NA	NA	NA	NA	NA	NA	NA	NA	0	1.643	1.872
418.5	8.93	10.29	12.46	30.51	33.94	34.98	0.03	4.232	6.24	31.83	34.39	35.08	5	1.008	1.132
421.5	9.8	13.2	16.24	29.86	34.19	35.44	0.29	6.809	11.02	31.15	34.48	35.49	5	1.207	1.354
425.5	0.55	7.496	12.36	32.9	34.49	35.05	-1.78	3.635	7.37	34.22	34.89	35.11	5	1.136	1.220
429.5	8.27	11.19	14.59	30.6	33.95	35.3	0.37	5.037	8.78	31.55	34.3	35.3	5	0.772	0.819
431.5	8.02	9.308	10.29	34.58	34.91	35.06	2.06	5.348	6.42	34.87	35.03	35.11	5	1.151	1.271
433.5	3.72	5.068	6.43	34.36	34.6	34.84	-0.15	0.193	0.54	34.77	34.78	34.79	2	1.298	1.433
437.5	12.36	13.55	15.68	28.58	32.23	35.37	0.29	5.781	9.46	31.15	33.79	35.35	5	1.071	1.323
441.5	NA	NA	NA	NA	NA	NA	NA	NA	NA	NA	NA	NA	0	1.569	1.739
443.5	-0.41	6.664	12.36	31.88	33.76	35.05	-1.24	2.587	7.37	33.88	34.67	35.11	5	1.078	1.211

Appendix D

Plates

Plate 1

	Core	Depth (cm)	Slide ref	size (μm)	view*	remarks
1-4 cyst of <i>Scrippsiella trifida</i>						
1	M23323	792.5	II 03	(36/45) x24	x1000, HF	
2					x1000, MF	
3					x1000, LF	
4	M23071	646	II 08a	32x24	x1000, MF	
5-8 <i>Operculodinium centrocarpum</i>						
5	M23323	760.5	I 06	\emptyset 39	x1000, HF	specimen with slightly shorter processes
6					x1000, MF	
7	M23323	830.5	IV 02	\emptyset 35	x1000, HF	oblique-apical view
8					x1000, MF	
9-12 <i>Nematosphaeropsis labyrinthus</i>						
9	M23323	760.5	I 03	\emptyset 33 \emptyset 61	x1000, MF	
10					x1000, LF	low-focus view on the cyst surface
11	M23323	782.5	I 08	\emptyset 35 \emptyset 65	x1000, HF	high-focus view on the cyst surface
12					x1000, MF	

* HF: High Focus

MF: Mid Focus = optical section

LF: Low Focus

◦ Composite picture, made by semi-transparently putting one photograph over another one taken at a slightly different focus depth

Plate 1

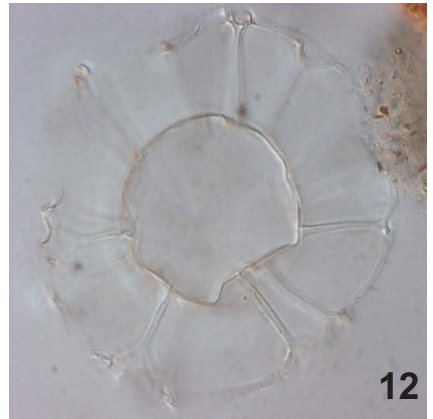
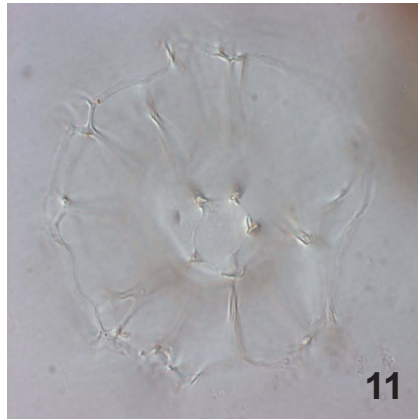
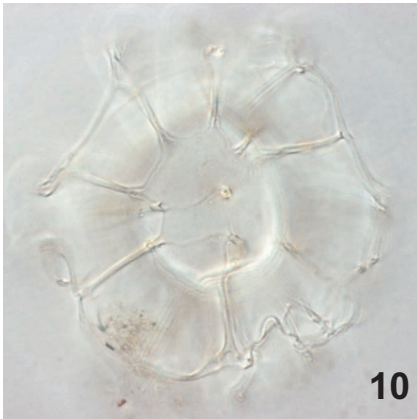
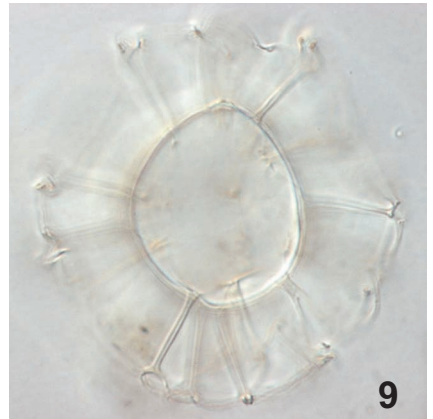
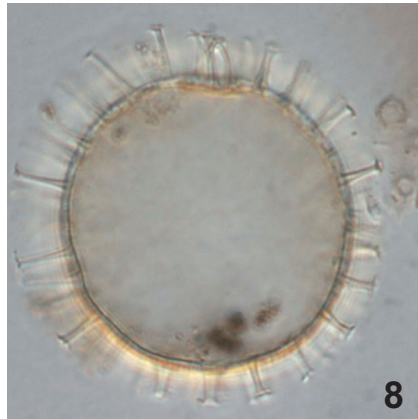
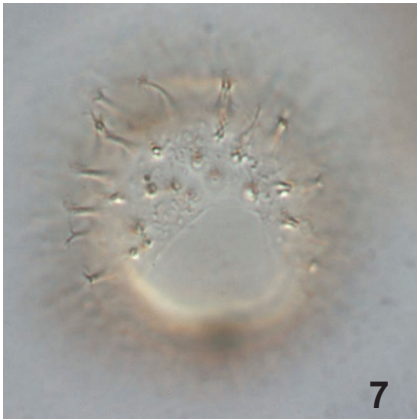
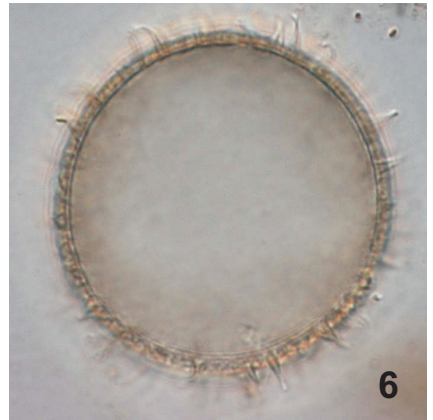
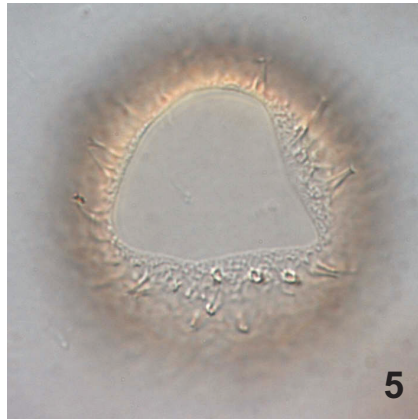
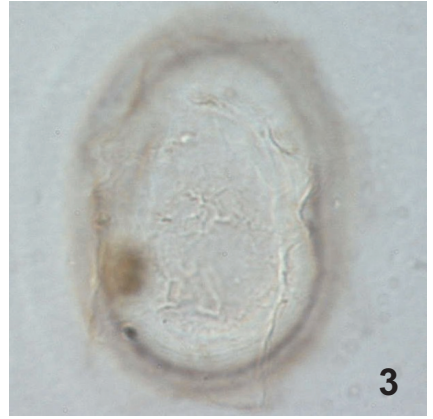
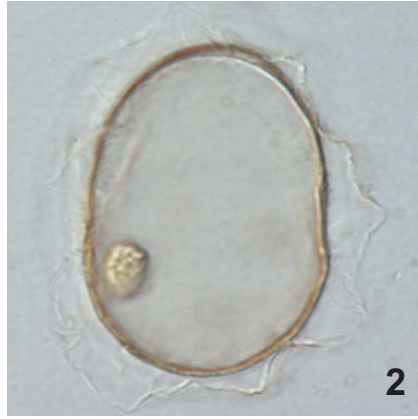
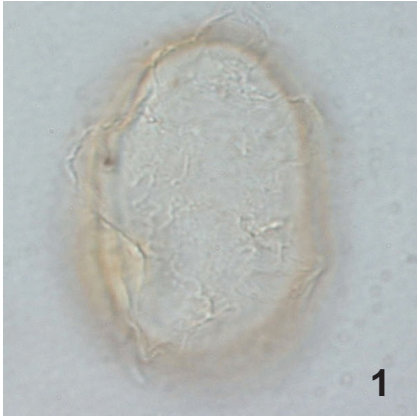


Plate 2

	Core	Depth (cm)	Slide ref	size (μm)	view*	remarks
1-5 <i>Ataxiodinium choane</i>						
1	M23323	766.5	III 03	\emptyset 29 \emptyset 55	x1000, HF	
2					x1000, MF	
3	M23323	770.5	III 07	\emptyset 39 \emptyset 56	x1000, LF	interior view on the archeopyle
4	M23323	790.5	I 07	\emptyset 38 \emptyset 54	x1000, HF	
5					x1000, MF	
6-12 <i>Nematosphaeropsis cf. labyrinthus</i>						
6	M23323	782.5	II 10		x1000	detail of "8", showing the pronounced sutural ridges (1.5 - 2 μm high)
7				\emptyset 40 \emptyset 80	x630, HF	paratabulation is well-expressed by marked
8					x630, MF	sutural crests between the process bases. This
9					x630, LF	differentiates <i>N. cf. labyrinthus</i> from typical <i>N. labyrinthus</i> cysts (see also
10	M23323	788.5	II 02c	\emptyset 29 \emptyset 64	x1000, HF	PLATE 5 in Rochon et al., 1999)
11					x1000, MF	
12					x1000, MF	slightly deeper focal depth with respect to "11"

* HF: High Focus

MF: Mid Focus = optical section

LF: Low Focus

◦ Composite picture, made by semi-transparently putting one photograph over another one taken at a slightly different focus depth

Plate 2

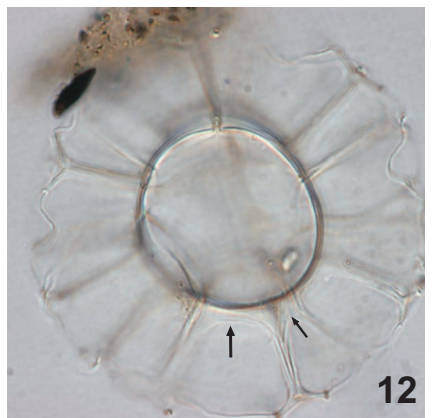
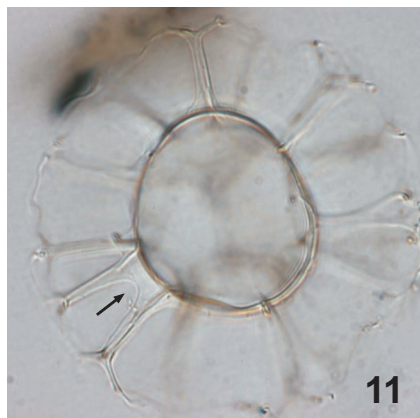
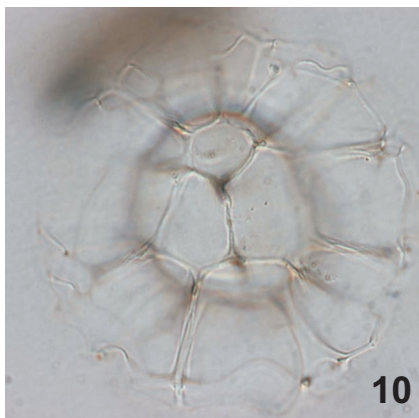
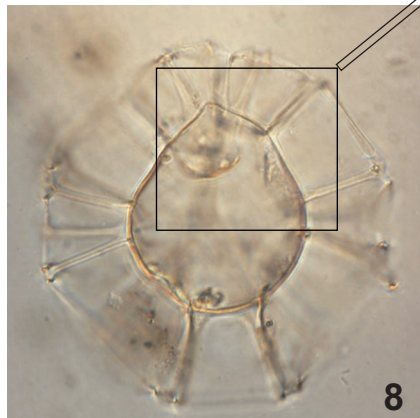
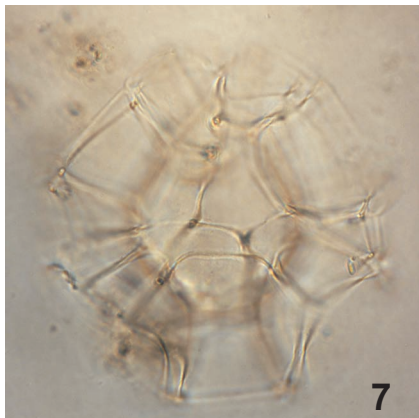
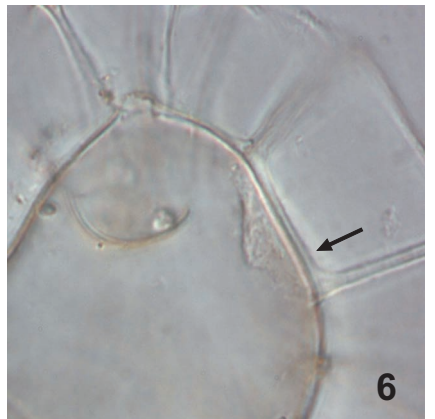
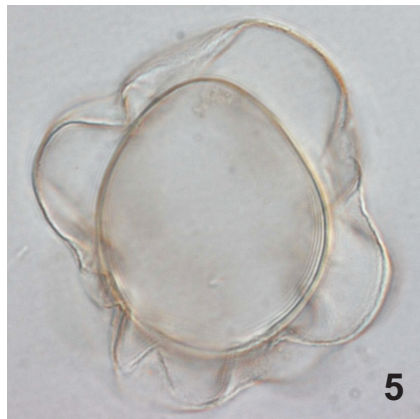
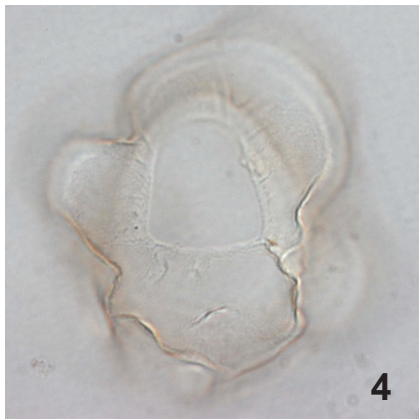
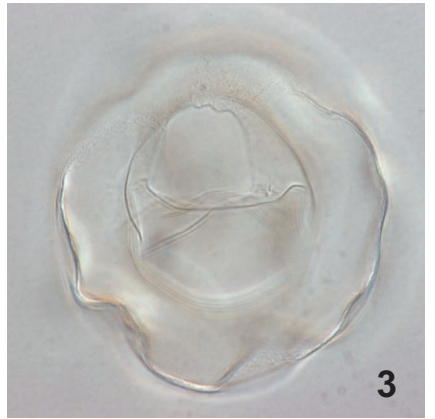
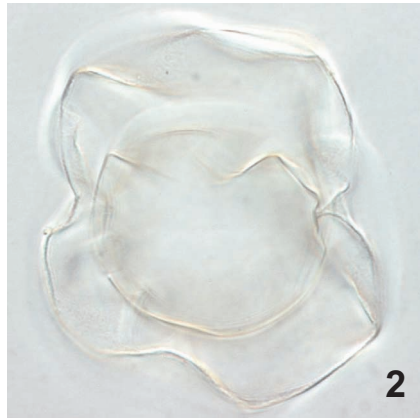
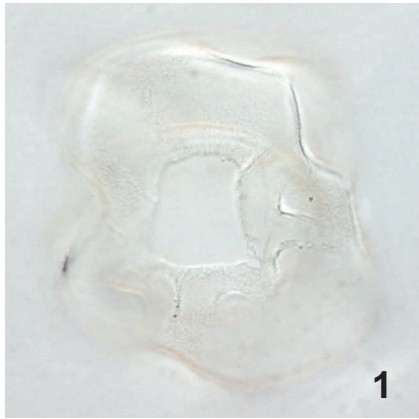


Plate 3

	Core	Depth (cm)	Slide ref	size (μm)	view*	remarks
1-2 <i>Nematosphaeropsis cf. labyrinthus</i>						
1	M23323	768.5	I 04	\emptyset 37 \emptyset 67	x1000, HF	see Plate 2
2					x1000, MF	
3-6 <i>Impagidinium pallidum</i>						
3	MD992277	398.5 [^]	III 01	\emptyset 75	x630, MF	
4	M23323	830.5	IV 06	\emptyset 56	x1000, HF	
5					x1000, MF	phase contrast
6					x1000, LF	
7-12 <i>Impagidinium sphaericum</i>						
7	M23323	770.5	III 01b	\emptyset 38	x1000, HF ^o	dorsal surface
8					x1000, MF	
9					x1000, LF ^o	inner view of ventral surface (sulcus and cingulum)
10	M23323	804.5	I 06	\emptyset 39	x1000, HF	right lateral view of right lateral surface
11					x1000, MF	
12					x1000, LF	left lateral interior

* HF: High Focus

MF: Mid Focus = optical section

LF: Low Focus

^o Composite picture, made by semi-transparently putting one photograph over another one taken at a slightly different focus depth

[^] original depth

Plate 3

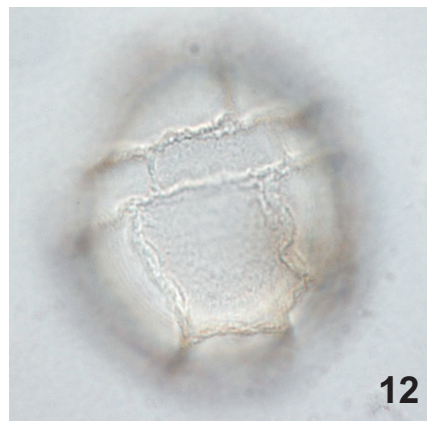
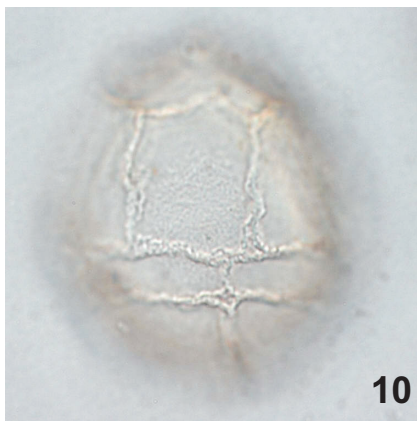
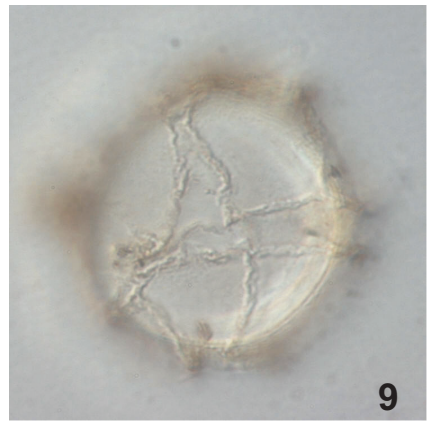
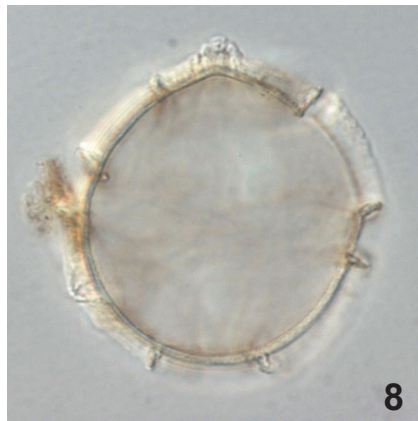
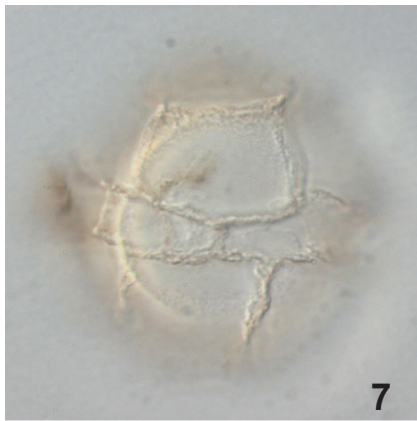
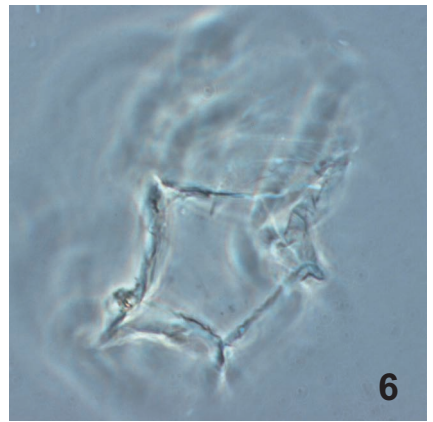
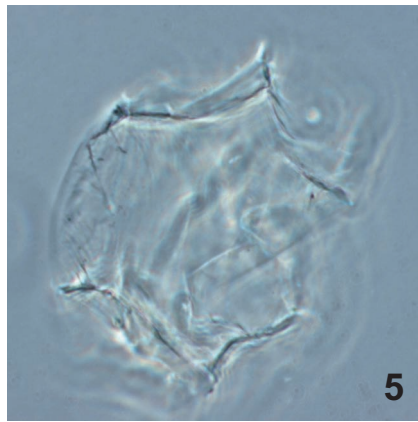
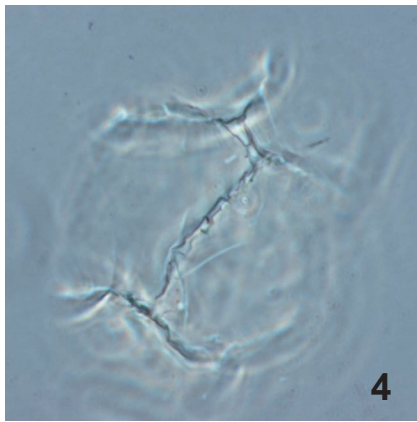
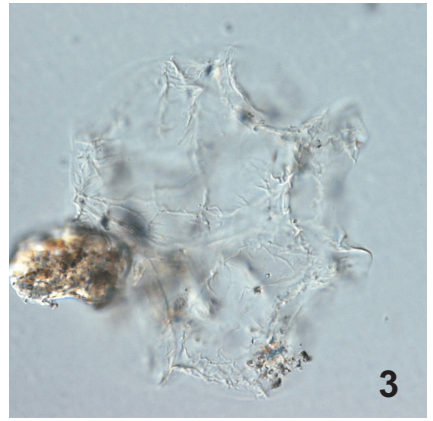
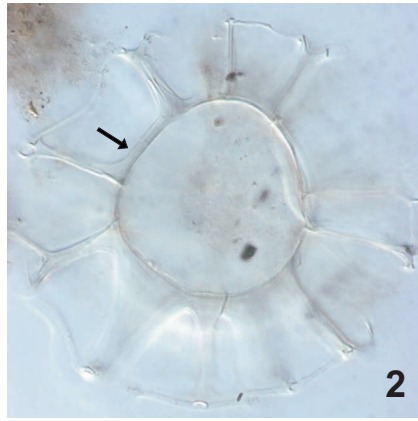
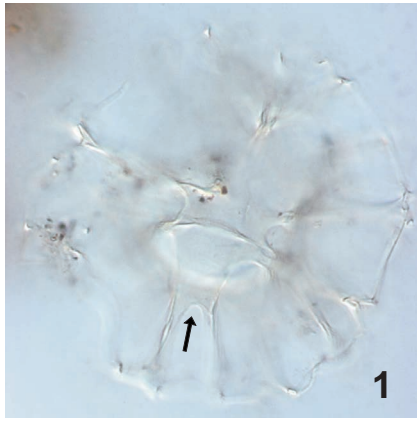


Plate 4

	Core	Depth (cm)	Slide ref	size (μm)	view*	remarks
1-5 <i>Lingulodinium machaerophorum</i>						
1	MD992277	438.5 [^]	II 01	\emptyset 46	x630, HF	dorsal surface with archeopyle
2					x630, MF	spines up to 25 μm long
3					x630, MF	slightly deeper focal depth with respect to "2"
<hr/>						
4	M23323	860.5	II 01	\emptyset 52	x630, HF	spines up to 25 μm long
5					x630, MF	
6-8 cyst of <i>Pentapharsodinium dalei</i>						
6	M23323	768.5	I 01	\emptyset 22	x1000, MF	
7					x1000, LF	
<hr/>						
8	M23323	782.5	II 09	\emptyset 26	x1000, MF	
9 <i>Spiniferites lazus</i>						
9	M23323	812.5	I 03	50x25	x1000, MF	note the fenestrate process shafts
10-12 <i>Spiniferites ramosus</i> s.l.						
10	M23323	814.5	II 04	\emptyset 35	x1000, MF	
11					x1000, MF	slightly deeper focal depth with respect to "10"
12					x1000, LF	

* HF: High Focus

MF: Mid Focus = optical section

LF: Low Focus

◦ Composite picture, made by semi-transparently putting one photograph over another one taken at a slightly different focus depth

[^] original depth

Plate 4

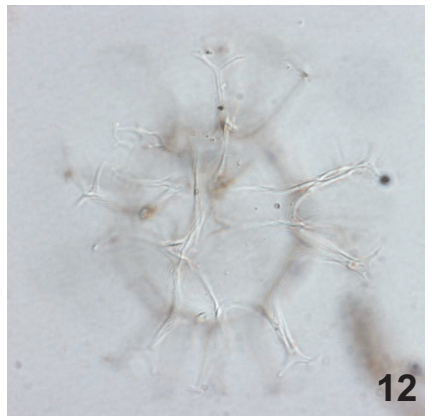
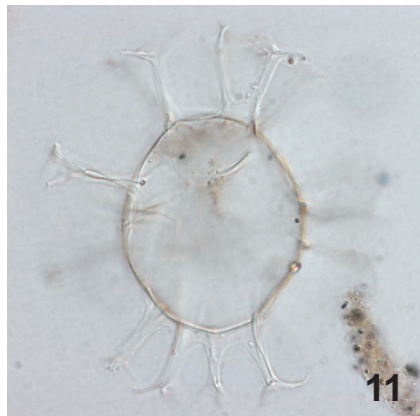
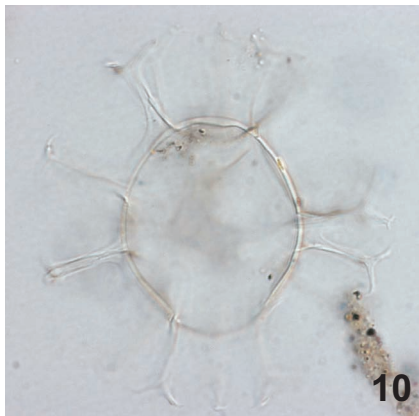
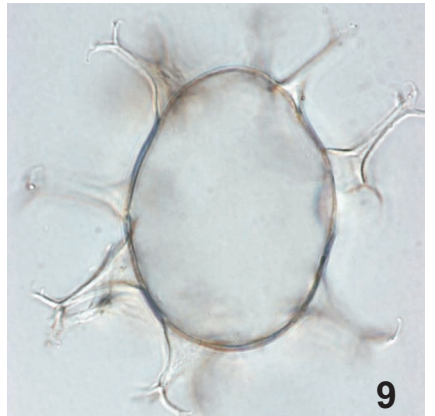
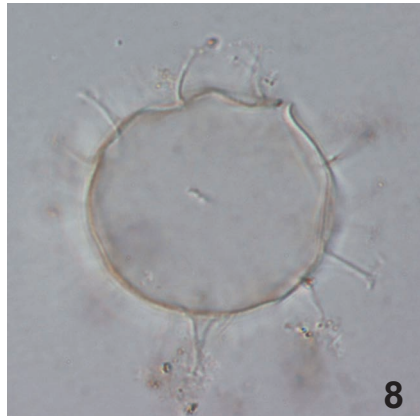
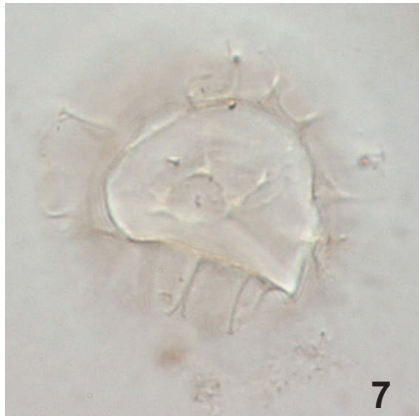
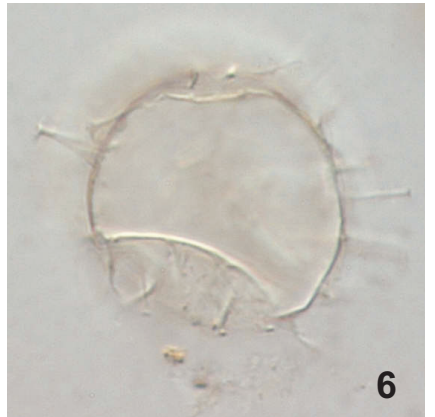
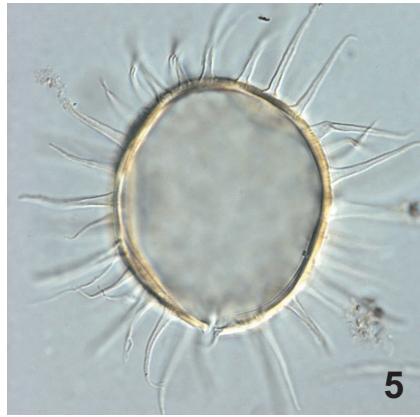
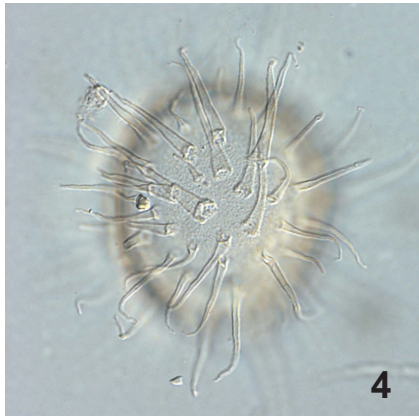
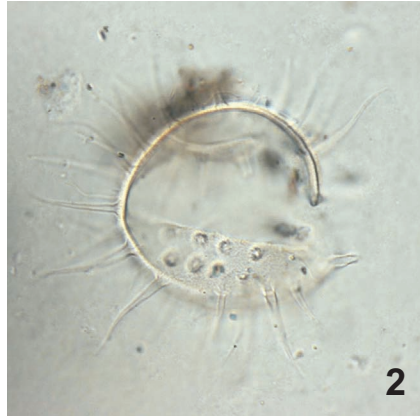


Plate 5

	Core	Depth (cm)	Slide ref	size (μm)	view*	remarks
1-3 <i>Spiniferites ramosus</i> s.l.						
1	M23071	653	I 02a	\emptyset 40	x1000, MF	
2					x1000, LF	
3					x1000, MF	note how some processes become fairly membranous
4-7 <i>Spiniferites hyperacanthus</i>						
4	M23323	788.5	II 01	\emptyset 61	x630, HF	antapical-ventral view of ventral surface
5					x630, MF	
6					x630, MF	slightly deeper focal depth with respect to "5"
7					x630, LF	oblique interior view of dorsal surface
8-12 <i>Spiniferites mirabilis</i>						
8	M23323	776.5	IV 08	\emptyset 49	x1000, HF	dorsal view of dorsal surface
9					x1000, MF	
10	M23323	770.5	III 09	\emptyset 52	x630, HF	ventral view of ventral surface
11					x630, LF	interior view of dorsal surface
12					x630, LF	slightly deeper focal depth with respect to "11"

* HF: High Focus

MF: Mid Focus = optical section

LF: Low Focus

◦ Composite picture, made by semi-transparently putting one photograph over another one taken at a slightly different focus depth

Plate 5

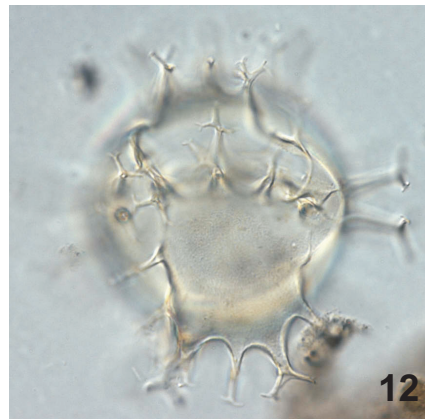
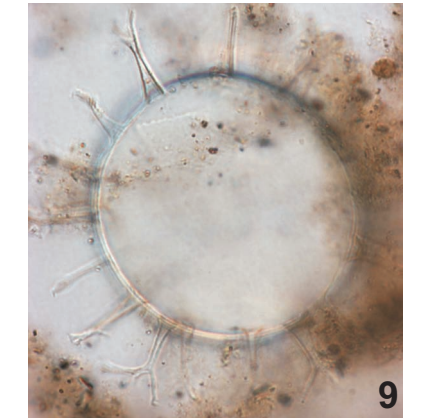
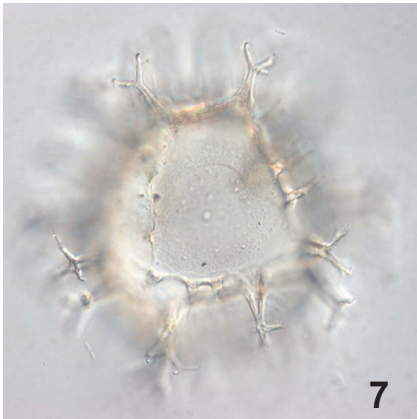
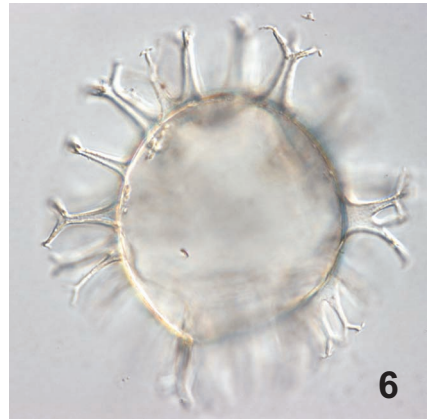
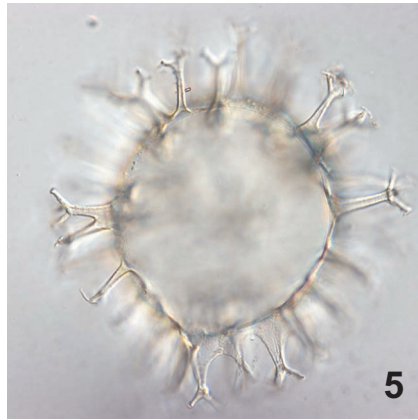
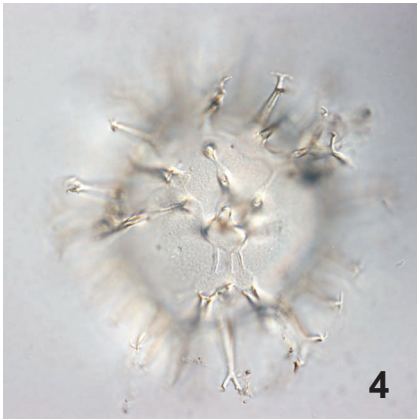
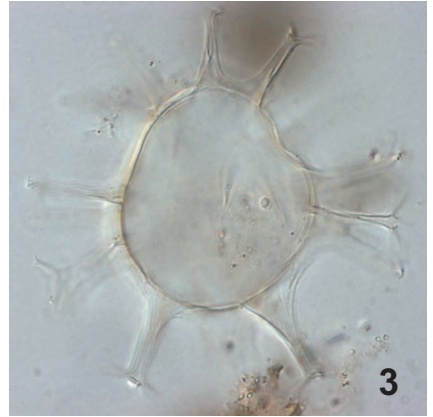
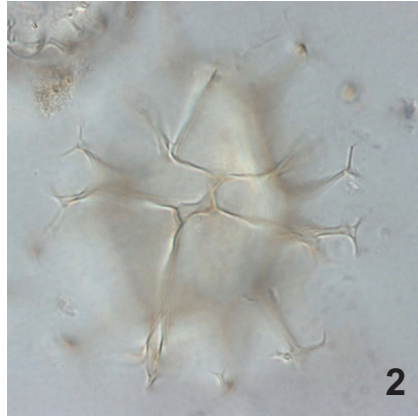
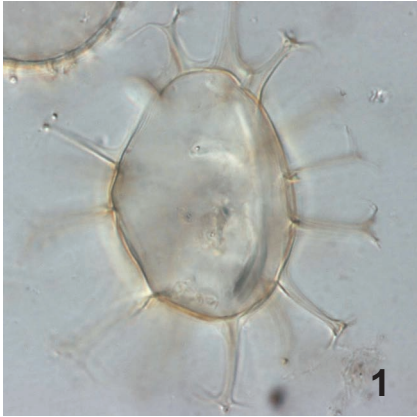


Plate 6

	Core	Depth (cm)	Slide ref	size (μm)	view*	remarks
1-6 <i>Spiniferites elongatus</i>						
1	M23323	770.5	III 11	46x31	x1000, HF ^o	dorsal view of dorsal surface
2					x1000, MF	
3					x1000, LF	interior view of ventral surface (sulcus)
4	M23323	834.5	III 08	51x28	x1000, HF ^o	dorsal view of dorsal surface
5					x1000, MF	pronouncedly membranous sutural crests
6					x1000, LF	interior view of ventral surface (sulcus)
7-12 <i>Spiniferites cf. elongatus sensu Harland and Sharp 1986</i>						
7	M23071	634.5	II 17a	44x29	x1000, HF ^o	note the strongly reduced processes and knob-like process tips.
8					x1000, MF	
9					x1000, MF	slightly deeper focal depth with respect to "8"
10	M23323	770.5	III 08	47x30	x1000, MF	see 7-9
11					x1000, MF	slightly deeper focal depth with respect to "10"
12					x1000, LF	interior view of dorsal surface

* HF: High Focus

MF: Mid Focus = optical section

LF: Low Focus

^o Composite picture, made by semi-transparently putting one photograph over another one taken at a slightly different focus depth

Plate 6

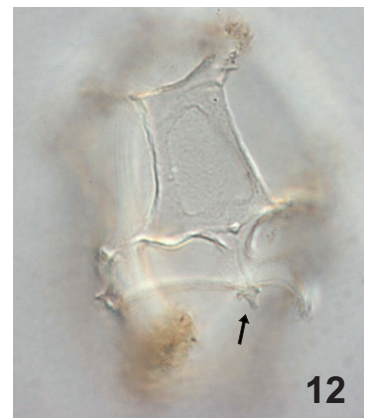
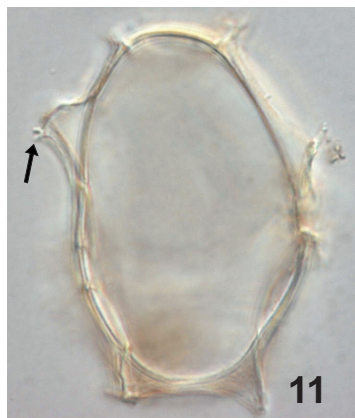
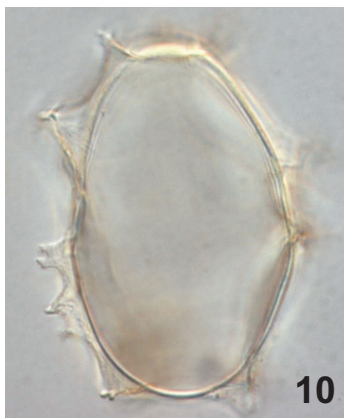
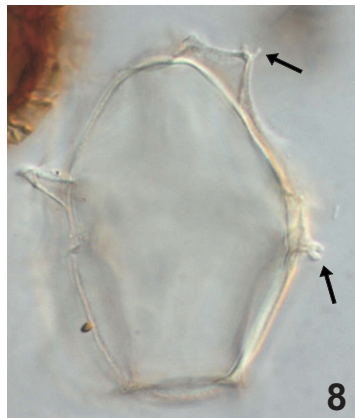
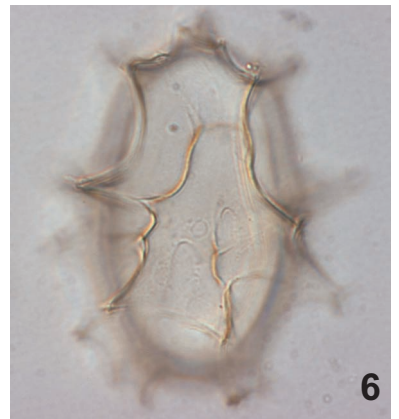
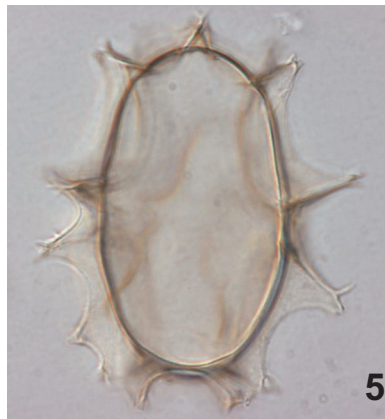
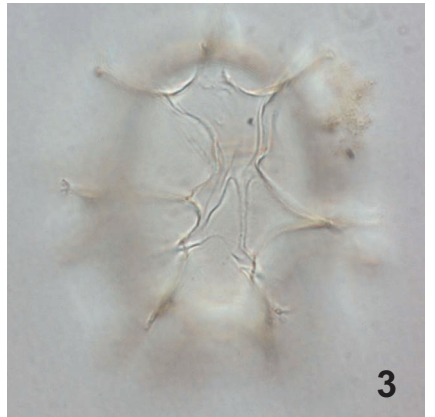
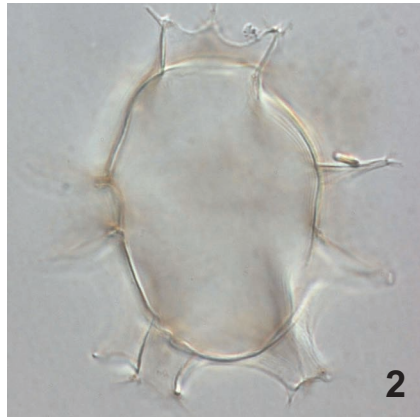
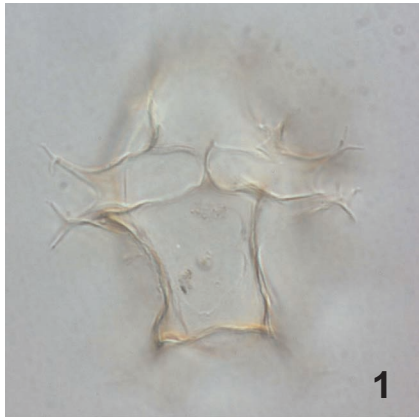


Plate 7

	Core	Depth (cm)	Slide ref	size (μm)	view*	remarks
1-7 <i>Spiniferites cf. elongatus sensu Harland and Sharp 1986</i>						
1	M23323	782.5	I 05	42x26	x1000, HF	ventral view of ventral surface (sulcus)
2					x1000, MF	
3					x1000, LF	interior view of dorsal surface
4	M23323	758.5	I 01	45x27	x1000, HF ^o	membranous crests, but with strongly reduced process
5					x1000, MF	shaft en tips
6	M23323	772.5	II 05	40x28	x1000, MF	see 4-5
7					x1000, MF	slightly deeper focal depth with respect to "6"
8-12 <i>Spiniferites cf. membranaceus</i>						
8	M23071	658	IV 32a	\emptyset 36	x1000, HF ^o	note the fused antapical processes. The membrane is, however, not fully developed like in typical S.
9	M23071	662	III 18a	\emptyset 32	x1000, MF	
10	M23323	834.5	III 02c	\emptyset 32	x1000, HF	<i>membranaceus</i> cysts
11					x1000, MF	note the membranous appearance of the whole cyst
12					x1000, LF	interior view of ventral surface

* HF: High Focus

MF: Mid Focus = optical section

LF: Low Focus

^o Composite picture, made by semi-transparently putting one photograph over another one taken at a slightly different focus depth

Plate 7

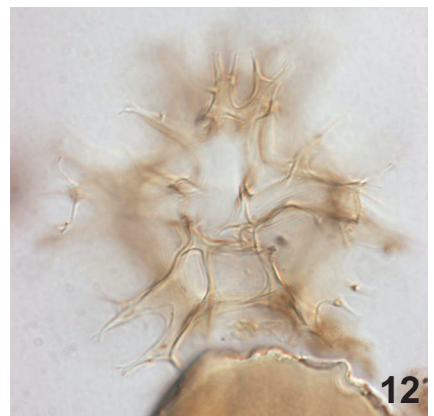
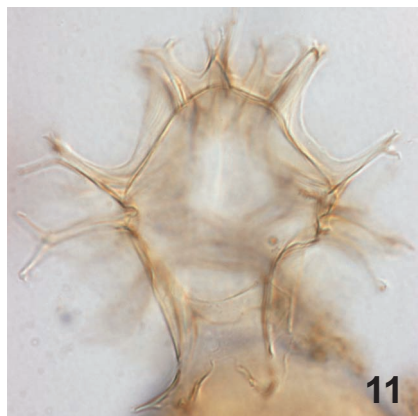
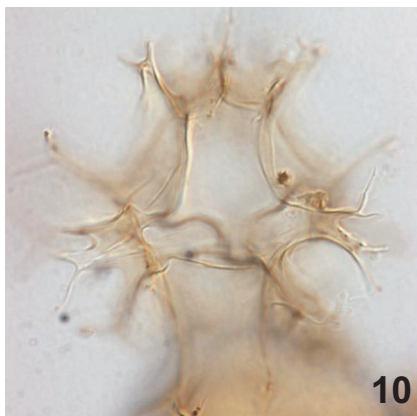
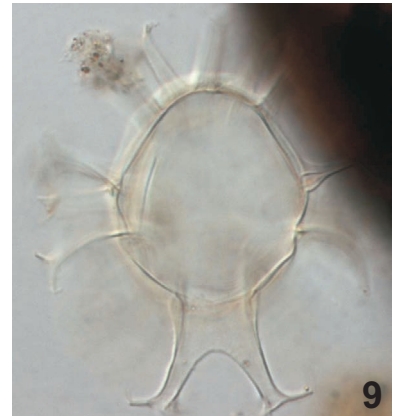
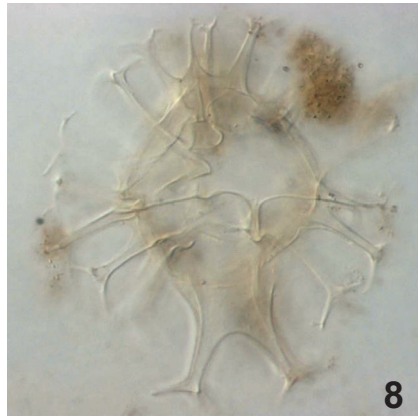
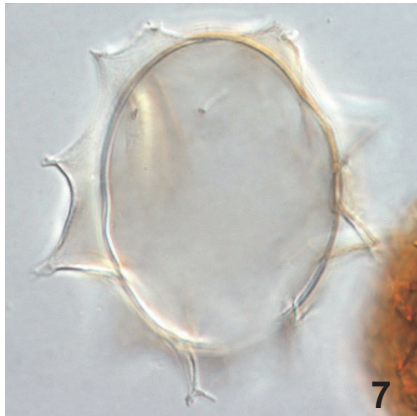
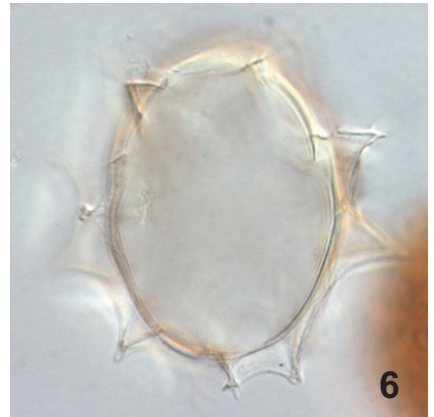
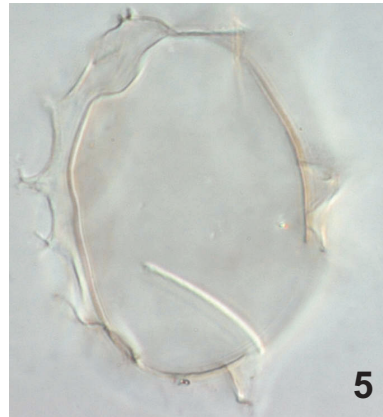
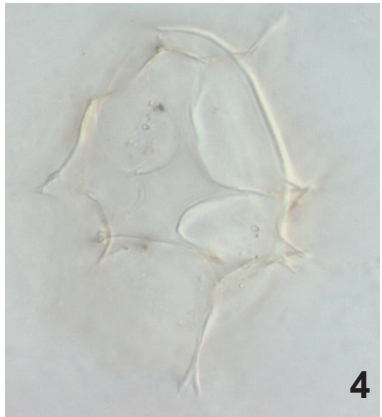
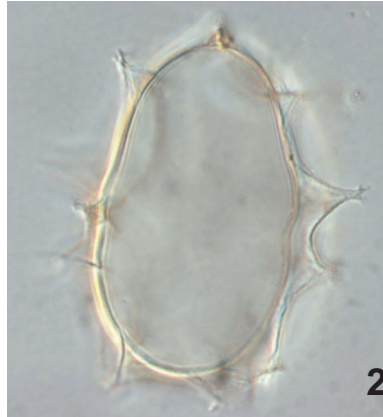
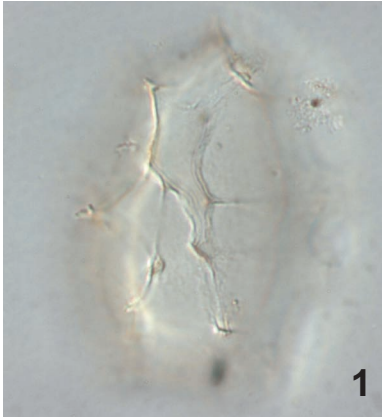


Plate 8

	Core	Depth (cm)	Slide ref	size (µm)	view*	remarks
1-5 <i>Bitectatodinium tepikiense</i>						
1	M23323	772.5	II 07	∅ 38	x1000, HF ^o	oblique-dorsal view of dorsal surface
2					x1000, MF	
3					x1000, LF	interior view of (ventral) surface
4	M23323	768.5	I 03	∅ 45	x1000, HF	dorsal view of dorsal surface
5					x1000, LF	note the free opercular plate inside the cyst
6-10 <i>Quinquecuspis concreta</i>						
6	M23071	646	III 18	80x66	x400, MF	note the outline of the archeopyle, with the operculum fully in place
7	M23323	784.5	I 06	88x75	x630, HF	apical-dorsal view. Note the free opercular plate inside the cyst
8					x630, LF	
9	M23071	648	II 16	75x63	x400, MF ^o	
10	M23071	649	II 11	76x68	x400, MF ^o	
11 cyst of <i>Polykrikos kofoidii</i>						
11	M23323	850.5	I 01	95x70	x630, HF	
12 cyst of <i>Polykrikos schwartzii</i>						
12	M23323	784.5	I 05	97x55	x630, HF ^o	

* HF: High Focus

MF: Mid Focus = optical section

LF: Low Focus

^o Composite picture, made by semi-transparently putting one photograph over another one taken at a slightly different focus depth

Plate 8

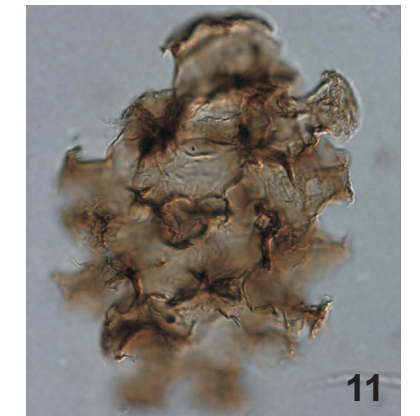
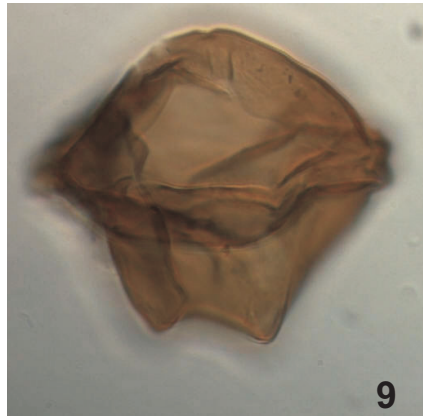
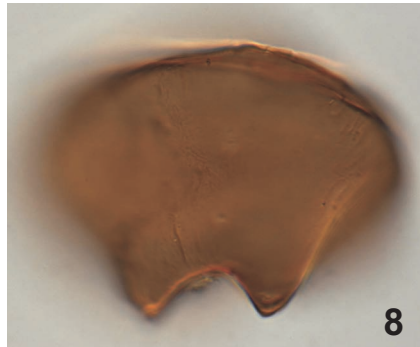
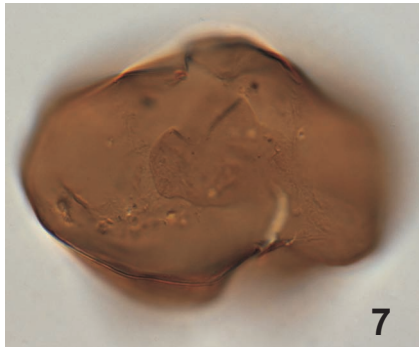
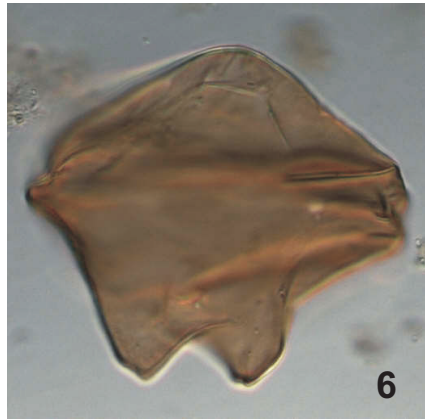
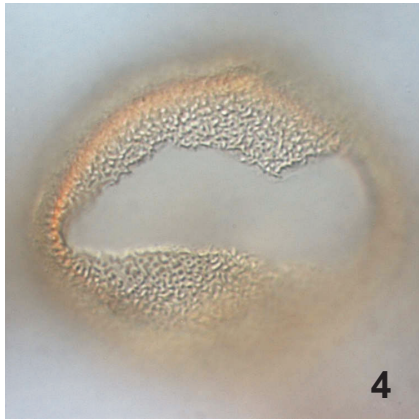
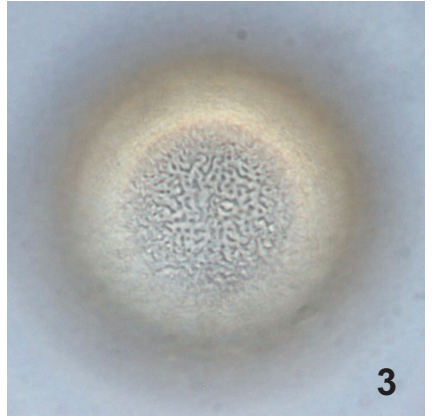
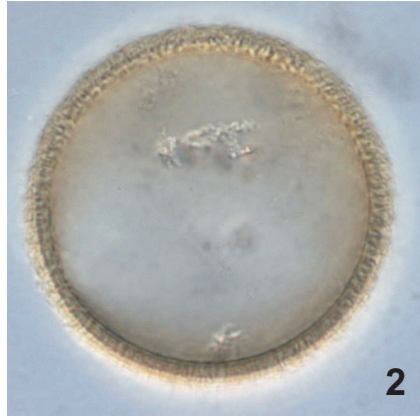
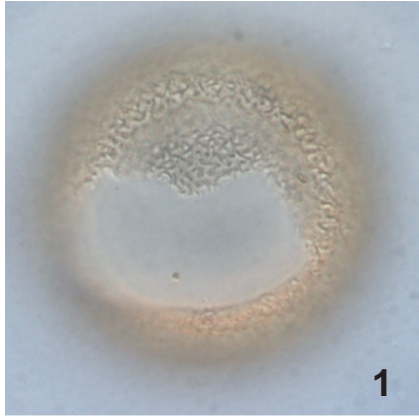


Plate 9

	Core	Depth (cm)	Slide ref	size (µm)	view*	remarks
1 <i>Brigantedinium cariaeoense</i>						
1	M23071	645	I 06	ø 43	x400, HF	
2-5 <i>Brigantedinium simplex</i>						
2	M23323	796.5	II 05	ø 36	x1000, MF	note the free opercular plate inside the cyst
3					x1000, LF	
4	M23323	800.5	II 05	ø 43	x1000, HF	ventral view of ventral surface, and free operculum
5					x1000, LF	interior view of dorsal surface
6 <i>Islandinium minutum?</i>						
6	M23071	642	III 15a	ø 36	x1000, LF	
7-12 <i>Protoperidinioid indet. cyst type A</i>						
7	M23323	794.5	I 06	ø 43	x1000, HF	for short description: see Plate 10
8					x1000, HF	slightly deeper focal depth with respect to "7"
9					x1000, MF	
10					x1000, LF	note the opening, possibly of the (intercalary?) archeopyle
11					x1000, LF	slightly deeper focal depth with respect to "10". The black dotted lines delineate what appear to be two opercular plates, adherent to the archeopyle margin
12	M23323	796.5	I 01d	38x28	x1000, LF	archeopyle?

* HF: High Focus

MF: Mid Focus = optical section

LF: Low Focus

◦ Composite picture, made by semi-transparently putting one photograph over another one taken at a slightly different focus depth

Plate 9

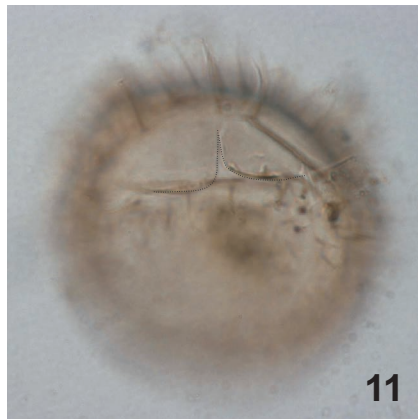
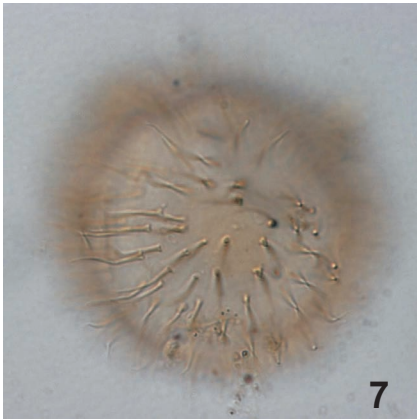
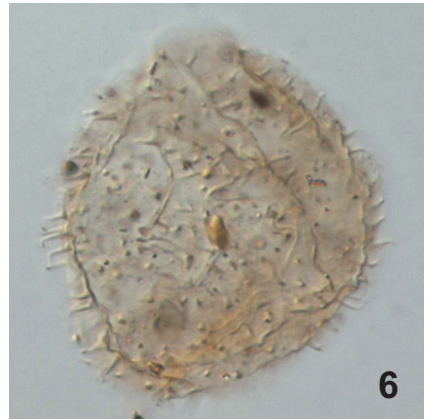
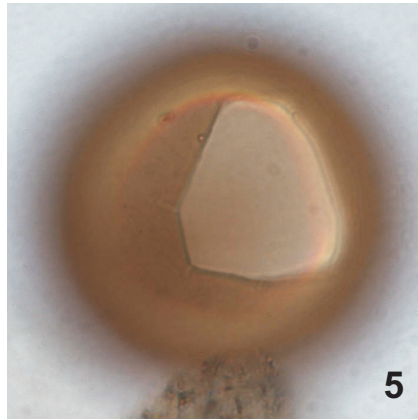
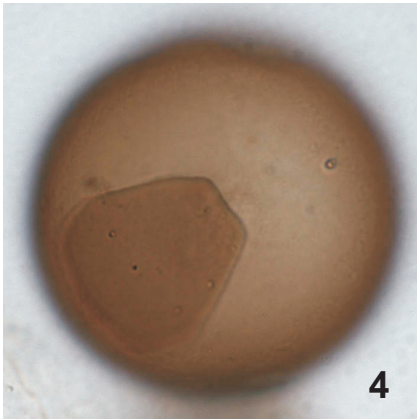


Plate 10

	Core	Depth (cm)	Slide ref	size (µm)	view*	remarks
1-12 Proto-peridinioid indet. type A						
1	M23071	642	III 10d	ø 38	x1000, HF	
2					x1000, LF	
3	M23071	648	II 20	ø 36	x1000, HF	long, slender and solid spines, slightly apiculocavate. Process tips acuminate. Cyst surface smooth to faintly granular, (light-)brown colour
4					x1000, MF	
5	M23071	649	II 07b	ø 46	x1000, HF	
6					x1000, MF	
7	M23323	794.5	I 01a	ø 29	x1000, MF	
8					x1000, LF	
9	M23323	796.5	I 04b	ø 34	x1000, HF	arrow: opening, due to partly detached opercular plate?
10					x1000, MF	
11	M23323	810.5	III 07d	ø 37	x1000, HF	
12					x1000, MF	

* HF: High Focus

MF: Mid Focus = optical section

LF: Low Focus

◦ Composite picture, made by semi-transparently putting one photograph over another one taken at a slightly different focus depth

Plate 10

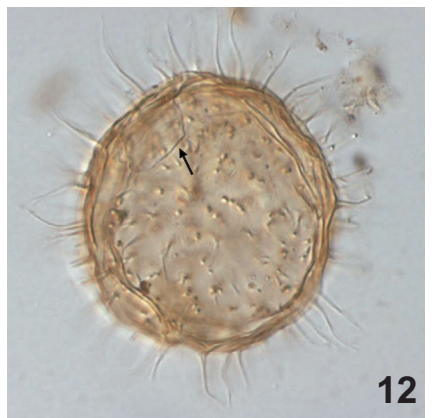
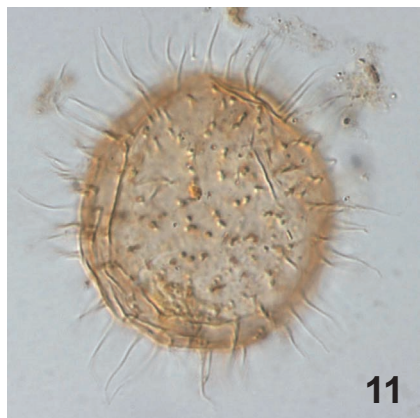
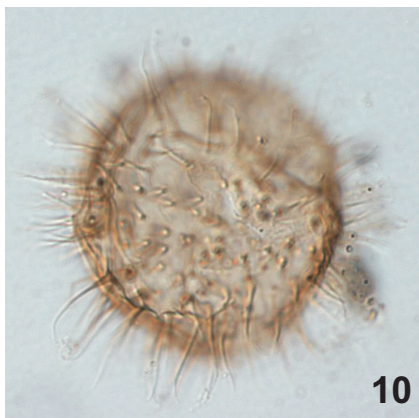
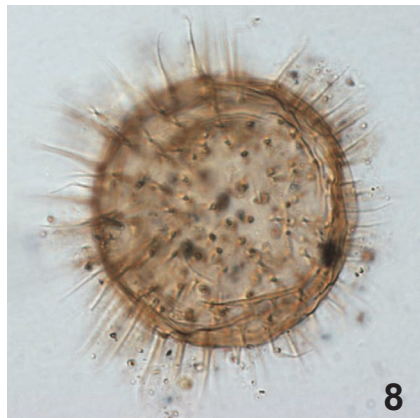
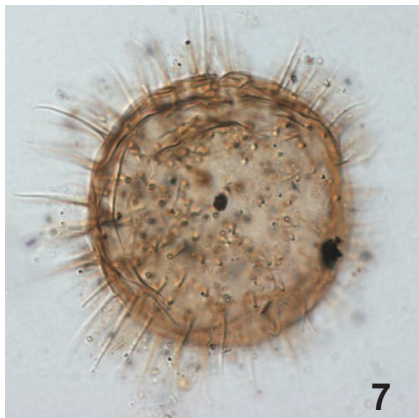
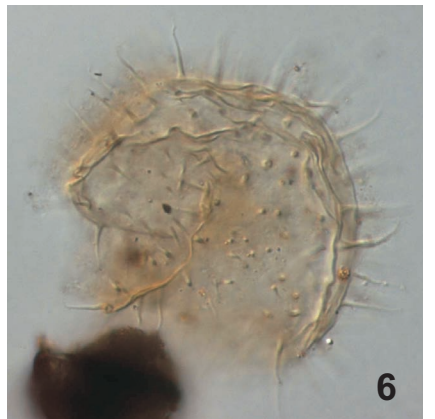
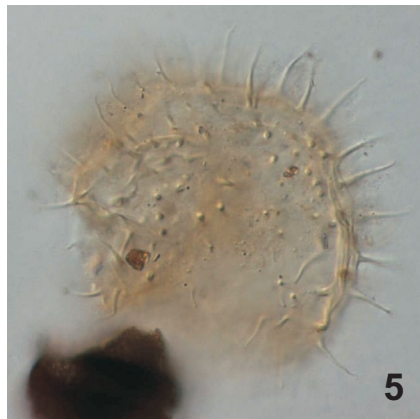
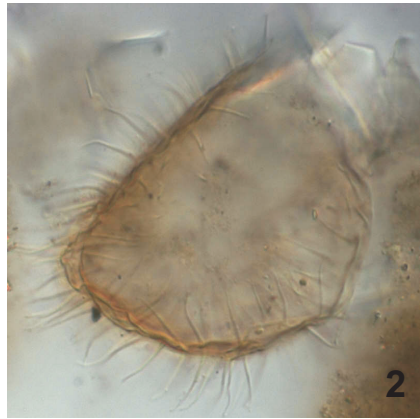
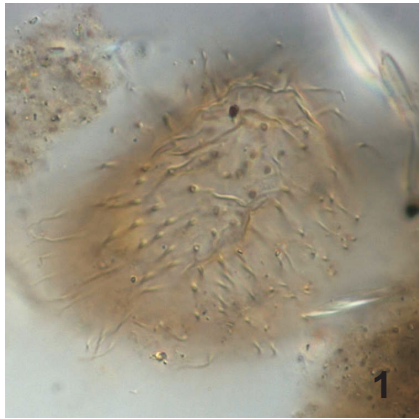


Plate 11

	Core	Depth (cm)	Slide ref	size (µm)	view*	remarks
1-3 <i>Selenopemphix quanta</i>						
1	M23071	642	III 18	ø 45	x1000, HF	
2					x1000, MF ^o	
3	M23323	794.5	I 05	65x51	x630 MF	
4-6 <i>Trinovantedinium applanatum</i>						
4	M23323	812.5	II 05	40x36	x1000, HF	
5					x1000, MF ^o	
6					x1000, LF	
7-12 <i>Trinovantedinium cf. applanatum</i>						
7	M23323	864.5	I 01	ø 43	x1000, HF	The <i>T. cf. applanatum</i> morphotype differs from <i>T. applanatum</i> in having heavier spines that are clearly hollow (apiculocavate) at their base (vs. solid), with markedly aculeate (vs. acuminate) process tips
8					x1000, MF	
9					x1000, LF	
10	M23323	864.5	I 02	41x36	x1000, MF	
11	M23071	636	I 03	50x38	x1000, MF	
12					x1000, MF	slightly lower focal depth with respect to "11"

* HF: High Focus

MF: Mid Focus = optical section

LF: Low Focus

^o Composite picture, made by semi-transparently putting one photograph over another one taken at a slightly different focus depth

Plate 11

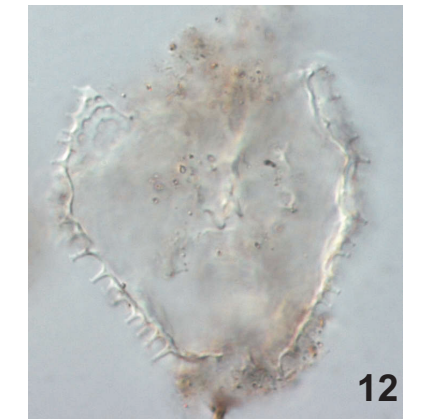
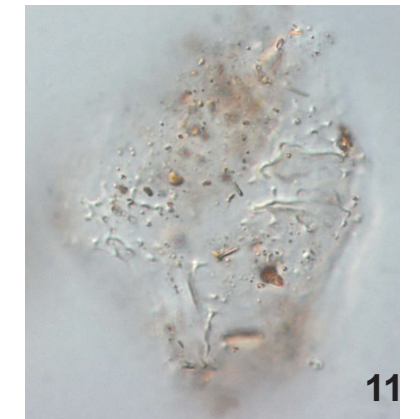
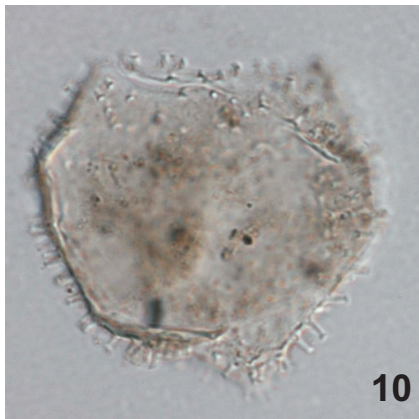
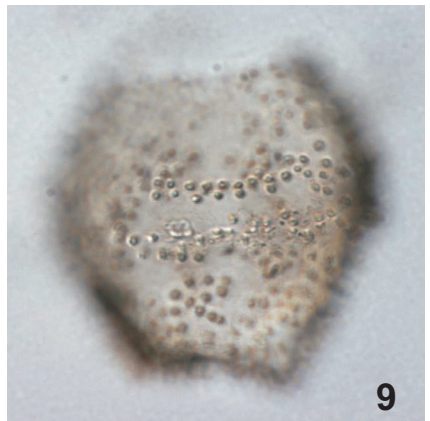
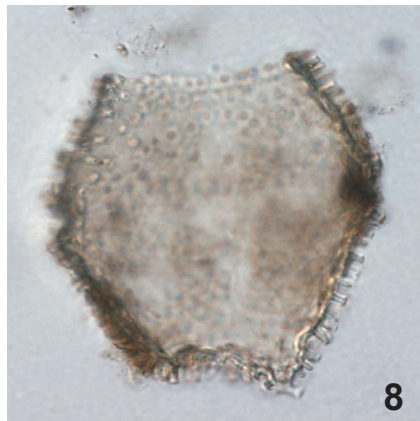
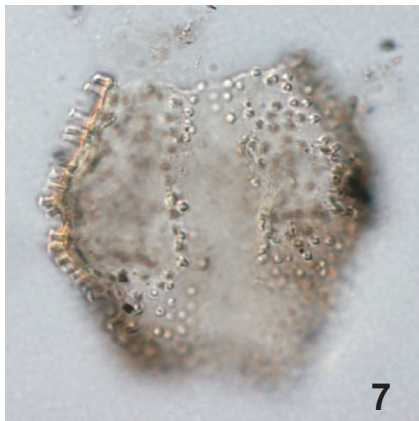
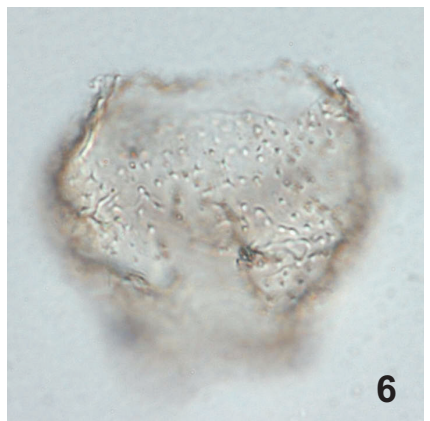
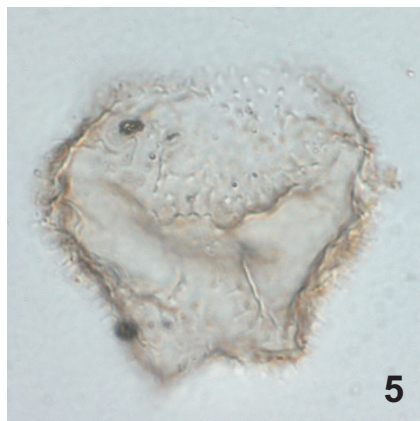
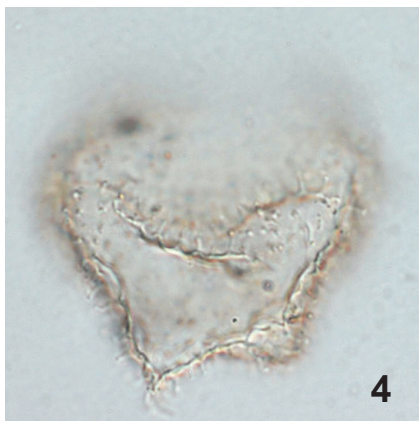
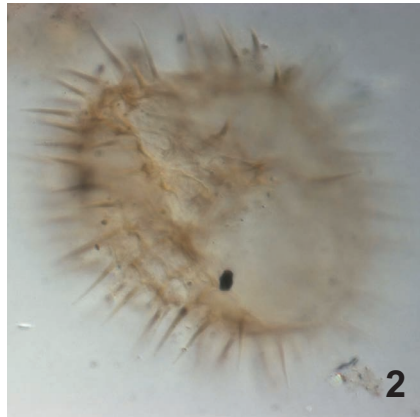
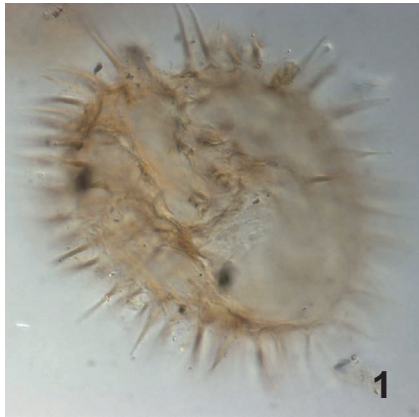


Plate 12

	Core	Depth (cm)	Slide ref	size (µm)	view*	remarks
1-4 Pyxidinospis reticulata						
1	M23071	636	I 04	ø 34	x1000, MF	
2					x1000, LF	
3	M23323	768.5	I 06	ø 35	x1000, MF	
4					x1000, LF ^o	
5-7 Tintinid lorica type 1						
5	MD992277	414.5 [^]	III 02	102x59	x630, MF	"Radiolarian-like" tintinid (?) lorica. Note the denticulate apertural margin
6					x630, LF	
7	MD992277	458.5 [^]	IV 01	275x85	x200	
8-9 Foraminiferal lining						
8	MD992277	414.5 [^]	III 01	L: 120	x630	
9	MD992277	426.5 [^]	III 01	ø 48	x1000	
10-12 Tintinid lorica type 2						
10	MD992277	410.5 [^]	IV 02	40x38	x1000, HF	small tintinid (?) lorica. Note the denticulate apertural margin
11					x1000, MF	
12					x1000, LF	
13-15 Palynomorph indet. type A						
13	MD992277	412.5 [^]	I 01	ø 75	x630, HF	unknown palynomorph, highly abundant at the MIS 5e/5d transition
14					x630, MF	
15					x630, LF	

* HF: High Focus
 MF: Mid Focus = optical section
 LF: Low Focus

^o Composite picture, made by semi-transparently putting one photograph over another one taken at a slightly different focus depth

[^] original depth

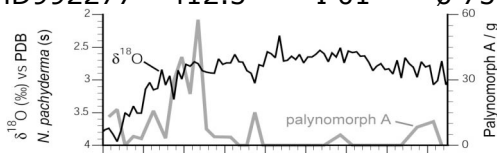
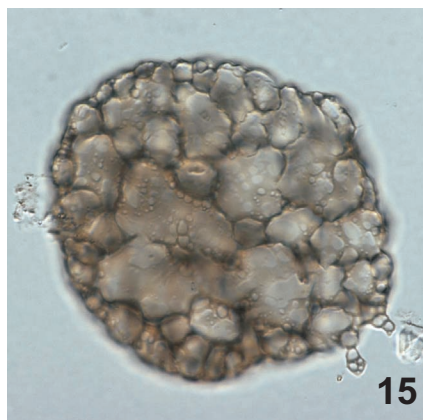
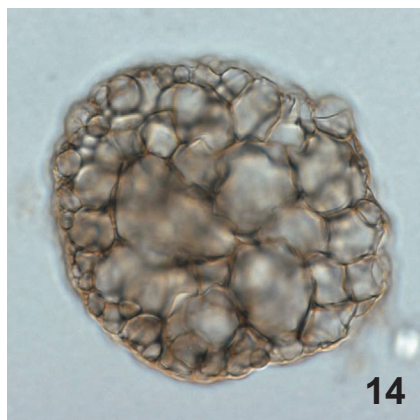
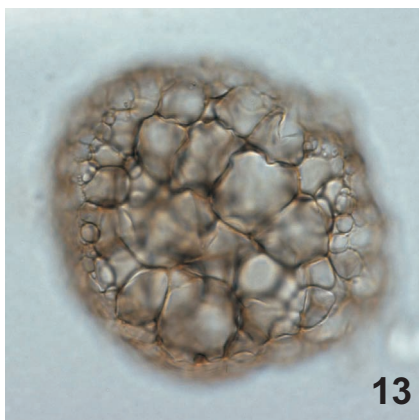
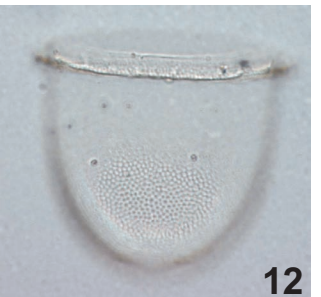
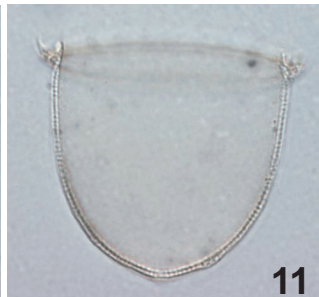
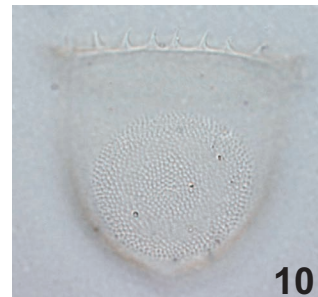
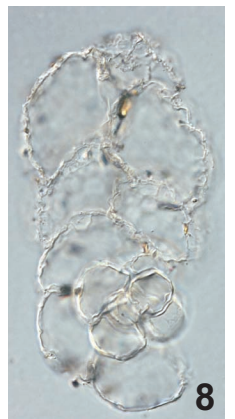
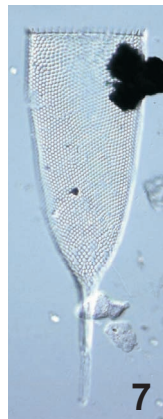
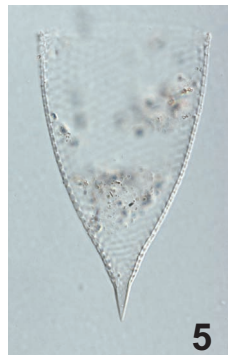
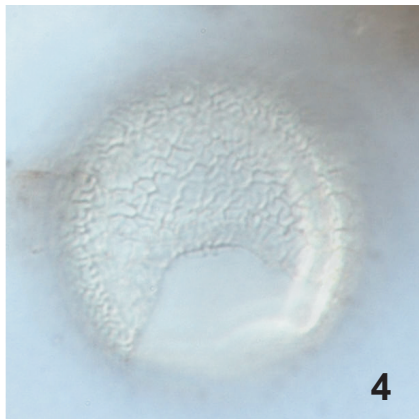
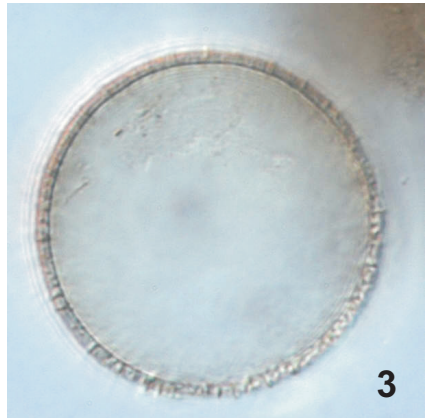
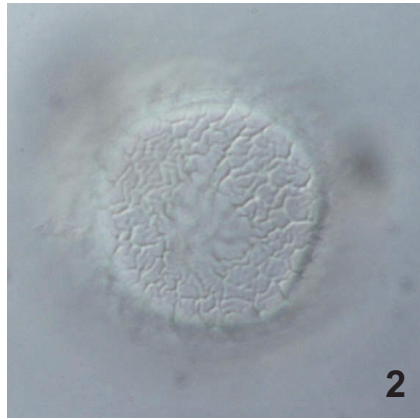


Plate 12



Curriculum Vitae

Personal Details

Name: Van Nieuwenhove
First names: Nicolas Frans Raphael
Date of birth: 7 June 1982
Place of birth: Ostend, Belgium
Nationality: Belgian
Current address:
 private Holtenauerstraße 92
 24105 Kiel, Germany
 work IFM-GEOMAR
 Wischhofstraße 1-3
 24148 Kiel, Germany
Tel.: +49 (0)431 600 2848
 +49 (0)176 2708 6802
Email: nvannieuwenhove@ifm-geomar.de
 nvnieuwenhove@googlemail.com



Research interests

Microfossils, dinoflagellate cysts and other palynomorphs, Quaternary climate and palaeoceanography of the Arctic and Subarctic

Academic Background

Period (dd.mm.yyyy)	Degree	Institution
01.10.2000-31.07.2004	Licentiate (~Master) Geology ¹	Universiteit Gent, Belgium
01.10.2004-07.07.2005	Master2 Biologie, Paléontologie et Océanologie Biologique ²	Université des Sciences et Technologies de Lille, France
Since August 2005: PhD-student at IFM-Geomar, Kiel		

Theses

¹ ***Chitinozoa biostratigraphy and chronostratigraphie of the Upper Ordovician Greenscoe section (Lake District, U.K.) (in Dutch)***

supervisors: Prof. Dr. J. Verniers, Universiteit Gent, Belgium
Dr. T. Vandenbroucke, Universiteit Gent, Belgium

² ***Biometrical study of the dinoflagellate cyst genus Bitectatodinium***

supervisors: Dr. T. Servais, Université des Sciences et Technologies, Lille, France
Prof. Dr. S. Louwey, Universiteit Gent, Belgium

Grants and Scholarships

- awarded the “2007 American Association of Stratigraphic Palynologists (AASP) Student Scholarship”

Short courses and workshops attended

- 10-12.11.2006: The 2006 International Workshop on Dinoflagellates and their Cysts: their ecology and databases for paleoenvironmental reconstructions (Copenhagen, Denmark)
- 29.01-02.02.2007: From the living dino to paleoenvironmental reconstructions; dinoflagellates – biological characteristics, ecology and their use for paleoclimate reconstructions (EUROPFOX, ECOLMAS; Bremen, Germany)
- 05.05.2008: Quantitative treatments and paleoceanographical reconstructions from dinocyst assemblages (Dino8; Montreal, Canada)

Scientific expeditions

- July 2006: 7-day field expedition to the Mezén territory (southeastern White Sea region), Russia, to sample Eemian outcrops along the Pyoza river.
- August 2007: 5-day ship expedition on board of the RV Maria S. Merian (Leg MSM 5/5) to the Fram Strait.

Peer-reviewed publications

- Van Nieuwenhove, N.**, Vandenbroucke, T.R.A., Verniers, J., 2006. Chitinozoan biostratigraphy of the Upper Ordovician Greenscoe section, Southern Lake District, UK. *Review of Palaeobotany and Palynology* 139, 151-169.
- Van Nieuwenhove, N.**, Bauch, H.A., Matthiessen, J., 2008. Last interglacial surface water conditions in the eastern Nordic Seas inferred from dinocyst and foraminiferal assemblages. *Marine Micropaleontology* 66, 247-263.
- Van Nieuwenhove, N.**, Bauch, H.A., 2008. Last interglacial (MIS5e) surface water conditions at the Vøring Plateau (Norwegian Sea), based on dinoflagellate cysts. *Polar Research* 27, 175-186.
- Mertens, K.N., Verhoeven, K., Verleye, T., Louwye, S., Amorim, A., Ribeiro, S., Deaf, A.S., Harding, I., De Schepper, S., Kodrans-Nsiah, M., de Vernal, A., Henry, M., Taoufik, R., Dybkjær, K., Poulsen, N.E., Feist-Burkhardt, S., Chitolie, J., González Arango, C., Heilmann-Clausen, C., Londeix, L., Turon, J.-L., Marret, F., Matthiessen, J., McCarthy, F., Prasad, V., Pospelova, V., Kyffin Hughes, J.E., Riding, J.B., Rochon, A., Sangiorgi, F., Welters, N., Sinclair, N., Christian, T., Soliman, A., **Van Nieuwenhove, N.**, Vink, A., Young, M. The absolute abundance calibration project: the Lycopodium marker-grain method put to the test. *Submitted to Review of Paleobotany and Palynology*.

Conference presentations

- Van Nieuwenhove, N.**, Bauch, H.A., Matthiessen, J.: *A comparative study of past surface ocean properties in the Subarctic using dinocysts and foraminiferal assemblages*. 02-07.04.2006, European Geosciences Union General Assembly (Vienna, Austria). (Poster).
- Van Nieuwenhove, N.**, Bauch, H.A., Matthiessen, J.: *Surface ocean properties of the Norwegian Sea during OIS5e, based on dinoflagellate cysts and foraminiferal assemblages*. 10-12.11.2006, The 2006 International Workshop on Dinoflagellates and their Cysts: their ecology and databases for paleoenvironmental reconstructions (Copenhagen, Denmark) (Poster).
- Van Nieuwenhove, N.**, Bauch, H.A., Matthiessen, J.: *Past surface ocean conditions from the last interglacial of the Norwegian Sea as reflected in paired microfossil records*. 10-14.12.2006, American Geophysical Union Fall Meeting (San Francisco, USA) (Poster).
- Van Nieuwenhove, N.**, Bauch, H.A.: *Surface ocean conditions in the Norwegian Sea during the last interglacial: evidence from dinocyst and foraminiferal assemblages*. 03-07.09.2007, 9th International Conference on Paleocanography (Shanghai, China) (Poster)
- Van Nieuwenhove, N.**, Bauch, H.A.: *Surface conditions and evolution of the Norwegian Sea during MIS 5e, based on dinoflagellate cyst assemblages*. 13-18.04.2008, European Geosciences Union General Assembly (Vienna, Austria) (Poster)
- Van Nieuwenhove, N.**, Bauch, H.A.: *The structure of the upper water column in the eastern Nordic Seas during the last interglacial (MIS 5e), based on dinoflagellate cysts*. 04-10.05.2008, Dino8 (Montreal, Canada) (Talk)
- Mertens, K., Amorim, A., Ribeiro, S., Deaf, A.S., Harding, I., De Schepper, S., de Vernal, A., Radi, T., Dybkjaer, K., Poulsen, N., Feist-Burkhardt, S., Chitolie, J., Gonzalez, C., Heilmann-Clausen, C., Kodrans-Nsiah, M., Londeix, L., Turon, J.-L., Marret, F., Matthiessen, J., McCarthy, F., Prasad, V., Pospelova, V., Hughes, J.K., Riding, J.B., Rochon, A., Sangiorgi, F., Marino, G., Welters, N., Sinclair, N., Thun, C., Soliman, A., **Van Nieuwenhove, N.**, Vink, A., Verhoeven, K., Verleye, T., Louwye, S., Young, M.: *The absolute abundance calibration project: the Lycopodium marker-grain method put to the test*. 04-10.05.2008, Dino8 (Montreal, Canada) (Talk by K. Mertens)

Erklärung gem. §10 Absatz 2 der PO der Mathematischen und Naturwissenschaftlichen Fakultät

Ich versichere hiermit, dass ich erstmalig an einem Promotionsverfahren teilnehme.

Außerdem versichere ich, dass die vorliegende Dissertation nach Inhalt und Form, abgesehen von den von mir angegebenen Quellen und Hilfsmitteln, sowie der Beratung durch meine akademische Lehrer und Betreuer, meine eigene Arbeit ist.

Weiterhin erkläre ich, dass ein Teil der Ergebnisse dieser Dissertation bereits veröffentlicht wurden, und Weitere Veröffentlichungen sind beabsichtigt.

Ich erkläre auch, dass die Dissertation unter Einhaltung der Regeln guter wissenschaftlicher Praxis entstanden ist.

Ort/Datum: _____

Unterschrift: _____